Physical modeling and study of the behavior of deep foundations of offshore wind turbines in sand

Ismat El Haffar

UNIVERSITE BRETAGNE SCIENCES LOIRE POUR L'INGENIEUR

CENTRALE NANTES

THESE DE DOCTORAT DE

L'ÉCOLE CENTRALE DE NANTES
COMUE UNIVERSITE BRETAGNE LOIRE

ECOLE DOCTORALE N°602
Sciences pour l'Ingénieur
Spécialité : Génie Civil

Par

Ismat EL HAFFAR

Physical modeling and study of the behavior of deep foundations of offshore wind turbines in sand

Thèse présentée et soutenue à l'IFSTTAR - Centre de Nantes, le 24-09-2018

Unité de recherche : IFSTTAR (Institut Français des Sciences et Technologies des Transports, de l'Aménagement et des Réseaux), GERS (Géotechnique, Environnement, Risques naturels et Sciences de la terre).

Rapporteurs:

Richard Jardine	Professeur, Imperial College, London
Pierre Breul	Professeur, Université Clermont Auvergne

Composition du Jury :

Président :	**Panagiotis Kotronis**	Professeur, Ecole Centrale de Nantes
Examinateurs :	**Cristina Tsuha**	Professeur, Université de São Paulo
	Christophe Dano	Maître de Conférences, Université Grenoble Alpes
Directeur de thèse :	**Luc Thorel**	Directeur de recherche, IFSTTAR
Encadrant de thèse :	**Matthieu Blanc**	Ingénieur des Travaux Publics de l'Etat, IFSTTAR

Acknowledgement

Firstly, I would like to express my sincere gratitude to my supervisors Luc Thorel and Matthieu Blanc for the continuous support of my Ph.D study and related research, for their patience, motivation, and immense knowledge. Their guidance helped me in all the time of research and writing of this thesis.

I would like to thank my thesis committee members for all of their guidance through this process; your discussion, ideas, and feedback have been absolutely invaluable.

I wish to thank the IFSTTAR and the Région Pays de Loire for their financial support to the thesis grants, within the context of which this study has been conducted.

My sincere thanks also goes to IFSTTAR Centrifuge team (Patrick Gaudicheau, Philippe Audrain, Alain Néel, Stéphane Lerat, Frantz Buisson, Alexandre Jagu) for their technical support and assistance during the centrifuge experimental campaign and also because they give me the opportunity to join their team and accepted me in the centrifuge little family as a Phd student. My thanks also goes also to Thomas Lenoir, Sophie Ricordel, Sandra Escoffier, Alberto Bretschneider, Jean Pierre David and the other members of the laboratory for the great times I spent with them in the last three years.

I thank my colleagues for the stimulating discussions and for all the fun we have had in the last three years.

To my closer friends, I express my gratitude for their unconditional friendship, support and patience throughout these years.

I would especially like to thank my amazing family for the love, support, and constant encouragement I have gotten over the years. In particular, I would like to thank my parents, my brothers, and my sister. I undoubtedly could not have done this without you.

Tables of contents

Abstract:

The axial and lateral capacity of piles jacked in Fontainebleau sand NE34 are studied using centrifuge modelling at 100×g.

The effect of the installation method, sand density and saturation, pile diameter and pile tip geometry (open or closed-ended) and pile roughness on the axial capacity of piles are firstly studied. A significant increase in the tension capacity is observed in cyclically-jacked piles unlike piles monotonically jacked at 100×g. The saturation of dense sand accelerates plug formation during pile installation. The increase in pile roughness and sand density increases significantly the shaft resistance of the piles tested here. For all the cases, pile capacities are compared with the current design codes for offshore wind turbines.

A parametric study of the effect of the installation method, load eccentricity and sand saturation on the lateral response of jacked piles is then realized using of an instrumented pile. The pile is loaded monotonically, then a thousand cycles are applied. A new methodology has been developed for determining of the constants needed in the integration procedure to identify the lateral displacement profile of the pile. The installation method influences directly the global (maximum moment and lateral displacement) and local behaviour (p-y curves) of the piles. The effect of the load eccentricity and sand saturation on the behaviour of the piles is also presented. In each case a comparison with the p-y curves extracted from the DNVGL code is realized.

Résumé Etendu:

Les fondations profondes transfèrent les charges d'une structure vers des couches géologiques situées à plusieurs dizaines de mètres sous la surface du sol. Les pieux doivent équilibrer les charges axiales ou latérales, par les interactions avec le sol environnant. Dans le domaine offshore, ces charges peuvent varier de manière monotone ou cyclique (généralement une somme de cycles due au vent, aux vagues ou au courant), ce qui complique encore le dimensionnement des pieux en prenant en compte les variations de l'interaction sol-structure.

Sous chargement axial, différents paramètres peuvent affecter la capacité axiale du pieu: méthode d'installation, diamètre du pieu, rugosité du pieu, géométrie de la pointe du pieu, densité et saturation du sable. Ces paramètres ont une influence directe sur la capacité de la pointe et sur le frottement latéral du pieu soumis à une charge axiale, ce qui génère des biais et des incertitudes multiples pendant le dimensionnement des pieux. Plusieurs études, réalisées dans le but de déterminer la capacité axiale des pieux, ont conduit à l'établissement des codes de dimensionnement, qui sont utilisés de nos jours pour le dimensionnement des pieux. Ces codes ne sont pas toujours bien adaptés aux applications offshore en raison de (1) les charges multiples appliquées sur les pieux et (2) les paramètres supplémentaires qui existent en milieu offshore par rapport au milieu onshore, comme la saturation totale du sable, la formation des bouchons dans les pieux ouverts et la complexité de la méthode d'installation.

Les charges latérales proviennent généralement des vagues, du courant, du vent et des tempêtes marines et sont appliquées à des excentricités différentes sur les structures offshores fixes. Les charges globales induisent sur les pieux, à des intensités différentes selon le type de structures et de fondations (monopieu, structure jacket sur pieux,…), des chargements monotones ou cycliques. Le dimensionnement des pieux sous chargement latéral est basé sur l'approche de transfert de charge appelée également courbes de réaction p-y. Cette méthode, basée sur la théorie des poutres, est largement utilisée pour dimensionner des pieux soumis à une charge latérale monotone, mais les effets des cycles ne sont pas encore bien identifiés. De plus, la capacité latérale d'un pieu peut également être affectée par la méthode d'installation du pieu, l'excentricité de la charge et la saturation du sable.

Pour mieux comprendre l'influence de ces paramètres sur la capacité axiale et latérale des pieux, une étude expérimentale paramétrique a été effectuée dans le sable de Fontainebleau NE 34 afin de quantifier l'effet de chaque paramètre sur le dimensionnement du pieu. La

modélisation en centrifugeuse est considérée comme la meilleure solution pour réaliser ce type de tests paramétriques de manière économique et dans des conditions contrôlées de chargement et d'homogénéité du sable. Deux montages expérimentaux ont été développés pour réaliser l'étude souhaitée sous chargement axial ou latéral à 100×g sur des pieux modèles à l'aide de la centrifugeuse géotechnique de l'IFSTTAR-Nantes.

Les objectifs de cette thèse sont:

- Étudier l'effet de la méthode d'installation, du diamètre du pieu, de la rugosité du pieu, de la géométrie de la pointe du pieu (ouverte ou fermée), de la densité et la saturation du sable sur la capacité axiale du pieu.
- Évaluer la performance des codes de dimensionnement de pieux sous chargement axial par rapport aux résultats expérimentaux.
- Etudier l'effet de l'excentricité de la charge, de la méthode d'installation du pieu et de la saturation du sable sur le comportement global (moment et déplacement) et local (courbes p-y) des pieux.
- Comparer les courbes p-y de la DNVGL et les courbes p-y extraites d'expériences sur des pieux instrumentés chargés latéralement.

Cette thèse est décomposée en deux: la première partie montre les tests réalisés sur les pieux sous chargement axial et les résultats obtenus. Alors que, la deuxième partie montre les tests des pieux sous chargement latérale et les résultats obtenus.

46 expérimentations de **chargement axial** ont été réalisées en utilisant un vérin hydraulique fixé sur le conteneur de sable de Fontainebleau NE34. Ce montage expérimental permet de mettre en place des pieux en utilisant différentes méthodes d'installation (fonçage monotone à 1×g, monotone à 100×g et cyclique à 100×g en utilisant diffèrents pas de chargement). Afin d'étudier l'effet de la rugosité du pieu, de la formation du bouchon et de la densité et saturation du sable, neuf pieux modèles, de différents diamètres et rugosités ont été foncés de 250 mm à 100×g dans de sable moyennement dense et dense de Fontainebleau sec et saturé.

L'étude sur l'effet de la méthode d'installation a été réalisée avec 6 tests à 100×g et de 250 mm de profondeur. Les méthodes d'installation réalisées sont le fonçage monotone à 1×g, le fonçage monotone à 100×g et le fonçage cyclique à 100×g avec des pas de fonçage allant de 2.5 mm à 25 mm. Cette étude a permis d'établir les résultats suivants :

1. Les pieux foncés ont une résistance à la compression trois fois supérieure à celle obtenue avec les pieux forés. Les pieux foncés d'une manière monotone à 100 × g offrent une capacité environ 8% plus élevée que celle des pieux cycliquement foncés.
2. L'impact des techniques d'installation sur la capacité de traction des pieux a été étudié. La différence la plus significative a été constatée pour les pieux foncés à 100 × g, s'ils sont foncés d'une manière monotone ou cyclique. Malgré la limitation de l'étude à un test pour chaque méthode d'installation et à une densité étudiée, la capacité en traction des pieux a clairement tendance à augmenter avec l'augmentation du nombre de pas d'installation. Les résultats montrent un gain de capacité d'extraction allant jusqu'à 67% avec l'augmentation des pas d'installation cyclique. L'explication discutée dans cette étude suggère qu'il pourrait exister une relation entre le gain de capacité et la dilatation et l'écrasement du sable habituellement observés dans les cas où des surfaces rugueuses sont en contact avec du sable dense.
3. Pour les deux approches, une comparaison avec les normes de dimensionnement a été faite. Les standards de dimensionnement se sont révélés très conservateurs par rapport aux résultats expérimentaux. De plus, aucune approche n'a été trouvée dans ces méthodes pour prédire le gain de capacité trouvé dans les tests d'arrachement.

L'effet de la densité et de la saturation du sable est ensuite étudié en réalisant des tests dans des conteneurs de sable moyennement dense (Dr=58%) et dense (Dr=99%) sec ou saturé :

1. La présente étude suggère d'abord que la saturation du sable dense a une influence importante sur la création de bouchons lors de l'installation de pieux.
2. Les pieux installés dans du sable sec présentent des capacités supérieures à celles des pieux installés dans du sable saturé en traction et compression.
3. Le déplacement en traction jusqu'à la rupture diffère selon les conditions de densité et de teneur en eau. Ses valeurs ne sont pas toujours égales à la valeur conventionnelle de 10% de B.
4. La rigidité initiale est affectée par la densité et la saturation du sable. La rigidité initiale augmente avec la densité du sable, qui est cependant plus faible dans le sable saturé que dans le sable sec. Une relation linéaire entre la force de fonçage et le volume encastré des pieux testés est décrite.

Des tests réalisés avec des pieux en acier de 4 diamètres différents (12,14,16 et 18 mm) permet également de discuter l'effet du diamètre du pieu:

1. La diminution du diamètre du pieu améliore la formation de bouchons dans les pieux ouverts.
2. Le rapport entre la capacité en traction et en compression diminue avec l'augmentation du diamètre.

L'étude sur l'effet de la géométrie de la pointe (ouverte ou fermée) a montré :

1. Les pieux ouverts ont des capacités en traction supérieures à celles des pieux fermés.
2. Le rapport capacité de traction/compression est systématiquement plus grand pour les pieux ouverts que pour les pieux fermés.

Une comparaison entre les résultats expérimentaux et les codes de dimensionnement existants (NF, ICP-05 et API et DNVGL) utilisés pour la réalisation d'éoliennes en mer montre que:

- En mode compressif, les codes de dimensionnement étudiés révèlent différents degrés de conservatisme par rapport aux résultats expérimentaux. ICP est le plus proche des résultats expérimentaux. Vient ensuite NF, dont les résultats sont approximativement la moitié des capacités expérimentales. Enfin, nous trouvons API et DNVGL, qui sont les codes de conception les plus conservateurs et qui donnent des résultats allant de 20% à 35% des capacités expérimentales sans les limitations suggérées dans les codes. Avec l'utilisation de ces limitations, les deux normes sont encore plus éloignées de la représentation du comportement réel des pieux.
- En mode de traction, la performance ICP est bonne dans le sable dense. Cependant, ICP et NF fournissent une surestimation des capacités de traction du pieu dans le sable moyennement dense. API et DNVGL surestiment également la capacité de traction dans le sable moyennement dense, tout en la sous-estimant dans le sable dense.
- La performance de la méthode ICP dans le cas de pieux ouverts semble dépendre de l'estimation précise de l'état de création de bouchon du pieu et du choix de la meilleure condition de bouchon entre les différentes conditions disponibles trouvées dans le code.

L'effet de la rugosité de pieu sur sa capacité axiale a été étudié en utilisant deux pieux possédant deux rugosités différentes (R_n = 0.014 et 0.33):

1. L'augmentation de la rugosité montre que la résistance à la traction augmente de 36% dans le sable dense et de 57% dans le sable moyennement dense. De plus, le frottement latéral en compression triple lorsque la rugosité augmente.

2. Les pieux rugueux, en effet, présentent des résistances de frottement à l'enfoncement et à l'arrachement trois fois plus élevées dans le sable dense que dans le sable moyennement dense. De plus, les pieux lisses révèlent des résistances de frottement à l'enfoncement et à l'arrachement quatre fois plus élevées dans le sable dense que dans le sable moyennement dense.
3. Le rapport de résistance au frottement entre la traction et la compression est de 0,8 dans le sable dense et de 1 dans le sable moyennement dense pour les pieux lisses. Les pieux rugueux présentent un frottement à l'enfoncement environ trois fois supérieur au frottement à l'arrachement dans les deux densités.
4. La comparaison des résistances expérimentales de frottement avec les résistances obtenues en utilisant les méthodes ICP montre que l'utilisation d'un angle de frottement de 15 ° et 20 ° pour des pieux lisses fournit une bonne estimation du frottement latéral déduit de l'ICP dans les sables à la fois moyennement denses et denses. Par ailleurs, 25 ° et 30 ° sont les angles de frottement utilisés dans l'ICP respectivement à afin de faire correspondre le frottement de traction des pieux rugueux dans le sable moyen et dense.

Les pieux offshore de structures jacket sont soumis non seulement à des charges axiales, mais également à de lourdes charges latérales provenant des vagues, du courant et du vent. Cela rend nécessaire d'étudier ces fondations également sous des chargements latéraux. Après l'étude réalisée sur les paramètres influençant la capacité axiale des pieux, cette thèse se concentre sur la capacité latérale des pieux.

Un nouveau montage expérimental, qui permet non seulement le fonçage en vol du pieu, mais également son chargement latéral en vol sans arrêter la centrifugeuse a été développé. Cela peut être réalisé en ajoutant un vérin électrique latéral au montage développé précédemment pour étudier la capacité axiale du pieu. De plus, un nouveau pieu modèle instrumenté a été développé possédant 16 niveaux de jauges à l'échelle 1/100 avec une profondeur d'encastrement de 200 mm. Ce pieu a été testé, en utilisant la centrifugeuse géotechnique à 100 × g, afin de déterminer les effets de la méthode d'installation (fonçage à 1×g et fonçage à 100×g), de l'excentricité du chargement et de la saturation du sable sur le comportement latéral de pieu sous chargement monotone et cyclique.

Une nouvelle méthode est développée pour la détermination des constantes requises pour la procédure d'intégration utilisée pour déterminer le profil de déplacement latéral du pieu. L'identification de la deuxième constante consiste à déterminer le centre de rotation du pieu à

l'aide du profil de réaction du sol. Une discussion complète de la méthode et de ses avantages est proposée dans la thèse. Cette méthode, appelée méthode incrémentale, permet d'établir les courbes p-y des tests effectués sur des pieux instrumentés, même si une seule condition limite peut être mesurée de manière fiable au cours des tests.

Après l'identification de la méthode de la double intégration, les effets de la méthode d'installation, de l'excentricité de la charge et de la saturation du sable sur le comportement global (déplacement du pieu et moment) et local (courbes p-y) sont déterminés.

A. Pour l'analyse de chargement monotone:

1. L'excentricité croissante de la charge produit une réponse plus douce des courbes p-y. DNVGL ne prend pas en compte l'effet de ce paramètre. Comme les effets d'excentricité de la charge ne sont pas très importants et pour des raisons pratiques, nous suggérons d'utiliser le même ensemble de courbes p-y pour évaluer la réponse du pieu lorsque différentes excentricités de la charge sont appliquées.
2. La saturation du sable s'est avérée être un paramètre important: 1) elle peut affecter le déplacement latéral avec une augmentation pouvant atteindre 57% du déplacement par rapport au sable sec. 2) la saturation du sable moyennement dense a entraîné une réponse plus faible d'environ 40% des courbes p-y par rapport au sable sec.
3. L'installation en vol de pieux provoque une diminution de 24% du déplacement latéral des pieux à la surface du sable. Ils ont également des valeurs maximales de moment inférieures et moins profonds qu'aux moments maximaux des pieux foncés à 1 × g. Les résultats précédents peuvent être attribués à la densification des couches de sable en surface. Les courbes p-y correspondant à ces pieux présentent un seuil final supérieur de 70% et une réponse initiale jusqu'à 45% plus rigide que les pieux installés à 1 × g.

La comparaison avec les courbes p-y du code DNVGL a montré que le code ne prend pas en compte l'effet de l'excentricité et de la méthode d'installation sur les courbes p-y. Pour le sable sec, la DNVGL a montré une rigidité 7 fois supérieure à celle expérimentale. Par contre, pour le sable saturé, le DNVGL était 4 fois plus élevé.

B. Pour l'analyse du chargement cyclique (jusqu'à 1000 cycles):

Le moment maximum dans le pieu au cours des cycles est analysé et il a été montré que sa valeur diminuait et devenait moins profonde avec l'augmentation du nombre des cycles. Le déplacement à la surface du sable est également présenté. Un examen détaillé et une

interprétation des courbes cycliques p-y d'un test sont ensuite présentés pour les différentes couches de sol.

1. L’accumulation du déplacement latéral du pieu diminue avec l’augmentation de l’excentricité, mais l’excentricité de la charge ne semble pas avoir d’effet important sur le développement des courbes cycliques p-y.
2. La saturation du sable montre une légère diminution de l’accumulation de déplacement latéral mais ne semble pas avoir d’effet important sur le développement des courbes cycliques p-y.
3. L'installation du pieu en vol induit généralement une diminution de l'accumulation du déplacement. En ce qui concerne les courbes p-y, les faibles profondeurs ont montré une amélioration de la réaction du sol à un meilleur taux pour le pieu installé à $1 \times g$ par rapport au pieu installé en vol. Par contre, dans les profondeurs importantes, le pieu installé en vol présente un taux de dégradation plus élevé au cours des cycles que le pieu installée à $1 \times g$.

Notations and Abbreviations

Latinas uppercases

A_b The gross end area of the pile

A_s The side surface area of pile

B Pile diameter

B_{inner} Inner diameter of the pile (m)

C_i Calibration coefficient

D Embedment length

D_r Relative density (%)

D_t Tension displacement

E_M Pressiometric modulus

E_p The modulus of elasticity of the pile

E_s The modulus of elasticity of the soil

F_r Failure force

G Centrifuge acceleration

H Horizontal applied load

H_c The half amplitude of the cyclic component

H_m The mean value of the applied lateral load

H_{min} The minimum horizontal load in the cycles

H_{max} The maximum horizontal load in the cycles

I_p The moment of inertia of the pile

K The coefficient of lateral earth pressure

M Moment

N Scale factor between prototype and model, intensity of the macro gravity field

N_q Dimensionless bearing capacity factor

P_s The perimeter of the foundation

R Radius of the application stresses

R_0 Radius between the rotation axes of the machine and the strongbox surface

R_1 Centrifuge radius

R_b Tip capacity

Rc Compression resistance

R_{inner} Inner radius

R_{outer} Outer radius

R_{max} Depth of asperities

R_n Normalized roughness

R_N Radius of the application of the centrifuge acceleration

R_s Shaft friction resistance

Rt Tension resistance

R_z The maximum height of the pile surface profile

R* Modified radius

U_c Coefficient of uniformity

V_m Inside volume of the test mold

Latinas lowercases

d_{50} Mean diameter of the sand

d_x The grain size, at which x% of particles by weight are smaller

e Void ratio of the material

e_{max} Maximum void ratio of the material

e_{min} Minimum void ratio of the material

f The unit skin friction capacity

f_{sol} Function dependent on the type of the soil and the values of q_c

g Earth gravity

h Model height

h^p Correspond to the prototype notation of h

h^m Correspond to the model notation of h

k_c Bearing factor dependent on the type of the soil and the installation method of the pile

m Mass of the mold and it content

m_d Dry weight of the sand

m_m Mass of the empty test mold

n Porosity

q_b Base capacity

q_c CPT resistance

p Soil reaction

y Lateral displacement

y_N Lateral displacement at the N cycle

z Depth coordinate

ω Rotation speed of the centrifuge

Greeks uppercases

ΔL Increment of soil length inside the pile

ΔD Increment of pile penetration depth

$\Delta\sigma'_{rd}$ The dilatant increase in local radial effective stress during pile loading

Greeks lowercases

ρ Density

ρ_d The unit dry weight of the material

ρ_{dmin} Minimum dry unit weigh

ρ_{dmax} Maximum dry unit weigh

ρ_s The dry unit weight of the solid particles

φ_{cs} The internal critical state friction angle

σ_{vm} Vertical stress

σ'_v The effective overburden pressure at the point in question

Δ The friction angle between the soil and pile wall

α Degradation factor of the lateral displacement

$\alpha_{pieu-sol}$ Dimensionless parameter which depend on the type of the pile and the type of the soil

τ_f The local shear stress

σ'_{rc} The local radial effective stress

List of figures

List of Tables

1 General introduction

Deep foundations transfer the loads of a structure towards geological layers located several tens of meters below the soil surface. The piles have to equilibrate axial or lateral loading, by the interactions with the surrounding soil. In the offshore domain, these loadings may vary as monotonic or cyclic (typically a summation of cycles due to wind, wave or current) which makes the design of the piles even more complicated in taking into account the variations of soil-structure interaction.

Under **axial loading**, different parameters can affect the axial capacity of the pile: installation method, pile diameter, pile roughness, pile tip geometry, sand density and saturation. These parameters influence directly the tip capacity (and bearing) and the shaft resistance of a pile submitted to axial loading, which put the design of the pile under multiple bias and uncertainties. Several studies, realized in order to design the axial capacity of piles, have led to establishing design codes, which are used nowadays for pile design. These codes are not always well adapted to offshore application because of (1) the multiple loadings applied on piles and (2) the additional parameters that exist in offshore in comparison with onshore area like full sand saturation, pile plugging and the complexity of the installation method.

Lateral loadings are usually originated from waves, current, wind and offshore storms and are applied at different eccentricity on the fixed offshore structures. The global loads induce on the piles, at different intensities depending on the type of structures and foundations (monopole, jacket on piles, …), monotonic or cyclic loading. Cyclic lateral loadings can be characterised by four parameters, additionally to the period: the maximum applied load (H_{max}), the cycle amplitude (H_c), the cycles number (N) and the type of the cyclic loading (one-way or two-way). The design of piles under lateral loading is based on the load-transfer approach called also p-y curves. This method based on the beam theory, is widely used to design pile under monotonic lateral loading, but the effects of cycles are not well identified yet. Moreover, the lateral capacity of a pile can also be affected by the installation method of the pile, the load eccentricity and the sand saturation.

For a better understanding of the influence of these parameters that affect the axial and lateral capacity of piles, a set of parametric experiments has been performed in Fontainebleau NE34 sand, to quantify the effect of each parameter on pile design. Centrifuge modelling is considered as the best solution to make such type of parametric tests in economical way and under controlled condition of loading and sand homogeneity. The use of instrumented model piles makes possible to analyse the effect of each parameter on pile capacity. This is why two

experimental set-ups have been developed in order to realize the desired study under axial or lateral loading on model piles using the beam geotechnical centrifuge of IFSTTAR-Nantes.

The objectives of this thesis are:

- To study the effect of installation method, pile diameter, pile roughness, pile tip geometry (open or closed-ended), sand density and sand saturation on the axial capacity of pile.
- To evaluate the performance of design codes used to design pile under axial loading toward the experimental results.
- To study the effect of load eccentricity, pile installation method and sand saturation on the global (moment and displacement) and local (p-y curves) behaviour of piles.
- To compare the DNVGL p-y curves and the p-y curves extracted from experiments on instrumented laterally loaded piles.

This report includes two chapters, where the data is presented at the prototype scale:

The first, one begins with a literature review on the parameters affecting the **axial capacity** of piles (installation method, pile diameter, pile tip geometry, sand density and saturation, pile roughness). Then, is presented the experimental set-up and the tests campaign realized. Finally the experimental results as well as the comparison with the design codes is analysed and discussed.

The second chapter focuses on **lateral loading** where a literature review on the different types of lateral loadings and the parameters (the installation method of the pile, the load eccentricity and the sand saturation) which can affect the lateral behaviour of piles is firstly presented. The new experimental set-up and the results of the realized tests are then presented and discussed.

A set of 8 appendixes presents the results at the model scale of each test, as well as ancillary information linked to the experiments.

2 Pile subjected to axial loading

2.1 Introduction

With the increasing size of the civil construction structures, the use of piles shows a greater interest. The increase of the size of the structures lead to that their weight increases proportionally. As consequence the traditional ways of the use of shallow foundation is not sufficient. Nowadays, the use of piles under these types of structures in order to transfer the load to deeper layers of soil is the leading solution.

In the offshore domain, the use of piles to maintain oils and gas structures was also widely used from the beginning of the exploitation of the offshore environment. Moreover, the construction of the offshore wind turbines profited from the development that was initially realized in the design of offshore piles in the construction of the oil and gas structures. Their design methods were applied to the foundation of the offshore wind turbines. But the fact that the condition in which the offshore wind turbines are constructed is different from the condition of the oil structure implies a lot of uncertainty about the use of the same design methods. The oil and gas platforms are heavy with high self-weight. Heavy self-weight (from 500 and up to 10000 tonnes) implies that the platform piles are in a compressed condition even when the structure is subjected to severe weather impacts tending to lift the platform. Conditions are different as regards offshore wind structures (smaller than 800 tonnes). Weather, in this case, may generate direct actual uplift loads on the piles, which must then be carefully designed to resist such stress.

The uncertainty that exist in the construction of the deep foundation of the offshore wind turbines makes necessary to study the different methods used in their design. This chapter will present the different methods used nowadays in the design of the foundation of the offshore wind turbines and the bias that exist about these methods. Moreover, the different parameters that have an influence on the design of the pile under axial loading are also presented.

The literature review will be followed by a presentation of the experimental campaign that was realized in this thesis in order to address the problem of uncertainty related to the design of offshore piles using centrifuge testing. The results of this experimental campaign are finally presented and analysed.

2.2 Literature review

2.2.1 Methods of installation of piles

Different methods of the installation of the piles exist. These methods can have an important influence on the axial capacity of the pile. According to the used method the soil around the pile at the end of the installation can be denser or looser than it initial state. This can impact directly the axial capacity that the pile can develop during its life time. The most used methods are presented as:

- Bored piles
- Driven piles
- Jacked piles

2.2.1.1 Bored piles

Bored piles known also as replacement piles were widely used in the past years due to the fact they are practical in big structure where large number of piles are needed. They are a commonly-used form of building foundation that provides support for structures, transferring their load to deeper layers of soil or rock that have sufficient bearing capacity and suitable settlement characteristics. They are popular in urban areas as there is minimal vibration. They are essentially preferred when the concrete piles are used. The principle of the construction of this type of piles is based on drilling a hole in which the steel reinforcement will be placed and the concrete will be poured in the case of concrete pile (Figure 2-1) or the pile tube will be placed in the case of steel piles.

During the construction of this type of piles they create a lot of perturbations in the soil which impact lately the axial capacity of the bored pile. Although the practical use of this type of piles, this installation method is considered to create piles that have the smallest axial capacity between all the cited installation methods.

2.2.1.2 Driven piles

Driving piles is considered as a displacement method because of the fact that the pile displaces the soil during its installation. The driving of these piles is realized with the use of large driving machines. As consequence, driving piles into the soil cause a high level of noise and ground vibration as well as ground movement. This is why it is not preferable for urban

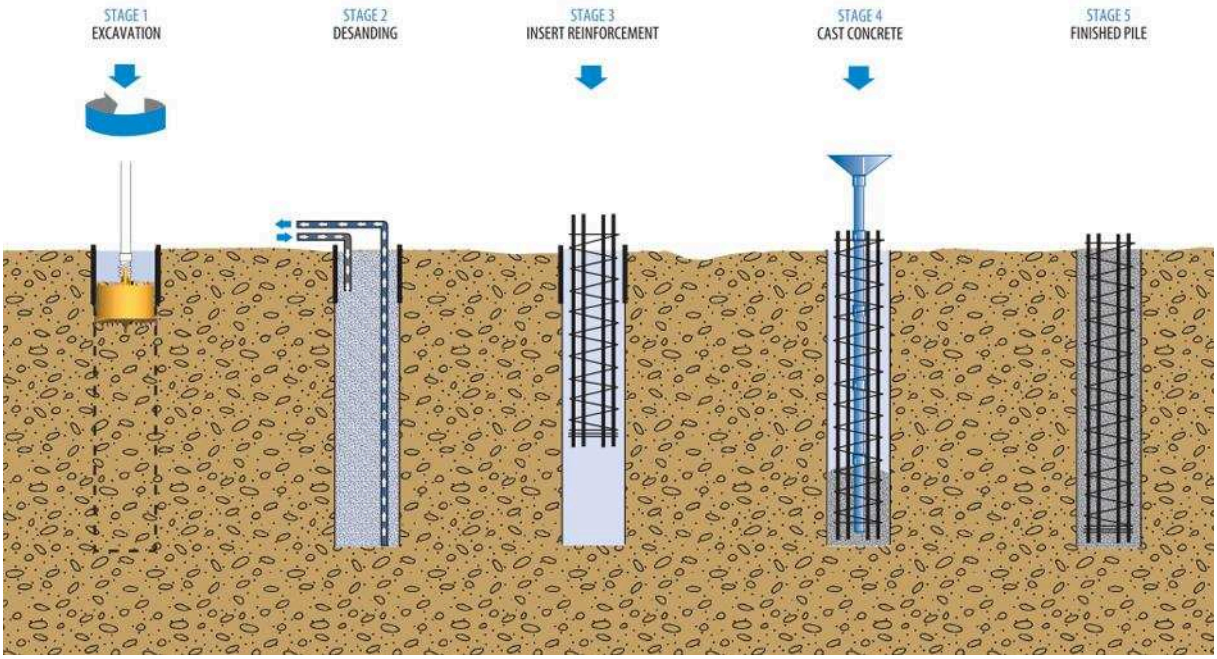

Figure 2-1: Bored piles construction

use. But this method is the main method used in the installation of the offshore piles which are the main objective of the studies in this thesis.

In the literature, the use and capacity of driven piles are extensively studied (Randolph et al. 1994; Jardine et al. 2005; Puech and Benzaria 2013). These studies have helped to reduce the uncertainty related to the axial capacity of driven piles. They have initiated the development of approaches and standards nowadays widely used in pile design (e.g., API, DNVGL, Eurocode 7, ICP (Jardine et al. 2005)).

2.2.1.3 Jacked piles

This method is developed as an alternative to the driving method in the urban area when piles with high level of axial capacity are needed. It is also considered as a displacement method and consists of jacking the piles in the soil with the use of a large hydraulic jack.

The use of jacked piles has received increasing attention in the past few years. The possibility of jacking piles without noise and vibration is indeed more suitable for urban use and more acceptable by current European recommended limits for noise and vibration (Eurocode 3, White et al. 2002). However, compared to driven piles, jacked pile behaviour remains largely unknown and little research has been devoted to the comparison of their respective capacities (Yu et al. 2012; Yang et al. 2006a).

2.2.2 Axial capacity of piles: tip and friction

The axial capacity of piles can be decomposed, in compression (R_c), to the shaft friction capacity (R_s) and the tip capacity (R_b). On the other hand, in tension (R_t) the capacity of the pile is generated only by the shaft friction (Figure 2-2).

$$R_c = R_s + R_b \text{ and } R_t = R_s \quad (1)$$

The shaft friction is generated from the contact between the pile and the lateral soil and depends on the level of contact of the pile with the surrounding soil. The pile installation method is the most important factor that can influence the shaft friction of the pile. The tip capacity is generated by the capacity of the soil compressed under the tip of the pile. It can be influenced by the installation method of the pile, it geometry and the shape of the tip.

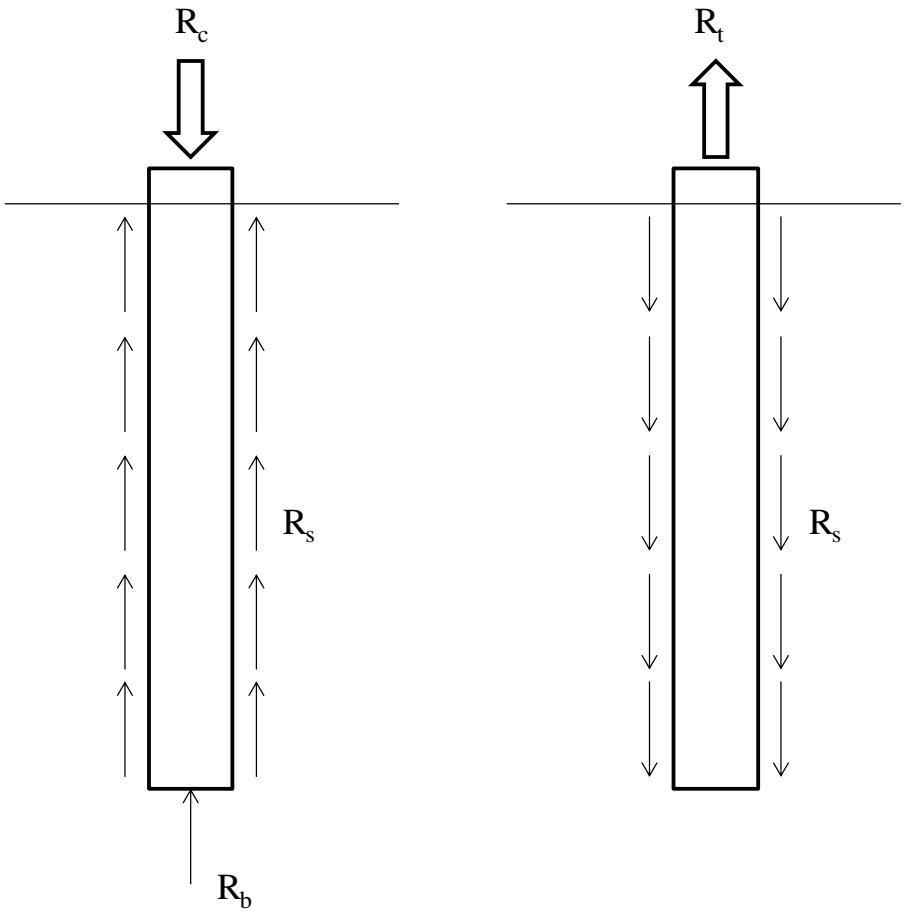

Figure 2-2: Axial capacity of pile decomposition

2.2.3 Design methods

Different design methods were developed in order to better design the pile foundations. In general the methods used in designing the piles are empirical or semi-empirical methods and they derived from laboratory or in-situ tests. These methods predict separately the shaft resistance and the tip capacity of the pile. In this section the design methods used in the design of piles in sand are presented.

The shaft resistance R_s and the tip capacity R_b are generally given by:

$$R_s = fA_s \text{ and } R_b = A_b q_b \tag{2}$$

Where:

f is the unit skin friction capacity

A_s is the side surface area of pile

q_b is the unit end bearing capacity

A_b is the gross end area of the pile

2.2.3.1 API and DNVGL

The API (American Petroleum Institute) standard developed by the American oil and gas industry is used to design offshore foundations of the oil and gas structures. DNV GL (2016) is based on the standard Design of offshore wind turbine structures (DNV 2004) and represents the current state of the art for design of the pile of the offshore wind turbines. API and DNVGL give similar formula for the design of offshore pile capacity.

Both standards are based on the hypothesis that the shaft friction and tip capacity increase linearly with the effective vertical stress σ_v'.

The unit skin friction is given for a depth z as:

$$f(z) = \beta \sigma_v'(\mathrm{z}) \tag{3}$$

where:

β is the dimensionless shaft friction factor for sands.

$\sigma_v'(z)$ is the effective overburden pressure at the depth z

In the absence of specific data, β values for open-ended pipe piles that are driven unplugged may be taken from Table 2-1. For full displacement piles (i.e. closed-ended or fully plugged open-ended piles) values of β may be assumed to be 25 % higher than those given in Table 2-1. For long piles, f(z) does not necessarily increase linearly with the overburden stress as implied by Equation 3. In such cases, it may be appropriate to limit f to the values given in Table 2-1.

The unit bearing capacity is computed using:

$$q_b(z) = \sigma'_v(z)\, N_q \tag{4}$$

N_q is a dimensionless bearing capacity factor given in Table 2-1. According to the pile type, the bearing capacity may be assumed to act over the entire cross section of the pile for plugged piles or on the pile annulus only for unplugged piles.

Although that the shaft friction and tip capacity are considered to increase linearly with the effective vertical stress, the standard gives limit values for the unit skin friction and the unit bearing capacity which can be used in the case of long piles. The use of limit values assumes the existence of a critical depth beyond which the shaft and tip capacities remain constant. The existence of a linear relationship between tip resistance and pile depth appears in many works found in the literature (e.g. Jamiolkowski et al. (2003), Kim et al. (2016)). Kim et al. (2016) show that this linear relationship exists up to a critical depth, beyond which the tip resistance is then almost constant. The hypothesis of the existence of the critical depth is well presented in Silva (2014). He cited that several authors have reported the measurement of limiting values, in laboratory model tests and in full-scale field tests (Kerisel 1961, Biarez and Gresillon 1972, Hanna and Tan 1973, Meyerhof 1976). Vesic 1970 realized field tests on instrumented piles and found that the increase of base resistance with increasing depth isn't linear and that the rate of increase, decreases with depth. Poulos and Davis 1980 suggested that the critical depth can be defined in the range of 10-20 times pile diameter after which a constant value should be considered. On the other hand, Silva (2014) explained also that several authors such as Kulhawly (1984), Fellenius and Altaee (1995), Kraft (1991), Randolph et al. (1994) have discussed the reality of a limiting value arguing that this idealization has little support and is difficult to explain in physical terms. Randolph et al. (1994) explained that nowadays it is commonly accepted that for a homogenous sand deposit the end-bearing resistance will continue to increase with depth but at a gradually decreasing rate.

Table 2-1 : Design Parameters for Cohesionless Siliceous Soil (API standard)

Density	Soil description	Shaft Friction factor, β	Limiting skin friction values (kPa)	N_q	Limiting Unit End Bearing Values (MPa)
Very Loose Loose	Sand				
Loose	Sand-Silt	Not applicable	Not applicable	Not applicable	Not applicable
Medium Dense	Silt				
Medium	Sand-Silt	0.29	67	12	3
Medium Dense	Sand Sand-Silt	0.37	81	20	5
Dense Very Dense	Sand Sand-Silt	0.46	96	40	10
Very Dense	Sand	0.56	115	50	12

2.2.3.2 French Standard

In the French standard, the determination of the tip and shaft resistance of the pile is based on the CPT tests or on pressuremeter test, but the main principles are similar. Many empirical values are also given in tables presented in the standard and used during the determination of the resistances.

The tip resistance formula in the NF 94 262 is directly related to the CPT profile and given as:

$$q_b = k_c \, q_{ce} \tag{5}$$

k_c is a "bearing factor" dependent on the type of the soil and the installation method of the pile and given in the table G.4.2.1 page 141 of the French standard.

q_{ce} is calculated using the following formula :

$$q_{ce} = \frac{1}{b+3a} \int_{D-b}^{D+3a} q_{cc}(z) \, . \, dz \tag{6}$$

with :

a= max{B/2,0.5m} where B is the width of the foundation

$q_{cc}(z)$ is the corrected CPT profile

h the height embedment of the foundation

b= min(a,h)

The lateral friction is given as:

$$R_s = P_s . \int_0^D q_s(z) . dz \tag{7}$$

P_s is the perimeter of the foundation

$q_s(z)$ is the unitary lateral friction at z given by this formula :

$$q_s(z) = \alpha_{pieu-sol} f_{sol}[q_c(z)] \tag{8}$$

$q_c(z)$ is the CPT resistance smoothed at the depth z.

$\alpha_{pieu-sol}$ is an dimensionless parameter which depend on the type of the pile and the type of the soil and given in the table G.5.2.2 of the French standard.

f_{sol} is a function dependent on the type of the soil and the values of q_c.

The f_{sol} functions are defined for the different type of soils by the following equations:

$$f_{sol}(q_c) = (aq_c + b)(1 - e^{-cq_c}) \tag{9}$$

The coefficients a,b and c are given in table G.5.2.2 of NF 94-262.

2.2.3.3 ICP-05 method

ICP (Imperial College Pile) is an empirical method based on tests realized using an instrumented pile on principally 6 sites between France and the UK. The pile is a 102 mm cylindrical steel pile with a conical tip. The sensor placed at it tip make possible the separation of the shaft and tip resistance.

Shaft friction of cylindrical piles

The shaft capacity is given as:

$$R_S = \pi B \int \tau_f \, dz \tag{10}$$

The local shear stress is :

$$\tau_f = \sigma'_v \tan \delta \tag{11}$$

δ is the interface angle of friction at failure and σ'_v is decomposed into two parts the local radial effective stress σ'_{rc} and the dilatant inc²rease in local radial effective stress during pile loading $\Delta\sigma'_{rd}$:

$$\sigma'_v = \sigma'_{rc} + \Delta\sigma'_{rd} \tag{12}$$

The local radial effective stress σ'_{rc} is given as :

$$\sigma'_{rc} = 0.029 q_c (\sigma'_v / P_a)^{0.13} (h/R)^{-0.38} \tag{13}$$

σ'_v is the free-field vertical effective stress

P_a = 100 kPa is the absolute atmospheric pressure

h : relative depth to tip.

R : pile radius (R =(R^2_{outer} - R^2_{inner})$^{0.5}$ for the case of open-ended piles)

h/R is limited to a minimum value of 8

The dilatant increase in local radial effective stress during pile loading is given as:

$$\Delta\sigma'_{rd} = 2G\Delta r/R \tag{14}$$

G : sand shear stiffness

$\Delta r = 2R_{cla} = 0.02\ mm$

R_{cla} : Pile roughness

<u>In the tension case :</u>

This equation $\sigma'_{rf} = 0.8\sigma'_{rc} + \Delta\sigma'_{rd}$ is used in place of the equation (12) for close-ended pile.

For open-ended pile in tension $\sigma'_{rf} = 0.9(0.8\sigma'_{rc} + \Delta\sigma'_{rd})$ will be used in place of (12).

<u>Base capacity of closed-ended cylindrical piles</u>

The determination of the base resistance is derived in this approach from CPT. A good selection of the q_c is mandatory as it can have an important effect on the tip capacity

calculation. ICP approach follows the suggestion of Bustamante & Gianeselli 1982 to average q_c over 1.5 pile diameters above and below the pile toe, providing that (i) the variation in q_c are not extreme and (ii) the depth intervals between the peak and trough q_c values are no greater than B/2. ICP mentioned that a q_c value below the mean should be adopted for design, if these conditions are not met as the base capacity may be controlled by a localized failure within any significant weaker layer.

The base capacity for closed-ended pile is given as:

$$R_b = q_b \pi B^2/4 \quad (15)$$

Where

$$q_b = q_c[1-0.5\log(B/B_{CPT})] \quad (16)$$

q_c average CPT end resistance at the founding depth.

B and B_{CPT} are the relative pile and CPT diameters.

A lower limit of $q_b = 0.3\ q_c$ is suggested for piles with B>0.9 m.

Base capacity of open-ended cylindrical piles

ICP differed several formulas for the determination of the base capacity of open-ended piles according to the state of the plugging that pile exhibits at the end of the installation.

A rigid basal plug is considered to develop during static loading if the following criteria are satisfied:

$B_{inner} < 0.02\ (D_r - 30)$ B_{inner} is in meters and D_r in % (17)

$B_{inner}/B_{CPT} < 0.083\ q_c/P_a$ Absolute atmospheric pressure P_a (18)

Fully plugged piles are considered to develop 50% of the end resistance of closed-ended piles of the same diameter after a pile head displacement of B/10:

$$R_b = q_b \pi R^2_{outer} \quad (19)$$

$$q_b = q_c[0.5-0.25\log(B/B_{CPT})] \quad (20)$$

Two lower limits must be applied according to ICP : (i) the fully plugged capacity should be no less than the unplugged capacity and (ii) q_b should not fall below $0.15q_c$.

Unplugged piles can sustain end bearing capacity on the annular pile base are only with $q_{ba} = q_c$

$$R_b = q_{ba}\pi(R^2_{outer} - R^2_{inner}) \quad (21)$$

2.2.4 Parameters that can affect the behaviour of piles

2.2.4.1 Installation methods

The installation method is a main parameter which affects the axial capacity of pile, because of the effect on the surrounding soil. The quality of the soil-pile contacts depends on the installation method, and so the lateral stresses applied on pile may vary from one method to another. Consequently, a significant difference in pile shaft friction may be induced (Puech 2013, Yang et al. 2006a).

The constructions of **drilled shaft or cast in place** piles are popular in urban area because of their advantages of having a minimal impact on existing foundations and producing relatively little noise (Fisher et al. 1995). However a disadvantage of drilled shafts is that their quality and performance can be affected by (and sensitive to) construction procedures (Petek et al. 2002). Also the high loosening of the surrounding soil induced during the installation of these types of piles put this type of piles in a disadvantage concerning the axial capacity in comparison with the other types of installation methods.

Driven piles are generally installed using drop hammers where a hammer with approximately the weight of the pile is raised to a suitable height and released to strike the pile head. The behaviour of driven piles can be differed if the pile is driven in cohesionless or cohesive soil. In cohesionless soil during the driving of high-displacement piles, adjacent soils will experience high compressive stresses, causing a build-up of large lateral effective stresses. This effect is most pronounced when driving high displacement piles into soil with high density. Such soils experience shearing as the pile is driven in, and they tend to dilate generating very high lateral contact stresses between the pile and the soil. On the other hand, in cohesive soil, driving high displacement piles strongly compresses adjoining soils and leads to a build-up of excess pore water pressure. This temporary build-up of excess pore water pressure coupled with the sensitivity of the clay causes the soil to lose a good fraction of its shear strength in the short term. This excess of pore water pressure dissipates over a time scale of a few weeks to a few months. As this occurs, the adjoining soil consolidates and

increases its strength (Swan). Lehane & White (2005), using centrifuge tests on pile installed by different methods in sand, remarked that the cyclic installation methods create either greater dilation during loading of the pile or stiffer confinement as a result of densification of the surrounding soil.

Jacked piles are installed using hydraulic jack. Their advantages over driven piles came from generating a lower level of noise and vibration during their installation (Yang et al. 2006b, Deeks et al. 2005). They are also considered to develop high capacity as a result of the preloading of the soil below the base (Zarrabi & Eslami 2016).

In the literature, different works were interested on the effect of the installation method on the axial capacity of piles. Puech & Benzaria (2013) realised in-situ tests using three different installation methods (driven, bored and screwed piles). The driven pile developed the highest compression capacity between the tested piles and the authors concluded that the higher the amount of soil displacement at installation, the higher the ultimate pile capacity. Other observation concerning the displacement at failure is also presented as the pile head displacement at failure is found to be lower for the displacement piles than for the non-displacement piles. In the literature, it is generally remarked that the jacked piles had higher capacity values than those of driven pile (Zarrabi et Eslami 2016, Yang et al. 2006a) and that the response of the drilled shaft and precast-in-place pile to loading were much weaker than the jacked and driven piles (Zarrabi et Eslami 2016). Deeks et al. 2005 found also that the stiffness of jacked piles is considerably higher than conventional driven or bored piles. Yang et al. 2006a have stated that jacked piles derive their resistance predominantly from shaft friction whereas the overall load carrying capacity of the driven piles is more evenly distributed between shaft and base. They also stated that the shaft resistance of the jacked piles is generally stiffer and stronger than that of the driven piles.

2.2.4.2 Pile tip

Pile tip is an important factor that can influence the axial capacity of piles. As presented before, standards suggested different formula for pile tip and shaft capacity depending on the type of pile tip. De Nicola and Randolph (1999) have used centrifuge testing for the evaluation of the API standard. They demonstrate the presence of bias in the type of pile as regards the calculation of the standard end bearing capacity. Testing shows that the experimental value of the Nq factor used for the calculation of the API end bearing capacity is 1.7 times higher than the recommended API values for open-ended pile tests. The tests carried

out on close-ended piles also show that the experimental values of Nq are on average 2.4 times higher than the recommended values. Similar results are found in Hossain and Briaud (1993).

Another key factor for offshore pile design is the plug formation, because the piles used for jacket structures are driven open-ended piles. During the installation of open-ended piles, if the pile is driven in an unplugged mode into the soil, the soil gets into the piles at a rate equal to the pile penetration rate. On the other hand, if the pile is driven in a plugged mode into the soil, a soil plug finally attaches itself to the inner surface of the pile, preventing additional soil from entering the pile. Measurement data show that plug length ranges between 10-20 % of the embedded length of the pile (Henke and Grabe 2008). Plugging is a real technical and economical problem. In very dense sand pile plugging can go as far as the available pile hammer becomes unable to drive the pile to design depth. The pile must then be pulled out and alternative solutions must be considered. Lehane and Randolph (2002) postulate that pipe piles driven into the soil in fully coring mode have some base capacities only slightly higher than those of non-displacement piles. Piles driven in fully plugged mode present base capacities that are similar to those of close-ended piles. Paikowsky and Whiteman (1990) also conclude that plugged piles behave almost identically to closed-ended ones and that under working loads both will have the same response. Plugging is a key factor, not only because it directly contributes to tip bearing capacity, but also because it indirectly contributes to the developed shaft capacity. More soil is displaced with a plugged pile than with a pile driven in a coring mode, which increases the effective stresses surrounding the pile (Iskander 2010). More generally, the degree of soil plugging can be represented using the Incremental Filling Ratio IFR (Paik et al. 2003, Lehane and Gavin 2001, Ko and Jeong 2015) defined as:

$$IFR = (\Delta L)/(\Delta D) \times 100 \tag{22}$$

where ΔL is the increment of the soil length inside the pile and ΔD is the increment of the pile penetration depth.

2.2.4.3 Sand density and saturation

The effect of density and saturation is taken into account normally in the standards by the use of effective stresses. The increasing number of the use of offshore piles makes necessary to validate this method of evaluation of the effect of density and saturation. De Nicola and Randolph (1999) demonstrate that the recommended end-bearing limits are very conservative in the case of dense sand. Gavin et al. (2011) report the study of Lings (1985) conducted to

assess the predictive reliability of the API method. Lings demonstrates the presence of a significant relative density bias, in which the API method prediction overestimates pile capacity in loose sand and significantly underestimates pile capacity in dense sand.

The effect of sand saturation wasn't a priority in the literature as it was considered that the water can dissipate easily in sand and no accumulation of the pore pressure can be created. As a result the use of effective stresses was considered to be satisfactory and no further studies have focused on the effect of saturation.

2.2.4.4 Pile material and roughness

Nowadays, the use of piles has increased significantly in all the domains of geotechnical and construction engineering. Piles are installed using different techniques (bored, jacked, driven) and different construction materials (steel, concrete, wood. The use of different construction materials affects skin friction between piles and soil (Potyondy 1961). The soil nature, the technical installations and the pile materials are classically taken into account in standards to determine the pile ultimate resistance (e.g., NF 94-262). A survey of the literature reveals that many studies have been conducted to examine the different parameters affecting skin friction between soil and pile materials (Aksoy et al. 2016, Potyondy 1961, Tiwari and Al-Adhadh 2014). Potyondy (1961) has been among the first to address this problem. Through direct shear testing, Potyondy studies concrete, steel and wood interfaces with different types of soil (sand, sandy silt, cohesive soil, silt and clay). The change in skin friction in relation to soil grain size distribution, moisture content, normal load, construction materials and surface finishing are observed. The increased use of jacked and driven steel piles gives more importance to well qualify the behaviour of the interface between steel and sand. With this aim in view, Uesugi and Kishida (1986b) propose some direct shear tests carried out between sand and steel plates of different roughness. They conclude that steel surface roughness, d_{50} of sand and sand type have a significant influence on coefficient of friction at yield between sand and steel. On the other hand, uniformity coefficient and normal stress have little influence on the friction coefficient at yield. The sand/steel interface is also discussed in Tejchman and Wu (1995) where the friction coefficient values obtained from the friction tests and the silo model experiments carried out between sand and steel of different roughness are summarized in a table. This study highlights the significant effects that both roughness and sand density have on the interface behaviour. Steel roughness is then classified as smooth, rough and very rough with, for each case, two different sand densities (loose and dense).

All these studies presented above have been conducted using shear testing devices. However, other studies present some experiments performed directly on piles in order to study uplift capacities resulting from the shaft resistance (Alawneh et al. 1999, Rao and Venkatesh 1985, Jardine et al. 1993). Rao and Venkatesh (1985) show that the uplift capacity increases with D/B ratio (D is the pile embedment depth and B is the pile diameter), pile roughness, soil density and particle size. Similar results are obtained by Alawneh et al. (1999) who suggest that pile installation method, initial sand conditions, pile roughness and pile end type are all significant variables affecting the ultimate uplift shaft resistance of a single pile in dry sand.

Among the discussed parameters affecting skin friction of steel piles, pile roughness is the key parameter. In the study conducted by Alawneh et al. (1999), the rough model piles tested increase by 12 to 54% in capacity compared with smooth model piles. Pile roughness not only affects the uplift capacity but also the ratio of the unit skin friction during pull-out to the push-in tests. Rao and Venkatesh (1985) also underline that the unit skin friction during pull-out tests is lower than during push-in tests by as much as 80% for rough piles. On the other hand, for smooth piles, the decrease ranges between 10 and 50%. This behavioural difference between smooth and rough piles suggests the existence of two different mechanisms, by which the increase in surfaces roughness causes the increase in peak strength (Lings and Dietz 2005). The first mechanism is related to smooth surfaces, where the movement of the particles is characterised by sliding at contact with the surface (Uesugi et al. 1988). The second mechanism is related to intermediate and rough surfaces, where the movement of the particles is increasingly characterized by rolling, resulting in dilation. Increase in roughness, and density increases dilation and, consequently, strength (Lings and Dietz 2005). Similarly, Uesugi and Kishida (1986a) suggest the use of the term “critical roughness”. They observe that, when the surface is smoother than the critical roughness, sliding motion occurs between steel and sand along the contact surface. They also report that Yajima et al. (1984) demonstrate that, when the surface roughness exceeds the critical value, shear failure occurs within the sand mass instead of sliding along the contact surface.

More generally, pile roughness is described using the term of “normalized roughness” introduced by Uesugi and Kishida (1986b). This normalized roughness is given by:

$$R_n = \frac{R_{max}}{d_{50}} \tag{23}$$

where d_{50} is the average diameter of the sand grains and $R_{\max}$ is the depth of the asperities on a profile length of d_{50}.

Lings and Dietz (2005) suggest that Kishida and Uesugi (1987) have chosen a profile length of d_{50} instead of a profile length of 2.5mm, as used originally by Yoshimi and Kishida (1981), to avoid elevated roughness measurements caused by the presence of wavy surfaces.

2.2.5 Conclusion

Different parameters can affect the axial capacity of piles (pile installation method, sand density and saturation, pile roughness and pile tip geometry (closed, open-ended). The existence of such number of parameters make necessary to investigate in details their effects on the capacity of piles. Centrifuge modelling is an interesting method in geotechnical engineering which permits the realisation of large number of tests in controlled conditions and in high level of accuracy. This experimental method is used in the present study in order to investigate the influence of the cited parameters on the capacity of piles. The objective of this study is also to test the standards used in the design of piles and to verify their capability to take into consideration the effect of the different parameters. The design methods appear to be very conservative in most of cases. For instance, the API already showed different bias concerning the effect of the density and saturation and pile tip on the axial capacity. Moreover, in other studies, database results are used to compare CPT-based methods with experimental ones (Schneider et al. 2008, Gavin et al. 2011). Gavin et al. (2011) reveal that the vertical tension loads applied on the foundations of wind turbines are much higher than those considered in the calibration of offshore design methods. Some conflicting results are also obtained here when these methods are tested to estimate the pile length required to support typical wind turbine loads. All these bias make necessary to realize a complete study that can compare the performance of these different standards toward experimental results.

2.3 Experimental campaign

2.3.1 Centrifuge modelling

Centrifuge modelling is a widespread experimental method in the field of geotechnical engineering. A small scale model is placed in a high gravity field to allow for the replication of the stress state in the full scale prototype. It was used in geotechnical studies from the 30's but became very popular in the 80's (Garnier 2001, Garnier 2002, Thorel et Garnier 2002). The use of the 5.5-m diameter swing arm centrifuge of IFSTTAR- Nantes is an important resource to study deep foundations as the use of thus large diameter centrifuge is essential to obtain a negligible gradient of g between the top and the bottom of the model pile.

The tests described in this thesis are carried out at an acceleration level of N = 100 times the earth gravity (100×g) on 1:100 scale model piles. In order to model the same stress state that exists in prototype scale some similitude factor must be respected (Table 2-2).

Table 2-2: Scale factors

Physical parameter	Scale factor
Acceleration	N
Length, displacement	1/N
Force	$1/N^2$
Stress	1
Density	1

Although the numerous advantages that centrifuge model offers such as versatility, it is always known that the use of this method to simulate in-flight geotechnical problems requires several abilities (mechanics, hydraulics, geotechnics, central-command, data acquisition …). An extensive work that was needed to develop the experimental campaign presented below in order to realize the different tests of the present study.

2.3.2 Model soil

The model soil is a poorly graded NE34 Fontainebleau sand (Table 2-3). Eight rectangular strongboxes (Table 2-5) are prepared with two different relative soil densities (58% ± 0.5 % and 99% ± 0.5 %, respectively) achieved by filling the strongboxes with sand using the air pluviation technique. The unit dry weight of these strongboxes is 1.59 g/cm^3 and 1.70 g/cm^3 for the medium dense sand and the dense sand respectively. More details on the model soil are

presented in the appendixes. Appendix 4 discusses the sand mass characterisation and preparation. Appendix 5 presents the procedure of determination of ρ_{dmin} and ρ_{dmax} and finally Appendix 6 presents the laser particle size distribution realized on the used sand.

As the present study is interested in the behaviour of offshore piles, the realization of tests in saturated sand is important. In order to saturate the sand, the strongbox is connected to a water tank by the underside up to full saturation which gives effective unit weight of 0.99 g/cm^3 and 1.04 g/cm^3 for the medium dense saturated sand and the dense saturated sand respectively.

Table 2-3 : Characteristics of the Fontainebleau NE34 sand

Sand	$U_C=d_{60}/d_{10}$	d_{50} (µm)	$\rho_{d\min}$ (g/cm^3)	$\rho_{d\max}$ (g/cm^3)	e_{min}	e_{max}
Fontainebleau NE34	1.53	210	1.46	1.71	0.549	0.753

U_c is the coefficient of uniformity (Silva 2014).

d_x is the grain size, at which x% of particles by weight are smaller (Silva 2014).

$\rho_{d\min}$, $\rho_{d\max}$ are minimum and maximum dry unit weigh tested in the lab according to the standard, respectively (NF P 94-059).

2.3.3 Model piles

As all the tests are realized at 100×g, the model piles presented here represent a prototype pile 100 times bigger.

Two types of model piles are used in this study: 1) a rigid aluminium rough pile (Figure 2-3 and Figure 2-5.b) instrumented with a 21-mm thick, 25-kN load sensor (XF3059 from Measurement) placed 25 mm from the pile tip; 2) a hollow smooth steel pile without instrumentation (Figure 2-4). The hollow pile can be an open or close-ended pile and 4 diameters are tested for this type of piles (12, 14, 16 and 18 mm) and have 1 mm as thickness. The both type have an embedded length of 250 mm. The different types of model piles are summarized in Table 2-4.

The installation of pile is realized by the use of a hydraulic jack presented in the experimental set-up of the (Figure 2-5.a). A 25-kN load sensor (FN3070 from FGP) is placed between the pile head and the hydraulic jack (Figure 2-5.a) to measure the pile total bearing capacity. The pile displacement is controlled using a magnetostrictive displacement sensor (1/3000350S010–1E01 from TWK).

Figure 2-3 : Detail of the rough instrumented model pile (pile 1 diameter=18mm)

Figure 2-4 : Smooth model pile

Table 2-4 : Model piles (model scale)

Piles	Roughness	External Diameter (mm)	Tip type
Pile 1 (instrumented)	Rough	18	Closed
Pile 2	Smooth	18	Closed
Pile 3	Smooth	18	Open
Pile 4	Smooth	16	Closed
Pile 5	Smooth	16	Open
Pile 6	Smooth	14	Closed
Pile 7	Smooth	14	Open
Pile 8	Smooth	12	Closed
Pile 9	Smooth	12	Open

2.3.4 Pile roughness measurement

The normalized roughness, $R_{n,}$ (§ 2.2.4.4) is used to define pile roughness. Garnier and König (1998) expected that a surface is considered as rough if $0.1< R_n < 1$. To obtain this roughness,

the pile surface is carefully machined. R_z (NF EN ISO 4287, 1998) for both piles is measured in laboratory conditions. R_z is equal to 69.8 µm for the rough pile and 2.88 µm for the smooth one and it is normalized using d_{50} = 0.21 mm of the Fontainebleau sand (Silva 2014). R_n is equal to 0.33 and 0.014 for the rough and smooth piles, respectively. Parts of these profiles are presented in Figure 2-6 for both piles.

2.3.5 Grains size effects

In centrifuge the model pile dimensions is much smaller than the prototype pile on the other hand the grain size is always the same. To avoid any effect that the small size of the model pile in comparison of the size of the sand grain (grains size effects) can create on any physical parameter measured, Garnier et al. (2007) have listed some factors between the pile diameter B and the sand mean grain size d_{50} that must be respected in centrifuge modelling.

For the bearing capacity $B/d_{50} > 35$ which is always respected in this study even for the smallest pile (12/0.21 = 57.1).

For the skin friction $B/d_{50} > 50$ or 100 which is always respected in this study even for the smallest pile (12/0.2 = 57.1) considering the case of factor equal to 50.

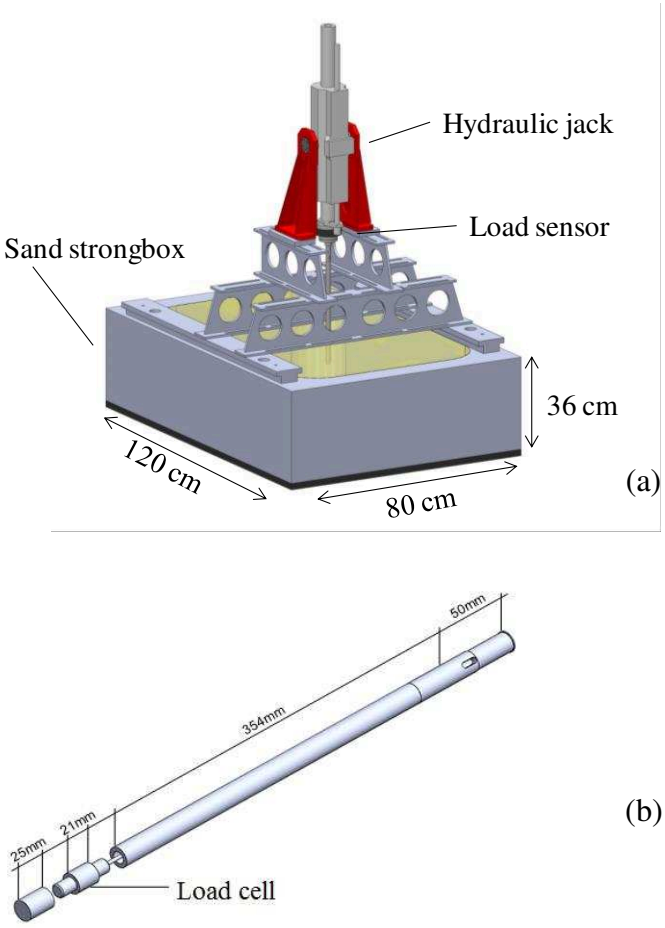

Figure 2-5 : (a) Experimental set up (inside dimensions), (b) Rough instrumented model pile

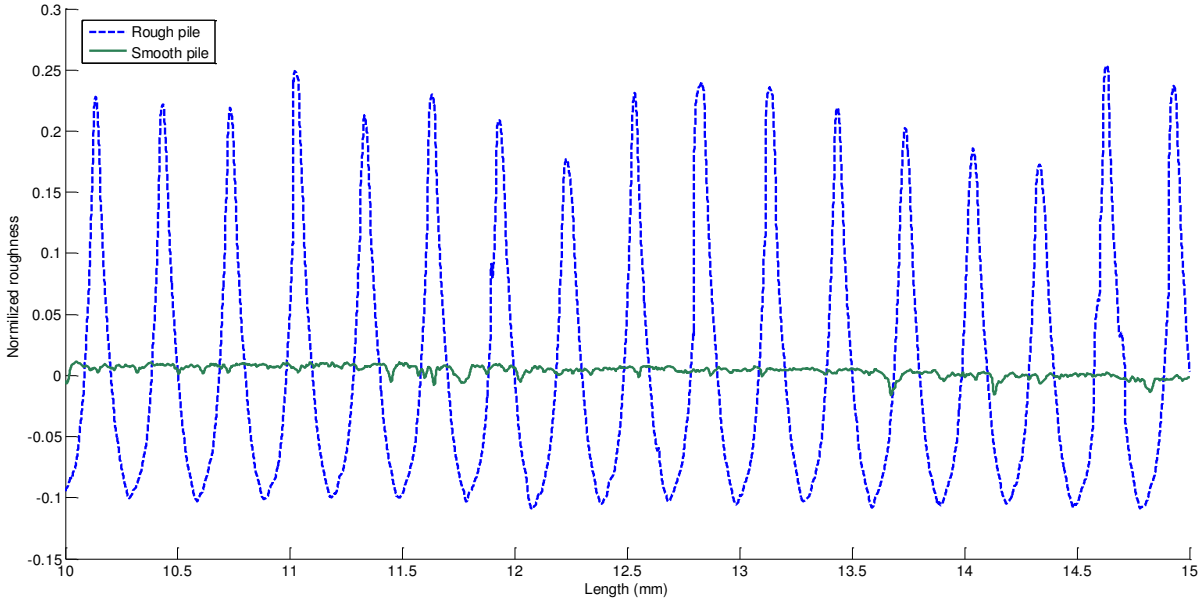

Figure 2-6 : Roughness profiles

2.3.6 Experimental campaign and tests table

The parametric study performed in the centrifuge on vertically loaded piles focused on the following parameters: Pile roughness, Pile diameter, tip shape (open or closed), installation process, sand density and saturated or dry sand.

The piles are loaded in tension but four of them were subjected to compression, before pull out test.

Before performing the loading test, a procedure of stabilisation is realized for each sand strongbox in order to make sure of the good homogeneity of the sand massif.

After the installation of the experimental set-up and before any tests is realized the strongbox is submitted to a cycles of ascend and descend of the centrifuge acceleration. In the present thesis and as all the tests will be realized at 100×g, the ascend of the acceleration will reach 100×g. In total 3 cycles of ascend and descend is realized for each strongbox before any test is realized. The CPT tests realized (B_{CPT} = 12 mm) afterward during the study confirm the good homogeneity of the tested strongbox (Appendix 4).

Table 2-5 lists the tests realized on the axial capacity of piles. In total eight strongboxes are used. In the present table even the tests which couldn't be completed due to a problem in the pile or the experimental set-up are presented. Some tests are only destined to be a primary tests or to be some repetitive tests and will not be fully discussed in the results section. Among the 52 tests planed, 46 have been analysed for the parametric study. The nomination is unique for each test but in the results chapter and before each group of tests a transitory table is presented where a new set of nomination is presented and used for the desired group of tests. The installation process is monotonic and performed at 100×g (M100), except in several mentioned cases.

Table 2-5 : Experimental campaign

Strong box	D_r (%)	Pile	Test name	Rough or smooth pile (R/S)	B (mm)	Open or closed pile (O/C)	Installation process	Comment
C1	58 (dry)	P1	C1P1S18O100G	S	18	O	M100	Compression and aluminium

								pile
		P2	C1P2S18C100G	S	18	C	M100	Compression and alum pile
		P2	C1P3R18C100G	R	18	C	M100	Compression
		P4						Wasted test
		P5	C1P5S18C100G	S	18	C	M100	aluminium pile
		P6	C1P6S18O100G	S	18	O	M100	aluminium pile
C2	99 (dry)	P1	C2P1R18C100G	R	18	C	M100	
		P2						Wasted test
		P3	C2P3R18C25	R	18	C	10 jacking strokes of 25 mm at 100×g	
		P4	C2P4R18C25	R	18	C	10 jacking strokes of 25 mm at 100×g	
		P5						Buckling
		P6	C2P6R18C10	R	18	C	25 jacking strokes of 10 mm at 100×g	
C3	99 (dry)	P1	C3P1R18C1G	R	18	C	M1	Compression
		P2	C3P2R18C1G	R	18	C	M1	
		P3						Buckling
		P4	C3P4R18C1G	R	18	C	M1	
		P5	C3P5R18C10	R	18	C	25 jacking strokes of 10 mm at 100×g	
		P6	C3P6R18C100G	R	18	C	M100	
C4	99 (dry)	P1	C4P1R18C50	R	18	C	50 jacking strokes of 5 mm at 100×g	
		P2	C4P2R18C100	R	18	C	100 jacking strokes of 2.5 mm at 100×g	
C5	99 (dry)	P1						Buckling
		P2						Buckling
		P3	C5P3S18O100G	S	18	O	M100	
		P4	C5P4S18C100G	S	18	C	M100	
		P5	C5P5S14O100G	S	14	O	M100	
		P6	C5P6S14C100G	S	14	C	M100	
		P7	C5P7S16O100G	S	16	O	M100	
		P8	C5P8S16C100G	S	16	C	M100	
		P1	C6P1S18O100G	S	18	O	M100	

C6	58 (dry)	P2	C6P2S18C100G	S	18	C	M100
		P3	C6P3S16O100G	S	16	O	M100
		P4	C6P4S16C100G	S	16	C	M100
		P5	C6P5S14O100G	S	14	O	M100
		P6	C6P6S14C100G	S	14	C	M100
		P7	C6P7S12O100G	S	12	O	M100
		P8	C6P8S12C100G	S	12	C	M100
C7	58 (saturated)	P1	C7P1S18O100G	S	18	O	M100
		P2	C7P2S18C100G	S	18	C	M100
		P3	C7P3S16O100G	S	16	O	M100
		P4	C7P4S16C100G	S	16	C	M100
		P5	C7P5S14O100G	S	14	O	M100
		P6	C7P6S14C100G	S	14	C	M100
		P7	C7P7S12O100G	S	12	O	M100
		P8	C7P8S12C100G	S	12	C	M100
C8	99 (saturated)	P1	C8P1S18O100G	S	18	O	M100
		P2	C8P2S18C100G	S	18	C	M100
		P3	C8P3S16O100G	S	16	O	M100
		P4	C8P4S16C100G	S	16	C	M100
		P5	C8P5S14O100G	S	14	O	M100
		P6	C8P6S14C100G	S	14	C	M100
		P7	C8P7S12O100G	S	12	O	M100
		P8	C8P8S12C100G	S	12	C	M100

As presented in the Table 2-5 four tests buckled during the installation of the corresponding piles in the dense sand. This is due to the very high density of the sand and the important length of the pile.

Each test results is presented at the model scale in appendix 1.

2.4 Results analysis

The different tests realized in the eight strongbox of Fontainebleau NE34 are grouped to focus on the study of a specific parameter that can influence the axial capacity of piles. These tests will be analysed in different sections and before each group of tests a transitory table is presented where a new set of names will be given for the discussed tests in the respective section. Also as mentioned before the experimental campaign realized for the installation of each set of tests will be presented before their respective tests.

The studied parameters are: The ultimate capacity, the effect of the installation method, the effect of sand density and saturation and pile tip type and finally the impact of pile roughness.

The results presented in the present study have already been published (El haffar et al. (2017)) or submitted to publication in journals.

2.4.1 Determination of ultimate capacity

For all the tested piles presented in this section Compression and/or tension tests are carried out after completion of pile installation. The determination of compression and tension capacities from the force–displacement curve is detailed in Blanc and Thorel (2016). The ultimate tension load is indicated by the minimum peak value. To determine the ultimate compression capacity the compression test curve needs to be presented on a log-scale graph. Once the curve is plotted two behaviours can be clearly identified: first a sharp increase in the force followed by a small one and these two behaviours can be represented by straight lines. The intersection of the two straight lines gives the ultimate compression capacity. When no compression test is performed after in-flight jacking, the final jacking force is considered as the ultimate compression capacity of the pile. This approach is in good accordance with the results obtained by Deeks et al. (2005), according to which failure occurs with a load equal to the installation force. The jacking and tension forces do not include pile self-weight. Consequently, the pile capacities presented in this section are capacities not taking account of their self-weight.

2.4.2 Effect of the installation method

The objective of this research, therefore, is to improve our understanding of the axial capacity evolution of jacked piles and propose a comparison with other installation methods. To achieve this, an experimental program is conducted on 100×g centrifuged model piles. The present section shows the findings of the detailed investigation carried out to examine static

axial capacity of close-ended piles in dense sand when applying different installation methods. The key feature of this analysis is the use of in-flight jacking installation techniques. This method is most representative of stress state susceptible to develop around prototype jacked piles.

Table 2-6 shows the new set of names given for the chosen tests to be presented in this section.

Table 2-6 : Transition table for tests nomenclature

Test	New name	Installation process
C3P1F18C1G	MJP1G	Monotonic at 1×g
C2P1F18C100G	MJP100G	Monotonic at 100×g
C2P4F18C25	CJP25	10 jacking strokes of 25 mm at 100×g
C2P6F18C10	CJP10	25 jacking strokes of 10 mm at 100×g
C4P1F18C50	CJP5	50 jacking strokes of 5 mm at 100×g
C4P2F18C100	CJP2.5	100 jacking strokes of 2.5 mm at 100×g

2.4.2.1 Pile installation and experimental campaign

Two different installation methods are compared: first, 1×g jacking used to model wished-in-place pile installation; then, in flight jacking used to represent installation effects and soil displacement occurring during jacked pile installation.

With the first method (MJP1G, Monotonic Jacked Pile at 1×g), the piles are jacked at 1×g to the desired embedded depth of 250 mm before application of the centrifuge acceleration and loading test itself (compression or tension).

With the second method, the piles are jacked in flight up to a depth of 250mm. The tests are carried out without stopping the centrifuge. Different types of jacking techniques are used:

- MJP100G (Monotonic Jacked Pile at 100×g): the piles are jacked monotonically at a speed of 0.1mm/s before a pull out test is performed at the same speed.
- CJP25 (Cyclic Jacked Pile): the piles are jacked using a series of jacking strokes, equal to 25 mm each, also at 0.1 mm. Between each stroke, the head force returns to zero. Then, the jacking pattern is repeated every 25mm until reaching the desired 250-mm embedded length. Similarly, a pull out test is performed at the end of the jacking phase (Figure 2-7).

- CJP10, CJP5 and CJP2.5 follow the same procedure as CJP25 with only stroke length differences, which are 10mm for CJP10, 5mm for CJP5 and 2.5mm for CJP2.5, respectively.

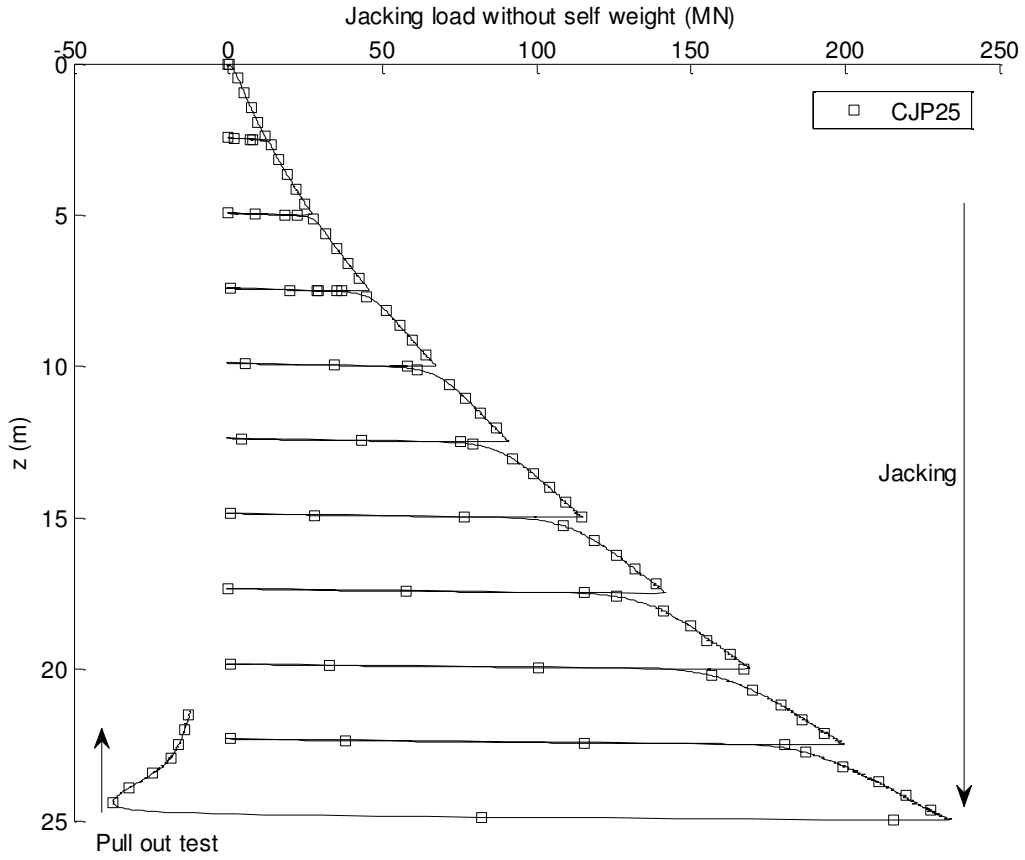

Figure 2-7 : Jacked pile using strokes of 2.5 m

2.4.2.2 Determination of shaft and tip resistance

All the six tests of this study are performed using model piles instrumented with a sensor placed at 2.5m from the pile tip (Pile 1 of Table 2-4). Sensor results, however, cannot be used directly to deduce tip capacity and shaft friction. The sensor measures the sum of the tip capacity and the shaft resistance for the first 4.6m at the bottom of the pile. In order to deduce shaft resistance along the entire piles, an experimental analysis method is developed in several steps:

1. Subtracting the tip sensor load ((b) on Figure 2-8) from head sensor load (curve (a) Figure 2-8) gives the shaft resistance for the first 20.4m of the pile ((c) in Figure 2-8).

2. Shifting up this curve on 4.6m gives the first 20.4m of the total shaft resistance ((d) in Figure 2-8).
3. By extending this curve up to 25m, using a 3rd order polynomial, the total shaft resistance is finally obtained.
4. The tip capacity ((e) in Figure 2-8) is deduced from the difference between total load and shaft resistance.

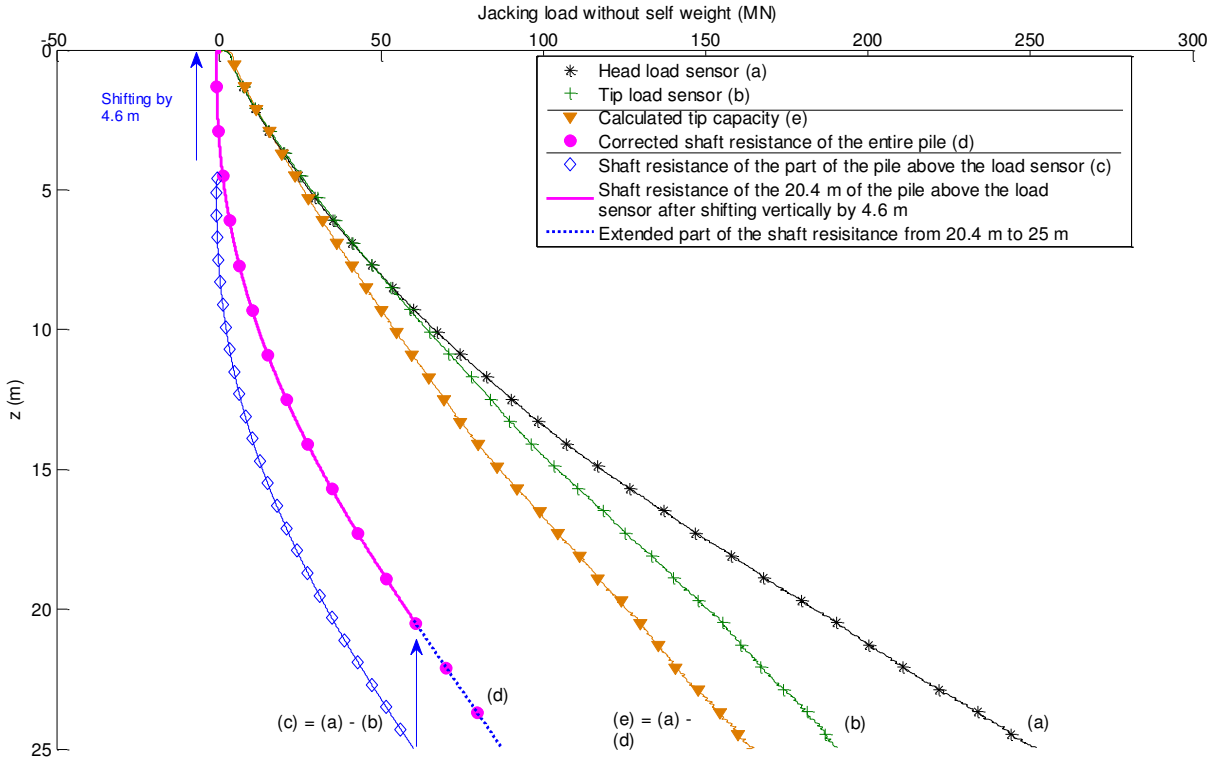

Figure 2-8 : Shaft and tip resistance decomposition

2.4.2.3 Compression test analysis

Compression force experimental results are presented in Table 2-7and Figure 2-9.

Initial comparison (Figure 2-9) clearly shows, as expected, the existence of a significant difference in compression force between piles jacked at 1×g and piles jacked at 100×g. The compression capacity of MJP100G, for instance, is three times higher than MJP1G. This difference has been found also in the work of Ko et al. (1984) where the bearing capacity of the piles installed at 1×g was found to be 40% less than that of the piles installed at 70×g.

A closer examination of the results reveals some differences between the piles jacked at 100×g (Figure 2-9.b, c, d). MJP100G has the highest compression capacity but there is neither clear trend nor clear relationship between compression capacity and stroke number. The

difference between cyclically and monotonically jacked piles may be accounted for by both shaft resistance and tip capacity (Table 2-7). The tip capacity decreases as the number of jacking strokes increases. This could be related to soil densification under the tip because the single direction only displacement of the pile MJP100G may cause a higher degree of densification of the soil under the pile tip compared to the cyclically jacked piles. On the contrary, MJP100G shaft resistance is the lowest among all the piles tested at 100×g (Table 2-7).

In addition, standard tip and shaft capacities used in pile design are presented in Table 2-7. Calculations using the ICP (Jardine et al. 2005) method are made with MJP100G tip capacity as value for the CPT. The friction angle between the rough pile and the sand is 30° here (Pra-ai 2013), which better suits present conditions (grain size, pile roughness…) than the 29° suggested in the ICP method. On the other hand, both API and DNVGL are more conservative than ICP and give results lower than the experimental tests.

Table 2-7 : Static ultimate capacities in compression and tension (prototype values)

Installation or design method	Compression			Tension		Tension/ compression (shaft resistance) (%)
	Total force [MN]	Tip capacity [MN]	Shaft resistance [MN]	Shaft resistance [MN]	initial tension stiffness [MN/m]	
MJP1G	74	-	-	-23	580	-
MJP100G	252	165	87	-30	309	34
CJP25	234	142	92	-37	341	40
CJP10	241	135	106	-46	452	43
CJP5	223	135	88	-47	474	53
CJP2.5	228	137	91	-50	523	55
ICP (30°)	174	136	38	-30	-	79
API and DNVGL	59	42	17	-17	-	100

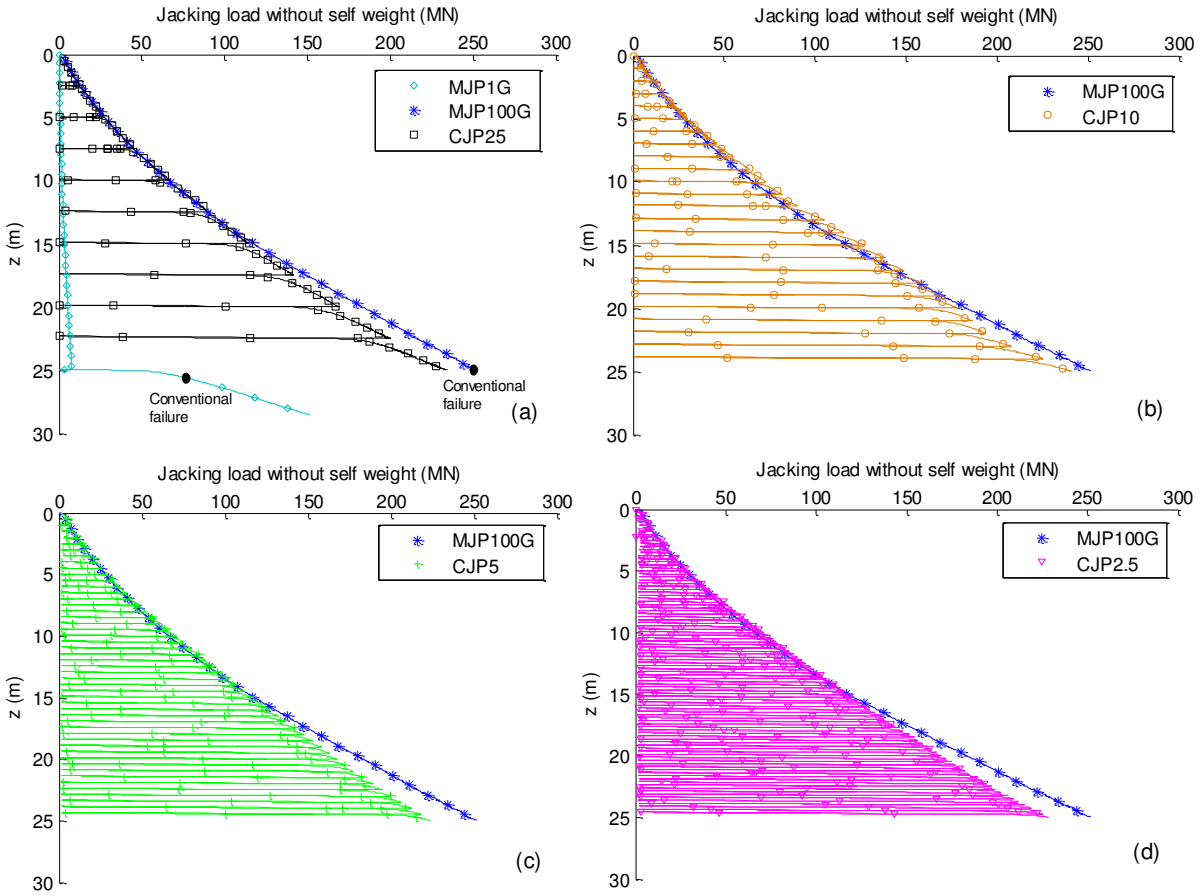

Figure 2-9 : Jacking load without self weight versus penetration depth for MJP100G (reference) and (a) MJP1G and CPJ25 – (b) CJP10 – (c) CJP5 – (d) CJP2.5

2.4.2.4 Pull out tests analysis

With the development of deep foundations in recent engineering projects, the use of piles, not only in compression but also in tension, is increasing. With this in mind, the pull out capacity of the piles installed according to the methods described is studied. Results are displayed in Figure 2-10 where only the tension part of the load-displacement curves is plotted. The tension displacement is normalized by the pile diameter B. In addition, the initial tension stiffnesses of the foundation are calculated for each test. They correspond to the slopes crossing the tensile displacement curve at the half of the maximum tension capacity. Main tests results are summarised in Table 2-7.

It should first be noted that the pull out capacity of MJP100G jacked at 100×g is 25% higher than that of MJP1G jacked at 1×g. This difference is not as high as with the compression capacity of both piles however. The difference between the pile capacity in compression and tension is not due solely to the mobilization of the tip capacity. The shaft resistance in

compression is twice the tensile shaft resistance. The shaft resistance ratio (tension to compression) obtained in this study is lower than the values of 0.7-0.8 found in the literature (Schneider et al. 2008). Despite having lower pull out capacity, it is noticed from Table 2-7 that the MJP1G initial stiffness is higher than the MJP100G one. For MJP1G, the g increase occurs while the pile is already installed. The soil surrounding the pile settles and rearranges which lead to an increase in the contact between soil and pile. This condition is assumed to be close to a wished-in-place pile behaviour. For MJP100G, the pull out test is undertaken directly after the jacking. The shearing mechanism along the shaft has to be reversed which required some displacement to be fully mobilized. The initial tension stiffness is then reduced.

On the other hand, when it comes to the comparison of the pull out capacity of piles jacked at 100×g using different stroke protocols; the graph clearly shows that the tension capacity of the piles increases with the number of strokes (cf. Table 2-7). Such results raise questions about (1) the gain in capacity with the increase of cyclic strokes and (2) the actual pile ultimate tension capacity that must be used for design methods.

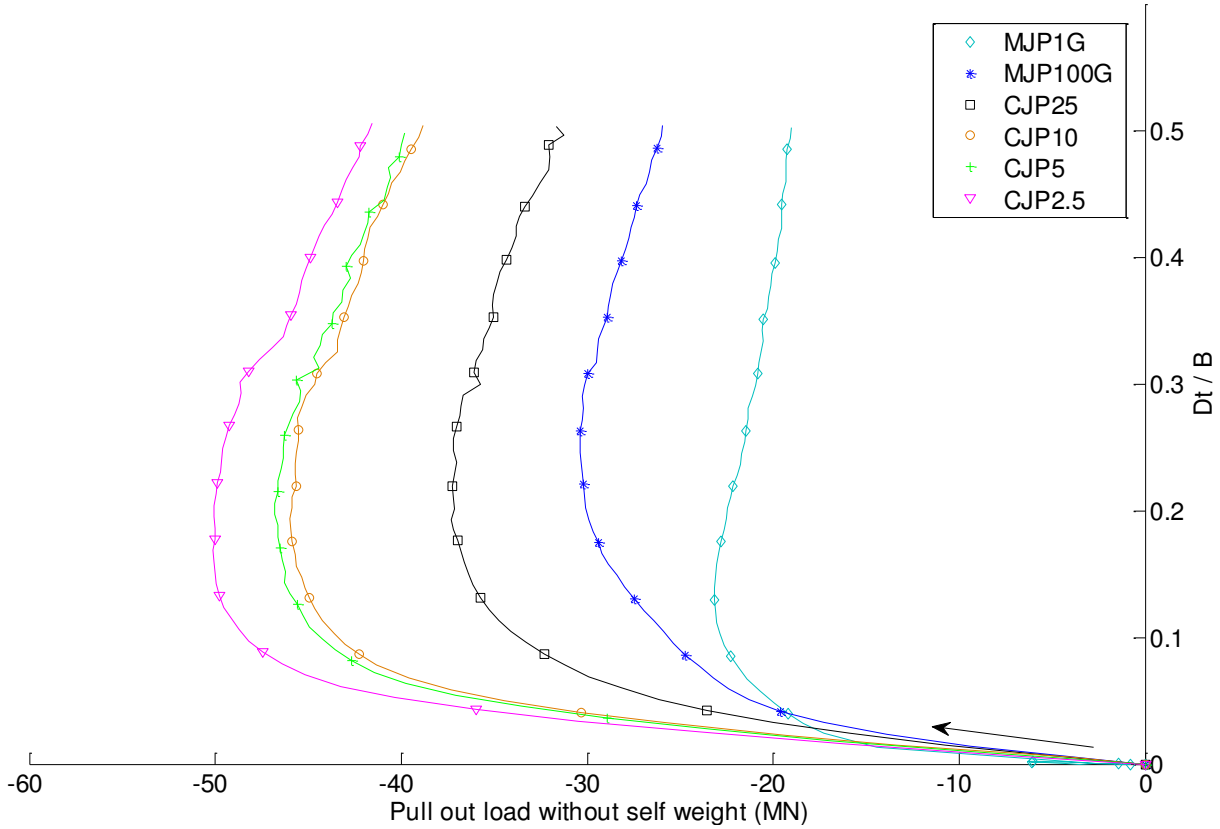

Figure 2-10 : Pull out tests

During the installation of displacement piles, the sand tends to dilate and generate high levels of lateral contact stresses with the piles. The effects of the dilation is also observed in the work of Lings and Dietz (2005).They observed i) in case of intermediate and rough surfaces in contact with the sand, the motion of the particles is increasingly characterized by rolling, resulting in dilation and ii) the increase in roughness and the increase in density bring about increased dilation and a resulting increase in strength. The dilation of the sand can be affected by the installation method used during the jacking of the piles. This phenomenon has been highlighted by Lehane and White (2005) where they have compared a monotonic and cyclic installation methods used during the jacking of a displacement piles. They have concluded that cyclic installation creates either greater dilation during pile loading or stiffer confinement as a result of densification of the surrounding soil. So the gain of capacity with the increase of cyclic strokes can be mainly related to the increase of sand dilation during the cyclic installation in comparison with the monotonic installation. Dilation can generate an increase in the pile radial stress applied, which is directly related to the shaft resistance of the pile and to the gain observed during testing. It is also noticed that this mobilization is more rapid in case of cyclic installation than the case monotonic installation. Table 2-7 show clearly that the initial stiffness in tension of piles installed at 100×g increases with the number of strokes. The results obtained in this study are also in good accordance with Lehane and White (2005) where they have revealed that the pull out capacity of their monotonically-installed piles was only 60% that of their cyclically-installed piles.

Another phenomenon, which is also related to this gain in capacity, is observed during the emptying of the strongbox containing the sand. The sand, indeed, is crushed near the shaft and under the tip of the piles. The grain size of sand in contact with the pile varies from its initial state and may cause an increase in the friction angle between piles and sand. Similar results are found in Yang et al. (2010) in their calibration chamber tests where the installation of displacement pile in pressurized sand (sand under high pressure) produces particle breakage. These results also underline the two phenomena discussed above, i.e., the sand around the displacement pile is over-consolidated at the end of the installation and has a final void ratio substantially below its initial e_{min} value. Their conclusion is that the sand response to further static loading is highly likely to be strongly dilatant.

Similarly to the above compression capacity, a comparison with design standards as regards pull out capacity is made and results plotted in Table 2-7. ICP provides a good estimation of

the capacity of the monotonically jacked pile at 100×g (MJP100G) whereas API and DNVGL results are once again conservative, just as in the case of compression capacity.

2.4.3 Effect of sand density and saturation and pile tip type

The objective of this study is to address the problem of uncertainty related to the design of offshore piles. Some tests are carried out in dense and medium dense sands, saturated and dry, to examine the effect of the density and of sand saturation. Moreover, testing is performed using open- and close-ended piles of different diameters to improve our understanding of the plugging effect on pile behaviour and the effect of pile diameter on pile plugging. In addition, a complete comparison between the experimental results and API, ICP-05, the French standard (NF) and DNVGL recommendations is proposed. This comparison is carried out to evaluate the standard performances against actual experimental results.

Table 2-8 shows the new set of names given for the chosen tests to be presented in this section. It is clear that the new names contain the mention of four strongboxes names C1, C2, C3 and C4 these are new set of names for the desired strongboxes containing these tests and must not be confused with the strongboxes mentioned in Table 2-5. In the present section 2.4.3 any mention of the strongboxes C1, C2, C3 and C4 is referenced to these new names given for the tests in the Table 2-8 and not of the original strongboxes of Table 2-5.

Table 2-8 : Transition table for tests nomenclature

Test	New name	Pile diameter (m)	D_r (%)	Dry/saturated (D/S)
C5P3S18O100G	C1O18	1.8	99	D
C5P4S18C100G	C1C18	1.8		
C5P7S16O100G	C1O16	1.6		
C5P8S16C100G	C1C16	1.6		
C5P5S14O100G	C1O14	1.4		
C5P6S14C100G	C1C14	1.4		
C6P1S18O100G	C2O18	1.8	58	D
C6P2S18C100G	C2C18	1.8		
C6P3S16O100G	C2O16	1.6		
C6P4S16C100G	C2C16	1.6		

C6P5S14O100G	C2O14	1.4		
C6P6S14C100G	C2C14	1.4		
C6P7S12O100G	C2O12	1.2		
C6P8S12C100G	C2C12	1.2		
C8P1S18O100G	C3O18	1.8	99	S
C8P2S18C100G	C3C18	1.8		
C8P3S16O100G	C3O16	1.6		
C8P4S16C100G	C3C16	1.6		
C8P5S14O100G	C3O14	1.4		
C8P6S14C100G	C3C14	1.4		
C7P1S18O100G	C4O18	1.8	58	S
C7P2S18C100G	C4C18	1.8		
C7P3S16O100G	C4O16	1.6		
C7P4S16C100G	C4C16	1.6		
C7P5S14O100G	C4O14	1.4		
C7P6S14C100G	C4C14	1.4		
C7P7S12O100G	C4O12	1.2		
C7P8S12C100G	C4C12	1.2		

2.4.3.1 Pile installation and experimental campaign

Each pile is jacked in flight at 100×g monotonically at a speed of 0.1 mm/s to simulate installation effects and soil displacement that takes place during the installation of displacement piles. The choice of a low jacking speed is important to prevent the build-up of pore-water pressure and ensure that both jacking and testing are conducted in drained conditions even in saturated sand. A pull out test is performed without stopping the centrifuge immediately after the installation of the piles to the desired embedded depth of 250 mm.

2.4.3.2 Bearing capacity tests

The effect of pile plugging, saturation and sand density on the behaviour of sand is examined using the results from the 28 loading tests are presented below.

Figure 2-11 illustrates the jacking tests carried out in dense sand strongboxes (dry and saturated). A first comparison between the open pile C3O18 and the closed-ended pile C3C18 (Figure 2-11.a) shows that, at the beginning of the loading phase and until the depth of 3 m is reached, the behaviour and initial stiffness of both piles is different. As the piles are driven deeper into the soil, their behaviour becomes similar and approximately the same capacity is

obtained at the end of the jacking phase. This observation may be accounted for by plug formation. On the other hand, in dry dense sand, C1O18 and C1C18 curves, in spite of different initial stiffnesses, are also different at the beginning of the jacking phase. Both piles behave differently until the depth of 13 m where the C1O18 curve starts to move upward to converge towards that of C1C18. Plug formation, here, does not start until the depth of 13 m.

A similar behaviour is observed for the 1.6-m diameter piles (Figure 2-11.b). The 1.4-m diameter piles, C1O14 and C1C14, jacked in dry sand (Figure 2-11.c) present the same behaviour than piles C1O18 and C1C18 whereas C3O14 and C3C14 behaviours are identical with no significant difference at early depth.

These results provide important data as regard the behaviour of open and closed piles and how it is affected by sand saturation. The behaviour of piles jacked in dry or saturated sands demonstrates the formation of plugging as the pile depth increases. This phenomenon is clearly influenced by the saturation of dense sand. As mentioned above, C3O18 behaves differently compared with closed pile C3C18 installed in similar conditions at early depth. Beyond a certain depth, it forms a rigid plug and then behaves like C3C18. On the other hand, during C1O18 testing, plug formation is initiated after a 13-m installation depth, beyond which C1O18 behaviour approaches that closed pile C1C18. We can conclude that the saturation of the sand speeds up plug formation against dry sand because plug appears at lower depth in saturated sand in contrast to dry sand.

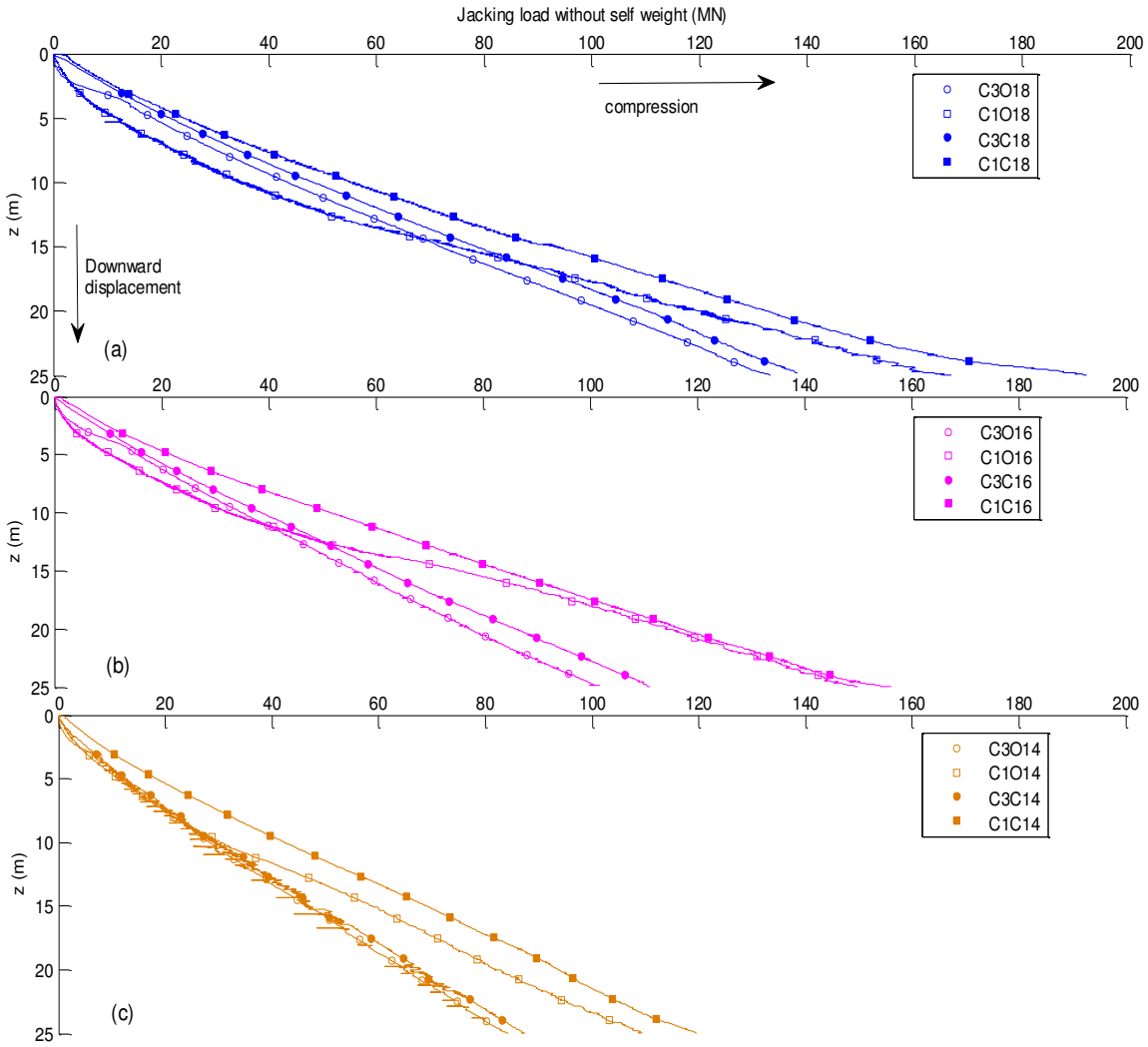

Figure 2-11 : Jacking load of piles installed in saturated or dry dense sands (a) B= 1.8m (b) B= 1.6m (c) B= 1.4m

Plug formation is also affected by pile diameter. As the pile diameter decreases from 1.8 m to 1.4 m, the difference between open and closed piles is decreasing until both pile types behave similarly as observed for C3O14 and C3C14.

Figure 2-12 displays the results for the piles tested in medium dense dry or saturated sand. In medium dense sand, the saturation does not affect plug formation. The open-ended piles jacked in dry or saturated sands develop plugging at the same time of their respective test. However, pile diameter effect on pile behaviour is still present. The difference between the performance of open-ended and close-ended piles decreases with the decrease in diameter until merging with a diameter of 1.2 m. This confirms the previous results, for which the decrease in pile diameter improves pile plugging causing open-ended piles to behave as close ended ones.

These results are in accordance with those of Kumara et al. (2016), which underlines that relatively small open-ended pile diameters produce a higher degree of soil plugging in both dense and loose sands. The study also found that a fully-plugged open-ended pile behaves similarly to a closed-ended pile. Lee et al. (2003) also report that at a driving depth equals to seventeen times the pile diameter, the base resistance of open-ended piles is approximately the same as that of closed-ended piles in similar conditions. The then obtained ratio of pile depth to pile diameter is close to the ratio determined in the present study.

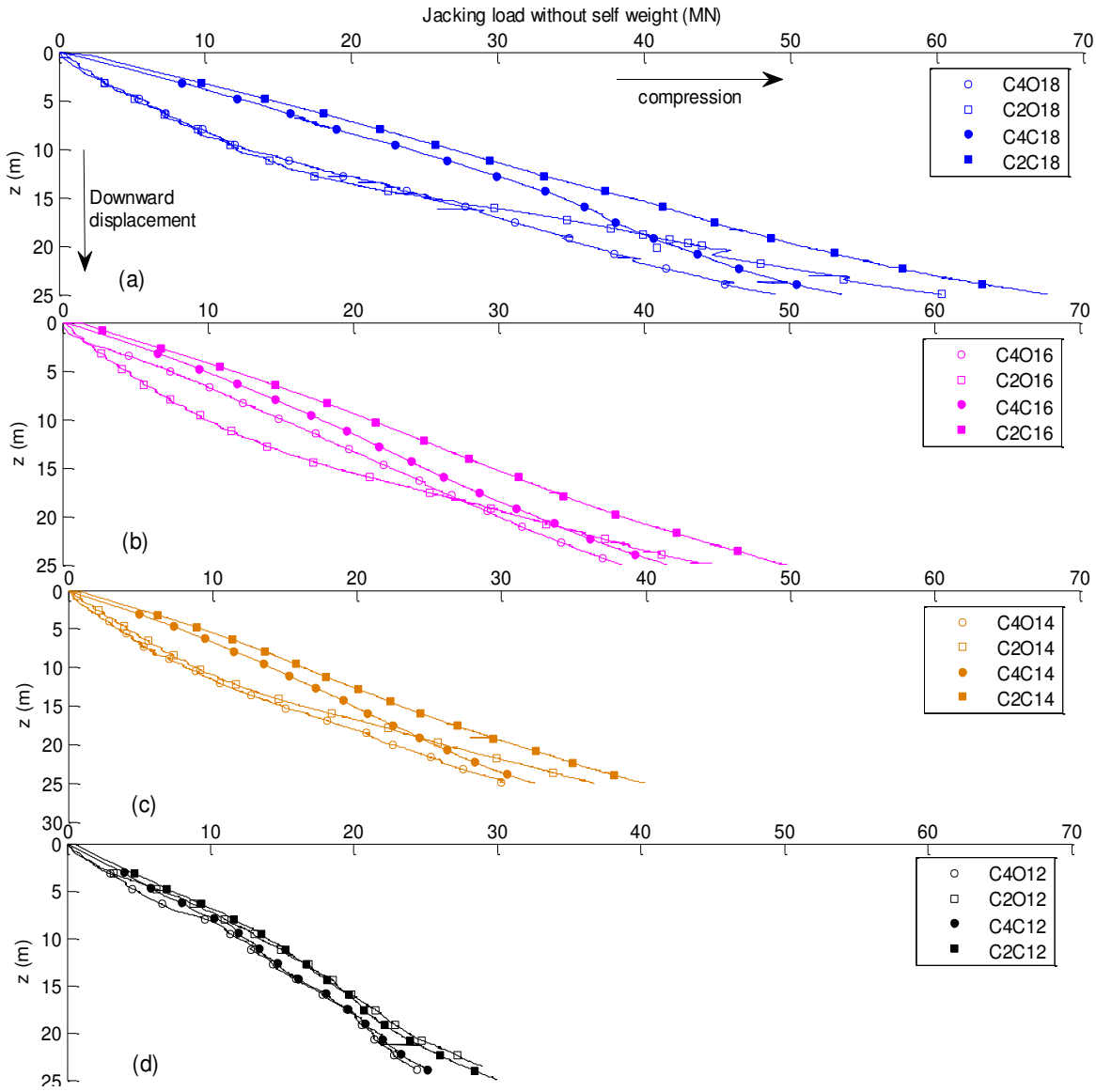

Figure 2-12 : Jacking load of piles installed in saturated or dry medium dense sands (a) B= 1.8m (b) B= 1.6m (c) B= 1.4m (d) B= 1.2m

Table 2-9 summarized the depths, at which plug formation starts for all the piles tested. The criteria used to determine plug initiation is the detection of a slope change and the beginning of inflection in the jacking load vs. depth curve.

When dismantling the tests, the size distribution of the grains forming the plug has been analysed using laser device (Appendix 6). Figure 2-13 presents the particle size distributions of intact Fontainebleau sand and of a sample taken from the sand that formed the plug inside the pile C1O16. For the plugged sand, the percentage of fine sand is clearly higher than the one obtained for the intact sand. The smallest sand particle diameter in the intact Fontainebleau sand is around 100 µm. On the other hand, in the plugged sand, 14 % of the total volume tested has a diameter smaller than 100 µm. Similar results were found by Altuhafi et al. (2018) on triaxial tests realized under high level of stresses. In this study, Altuhafi et al. (2018) obtained particle breakage in the sand specimens sheared under 6.5 MPa. Another comparable particle breakage was noted in the work of Yang et al. (2010) where they concluded that breakage was only evident in tests where the pile tip effective stresses exceeded around 7 MPa.

For C1O16, the sand plug appears at the pile tip for an embedded length of 13m and for an external applied load of 70 MN. The shaft friction of the 13 m embedded pile is less than tension capacity of the 25 m embedded pile (27 MN). The pile tip resistance at 13 m is then higher than 43 MN. The stress under the pile tip is then higher than 20 MPa and largely above 7 MPa given by Yang et al. (2010). It proves that, before the plug formation, the sand particles, which go inside the pile, may have crushed during the pile installation.

2.4.3.3 Pull out capacity tests

The pull out resistance of the piles is plotted according to the tension displacement normalized by the pile diameter in Figure 2-14 (dense sand) and Figure 2-15 (medium dense sand). The results show that the pull out resistance of the piles installed in saturated sand is lower than for the piles installed in dry sand. The explanation is the same as in the bearing capacity section where piles installed in saturated sand mobilize surrounding effective stress only instead of total stress as in dry sand. Moreover, Figure 2-14 and Figure 2-15 show that the pull out capacity of open-ended piles is higher than that of closed ones. Open-ended piles, indeed, may add inner friction to the external shaft resistance. Nevertheless, the difference between open-ended and closed piles is not significant enough which demonstrate that plug formation prevents too much sand from entering into the pile and mobilizing the internal

friction. If plug formation is not initiated and the pile is jacked in a full coring mode, the higher internal pile friction must have a bigger influence on the difference between open and closed pile tension capacities.

Table 2-9 : Depth of plug formation

	B/ d_{50}	86		76		66		57
		z	z/B	z	z/B	z	z/B	z
Dry	D_r = 58%	16 m	8.9	14 m	8.8	14 m	10	0 m
	D_r = 99%	13 m	7.2	13 m	8.1	11 m	7.9	-
Saturated	D_r = 58%	16 m	8.9	2 m	1.3	14 m	10	0 m
	D_r = 99%	3 m	1.7	3 m	1.9	0 m	0	-

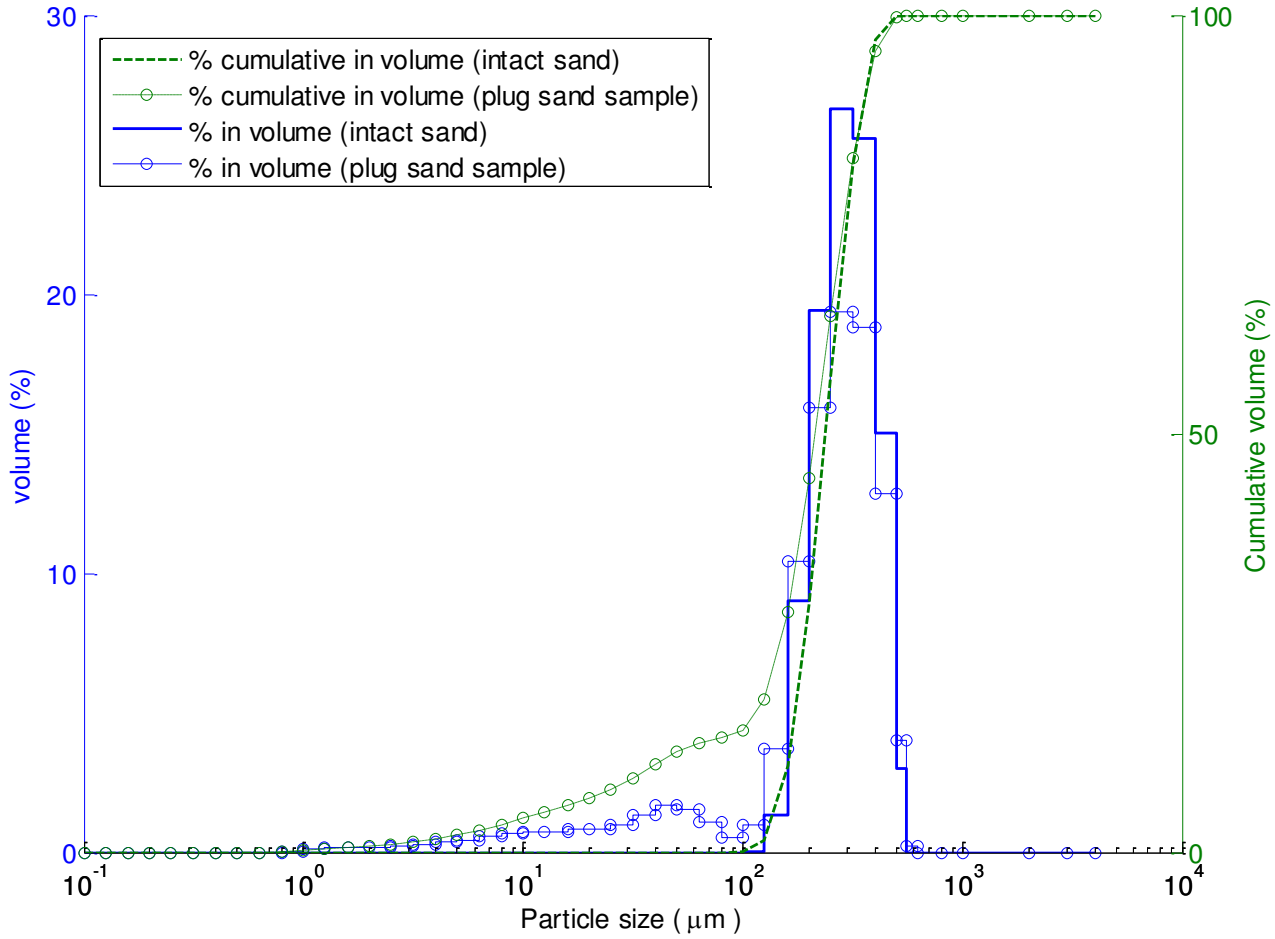

Figure 2-13 : Particle size distribution for intact Fontainbleau sand and plug sand sample

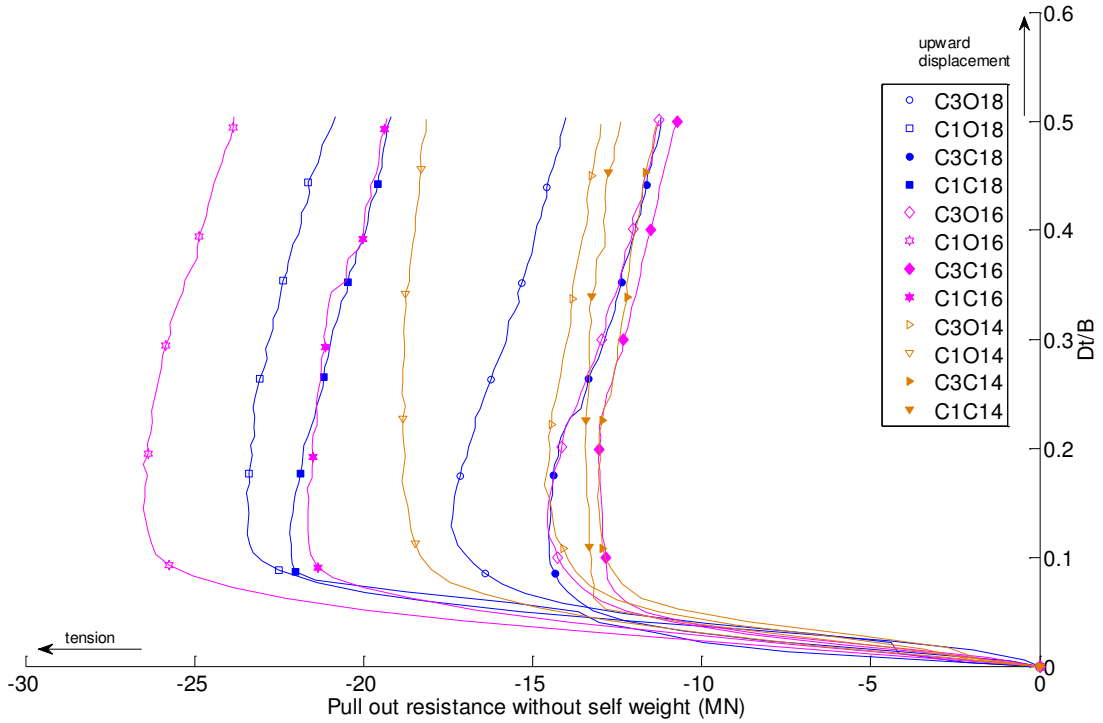

Figure 2-14 : Pull out resistance of piles installed in saturated or dry dense sands

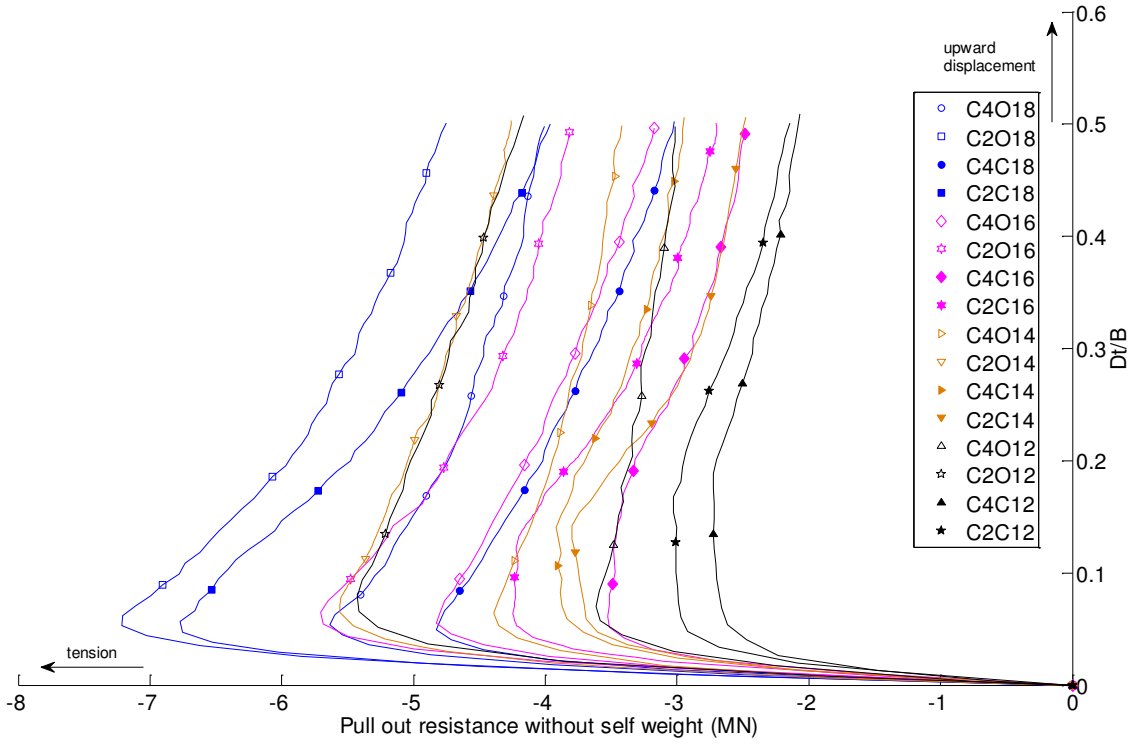

Figure 2-15 : Pull out resistance of piles installed in saturated or dry medium dense sands

2.4.3.4 Ultimate load

The ultimate compression capacity of all the piles tested is presented in Figure 2-16, which highlights the previous results, i.e., that the ultimate capacity of open-ended piles is similar to

closed ones. Two significant findings of this figure are: (1) the ultimate compression capacities of piles jacked in dry sand is substantially higher than that of the piles jacked in saturated sand because, in saturated sand, the pile capacity results from the effective stresses and not from the total stresses like in dry sand, (2) the ultimate compression capacity in dense sand is higher than that in medium dense sand for both dry and saturated sands. This observation is consistent with the work of Paik and Salgado (2003), in which the ultimate unit base resistance increases significantly with increasing relative density and horizontal stress.

As for compression mode, the ultimate tension capacities of the piles are presented in Figure 2-16. The results clearly show that the piles installed in dense sand have a higher uplift capacity than those installed in medium dense sand. One reason for this is the increase in both effective and friction angles between piles and soil due to the increase in the soil relative density (Gaaver 2013).

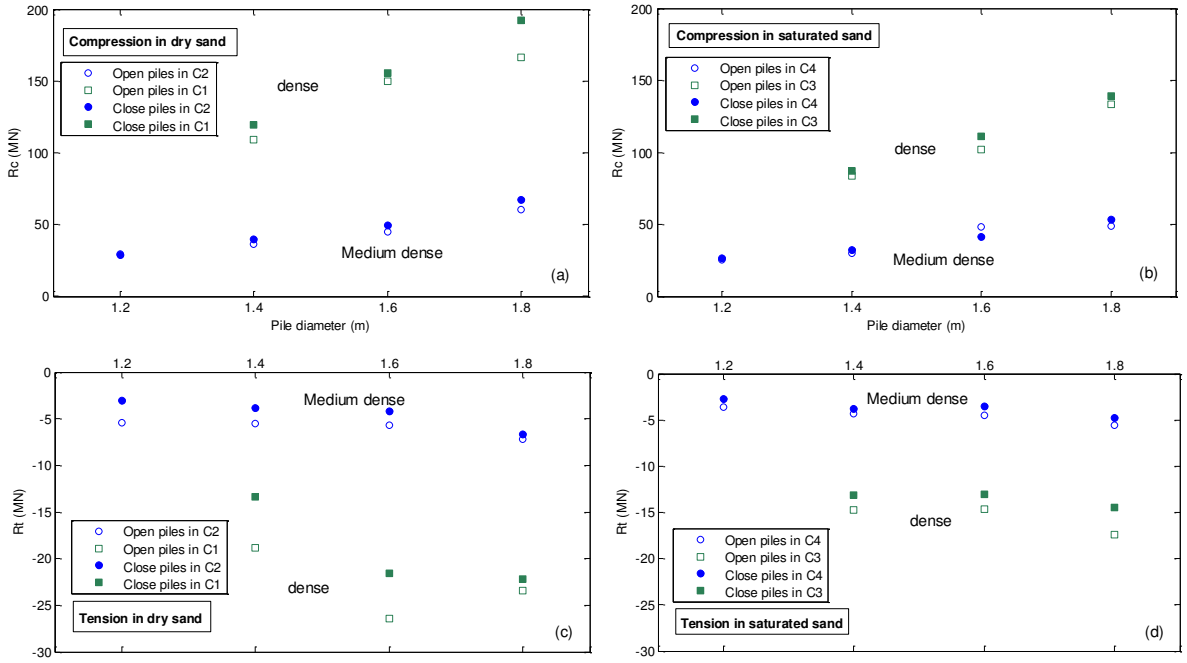

Figure 2-16 : Ultimate capacity in compression mode (Rc) and in tension (Rt): (a) Rc for dry sand – (b) Rc for saturated sand – (c) Rt for dry sand – (d) Rt for saturated sand

2.4.3.5 Ratio of the tension to the compression resistance

It is recognized that the main difference between tension and compression capacities comes from tip capacity. However, some studies show that this difference can also result from the shaft resistance. It is also generally agreed that the unit skin friction is higher in compression than in tension (Foray et al. 1998, De Nicola and Randolph 1994). Foray et al. (1998) have shown that, in addition to the changes in the radial stresses along the pile shaft related to the

loading path, this difference in skin friction can also be attributed to some residual loads induced by pile driving and generating negative friction stresses along the pile shaft. Gaaver (2013) also points out that Poulos and Davis (1980) recommend that the estimate of the pile uplift capacity should be two thirds that of the downward shaft resistance.

Guefrech et al. (2012), for "non-displacement" rough piles in centrifuge, simulating a prototype with B = 0.42 m and D = 13 m installed in a dense dry Fontainebleau sand, obtained $R_t/R_c = 0.68$

This ratio is plotted in Figure 2-17. With the exception of a few cases (the 1.4-m diameter piles in C1 and the 1.2-m diameter piles in C4), the tension to compression capacity ratio decreases as diameter increases. As shown in Figure 2-16, this can be accounted for by the fact that the compression capacity increase with pile diameter is sharper than the traction capacity increase with pile diameter. A possible explanation is that the compression capacity depends on both tip and shaft resistances. The tip capacity increases parabolically with pile diameter in contrast to tension resistance dependent only on shaft resistance, which rises linearly according to diameter.

Another key observation is that the open-ended pile ratio is always higher than the close-ended pile ratio. As noted above, open-ended piles appear to mobilize higher tension capacities, and an almost similar compression capacity.

The very higher R_t/R_c ratio obtained by Guefrech et al. (2012) for non-displacement pile is certainly linked to the installation method, to the experimental procedure and the higher slenderness of the pile.

2.4.3.6 Pile displacement until tension failure

The displacement until failure is usually considered around 10% of B. However, although useful for engineering practice, there is no basis for thinking this choice is true for all types of pile. Figure 2-18 presents the pile displacements until tension failure. The first two figures display displacement until tension failure for all the tested piles while the other two display the same displacement against B.

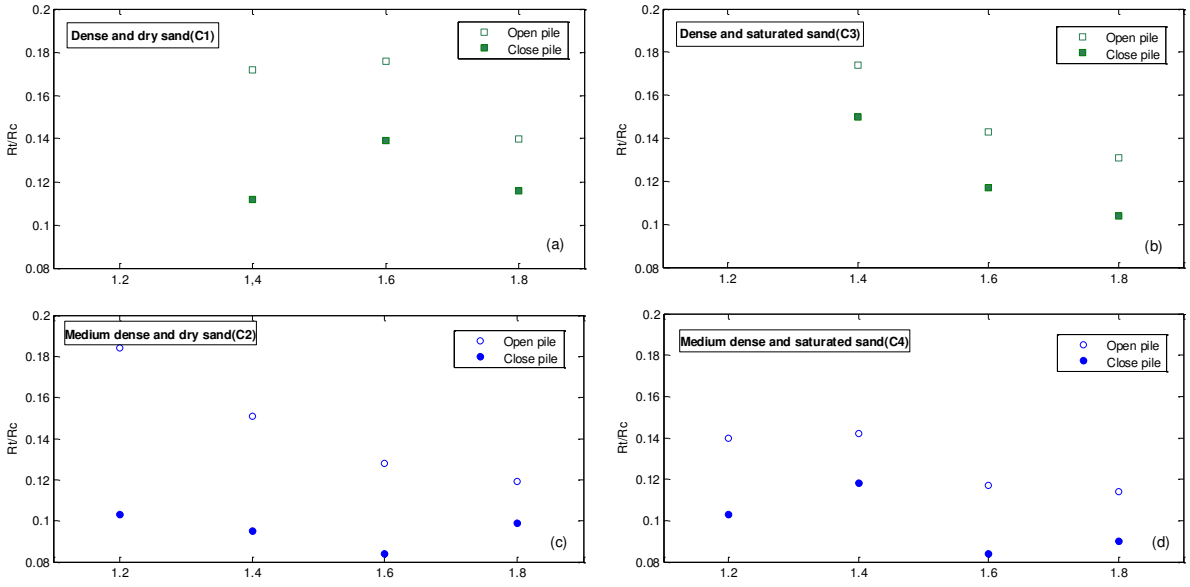

Figure 2-17 : Tension/compression capacity: (a) for dense and dry sand – (b) for dense and saturated sand – (c) for medium dense and dry sand – (d) for medium dense and saturated sand

The displacement until failure depends on density and degree of saturation. The piles in the saturated strongboxes present greater displacement until failure than the piles in the dry ones. Moreover, the piles in the dense strongboxes show greater displacement than those in medium dense respective strongboxes. The average failure displacement ratio in dense dry sand C1 is 14% compared to 7% for medium dense dry sand C2. The average failure displacement ratio of the piles in dense saturated sand C3 is 19% compared to 10% for saturated medium dense sand C4. These results demonstrate that the general assumption that the failure displacement ratio is 10% of B is not always valid. Many factors can affect this ratio. It also proves that the displacement until tension failure increases with the increase in density and saturation.

Finally, a closer analysis of the failure displacement ratio reveals that it shows a decrease as pile diameter increases whatever the density and water content conditions.

These results are consistent on the fact that, in saturated sand, water maintains smoother contact between sand and pile. In the tension mode, the pile, therefore, is more freely to slide, which produces higher displacement until failure. Sand density effect can also be produced by the high lateral stress and contact between dense sand and pile, which then requires greater displacement to mobilize all the frictions with sand. More work needs to be carried out to understand these results better in order to develop a comprehensive approach, which can take into account sand density, sand saturation and pile diameter. Maybe the numerical simulation by discrete element method should give information on those phenomena.

2.4.3.7 Initial tension stiffness

The calculated initial tension stiffness of the tested piles is presented in Figure 2-19. The initial stiffness corresponds to the slope, which crosses the tension displacement curve at half of the maximum traction capacity.

These results highlight the impact of the density on the initial tension stiffness of the piles in both dry and saturated sands. The stiffness is higher in dense sand than in medium dense sand. Moreover, stiffness is affected by sand saturation at the same dry density. In saturated sand, the stiffness is lower than in dry sand for both medium dense and dense sands. The effect of sand density and saturation on the initial stiffness can be explained by the reduction in the lateral stress between dense and medium dense sands and between dry and saturated sands. This reduction in lateral stresses may lead to a diminution of the shaft friction. For the same displacement, the piles mobilize lower shaft friction in medium dense sand in comparison with dense sand and in saturated sand in comparison with sand at the same dry sand density.

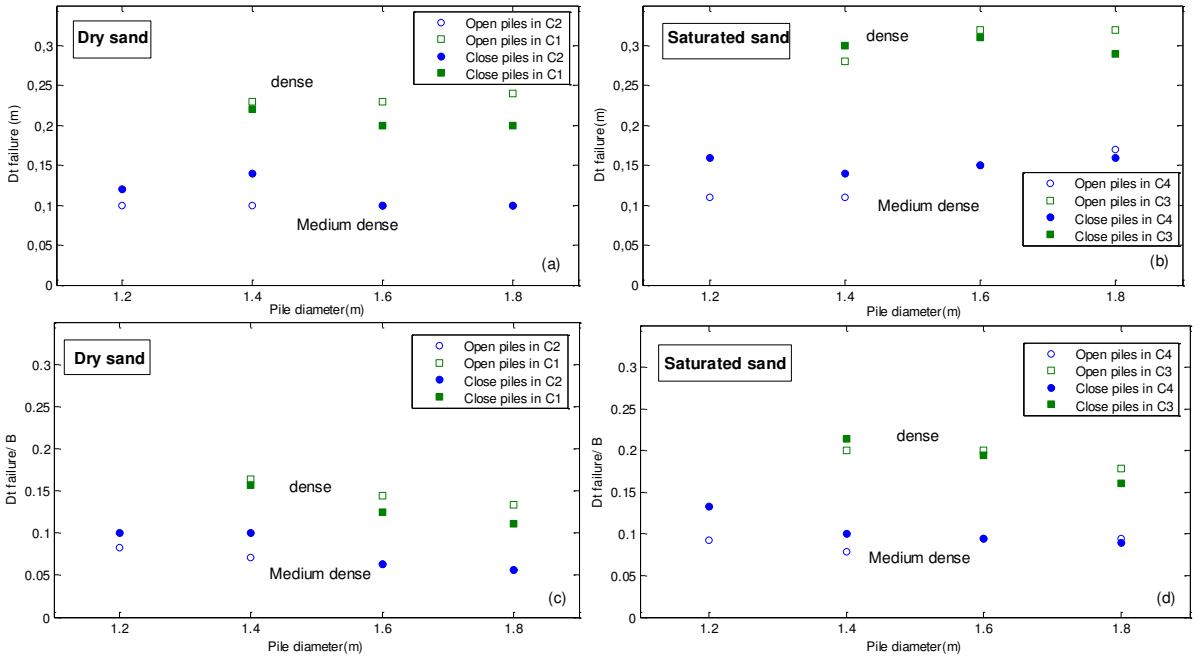

Figure 2-18 : Pile failure displacement ratio: (a) for dry sand – (b) for saturated sand – Pile failure displacement ratio (c) for dry sand – (d) for saturated sand

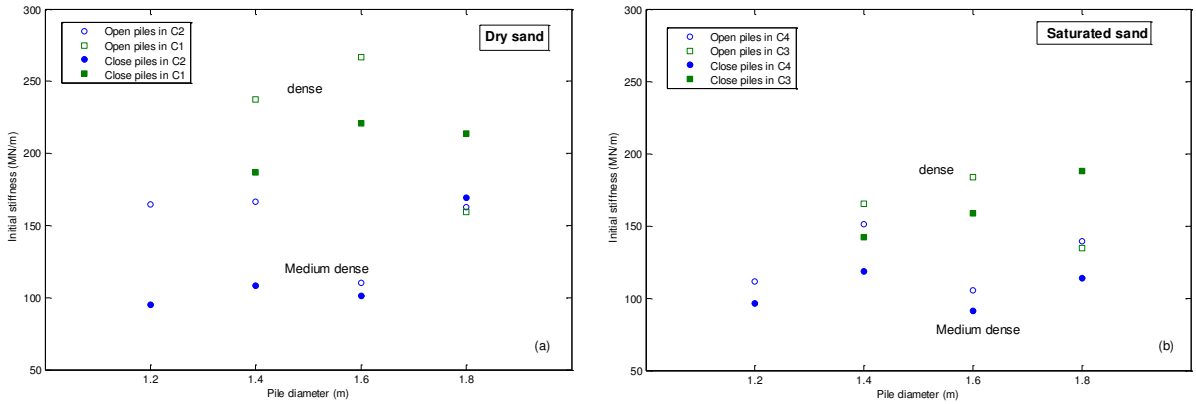

Figure 2-19 : Initial pile tension stiffness: (a) for dry sand – (b) for saturated sand

2.4.3.8 Embedded volume versus jacking load

The existence of a linear relationship between tip resistance and pile depth appears in many works found in the literature (Jamiolkowski et al. (2003), Kim et al. (2016)). Kim et al. (2016) shows that this linear relationship exists up to a critical depth, beyond which the tip resistance is then almost constant. Moreover, the slope of the linear curve and the critical depth both increase with the increase in the relative density. In the other hand and because of the use of a displacement installation method in this study, it was interesting to test the existing of such relationship between the total force required to jack a pile and its embedded volume (volume of the embedded part of the pile). In Figure 2-20, a linear relationship between the embedded volume of the close-ended piles and their jacking load is observed. Although there is no definitive explanation for the existence of such a linear relationship, it is very probable that this result is related to the amount of sand displaced. The experimental piles, indeed, are installed using a displacement method known to generate great sand displacements as jacking progresses. The relationship is verified whatever the sand density and the saturation. It also provides the designer a choice, for a desired jacking load, between the use of longer piles with a small diameter or larger ones with smaller length. The linear relationship between embedded volume and jacking load also shows similarities with the relationships available in the literature between tip resistance and depth. It appears here that the experimental piles have not yet reached the critical depth where the forces tend to stabilize. The relationship between force and embedded volume may, therefore, be critical for pile designers. The relationship with the embedded volume is certainly linked to that between tip capacity and CPT profile.

A survey of the literature reveals that little research is focusing on this subject. Still, some similar results are discussed in Robinsky et al. (1964). The authors present the results obtained from the study conducted on two straight sided piles of different diameters and one

tapered pile. According to them, each pile presents a straight-line relationship between its embedded volume and its respective capacity. However, in this case, slopes are different contrary to the results obtained in the present work.

The same study is conducted on the open-ended piles. The results are presented in Figure 2-21. Most of the piles also display a straight-line relationship between embedded volume and jacking load. However, the slopes are different contrary to close-ended piles. The only exception is for the results of the open-ended piles installed in the dense and saturated sand, C3. In this case, the lines have the same slope. As discussed above in the first section, this can be accounted for by the fact that plug formation is initiated at a very shallow depth in this high density and saturation strongbox and the open-ended piles then behave similarly to close-ended piles.

The relationship exists only between piles embedded volume and jacking load in compression mode. No relationship is found between the pile tension capacity and the embedded volume achieved at the end of the jacking phase.

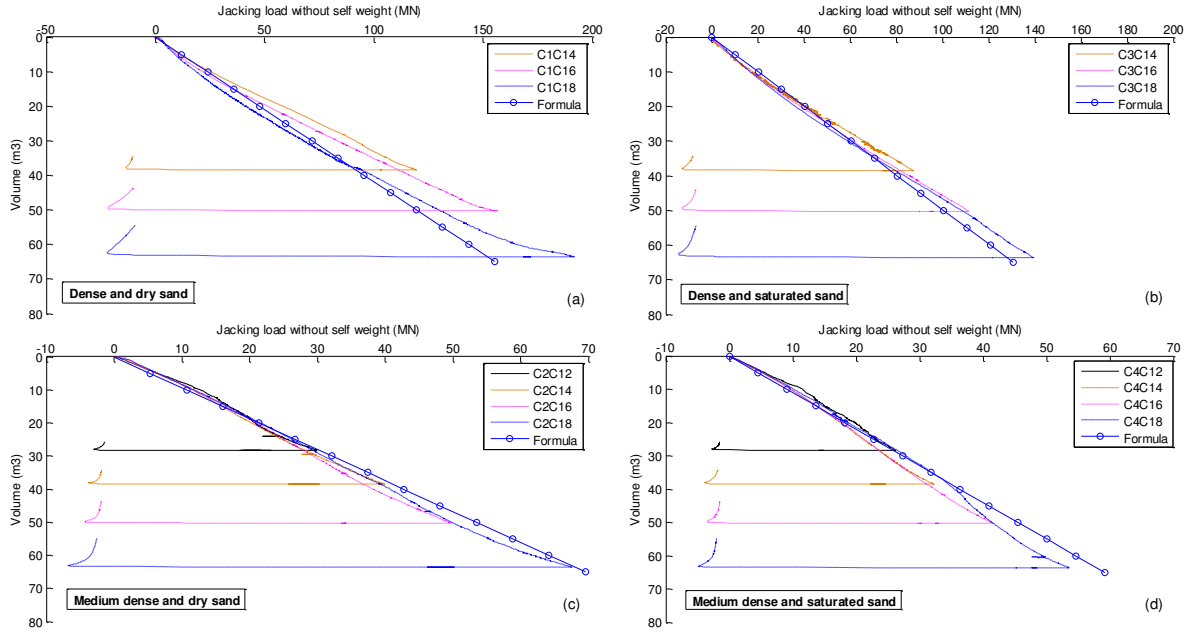

Figure 2-20 : Closed pile embedded volume versus jacking load: (a) for dense and dry sand – (b) for dense and saturated sand – (c) for medium dense and dry sand – (d) for medium dense and saturated sand

The fact that all the curves of the close-ended piles tested in each strongbox have a linear relationship between the embedded volume and the vertical load whatever their diameter points out the fact that this relationship depends on the sand density and the friction angle of

contact between the pile and sand and is independent from the pile diameter. With this aim in view, for each strongbox, a straight line with a slope k is plotted in Figure 2-20. k takes four different values depending on the density and the saturation states. It is equal to 2.39, 1.07, 2.014, 0.91 MN/m^3 respectively for the strongboxes C1,C2,C3 and C4. The presented slope values predict the experimental results with some uncertainties of less than 5% for strongboxes C2, C3 and C4, with the exception of strongbox C1, for which the uncertainty reaches 20% in comparison with the experimental results.

The lines used in Figure 2-20 are plotted in Figure 2-21 for open piles. The theoretical line plotted in Figure 2-21.b confirms the above conclusion that plug formation takes place from the start of the installation phase in this strongbox with piles performing similarly to close-ended piles. The line in dry strongbox C2 presents slope similar to that of pile C2O12, plugged from the beginning of the jacking phase. As for the other piles in C2, the initial slope is significantly below what it should be with regard to the theoretical line. However, as the embedded volume increases and as the plug is developing, the slope of the curves changes and becomes more rigid. The initial slope of these piles can then be considered as the "unplugged slope". Thus, if plugging did not appear, the slope would certainly remain unchanged. Plug formation affects pile behaviour, which then becomes more similar to that of closed piles. Similar results are observed for C1 and C4.

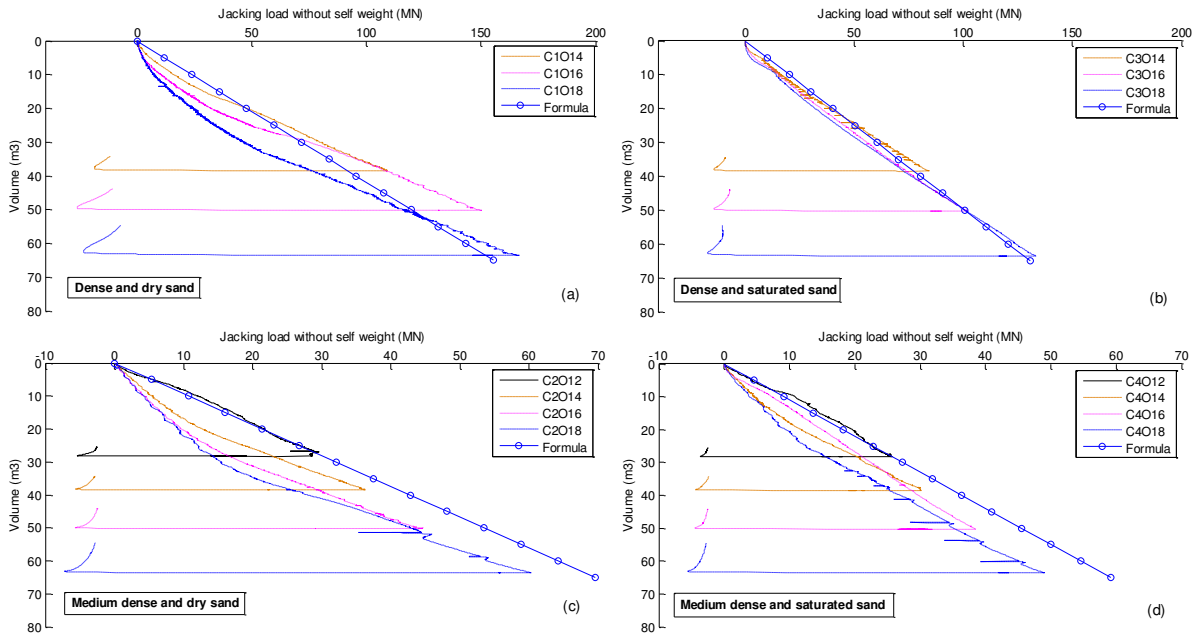

Figure 2-21 : Open pile embedded volume versus jacking load: (a) for dense and dry sand – (b) for dense and saturated sand – (c) for medium and dry sand – (d) for medium and saturated sand

2.4.3.9 Comparison between experimental results and standards

The second part of this study is devoted to the comparison between the experimental results and the standards used for offshore wind turbine design.

The standards examined in this study are: ICP, which is a CPT based method, NF, API and DNVGL. A CPT test is carried out in each strongbox to determine the CPT curve required for both ICP and NF calculations (Appendix 4). Two friction angles (18° for medium dense sand and 23° for dense sand) are chosen because they are considered to be the most representative of the present conditions (grain sizes, density, pile roughness…) (Prai-ai, 2013).

2.4.3.9.1 Close-ended piles

Close-ended piles are first considered. The comparison between standard and experimental results is presented in Table 2-10. The choice of addressing close-ended piles only is related to their well-known tip conditions, which, contrary to open-ended piles, remove uncertainty as regards tip condition. Open-ended pile performances can differ depending on plugging and, therefore, will be studied in a next phase of comparison. The conditions and values of the coefficients used in the standards are presented in the next paragraph.

First, two conditions are examined for API and DNVGL standards: a first one without the limitations suggested in API and DNVGL standards, and the second one with the use of these limitations in order to investigate in detail the nature of their objectives:

- In medium dense sand, the N_q value used is 12, the limiting skin friction value is 67 kPa and the limiting unit bearing value is 2.9 MPa.
- In dense sand the N_q value used is 40, the limiting skin friction value is 95.7 kPa and the limiting unit bearing value is 9.6 MPa.

As regards NF, the used sand with a pile of class 4 (the pile classification proposed in the standard) give a K_c value equal to 0.4 and a $\alpha_{pile\text{-}soil}$ value equal to 0.85.

Table 2-10 : Static ultimate capacities in compression and tension modes (prototype values)

Pile name	Compression					Tension				
	Exp.	ICP	NF	API and DNVGL without limitation	API and DNVGL with limitation	Exp.	ICP	NF	API and DNVGL without limitation	API and DNVGL with limitation
C1C18	192	164	79	54	34	-22.2	-22.2	-10.8	-12.2	-9.8
C1C16	156	140	64	44	28	-21.6	-19.5	-9.6	-11	-8.7
C1C14	120	116	50	35	22	-13.4	-16.6	-8.4	-9.6	-7.6
C2C18	68	60	36	21	14	-6.7	-6.6	-9.8	-8.8	-6.9
C2C16	50	51	29	17	12	-4.2	-5.8	-8.7	-7.9	-6.2
C2C14	40	42	23	14	10	-3.8	-5	-7.6	-6.9	-5.4
C2C12	29	34	18	11	8	-3	-4.2	-6.5	-5.9	-4.6
C3C18	139	129	45	33	32	-14.5	-16.3	-10.4	-7.5	-7.4
C3C16	111	110	52	27	26	-13	-14.2	-9.2	-6.7	-6.6
C3C14	87	92	41	22	21	-13.1	-12.3	-8.1	-5.9	-5.8
C4C18	54	48	30	13	13	-4.8	-5.1	-9.3	-5.5	-5.4
C4C16	42	41	25	11	11	-3.5	-4.5	-8.3	-4.9	-4.8
C4C14	32	34	20	9	9	-3.8	-3.9	-7.3	-4.3	-4.2
C4C12	26	27	16	7	7	-2.7	-3.2	-6.2	-3.7	-3.6

As for compression mode (Table 2-10), the experimental results exceed the results obtained with the standards for most of the piles tested. The ICP method gives the values closest to the experimental ones. The use of the effective stress in the method allows for the estimation of the difference in the pile capacities in dry and saturated sands. On the other hand, NF results appear more conservative than ICP ones and are that of approximately half of the experimental results achieved with the model piles. NF results are more accurate in the case of medium dense sand than in dense sand. The difference between ICP and NF results mainly from the calculation of the base resistance. Both methods are based on the CPT test for this calculation but NF, however, proposes an empirical value to determine the end bearing capacity from the CPT resistance (q_c). This value is generally well below the coefficient obtained with the formula used in ICP and multiplies the q_c value of the CPT. Finally, API

and DNVGL standards appear as the most conservative calculation methods for all the piles tested with results ranging from 20% to 35% of the experimental values in the case of the API and DNVGL without limitation. The additional limitation suggested in API and DNVGL makes them even more conservative while far from representing the real capacity of the tested piles. Figure 2-22 represents the experimental vs calculated results obtained from the design codes and confirm the above discussed results about the conservative behaviour of the design code. The four curves presented in this curves are always higher than the bisectrix which proves that the experimental capacities are always bigger than the calculated ones. Foray et al. (1998) conclude that API may be considered conservative because it underestimates pile end bearing capacity. They also report that piles driven in dense to very dense sands can develop significantly higher bearing capacities than those calculated using the current API design method, especially when the sand is overconsolidated. Some previous studies have criticized the use of the limitation in the API method. Foray et al. (1998) show that, in agreement with the work of Kraft (1990) and Foray et al. (1993), there is no evidence of the existence of limiting values for both end bearing and skin friction resistances, at least for the piles driven in sand up to a 60 to 80 m penetration depth.

As regards tension, ICP demonstrates good performance in dense sand with, however, a small overestimation of the pile tension capacity in medium dense sand. NF provides capacity values, which are that of approximately half of the experimental ones in dense sand. NF results are even problematic for piles installed in medium dense sand because the overestimate, in this case, is more than twice that of the real experimental pile capacities. API and DNVGL present a large underestimation of the pile tension capacities in dense sand. For piles installed in medium dense sand, they, on the other hand, like NF, tend to overestimate the tension capacity. Figure 2-23 confirm also these results as it is clear that the NF and the API tend to overestimate the experimental results in medium dense sand (the low values in the figure) and underestimate the experimental results in dense sand.

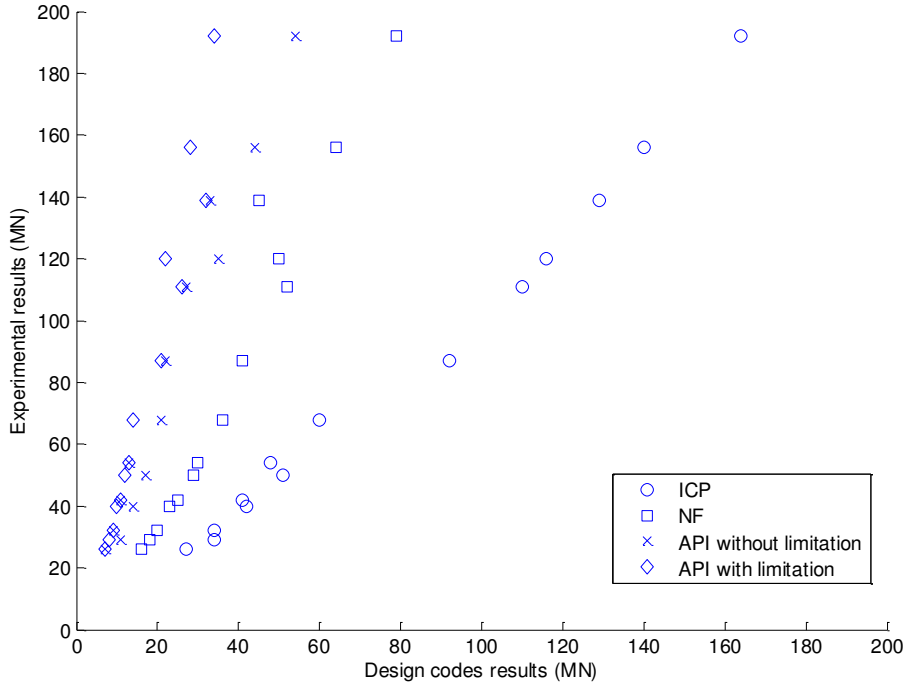

Figure 2-22 : Experimental vs design codes results (compression)

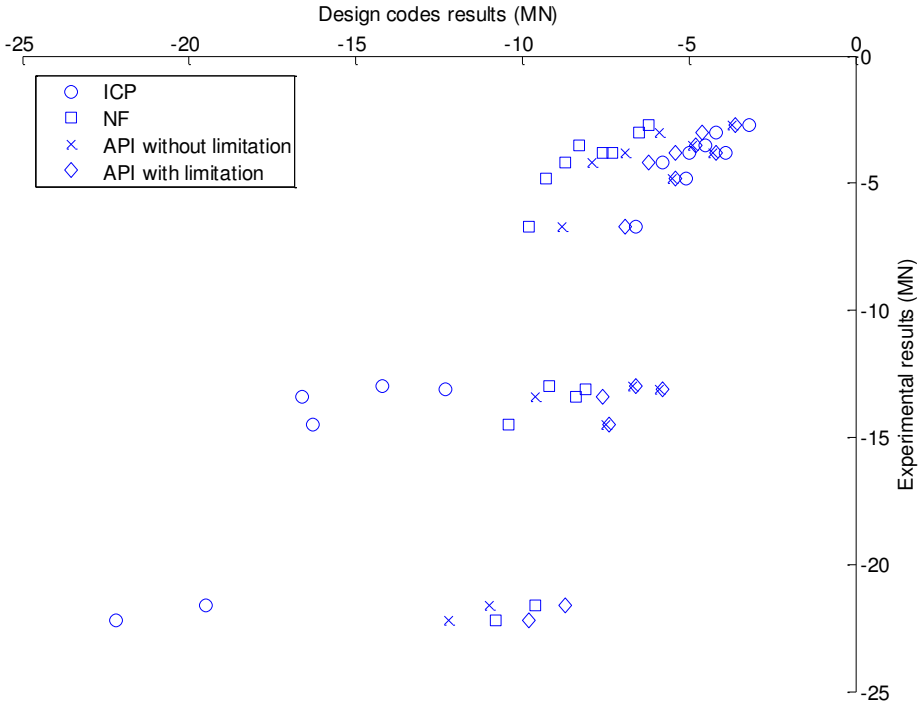

Figure 2-23 : Experimental vs design codes results (tension)

It is clear from the general comparison discussed in this section that more work needs to be carried out on the existing standards used for offshore wind turbine design to improve their performances. Alwaneh et al. (1999) report that the studies by Toolan et al. (1990), Randolph et al. (1994), Jardine et al. (1998), and many others underline the limitations of the API code

design guidelines for tension piles, especially where loose and dense sands are found. They, consequently, advocate for the development of new alternative design methods. A large underestimate is observed in most cases, which can have a real economical impact on the cost of the construction of offshore wind turbines. Therefore, the enhancement of existing standard performances can generate a significant cost reduction in the geotechnical part of wind turbine design, a part, which is generally estimated as 25% of the total cost of the offshore wind turbine.

2.4.3.9.2 Open-ended piles

Open-ended pile axial capacity is difficult to predict because of its dependence on the plugging percentage of the pile tip. API does not provide a detailed description and study of pile tip capacity depending on the plugging state. It only suggests that the pile end-bearing capacity may affect the entire pile section of plugged piles while being limited to the annular section of unplugged piles. NF provides different empirical coefficients depending on the type of pile (open-ended or close-ended). On the other hand, ICP recommends a specific formula for open-ended pile shaft friction including a modified radius $R^* = (R^2_{outer} - R^2_{inner})^{0.5}$ instead of the normal radius used for close-ended piles. Moreover, ICP proposes different formulas to calculate the open-ended pile tip capacity depending on the plugging state. The three different plugging conditions presented in ICP are: unplugged piles, fully plugged piles and rigid basal plug.

In order to examine the performances of the ICP method as regards plugging conditions, a detailed analysis of the axial capacity of piles C1O18, C1O14, C2O18 and C2O12 is carried out. Figure 2-24 presents the results obtained for the largest and the smallest piles installed in the medium dense strongbox C2. The axial capacity of these piles is compared with the axial capacity provided by ICP under three different tip conditions (close-ended, fully plugged and unplugged pile).

The experimental piles appear far from the unplugged state described by ICP. A very different behaviour is observed between the largest piles and the smallest one. At the beginning of the jacking phase, the largest pile C2O18 behaves almost identically to the fully plugged piles. However, as jacking progresses, the pile behaviour evolves into that of close ended piles. At the end of the jacking phase, C2O18 has a capacity similar to close-ended piles. ICP, here, cannot take the existence of the rigid plug that forms during jacking into account. On the other hand, the behaviour of the smallest pile C2O12 is similar to the close-ended pile conditions

considered in the ICP method. This pile satisfies one of the ICP conditions, which considers that the pile can develop a rigid basal plug during static loading ($D_{inner} < 0.02(D_r - 30)$). In tension mode, ICP underestimates the tension capacity of the tested piles under all the conditions but give a good estimation of the residual value of piles. Similar results are also observed with the analysis of C1O18 and C1O14.

The performance of the ICP method in the case of open-ended piles depends on the accurate estimate of the pile plugging state and on the choice of the best plugging condition between the different available conditions found in the design code. Further studies are needed to reduce uncertainties about open-ended pile behaviour and create a consistent database for improving existing design codes in the area of open-ended pile behaviour.

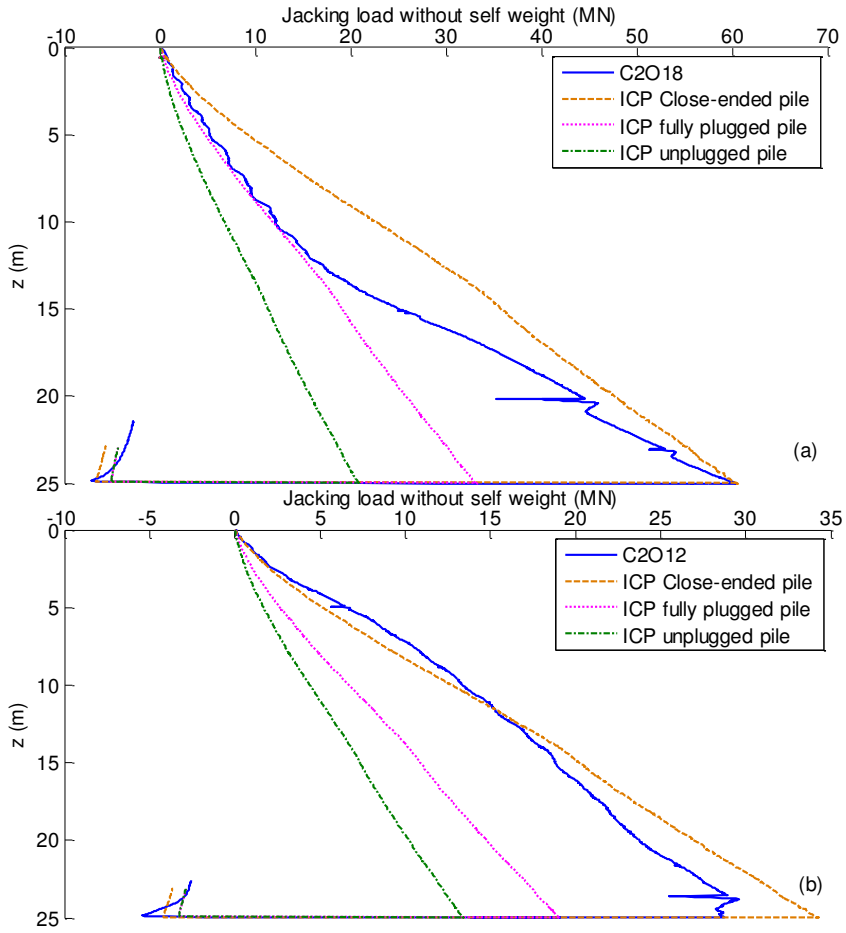

Figure 2-24 : Open piles in C2: (a) for C2O18 – (b) for C2O12

2.4.4 Impact of pile roughness

The present section reports a study conducted to examine the impact of pile roughness on shaft friction developed during the installation of jacked piles in dry sand. With this aim in view, two piles of different roughness (Pile 1 and 2 from Table 2-4) are tested in two different

sand densities to study the shaft resistance that rough and smooth jacked piles can develop in dense and medium dense sands. The choice of jacked piles is guided by the observation according to which shaft resistance can also be affected by the installation method. Moreover, the use of jacked piles (which can be placed using a hydraulic jack) has increased considerably in recent years. The possibility of jacking piles without noise and vibration make these piles more suitable for urban use and a more acceptable method for current European recommended limits (Eurocode 3, White et al. 2002). In order to eliminate any risk of introducing other parameters, which may affect pile shaft resistance and focus only on the effect of piles roughness on shaft resistance, all the piles are jacked identically at 100×g.

Table 2-11 shows the new set of names given for the chosen tests to be presented in this section. The test name contains the following information 1) surface roughness (R for rough and S for smooth), 2) sand density (D for dense and M for medium). For example, PRD is the rough pile jacked in dense sand.

Table 2-11 : Transition table for tests nomenclature

Test	New names	Pile roughness (R_n)	Sand density (D_r in %)
C2P1F18C100G	PRD	0.33	99
C1P3F18C100G	PRM	0.33	58
C5P4S18C100G	PSD	0.014	99
C6P2S18C100G	PSM	0.014	58

2.4.4.1 Pile installation and experimental campaign

The piles are jacked in flight at 100×g to the desired embedment depth of 250 mm to simulate installation effects and soil displacement that takes place during the installation of displacement piles. Pull out and/or compression tests are performed without stopping the centrifuge immediately after pile installation.

2.4.4.2 Determination of shaft and tip resistance

The tests conducted to examine rigid rough piles are carried out using some model piles instrumented with a sensor placed 2.5m from the pile tip (Pile 1 of Table 2-4). The sensor results, however, cannot be used directly to deduce the tip capacity and the shaft friction. The sensor measures the sum of both the tip capacity and the shaft resistance for the first 4.6 m at the bottom of the pile. In order to deduce shaft resistance along the entire pile, an

experimental phased analysis methodology is developed and applied on PRD. This procedure is already explained in section 2.4.2.2.

The same experimental method is also applied to the rough piles jacked in medium sand (PRL) to separate the tip capacity from the shaft resistance.

As all the piles are jacked identically and have the same dimensions, tip capacity should not be different for rough and smooth piles. This similarity in tip capacity results is used to deduce the shaft resistance of the smooth piles from their total capacity by subtracting the tip capacity of the rough piles from the total capacity of the smooth piles. As shown in Figure 2-23, the tip capacity ((a) in Figure 2-25) of pile PRD is used to deduce the shaft resistance of pile PSD ((c) in Figure 2-23) from its total capacity ((b) in Figure 2-25). The same method is used to deduce the shaft resistance of pile PSM from its total capacity using the tip capacity of pile PRM.

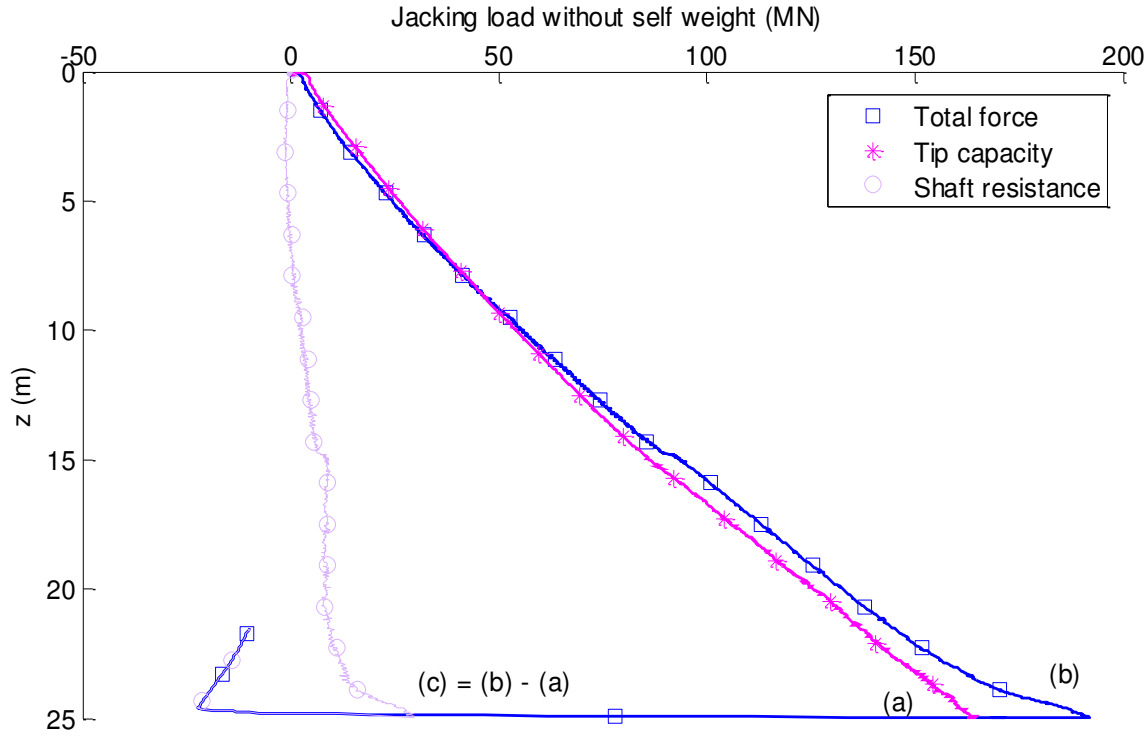

Figure 2-25 : Shaft and tip resistance decomposition of pile PSD

2.4.4.3 Effect of roughness on pile shaft resistance

Although it is generally agreed that pile roughness can affect pile shaft resistance, little research is focusing on this problem in the literature and few studies are conducted directly on some instrumented piles in order to examine roughness effect. Alawneh et al. (1999) suggest that rough piles present a capacity increase ranging from 12% to 55% compared to smooth

model piles. They also observe that the lateral earth coefficient increases as pile roughness increases. This indicates that pile surface roughness enhances the tendency for sand to dilate during uplift loading, which in turn increases the magnitude of the radial effective stress against the pile surface. In the present study, the overall shaft resistance of the entire piles is examined during the jacking phase and pull out tests are carried out to study the effect of roughness on this resistance.

PRD and PSD results are presented in Figure 2-26. As discussed above, the tip capacity of both piles is considered identical. Then, the shaft resistances are obtained from the difference in this tip capacity and the total force of the piles. The same method is used to obtain the shaft resistances of piles PRM and PSM as shown in Figure 2-27.

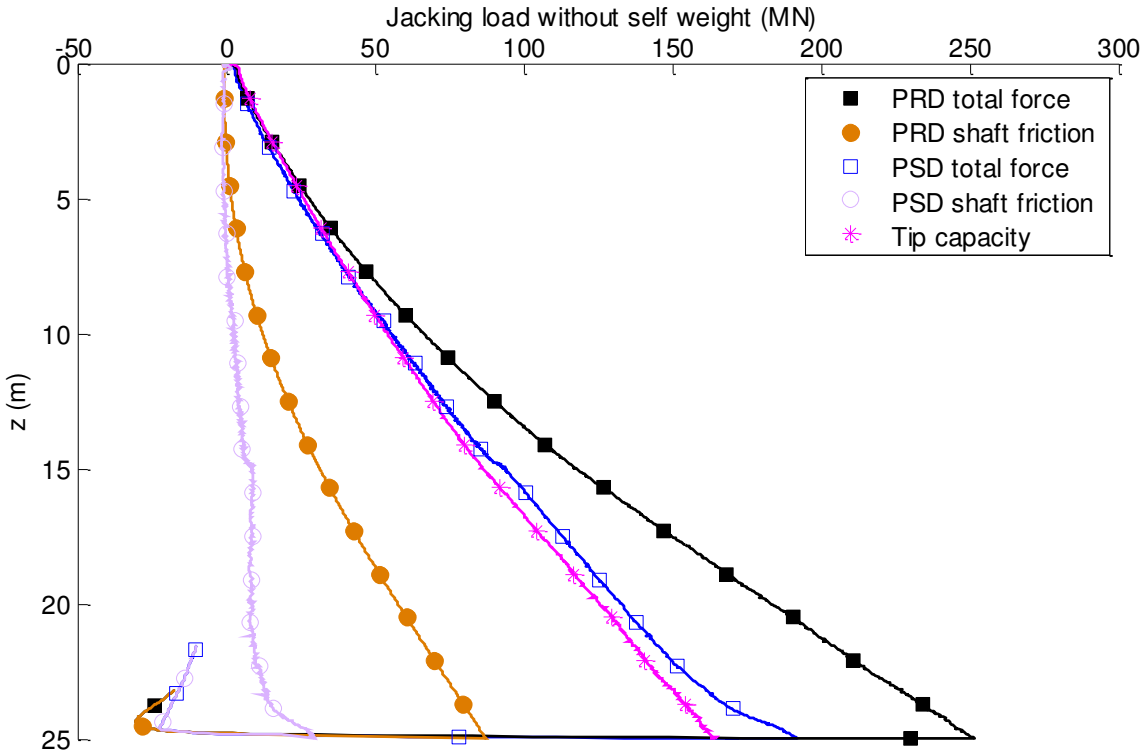

Figure 2-26 : PRD/PSD comparison

In Figure 2-26, from the beginning of the jacking phase and down to a depth of 5 m, the shaft resistances of both piles display very small values. The shaft resistance appears not to be mobilized at shallow depth. As jacking progresses, pile PRD presents a sharp increase in shaft resistance as depth increases until reaching an overall push-in shaft resistance of 87 MN at the end of the jacking phase. On the other hand, pile PSD presents a small shaft resistance increase as depth increases until reaching 27 MN of push-in shaft resistance at the end of the jacking phase. The pull-out tests carried out after completion of the jacking phase reveal that

PRD and PSD both mobilize a pull-out shaft resistance of 30 MN and 22 MN, respectively (Table 2-12).

The same comparison is made with the results obtained in Figure 2-25. From the beginning of the jacking phase and down to a depth of 5 m, the shaft resistances of both piles display similar results and very small values. At the end of the jacking phase, pile PRM reaches an overall push-in shaft resistance of 30 MN. On the other hand, pile PSM reaches a push-in shaft resistance of 7 MN at the end of the jacking phase. The pull-out tests carried out, after completion of the jacking phase for PSM and after the compression test for PSD, reveal that PRM and PSM both mobilize a pull-out shaft resistance of 11 MN and 7 MN, respectively.

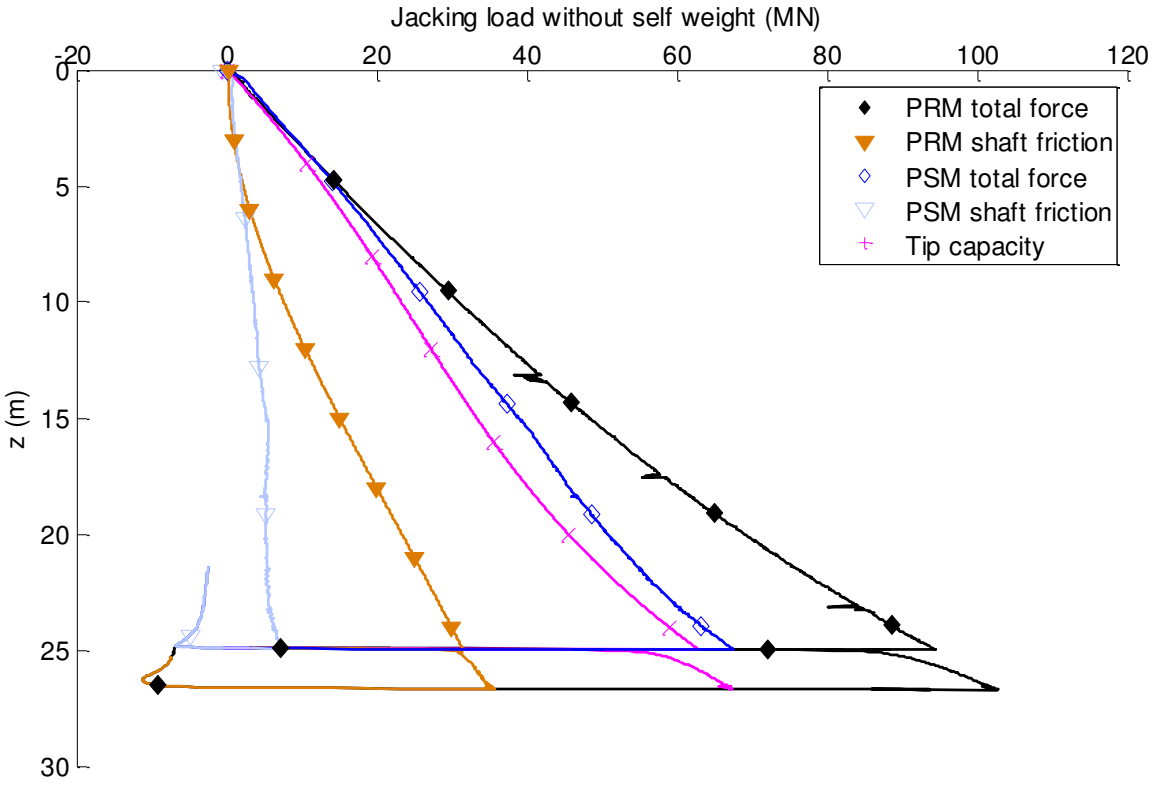

Figure 2-27 : PRM/PSM comparison

The comparison of the results reveals a very significant roughness effect on the pile skin friction. As regards pull-out capacity, the roughness increase, in dense sand, causes an increase of about 36% in pull-out capacity. On the other hand, in medium sand, PRM mobilizes more than 57% of shaft resistance than PSM. These levels of increase in pull-out shaft resistance are comparable to those found by Alawneh et al. (1999) and presented above. However, the most important shaft resistance increase is obtained during push-in tests. The

rough piles present a shaft resistance three times higher than that of the smooth piles in both dense and medium sand.

Table 2-12 : Static ultimate capacities in compression and tension modes (prototype values), the results of ICP are those obtained with Rcla = 0.01 mm.

Installation or design method	Compression			Tension
	Total force [MN]	Tip capacity [MN]	Shaft resistance [MN]	Shaft resistance [MN]
PRD	252	165	87	-30
PRM	91	61	30	-11
PSD	192	165	27	-22
PSM	68	61	7	-7
ICP PRD (30°)	174	136	38	-30
ICP PRM (25°)	63	52	12	-11
ICP PSD (20°)	160	136	24	-19
ICP PSM (15°)	59	52	7	-6

2.4.4.4 Impact of sand density on the behaviour of piles of different roughness

Rao and Venkatesh (1985) demonstrate that, with the increase in density, the ultimate uplift capacity increases whereas the shaft load is mobilized at a faster rate. As dilation is higher in dense sand than in loose sand, the shaft resistance of rough piles can be affected by the density. Alawneh et al. (1999) suggest that pile surface roughness enhances the tendency of the sand to dilate during uplift loading.

The results of the comparison between the rough piles in dense and medium sand (Figure 2-28) confirm that the shaft resistance of both piles is similar down to a depth of approximately 6 m. As jacking progresses, PRD presents a greater shaft resistance increase than PRM. At the end of the jacking phase, PRD has mobilized some skin friction three times higher than PRM. In the first 10 m, PSM presents higher friction (Figure 2-29) than PSD. However, at the end of the jacking phase, PSD has already reached a shaft resistance value roughly four times higher than the PSM resistance.

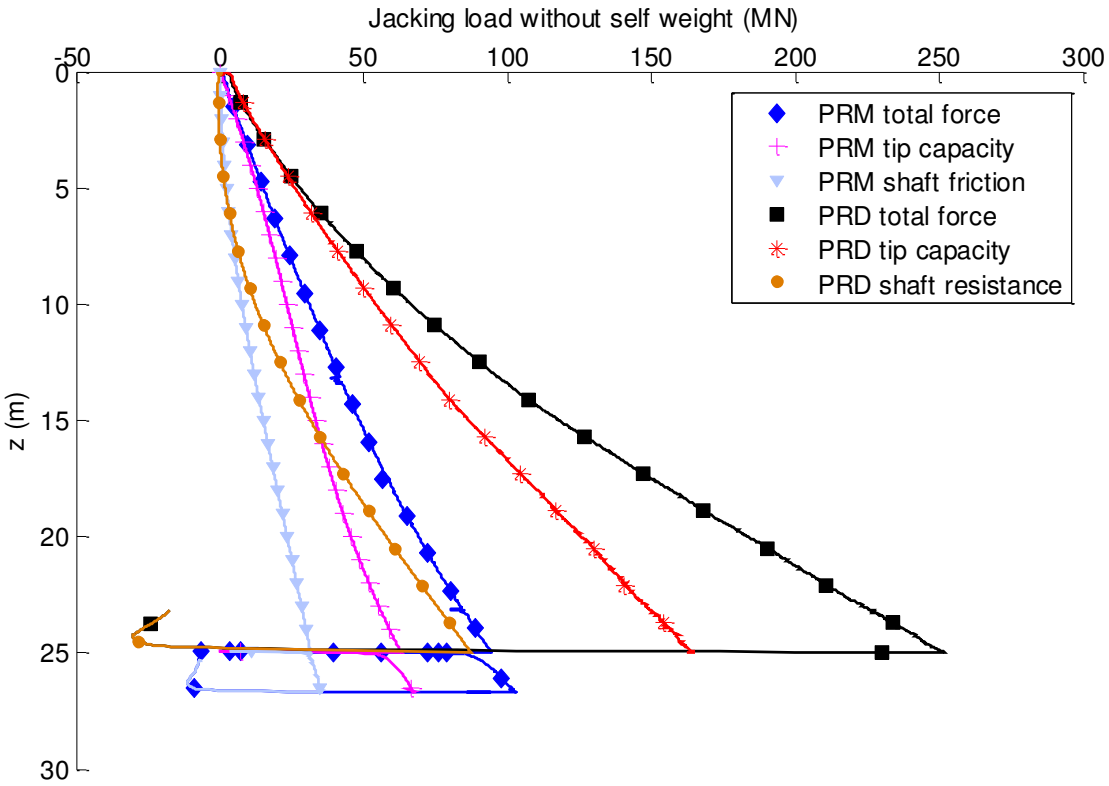

Figure 2-28 : PRD/PRM comparison

The comparison of the results shows a noticeable difference between push-in and pull-out shaft resistances. It also reveals that roughness affects the ratio between both resistances. This difference is well underlined in the literature. The results found in the literature generally show that the unit skin friction is higher in compression than in tension (Foray et al. 1998, De Nicola and Randolph 1994). Foray et al. (1998) also report that in addition to the changes in radial stresses along the pile shaft related to the loading path, the difference in skin friction may also be attributed to some residual loads produced by driving and generating negative friction stresses along the pile shaft when tension loads are applied. As regards the smooth piles, the ratio of the pull-out resistance to the push-in shaft resistance is around 0.8 for PSD and 1 for PSM. These values are in good accordance with those found in Gaaver (2013), who report that Poulos and Davis (1980) recommend that the estimate of the pile uplift capacity should be two thirds that of the downward shaft resistance. Schneider et al. (2008) underline that pile design methods use a value between 0.7 and 0.8 for the ratio between push-in and pull-out shaft resistances. On the other hand, for the rough piles, the push-in shaft resistance is about three times the pull-out resistance. This ratio is higher than the values found in the literature. This high ratio can be derived from the combination of the effects of the high

density with the high roughness of the piles which makes rough pile push-in shaft resistance higher than usual values.

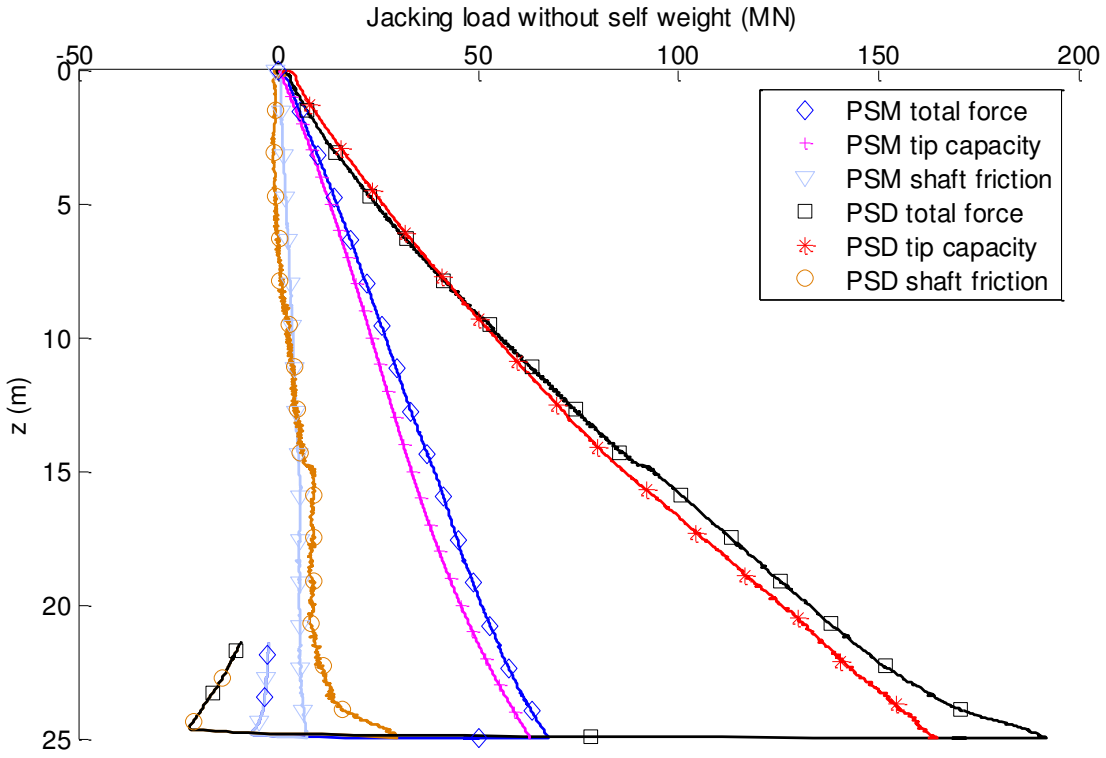

Figure 2-29 : PSM/PSD comparison

After the comparison between pile shaft frictions, a comparison of the skin frictions (shaft friction divided by the lateral surface of the pile) mobilized during the tests is made. The skin friction analysis of the PSM tests clearly shows the presence of a unit skin friction value ranging between 100 and 150 kPa during the jacking phase and equivalent to 100 kPa at maximum tension capacity. As regards the PSD pile, between jacking depths of 10 m to 20 m, the skin friction is about 200 kPa. At depths greater than 20 m, skin friction sharply increases up to 400 kPa at the end of the jacking phase and 350 kPa at ultimate tension. Pile PSM skin friction value is not far from the limit skin friction value recommended by the standards (90 kPa for NF P 94-262 and between 67 and 115 kPa for API RP2GEO 2011 and DNVGL). Pile PSD, on the other hand, presents some values higher than the standard limit skin friction in both compression and tension modes, an observation, which may be due to a very high density level.

The same analysis is then repeated for piles PRM and PRD. PRM shows an increase in skin friction as jacking progresses until reaching a value of about 500 kPa at the end of the jacking

phase and about 170 kPa at the ultimate tension. PRD reaches a very high skin friction value of 1350 kPa at the end of the jacking phase and about 500 kPa at the ultimate tension. The very high skin friction values, measured in this study, far exceed the value recommended by the standards as skin friction limit. This value can be explained, as mentioned above, by the very high density level and the pile roughness, which both play an important role as regards skin friction mobilization. A survey of the literature on high skin friction levels reveals a low number of studies focusing on this subject. In the research work of Clausen et al. (2005), a skin friction value of 200 kPa in tension is obtained. The authors also present a comparison with API, from which they conclude that API (API RP 2A 1993) results may be too pessimistic in very dense sand. Moreover, Clausen et al. (2005) determine a local skin friction value for long piles (down to a depth of 47 m) that reaches 550 kPa in tension for depth beyond 38 m. They also suggest that API skin friction values may be underestimated in comparison with some other deep foundation design methods such as Fugro (2004) (Kolk et al. 2005), NGI-99 and MTD-96 (Jardine & Chow (1996)).

The unit skin friction shows to be variable during the installation of the pile especially in the dense sand. In dense sand the profile of shaft friction showed to not increase linearly with depth. The shaft friction in dense sand can be strongly affected by the disturbance and the dilatant of the sand during the installation of displacement pile which also can increase with the increase of the depth and the lateral stresses.

Density also affects pile tip capacity. The pile tip capacity in dense sand is about three times higher than that in medium sand. This observation is consistent with the research work of Paik and Salgado (2003), which demonstrates that the ultimate unit base resistance increases significantly with increasing relative density and horizontal stress.

2.4.4.5 ICP comparison

Efforts have been conducted lately to assemble field tests in databases. These tests have been employed to check the validity of design methods for piles driven in sands (Lehane et al. 2017, Yang et al. 2017). The Imperial College Pile (ICP-05) showed a good performance in the previous studies and it is well used in Northern European offshore oil, gas and wind-energy projects. The second part of this study is dedicated to the comparison of the present centrifuge experimental results with those of the ICP method.

In the ICP method, there are two parameters that have to be taken into consideration to estimate the effect of the pile roughness on the shaft friction: (1) the friction angle δ_{cv} between

the pile and the surrounding sand and (2) the centre line average roughness R_{cla}. The friction angle δ_{cv} depends on the normalized roughness of the pile that is not impacted by centrifuge scaling laws. The centre line average roughness R_{cla} enters in the calculation of the dilatant increase of local radial effective stress ($\Delta\sigma'_{rd}$) during pile loading. In the ICP method, R_{cla} is inversely proportional to the radius of the pile. R_{cla} is also a length value impacted by scaling laws (N times higher in prototype scale than in model scale). As these two parameters can influence in separate way the shaft friction of the pile, the effect of each parameter on the calculation of the shaft friction is treated separately.

In the case of large diameter pile, δ_{cv} effect is more important than R_{cla} effect . $\Delta\sigma'_{rd}$ may contribute less than 5% of the capacity for piles with diameter larger than 1 m (Jardine et al., 2005). This is why the focus is made firstly on δ_{cv} effect with R_{cla} fixed here at R_{cla} = 0.01 mm to represent a slightly rusted steel pile. δ_{cv} used is varied until the resulting ICP shaft friction values best match with the experimental ones. Then, the δ_{cv} obtained is compared with other results found in the literature from studies (Tejchman and Wu (1995), Pra-ai (2013)) conducted with the same density and roughness levels than those used in this work.

Afterwards, the second step, R_{cla} effect of is studied by repeating these calculations using the R_{cla} prototype value (N times the model one).

The ICP pile capacity is calculated using the CPT test results described above. The use of the CPT method has always been problematic as regards centrifuge modelling due to the large CPT diameter used in laboratory conditions in comparison with the on-field one. This lead to a q_b/q_c ratio, in the case of the tests presented in this study, of 0.92 for medium sand and of 0.97 for dense sand. This ratio is higher than what is traditionally used in the literature but, however, not very different from White and Bolton (2005), who obtain a ratio of 0.9 from a database of 20 load tests by taking into account the effects of the partial pile embedment into the bearing stratum and the partial mobilization of base resistance. This result and the limitation that exists when using the centrifuge modelling both account for the use of the obtained CPT test results in the ICP calculation. Moreover, the ICP formula already considers the CPT diameter effect by normalizing the pile diameter by the CPT diameter. This consideration reduces some uncertainties related to the use of such adopted CPT results.

As regards the smooth piles, Figure 2-30 and Figure 2-31 display the comparison between experimental and ICP results for PSD and PSM, respectively. With the use of a friction angle

of 15° for PSM and 20° for PSD, the experimental results satisfactorily agree with the ICP shaft friction in both compression and tension modes (Table 2-12). The angles of friction obtained are in good accordance with the angles proposed by Tejchman and Wu (1995) and Pra-ai (2013) for smooth piles in dense and medium sand. ICP, on the other hand, slightly underestimates both the tip and total capacities for both piles (Table 2-12). The use of the prototype values of the roughness in the case of smooth piles (R_{cla} = 0.037 mm) has a minor effect on the results of the shaft friction.

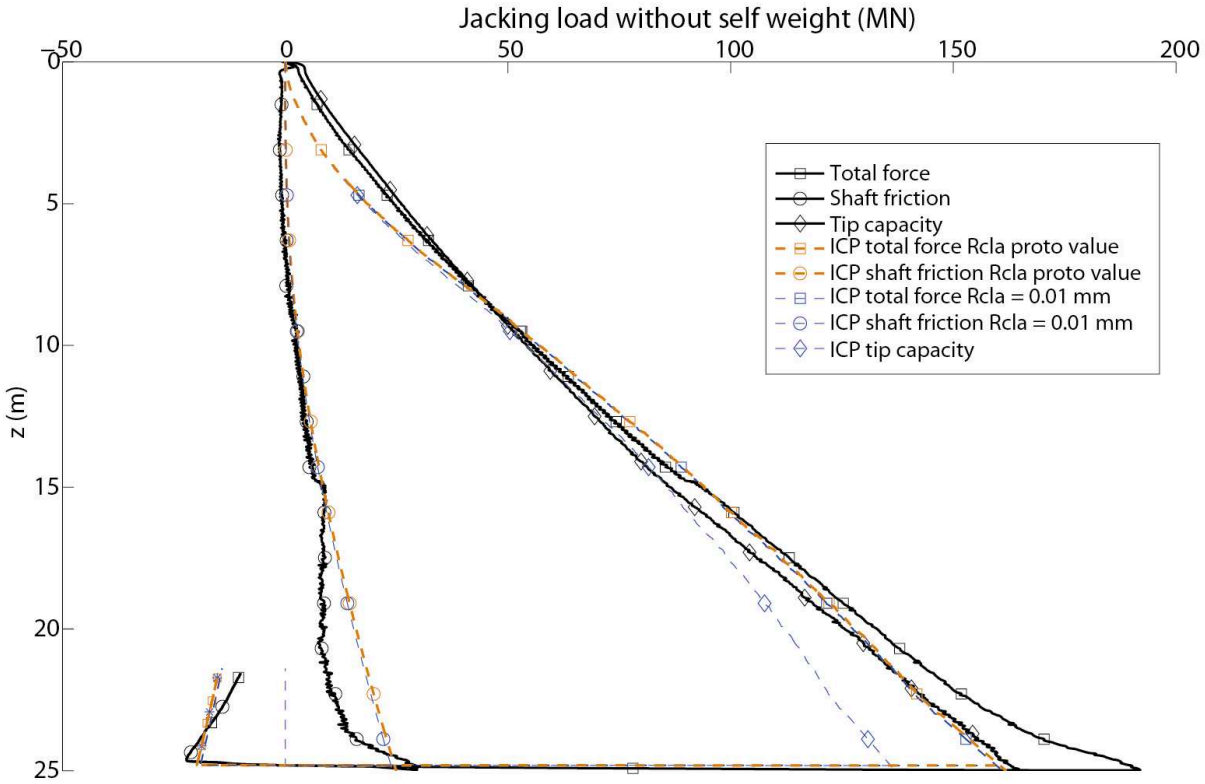

Figure 2-30 : PSD/ICP comparison

As regards the rough piles, Figure 2-32 and Figure 2-33 display the comparison between ICP and experimental results for piles PRD and PRM, respectively. The objective here is to determine at which angle ICP matches the pile tension resistance and measure the corresponding push-in shaft resistance. The reason why the comparison is made, with priority placed on the tension part of the pile, is that, as explained before, the pile push-in shaft resistance shows a very high force level, which cannot be obtained with the current standards. With the use of an angle of friction of 25° for PRM and 30° for PRD both ICP and the experimental tension capacities satisfactorily agree (Table 2-12). In compression mode, however, ICP provides a value about half that of the push-in shaft resistance. As seen before,

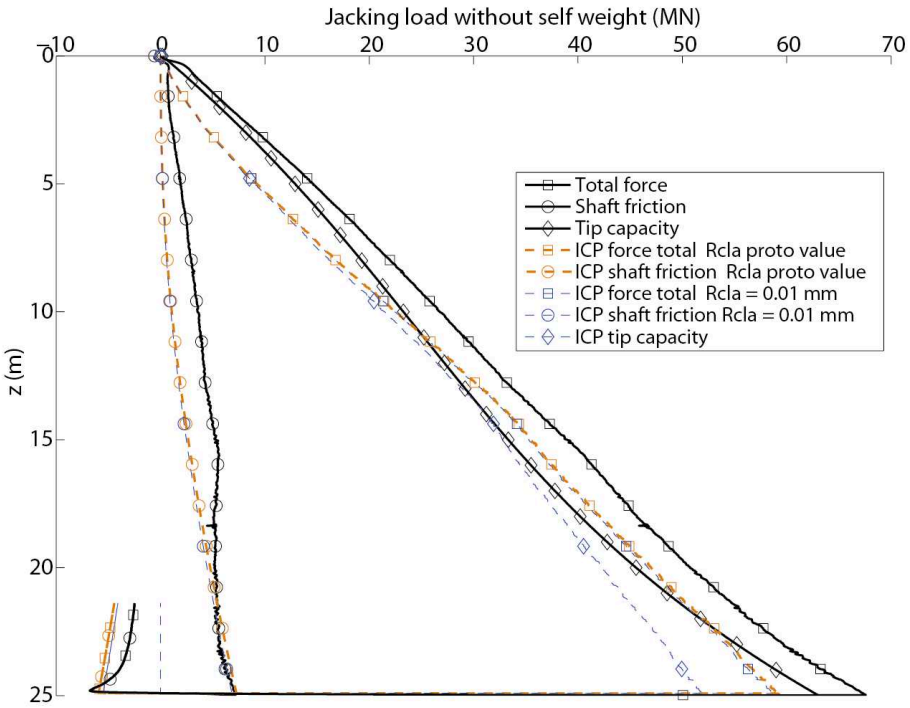

Figure 2-31 : PSM/ICP comparison

this result is expected to be due to the high experimental shaft resistance level. This high force level can be due to the very high density and roughness levels, which can also lead to high dilation and sand particle breakage during the jacking phase. The angles of friction obtained from the tension part of the piles are in good accordance with the angles found in Tejchman and Wu (1995) and Pra-ai (2013) for rough piles in dense and medium sand. Using the ICP method, the underestimate of push-in shaft resistance also produces an underestimate of the pile total capacity. In the case of the rough piles, the use of R_{cla} prototype value (1.8 mm) induces a big difference in the results. For example, the tension capacity in Figure 2-33 obtained by the ICP is about 66 MN compared to the 11 MN obtained from the experimental results. R_{cla} is in this case very high. It may be outside of the domain of validity of the ICP formulation. This is why the results obtained from using the prototype values of the R_{cla} can't be considered as reliable in the case of our rough model piles.

To conclude, the use of some reasonable angles of friction provides a good estimate of the experimental shaft resistance using the ICP method. On the other hand, the effect of the roughness can be considered as minor in the case of smooth piles but in the case of rough piles the effect of this parameter on $\Delta\sigma'_{rd}$ still not well quantified in the case of the centrifuge modelling because the use of the prototype values of the roughness can put the pile roughness

outside of the domain of validation of the design methods. For small scaled model in centrifuge, only the normalized roughness (divided by d_{50}) can be used in the design.

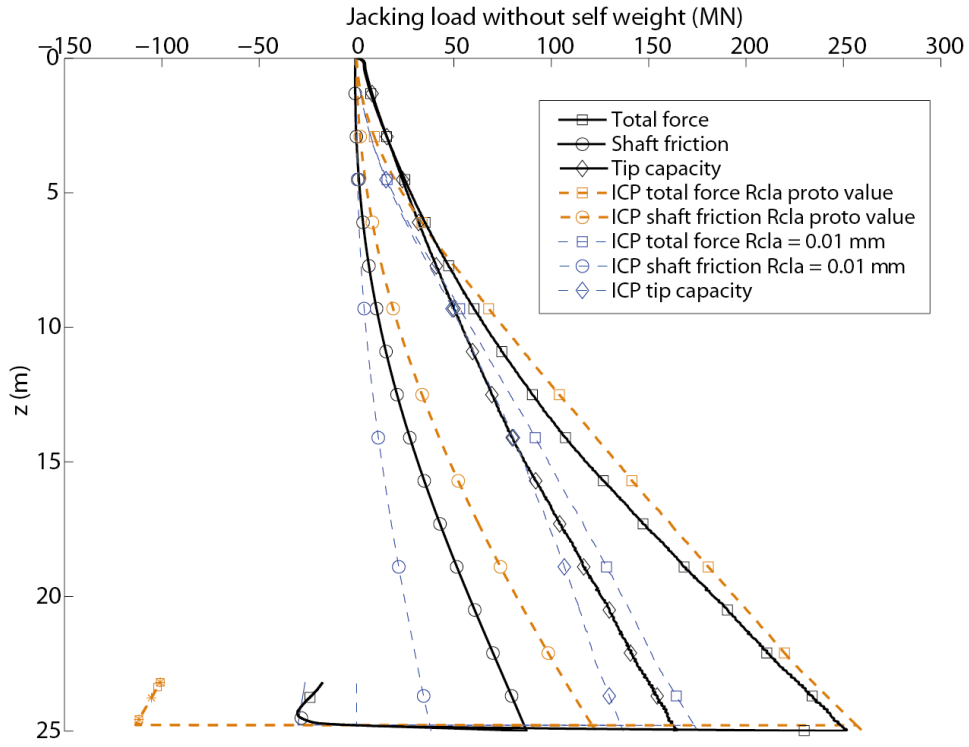

Figure 2-32 : PRD/ICP comparison

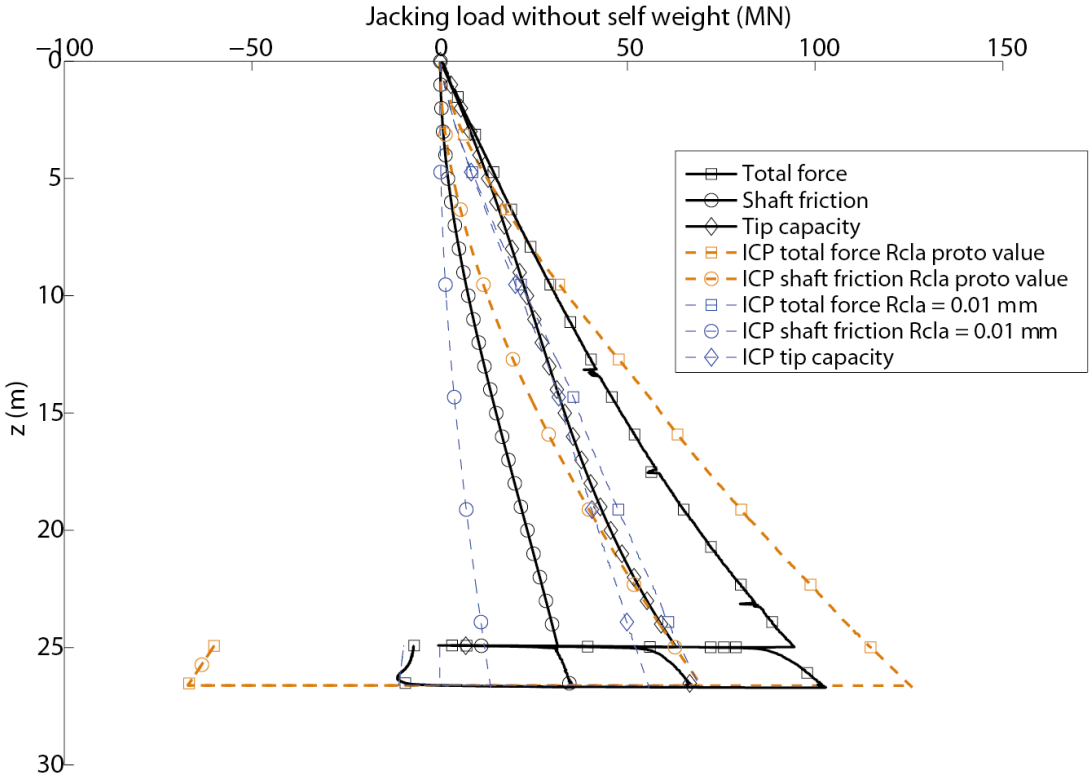

Figure 2-33 : PRM/ICP comparison

2.5 Conclusion

Model piles at scales 1/100 with an embedment depth of 250 mm have been tested, using geotechnical centrifuge at 100×g, in order to determine the parameters that can affect the axial capacity in sand. Based on a total number of 46 tests, 6 parameters have been investigated.

A. Firstly, different **installation techniques** have been compared:
   1. Jacked piles have a resistance **in compression** three times higher than that obtained with wished-in-place piles. The monotonically jacked piles at 100×g provide a capacity approximately 8% higher than the cyclically jacked piles.
   2. The impact of installation techniques on the **pull out** capacity of the piles has been studied. The most significant difference has been found for piles jacked at 100×g if they are jacked monotonically or cyclically. Despite the limitation to the study to one test for each installation method and to one studied density, the pull out capacity of the piles showed a clear tendency to increase with the increasing number of the installation strokes. The results show a pull out capacity gain of up to 67% with increasing cyclic installation strokes. The explanation discussed in this study has proposed that a possible relationship may exist between the gain in the capacity and the dilation and crushing of sand usually observed in cases where rough surfaces are in contact with dense sand.
   3. For both approaches a comparison with design standards has been made. Standard design has proved very conservative compared to experimental results. In addition, no approach has been found in these methods to predict the gain in capacity found in the pull out tests.

B. The effect of **sand density** and **saturation** is then studied:
   1. The present study first suggests that the saturation of dense sand has significant influences on plug creation during pile installation.
   2. The piles installed in dry sand present some greater capacities than the piles installed in saturated sand in both tension and compression modes.
   3. The displacement until tension failure differs depending on the density and water content conditions. Its values do not always equal the conventional value of 10% of B.

4. The initial stiffness is affected by sand density and saturation. The initial stiffness increases with sand density being, however, lower in saturated sand than in dry sand. A linear relationship between the jacking load and the embedded volume of the tested piles is described.

C. The effect of **pile diameter** is also discussed:

1. The decrease in pile diameter enhances plug formation in open-ended piles.
2. The ratio of the tension to the compression capacity decreases as diameter increases.

D. Concerning the effect of **pile tip geometry** (open or closed-ended):

1. Open-ended piles showed greater tension capacities than closed ones.
2. The ratio of the tension to the compression capacity is systematically larger for open-ended piles than for closed-ended piles.

Table 2-13 resume the effect of the different parameter on the compression and tension capacities.

A comparison between the experimental results and the existing design codes used for offshore wind turbine design shows that:

- In compression mode, the design codes studied reveal different degrees of conservatism in comparison with the experimental results. ICP is closest to the experimental results. Then comes NF, whose results are approximately half of the experimental capacities. Finally, we find API and DNVGL, which are the most conservative design codes and give results ranging from 20% to 35% of the experimental capacities without the limitations suggested in the codes. With the use of these limitations, both standards are even further removed from the representation of the real pile behaviour.
- In tension mode, ICP performance is good in dense sand. However, both ICP and NF provide a large overestimate of the pile tension capacities in medium dense sand. API and DNVGL also overestimate the tension capacity in medium dense sand while underestimating it in dense sand.
- The performance of the ICP method in the case of open-ended piles appears to depend on the accurate estimate of the pile plugging state and on the choice of the best plugging condition between the different available conditions found in the design code.

Table 2-13 : Effect of the studied parameters on R_c and R_t

	Density (↗)	Saturation (↗)	Open ⟶ Closed-ended	B (↗)
R_c	↗	↘	↗	↗
R_t	↗	↘	↘	↗

E. the effect of **pile roughness** on the shaft friction is finally discussed:

1. The increase of roughness show that the pull out shaft resistance increases by 36% in dense sand and by 57% in medium sand. The push-in shaft friction, moreover, triples as roughness increases.
2. Rough piles, indeed, present push-in and pull-out shaft resistances three times higher in dense sand than in medium sand. Smooth piles, moreover, reveal some push-in and pull-out shaft resistances four times higher in dense sand than in medium sand.
3. The shaft resistance ratio of tension to compression is 0.8 in dense sand and 1 in medium sand for smooth piles. Rough piles present a push-in friction about three times higher than the pull-out friction in both densities.
4. The comparison of the experimental shaft resistances with the resistances obtained using the ICP methods show that the use of a friction angle of 15° and 20° for smooth piles provides a good estimate of the ICP shaft friction in both medium and dense sand. On the other hand, the 25° and 30°, respectively, are the friction angles that used in the ICP to match the tension shaft friction of rough piles in medium and dense sand.

This research provides some interesting findings, which are needed in the field of understanding the behaviour of offshore piles better. It shows also that if more work are carried out to improve the performance of the existing standards used in the field of offshore pile design such improvement can generate a significant cost reduction in the geotechnical part of wind turbine construction.

3 Pile subjected to lateral loading

3.1 Introduction

The offshore piles of jacked structures are submitted not solely to axial loading but also to severe laterals loads originated from the waves, the current and the wind. This makes necessary to study these foundations also under lateral loadings.

After the presentation in the previous chapter of the parameters influencing the axial capacity of piles, this chapter is focusing on the lateral capacity of piles using centrifuge modelling of instrumented piles. The inside instrumentation of the flexible piles used for the lateral loading induces a closed-end. The offshore piles driven in reality are on the other hand open-ended steel piles. This is why parameters like the roughness and the pile tip type (open or closed) which cannot be studied using instrumented piles are presented in the first chapter.

In order to design piles under severe lateral loads DNVGL-ST-0126 (DNV GL,2016) method is used, which is based on the load-transfer approach known also as the p-y method. The pile behaviour is modelled according the beam theory and the soil is simplified as a series of nonlinear springs (Figure 3-1). These springs are described by using the p-y curves or reaction curves, which define the load displacement relationship for the soil/pile interactions between soil and pile. The pile design p-y curves considered for design are monotonic functions that can possibly reach a plateau for large displacements. Initially, the p-y model has been developed by Matlock (1970) for soft clay, and by Reese et al. (1974) for sand. Gradually, however, others p-y models have been developed for both sand and clay (Murchison and O'Neill 1984, Kondner 1963, Scott 1980, Wesselink et al. 1988). Others tried to develop simpler method as the characteristic load method developed by Duncan et al. 1994. Note especially the research works by Reese et al., 1974 and O'Neill and Muchinson, 1983, which led to the establishment of recommendations in standards for oil and gas installations (DNV, 1977 and API, 1993). In 2004, these recommendations have been adopted in the standard Design of offshore wind turbine structures (DNV 2004), on which the DNV GL 2016 Standard is based. This standard represents the current state of the art for the design of offshore wind turbine piles.

In this chapter the methods used for design of laterally loaded piles as well as the parameters that can influence their lateral capacities are presented. The literature review will be followed by the experimental campaign realized on 18 mm instrumented pile using centrifuge modelling at 100×g. Monotonic lateral loading followed by cyclic loading are applied on the piles. The effect of the installation method of the pile, load eccentricity, sand density and

saturation on the lateral capacity of piles is studied. The moment profiles and the lateral displacement of the pile are also presented. Finally, the monotonic and cyclic p-y curves of the different tests are obtained and compared with the p-y curves of the DNVGL code.

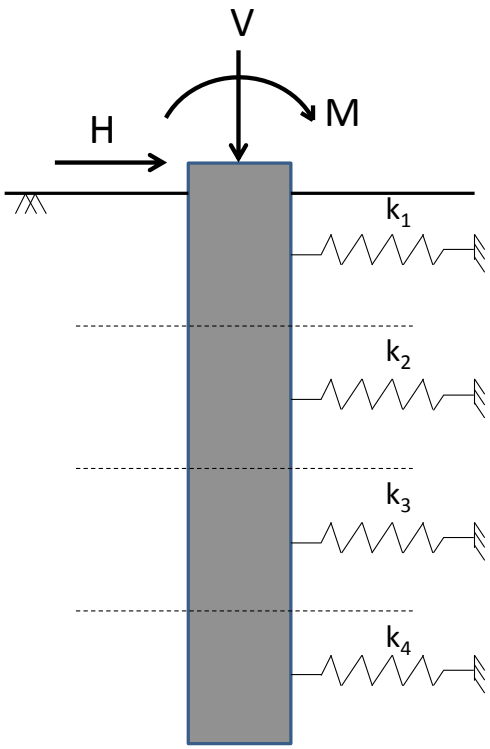

Figure 3-1 : p-y model for lateral loading (for 4 layers discretization)

3.2 Literature review

3.2.1 Classification of piles under lateral loading: flexible and rigid

The response of pile under lateral loading depends on its flexular rigidity and the rigidity of the soil surrounding it so on the soil-pile relative stiffness. In general piles are classified under three types: flexible, semi-rigid and rigid depending on its transfer length (Menard et al. 1969, Frank 1999) defined by the following formula:

$$l_0 = \sqrt[4]{\frac{4E_pI_p}{E_s}} \tag{24}$$

Where:

E_p is the modulus of elasticity of the pile

I_p is the moment of inertia of the pile (m^4)

E_s is the modulus of elasticity of the soil

This transfer length is then compared with the embedded depth of the pile (D). If this depth D $< l_0$the pile is considered rigid, D $> 3l_0$ the pile is flexible and if $l_0<$ D $< 3l_0$ the pile is semi-rigid. This classification assumes homogeneous soil and pile properties, which corresponds in most of the cases to a very simple geotechnical model.

This classification is important because the behaviour of the pile is dependent on its rigidity. In the case of short rigid pile, the behaviour of the pile is controlled by its displacement and rotation. As the pile is very rigid it undergoes an overall movement as one stiff element and the lateral deformation of the pile is negligible compared to its displacement and rotation this is generally the case of large monopiles used in offshore construction. On the other hand, in the case of elongated flexible pile, its movement is essentially dependant on its deformation. The shallow layers of the soil are the most mobilized and resist to the movement of the pile. The tip of the pile is generally considered fixed in the soil and no displacement is considered to occur there.

3.2.2 Different types of loadings

The types of loadings that can be applied laterally on piles are listed under two categories:

- Monotonic loadings: the pile is subjected to a monotonic force at the head.

- Cyclic loadings: the pile is normally subjected to a series of identical cycles. This cyclic loading can be either one-way or two-way loading and can be identified using the following parameters:
  - The number of cycles N and the frequency of the cyclic loading
  - The mean value of the applied lateral load H_m
  - The half amplitude of the cyclic component H_c

These parameters are presented in Figure 3-2. The load csiman oscillates between $H_{max} = H_m + H_c$ and $H_{min} = H_m - H_c$ and the sign of the ratio H_{min}/ H_{max} is used to determine if the loading is two-way or one-way. Two-way if it is negative and one-way if it positive.

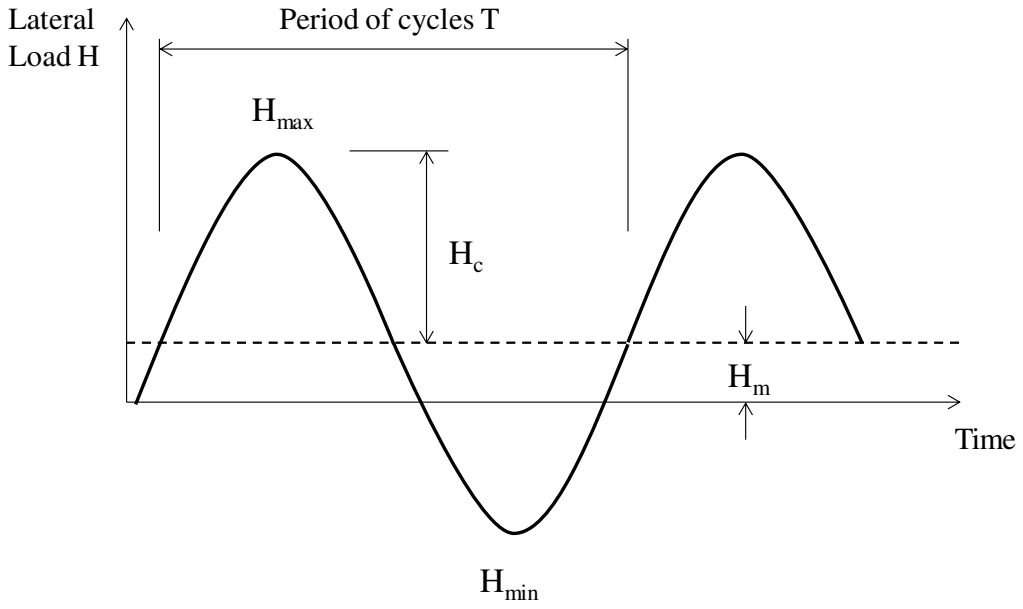

Figure 3-2 : Parameters of the cyclic lateral loading

3.2.3 Design of laterally loaded piles

As it is mentioned before the design of a pile under lateral loading is based on the load-transfer approach. This method models the pile behaviour following the beam theory and the soil is simplified as a series of nonlinear springs (Figure 3-1). The springs are described by the p-y curves or reaction curves which define the load displacement relationship for the interaction between soil and pile.

For the methods based on reaction curves, the soil reaction p is related to the displacement y at a determined depth z by a coefficient of soil reaction k following this expression:

$$p(z) = k(z).y(z) \tag{25}$$

k(z) is expressed in N/m^3

p(z) is soil pressure in N/m^2

y(z) is the horizontal displacement in m

This expression can be equally written in the form:

$$P(z) = E_s(z).y(z) \tag{26}$$

Where: P is the soil reaction in N.m and E_s is the soil modulus reaction taken into account that $E_s = k.B$ (B is the pile diameter).

So what is important is to determine the expression of the soil modulus E_s. In the literature different authors were interested in this coefficient and different expression are proposed:

- Terzaghi (1955) suggests the following expression for sand:

$$E_s = 0.74A\gamma z \tag{27}$$

Where:

A is a dimensionless coefficient function of the sand density (Table 3-1).

γ is the density of the soil

z is the depth

Table 3-1 : Coefficient A versus sand density

Sand density	Loose	Medium	Dense
A	100-300	300-1000	1000-2000

- Ménard et al. 1969 give an expression of the coefficient E_s in function of the pressiometric modulus E_M , the pile diameter B, a reference diameter B_0 equal to 0.6 m and a coefficient α dependent on the soil type.

$$\frac{E_s}{E_M} = \begin{cases} \dfrac{3}{\frac{2}{3}\left(\frac{B_0}{B}\right)\left(2.65\frac{B}{B_0}\right)^{\alpha} + \frac{\alpha}{2}} & \text{for } B > B_0 \\ \dfrac{18}{4(2.65)^{\alpha} + 3\alpha} & \text{for } B < B_0 \end{cases} \tag{28}$$

- Poulos (1971) took a strong hypothesis when suggesting a modulus coefficient constant with the depth and depending only on the soil type (Table 3-2)

Table 3-2 : Mean values of E_s for cohesionless soil

Sand density	Interval of the values of E_s (MPa)
Loose	0.896-2.068
Medium	2.068-4.137
Dense	4.137-9.652

The method based on the use of p-y curves to express the relation between the soil reaction and its displacement is the one used normally in the standards to design piles under lateral loadings. These curves can be obtained from in-situ or laboratory tests and their expression is different depending on the corresponding standards. The expression of the p-y curves in the API and DNVGL is presented in the following section.

In general API and DNVGL give similar functions for the p-y curves. The p-y curves considered for design are monotonic functions, that reach possibly a plateau for large displacement. Initially the p-y model was developed by Matlock (1970) for soft clay, and Reese et al. (1974) for sand but eventually others p-y models were developed for sand and clay (Murchison and O'Neill 1984, Kondner 1963, Scott 1980, Wesselink et al. 1988). Although all these important studies, the work of Reese et al. 1974 and O'Neill and Muchinson (1983) led to the recommendations in the standards (DNV, (1977) and API, (1993)) for oil and gas installations. In 2004 these recommendations were adopted in the standard Design of offshore wind turbine structures (DNV, 2004) on which the standard cited above (DNV GL, 2016) is based. This standard represents the current state of the art for design of the pile of the offshore wind turbines.

The soil reaction is a hyperbolic formula having as a limit the ultimate reaction of soil for high displacement.

$$P = AP_u \tanh\left(\frac{kz}{AP_u} y\right) \tag{29}$$

Where :

A factor depending on the type of the loading

$$A = \begin{cases} 0.9 \text{ for cyclic loading} \\ \left(3 - 0.8\frac{z}{B}\right) \geq 0.9 \text{ for static loading} \end{cases}$$

z is the depth (m)

y is the lateral displacement (m)

k is the initial modulus of subgrade reaction given in Figure 3-3

P_u is the static ultimate lateral resistance recommended to be calculated as :

$$P_u = \begin{cases} (C_1 X + C_2 B)\gamma' X & \text{for } 0 < X \leq X_R \\ C_3 B \gamma' X & \text{for } X > X_R \end{cases}$$

Where the coefficients C_1, C_2 and C_3 depend on the friction angle φ as shown in Figure 3-4 and where X is the depth below soil surface and X_R is a transition depth, below which the value of $(C_1 X + C_2 D)\gamma' X$ exceeds $C_3 D \gamma' X$. Further, B is the pile diameter and γ' is the submerged unit weight of soil.

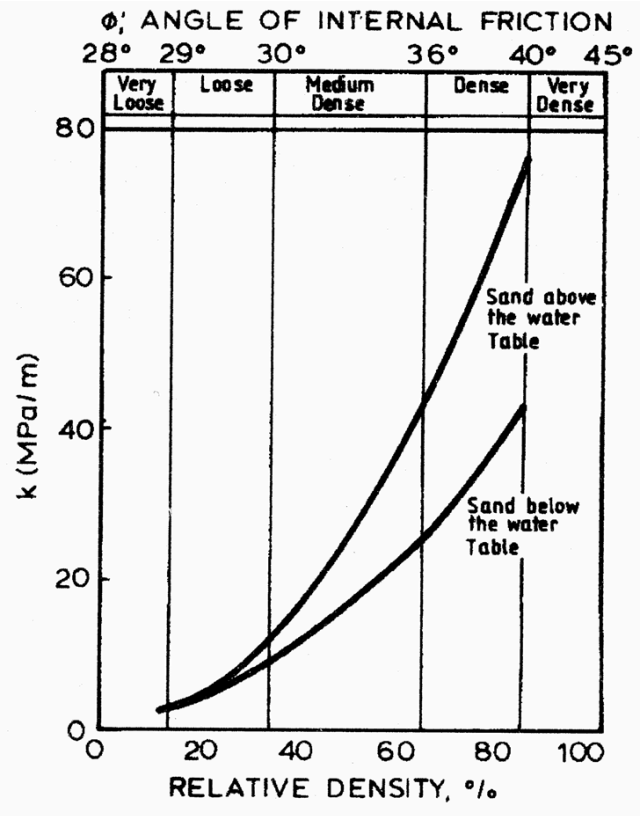

Figure 3-3 : Initial modulus of subgrade reaction k as function of friction angle φ (DNVGL 2016)

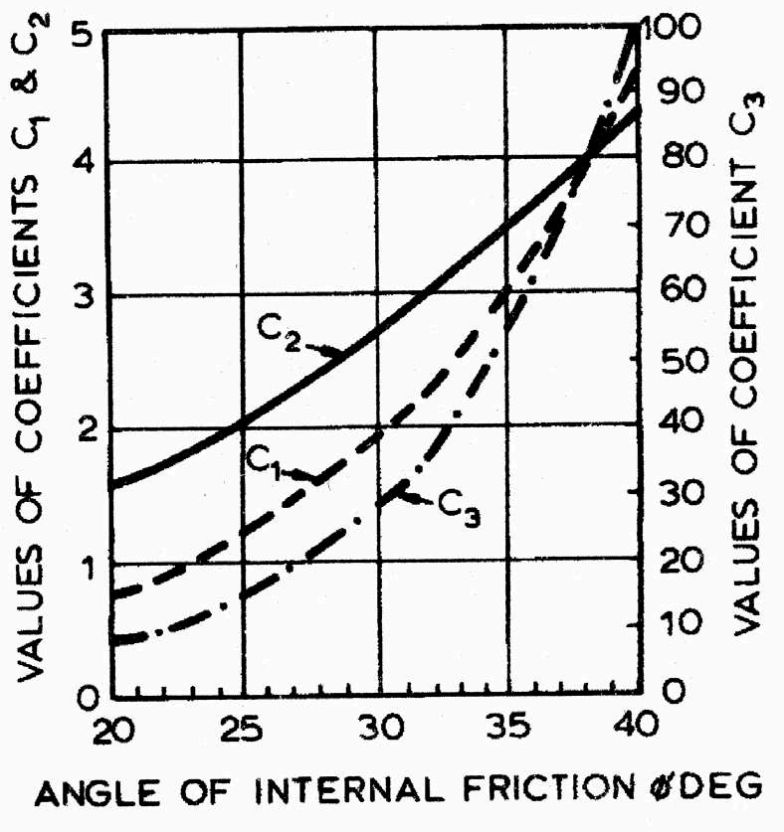

Figure 3-4 : Coefficients as functions of friction angle (DNVGL 2016)

3.2.4 Parameters that can affect lateral behaviour of piles

3.2.4.1 Pile installation method

In the literature, despite the existence of a few in-situ studies (Baguelin and Jézéquel (1972), Bigot et al. (1982)), centrifuge modelling is predominantly used to investigate the lateral behaviour of piles (Mezazigh et al., 1994, Mezazigh, 1995, Rosquoet et al., 2007, Dyson and Randolph, 2001, Rakotonindriana, 2009). Scott (1981) is cited by Kong and Zang (2007) as the first author to model laterally loaded piles in a centrifuge. In this study, a small model pile is installed at 1×g while another larger pile is installed by raining the sand around it. The results show that neither installation method represents the prototype conditions accurately. Jacking (or driving) model piles in flight better simulates prototype conditions, in particular lateral stress distribution after completion of the installation. Some other studies carried out to examine these effects are presented in the works of Kim et al., (2004) and Dyson and Randolph, (2001). Both studies demonstrate the significant effect of pile installation methods on the stiffness of the load transfer curve. Kim et al. (2004) present the load-displacement curves and the p-y curves at 1B, 3B and 6B, respectively, for a preinstalled pile and some piles driven at different driving energies. They show that the lateral pile loading of driven

piles is higher than for the preinstalled pile and that it increases as the driving energy increases. They also observe that the soil-pile reactions of the load-transfer curves at a certain depth are larger for driven piles than for the preinstalled pile and that the soil-pile reactions of the driven piles increase as the driving energies increase. On the other hand, Dyson and Randolph (2001) have studied four different installation methods to quantify their influence on the lateral response. They present the pile head load-displacement responses and the load-transfer curves derived from the tests at two depths of 1.3 and 5B, respectively. Pile head load-displacement responses are given in the stiffness decreasing order; driven piles, piles jacked at 160×g, 1×g and, finally, preinstalled piles. The stiffness of the load-transfer curves follows the same trends as the pile head response at shallow depths but the differences are substantially reduced with a depth of five diameters. In the experimental campaign conducted by Huang et al. (2001) where both bored and driven groups piles are used, bored pile installation proves to have a loosening effect on the surrounding soil down to a depth of approximately 6 m. This can cause the soil to reduce its capacity to resist lateral loading within the bored pile group. The installation of driven precast concrete piles, on the other hand, appears to increase the density of the surrounding soil. McVay et al. (1994) have been among the first to individually drive a nine-pile groups in-flight and then laterally load them without stopping the centrifuge. An increased lateral resistance of the piles is observed when driven at the prototype stress levels compared with the 1×g installation. Significant sand dilation is observed at the 1×g installation compared with the 45×g installation in dense sand.

3.2.4.2 Load eccentricity

Another factor, which might influence pile lateral behaviour is load eccentricity above the soil surface. Yan and Byrne, (1992), have found that pile head loading eccentricity significantly affects pile head response and bending-moment distribution. A higher loading eccentricity causes a higher bending moment in the pile and a softer pile head response. The depth of maximum bending moment, however, does not change significantly with the loading eccentricity. These authors have also underlined that loading eccentricity affects the soil-pile interaction at shallow depth. Higher loading eccentricity leads to softer P-y curve. At deeper depths, however, the effect is insignificant. Hokmabadi et al., (2012), conclude that one of the most significant parameters influencing monopile behaviour and, particularly pile head displacement prediction is monopile free length. According to this study, pile head displacement increases significantly when the pile free length increases. Despite these findings on the influence of the installation method and of load eccentricity on the lateral

behaviour of piles found in the literature, DNVGL methods do not take these relevant factors into account.

3.2.4.3 Sand saturation

Pile lateral behaviour is significantly affected by sand saturation. In DNVGL, this factor is taken into account by changing the effective sand weight and the k factor that can be deduced from the DNVGL code and depends on sand density and saturation. The influence that causes sand saturation on pile lateral response has always been taken into account in design codes by using effective stress and dimensional approaches. This consideration is based on the fact that piles behave like in drained conditions in sand. Consequently, using effective stress makes it possible to take the saturation effect into account. However, with the development of offshore structures, like offshore oil structures and offshore wind turbines, installed in fully saturated sand, increasingly raised the problem of the structure pile lateral response. Phanikanth et al. (2010) use the method of the subgrade reaction proposed by Reese and Matlock (1956) to develop a Matlab program that allows for the behaviour study of laterally loaded piles. The parametric study described illustrates the response of laterally loaded piles in three different sand densities: loose, medium and dense. For each sand density studied, a dry or submerged condition is stipulated. As regards short rigid piles, the transition from the dry to the submerged condition causes an increase in deflection of about 58%, 30% and 27% for loose, medium and dense sand, respectively. As for flexible piles, the increase is of 33% 22% and 25% for loose, medium and dense sand, respectively. Despite the importance of previous studies on saturation effects on pile lateral behaviour, experimental work is always appreciated and essential to clarify any bias or incertitude that may exist in this domain. This is why experimental campaigns, during which the saturation effects can be examined, are necessary.

3.2.4.4 Effect of cycles

Cycles can affect not only the global behaviour of piles (pile displacement and moment) but also the local behaviour represented by the p-y curves. Moreover, the effect of cycles on the lateral behaviour of piles can itself be affected by the installation method of piles, the load eccentricity and sand saturation.

3.2.4.4.1 Global behaviour

The effect of the cycles on the lateral displacement of the pile head and on the maximum moment in the pile are between the main parameters that was discussed during the studies on the lateral cycle behaviour of piles in the literature.

It is known that the cyclic loading usually lead to an increase of the pile head displacement which makes essential to study this increase to be sure that the pile will still be in acceptable limit of displacement after the cyclic loading. Two main laws can be found in the literature for the expression of the piles displacement as function of the number of cycles: (1) The logarithmic law: $y_N/y_1 = 1+\alpha \ln N$ (Lin & Liao (1999)), and (2) the power law: $y_N/y_1 = N^m$ (Long & Vanneste (1994)). y_1 and y_N are the pile head lateral displacements when first loading is applied at N^{th} cycle, respectively. Coefficient α, called degradation parameter, represents the displacement amplification due to the cycles.

In the report of the Solcyp Project (2017), an extensive literature review of the different coefficient α values obtained is presented and summarized in Table 3-3. Depending on the authors, α ranges from 0.087 to 0.25. The degradation parameter is also highly dependent on soil density, installation method and type of cyclic loading. Lin and Liao (1999) propose a detailed expression of α (see Table 3-3) including three parameters directly dependent on soil density, installation method and type of cyclic loading: (1) k_1 is a decreasing function of soil density, which varies from 1.3 (for loose sand) to 1 (for dense sand), (2) k_2 depends on the pile installations mode (k_2 generally varies from 0.8, if pile installation disturbs soil characteristics by increasing density, and 1.8 if it does not) (3) k_3 depends on the type of cyclic loading and varies from 0.09 for two-way cycles to 1 for one-way cycles. As regards the expression of the power law, the coefficient m quantifies pile head displacement amplification in relation to the cycles. With a goal similar to the logarithm expression, Solcyp Recommendations (2017) present an extensive literature review of the values of m obtained in various conditions of soil density, pile installation method and cyclic load characteristics (Solcyp Recommendations, Table 8.5, p.247). Despite the considerable amount of effort devoted to this subject in the literature, more work needs to be carried out to improve our understanding of the cycle impact on pile head displacement. Many coefficients might affect pile head displacement. While some of them, like installation method and sand density, have already been addressed in a number of studies, we need more information to understand these parameter effects better. Moreover, some important parameters for the design of offshore wind turbines, like loading eccentricity, have not yet been investigated.

As regards the maximum bending moment inside the piles, some authors note an increase in the maximum moment values when the number of cycles increases. The depth of the maximum moment also increases with the number of cycles (Meimon et al. 1986, Hadjadji et al. 2002, Verdure et al. 2003, Rosquet et al. 2007). The maximum moment increase can be attributed to the decrease in the reactions occurring at the soil surface and to load transfer to the deeper layers.

Table 3-3 : Overview of values put forward for the coefficient α in the case of sandy soils

Authors	Type of cyclic loading	Degradation parameter α	Comments
Bouafia (Bouafia 1994)	One-way $H_{min}/H_{max} = 0$	0.18-0.25	Extremely low number of cycles (4-5)
Lin and Liao (Lin & Liao 1999)	$-1<H_{min}/H_{max}<0.1$	$\alpha = 0.032 \frac{L}{T} k_1 k_2 k_3$ (varies from 0.02-0.24)	α depends on the soil density, the mode of installation of the pile and the type of cyclic loading (α does not depend on H_{max} and is greater for one-way loading)
Hadjadji et al. (2002)	One-way $H_{min}/H_{max} = 0.33$	0.087	The pile underwent various lateral stresses before the cyclic sequence of 10000 cycles
Verdure et al. (2003)	One-way $H_{min}/H_{max} \geq 0$	α varies from 0.04 to 0.18 depending on the ratio H_c/H_{max}	$\alpha = 0.18(H_{max} - H_{min})/H_{max}$
Rosquet et al. 2007	One way	$\alpha = 0.08\left(\frac{H_{max} - H_{min}}{H_{max}}\right)$	
Li et al. (2010)	One-way $H_{min}/H_{max} = 0$	0.17-0.25	α increases slightly with H_{max}
Peralta (2010)	One-way $H_{min}/H_{max} = 0$	0.21	α is independent of H_{max} (flexibles piles)

3.2.4.4.2 Local behaviour

A survey of the literature reveals that a considerable amount of effort has been devoted to the problem of cyclic lateral loading effects on pile behaviour (Lin et Liao 1999, Le Blanc et al. 2010a, Achmus et al. 2009, Le Blanc et al. 2010b). A decent number of approaches are proposed for improving the consideration of the effect of cyclic lateral loading by the reduction of the static coefficient value of the soil reaction (Prakash 1962, Broms 1964, Davisson and Salley 1968, Alizadeh and Davisson 1970). The p-y model developed by Reese

et al. (1974) considers the cyclic loading effect by using a degradation factor empirically obtained to predict the cyclic p-y relationships based on the static p-y curves. Li et al. (2010) indicate that, under this approach, the cyclic p-y curves are independent of the number of cycles. Long and Vanneste (1994) have collected the data from thirty-four full-scale cyclic lateral loading tests conducted on piles in sand to identify the factors affecting cyclic behaviour. Data include soil density, pile type, installation method and cyclic loading characteristics. They also enhance the p-y approach by considering the effect of the number of cycles. However, a maximum of only fifty lateral loading cycles is carried out in the tests considered. Achmus et al. (2009) also point out this problem and specify that the p-y curves established under cyclic loading conditions are based on field tests performed with less than 200 cycles. Moss et al. (1998) emphasize that p-y curves do not account for the permanent deformation, which accumulates with increasing cycles. The qualitative results obtained by Chang and Whitman (1988), Little and Briaud (1988) and Kramer and Heavey (1988) show that the pile behaviour differs whether the applied load is one-way or two-ways. One-way loading produces higher cumulative stresses and deformations (Verdure et al. 2003).

3.2.5 Conclusion

With all these factors that can influence the behaviour of the piles, the necessity of high quality cyclic tests in controlled conditions and with the possibility to realize large number of cycles is highly needed, in order to (1) examine the influence of installation method, load eccentricity and sand saturation on the lateral behaviour of piles (2) calibrate the design approaches upon these tests. In this field of activity, centrifuge testing is the most adequate, economic and recommended experimental method. In the literature, centrifuge testing is predominantly used by several authors in order to investigate the pile lateral response (Rosquoet 2004, Khemakhem 2012, Zhang et al. 2011,Klinkvort 2012). With this aim in view, a detailed experimental investigation carried out in the centrifuge to examine the influence of installation method, load eccentricity and sand saturation and cycles on the lateral behaviour of piles in medium dense sand.

3.3 Experimental campaign

3.3.1 Model soil

The model soil is a poorly graded NE34 Fontainebleau sand (Table 2-3). Six rectangular strongboxes (Table 3-4) are prepared with two different relative soil densities (58% ± 0.5 % and 99% ± 0.5 %, respectively) achieved by filling the strongboxes with sand using the air pluviation technique. The unit dry weight of these strongboxes is 1.59 g/cm^3 and 1.70 g/cm^3 for the medium dense sand and the dense sand respectively. More details on the model soil are presented in the appendixes. Appendix 4 discusses the sand mass characterisation and preparation. Appendix 5 presents the procedure of determination of ρ_{dmin} and ρ_{dmax} and finally Appendix 6 presents the laser particle size distribution realized on the used sand.

Two boxes are connected to a water tank by the underside up to full saturation, which gives an effective unit weight of 0.99 g/cm^3 and 1.04 g/cm^3 for the medium dense saturated sand and the dense saturated sand respectively.

3.3.2 Model pile

Two types of 18 mm-diameter model piles of are used: (1) a rigid full aluminium rod with an embedded depth of 200 mm on model scale, i.e., an embedment depth of 20 m on the pile prototype scale. (2) The second model pile is a 1.5-mm thick flexible aluminium close-ended pile with an embedded depth of 200 mm, i.e., a thickness of 0.15 m and a depth of 20 m on prototype scale. This model pile is equivalent to a prototype pile with a bending stiffness of 19.74 GN.m2 at 100×g.

The flexible pile (Appendix 2) is instrumented from inside using 16 levels of quarter-bridge strain gages diametrically opposed for bending moment measurement. The difference between the results of the two gages located in the same level is calculated. Then this result is multiplied by the coefficient obtained from the calibration of the pile under lateral loading to obtain the bending moment at each level. Pile instrumentation from inside is a key aspect of the present study and gives the present study an important advantage and opportunity to jack piles, even in flight, without damaging the strain gages. The pile external geometry and roughness (R_n = 0.011) are perfectly controlled. The transfer length l_0 calculated for this pile using the method described by Rosquet (2004) is 6.29, which gives a value of 3.18 for the B/l_0 ratio. This result is lower than the ratio obtained for the pile studied by Rosquet (2004) (4.3).

We can therefore consider that the pile studied in the present work is more rigid than the pile studied by Rosquet (2004).

The ratio of the pile diameter B to the Fontainebleau sand d_{50} is 18/0.21 = 85.7, a result, which is higher than the minimum limit (45) recommended by (Garnier et al, 2007) to eliminate all grain size effects.

3.3.3 Experimental campaign and tests table

The parametric study performed in the centrifuge on laterally loaded piles focused on the following parameters: installation process, load eccentricity and sand saturation. Moreover, the effect of these parameters on the cyclic behaviour of piles is studied by realizing up to 1000 cycles after the monotonic loading.

Before performing the loading test, a procedure of stabilisation is realized for each sand strongbox in order to make sure of the good homogeneity of the sand massif.

After the installation of the experimental set-up and before any tests is realized the strongbox is submitted to a cycles of ascend and descend of the centrifuge acceleration. In the present thesis and as all the tests will be realized at 100×g, the ascend of the acceleration will reach 100×g. In total 3 cycles of ascend and descend is realized for each strongbox before any test is realized. The CPT tests realized afterward during the study confirm the good homogeneity of the tested strongbox (Appendix 4).

Table 3-4 lists the tests realized on the lateral capacity of piles. In total six strongboxes are used. The nomination is unique for each test but in the results chapter and before each group of tests a transitory table is presented where a new set of nomination is presented and used for the desired group of tests.

Only the tests realized in the medium dense sand (D_r = 58%) are fully analysed and presented in the results analysis section. The tests realized in the very dense sand (D_r = 99%) were initially realized in order to test different densities and they are not discussed in the results section but the results of these tests are presented in model scale in the Appendix 1.

Table 3-4 : Experimental campaign

Strongbox	D_r (%)	Pile	Test name	Rigid of flexible pile (R/F)	High or low eccentricity (H/L)	Jacking at 1×g or 100×g (1G or 100G)	H_{min} (N)	H_{max} (N)	Nb of cycles	Comment
C9	58 (dry)	P1	C9P1RL100G	R	L	100G	-	-	-	
		P2	C9P2RL1G	R	L	1G	-	-	-	
		P3	C9P3RH100G	R	H	100G	-	-	-	
		P4	C9P4RH1G	R	H	1G	-	-	-	
C10	99 (dry)	P1	C10P1RH100G	R	H	100G	The max value of the force sensor wasn't sufficient			
		P2	C10P2RH100G	R	H	100G	-	-	-	
		P3	C10P3RH1G	R	H	1G	-	-	-	
		P4	C10P4RL1G	R	L	1G	-	-	-	
		P5	C10P5RL100G	R	L	100G	-	-	-	
C11	58 (dry)	P1	C11P1FL1G	F	L	1G	-	-	-	
		P2	C11P2FL1G	F	L	1G	50	500	200	
		P3	C11P3FL100G	F	L	100G	50	500	1000	
		P4	C11P4FH1G	F	H	1G	40	400	1000	
		P5	C11P5FH100G	F	H	100G	40	400	1000	
C12	58 (saturated)	P1	C12P1FH1G	F	H	1G	40	400	1000	
		P2	C12P2FH100G	F	H	100G	40	400	1000	
		P3	C12P3FL1G	F	L	1G	50	500	1000	
		P4	C12P4FL100G	F	L	100G	50	500	1000	
		P5	C12P5FL1G	F	L	1G	50	500	1000	f = 1 Hz
C13	99 (saturated)	P1	C13P1FL1G	F	L	1G	50	500	1000	
		P2	C13P2FL100G	F	L	100G	50	500	1000	Problaser
		P3	C13P3FH1G	F	H	1G	40	400	1000	
		P4	C13P4FH100G	F	H	100G	40	400	1000	

		P5	C13P5FL1G	F	L	1G	50	500	1000	f = 1 Hz
		P6	C13P6FL1G	F	L	1G	50	500	1000	
		P7	C13P7FL1G	F	L	1G	50	500	1000	f = 4 Hz
C14	99 (dry)	P1	C14P1FL1G	F	L	1G	50	500	1000	
		P2	C14P2FL100G	F	L	100G	50	500	100	Prob laser
		P3	C14P3FH1G	F	H	1G	40	400	1000	
		P4	C14P4FH100G	F	H	100G	40	400	1000	

3.4 Results analysis

This section can be decomposed into two essential parts. In the first part, the monotonic lateral behaviour of piles is discussed and the detailed experimental investigation carried out to examine the influence of installation method, load eccentricity and sand saturation on the lateral behaviour of piles in medium dense sand is presented. The monotonic loading is followed by a cyclic one-way loading up to 1000 cycles. The results of the cyclic tests are presented in the second part of this section. The use of the one-way cyclic loading is selected as this type of loading is considered as the worst case of loading in sandy soil. The effects of sand saturation, pile installation method and load eccentricity on the lateral behaviour of piles under large number of cycles are discussed. After the experiment, a full analysis is completed. This complete analysis includes the analysis of the pile general behaviour such as pile deflection and bending moment profiles for each case, and the analysis and comparison of the experimental p-y curves. A full comparison between experimental monotonic p-y curves and DNVGL ones is also made. The performance results of the DNVGL curves versus experimental ones are discussed. The objective of this experimental program is to fill the lack in the studies of the effects of the selected parameters which influence largely the behaviour of the piles of wind turbines under high number of cycles.

The results presented in the present study are already been published or submitted to publication in journals.

3.4.1 Pile installation and loading

Extensive work has been undertaken to develop an innovative experimental campaign. Thanks to this earlier work it becomes possible to carry out the specific steps required for both installation and loading of the piles studied. The experimental set-up (Figure 3-5) includes a hydraulic jack to jack piles in place and an electric actuator used for lateral loading. A 25-kN ± 0.25 kN load sensor (FN3070 from FGP) located between the pile head and the hydraulic jack measures the total bearing capacity of the pile. Pile displacement is determined using a magnetostrictive displacement sensor (1/300350S010–1E01 from TWK), which controls the displacement of the hydraulic jack. Lateral loading is measured using a 2.5-kN ± 0.025 kN load sensor (F521-06TC from TME) located at the tip of the electric actuator. The displacement of this jack is provided by a sensor, manufactured by Exlar and integrated inside the jack. A lateral laser (OCX7-11170024 from the company BAUMER) is mounted on the

front of the installed pile to measure pile lateral displacement at a height of 12 mm above sand surface.

Two different installation methods are tested. In the first method, the pile is first jacked at 1×g to model wished-in-place pile installation then the centrifuge acceleration is applied and the lateral loading is realized. The second method consists in first jacking the pile in-flight at a speed of 0.1 mm/s to simulate installation effects and soil displacement that takes place during the installation of displacement piles, then applying lateral loading without stopping the centrifuge. For each case and in each strongbox, lateral loading is carried out at some elevations of 1.67B or 3.89B above the sand surface. Loads are applied in force controlled mode at a constant speed of 1 N/s for the flexible piles (Figure 3-6), and in displacement controlled mode at a constant speed of 0.1 mm/s for the rigid piles. The maximum loading reached depends on the type of model pile used for the test: (1) the rigid pile is loaded until failure (2) the flexible pile is loaded up to the desired lateral force of 500 N for an eccentricity of 1.67B; and up to 400 N for an eccentricity of 3.89B. The loading limits of the flexible pile are chosen in order to remain within the elastic limit of the piles.

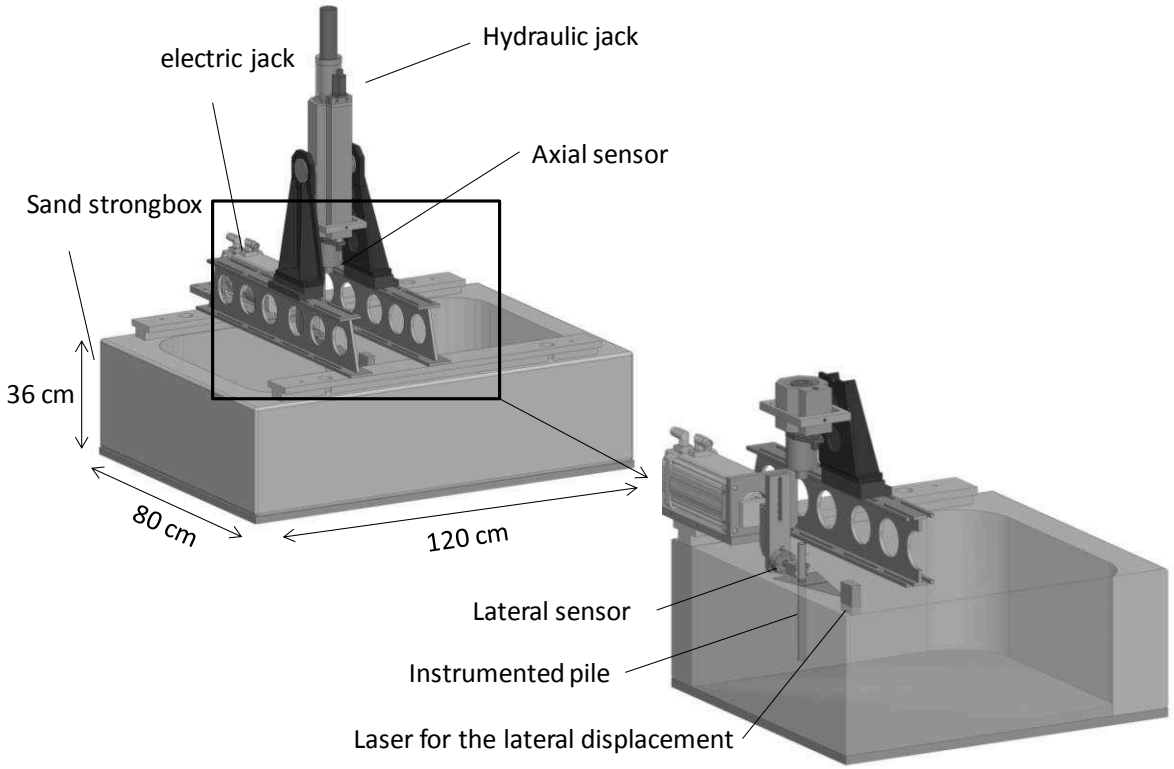

Figure 3-5 : Experimental set up (inside dimensions)

After the monotonic loading up to the desired maximum load the flexible pile is submitted to cyclic loading with frequency of 0.2 Hz between the H_{max} (maximum monotonic load) and H_{min} (minimum load) (Figure 3-6). As explained in the literature section, in sandy soil the ratio $H_{min}/ H_{max} = 0$ is considered as the worst type of loading for laterally loaded piles. In the context of the present laboratory setting, it is not possible to use $H_{min} = 0$ to maintain the electrical lateral jack in contact with the pile during loading without losing control of it. H_{min} is then set at 0.1 H_{max} to model the worst possible loading within the present experimental context. The same type of cyclic loading is applied for all the tests conducted so that investigation remains focused on the parameters to be studied and will not be affected by the type of loading. The literature, indeed, already contains a decent number of studies devoted to study the effect of the loading type.

Some tests are limited to 100 or 200 cycles because the laser provides unreliable results for a greater numbers of cycles.

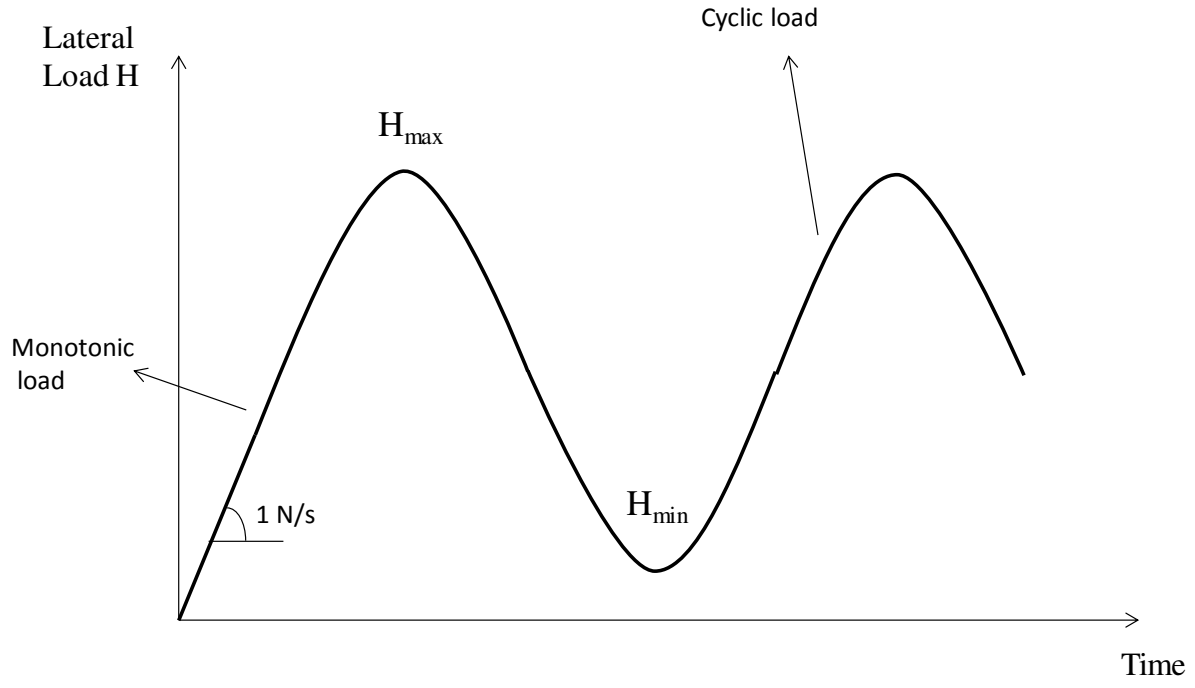

Figure 3-6 : loading sequence of flexible piles

3.4.2 Monotonic loading tests

This section examines the influence of installation method, load eccentricity and sand saturation on the lateral monotonic behaviour of piles in medium dense sand.

Table 3-5 shows the new set of names given for the chosen tests to be presented in this section.

Table 3-5 : transition table for tests nomenclature

Test	New name	Dry or saturated sand (D/S)	Rigid or flexible pile (R/F)	High or low eccentricity (H/L)	Jacking at 1×g or 100×g (1g or 100g)
C9P2RL1G	DRL1g	D	R	L	1g
C9P1RL100G	DRL100g	D	R	L	100g
C9P4RH1G	DRH1g	D	R	H	1g
C11P2FL1G	DFL1g	D	F	L	1g
C11P3FL100G	DFL100g	D	F	L	100g
C11P4FH1G	DFH1g	D	F	H	1g
C12P3FL1G	SFL1g	S	F	L	1g

3.4.2.1 Failure reference tests (rigid piles)

Soil rupture is examined using a rigid pile laterally charged in a displacement controlled mode. The failure tests are performed in medium dense dry sand for both installation methods and different load eccentricities. The failure force is defined as the intersection between the tangent at the origin and the tangent at large displacement on the load-displacement curve (Figure 3-7). The analysis of the failure force of the different piles is presented in Table 3-6. The results clearly show that the failure force is influenced by pile installation method and load eccentricity. (1) Pile installation at 100×g has naturally enhanced soil response. This can be explained by the densification of the surrounding soil during pile in flight installation and increase in horizontal stress on the pile shaft. (2) Increasing load eccentricity decreases failure forces. This observation can be anticipated since, for rigid pile, the kinematics of laterally loaded piles concerns only rotation. An increase in the lever arm therefore causes a decrease in the force for the same rotation.

The results achieved with rigid piles are used as references for the load intensity range that will be applied to flexible piles.

Different methods for the calculation of the ultimate lateral resistance of piles are described by Hansen (1961), Broms (1964) and Bouafia (1994). In this study, the experimental results are compared with the theoretical values obtained using Broms' relationship (Table 3-6):

$$H_r = \frac{\gamma D^3 B K_p}{2(h+D)} \tag{30}$$

where :

H_r is the failure force, γ the density, D the embedded length, B the pile diameter, h the height of the loading point, K_p the coefficient of earth pressure.

Broms results overestimate the experimental results by 20% and 30% for the lower load eccentricity using installation methods at 1×g and 100×g, respectively. As regards the higher load eccentricity, the difference is even greater with an overestimation of up to 54% for the pile installed at 1×g.

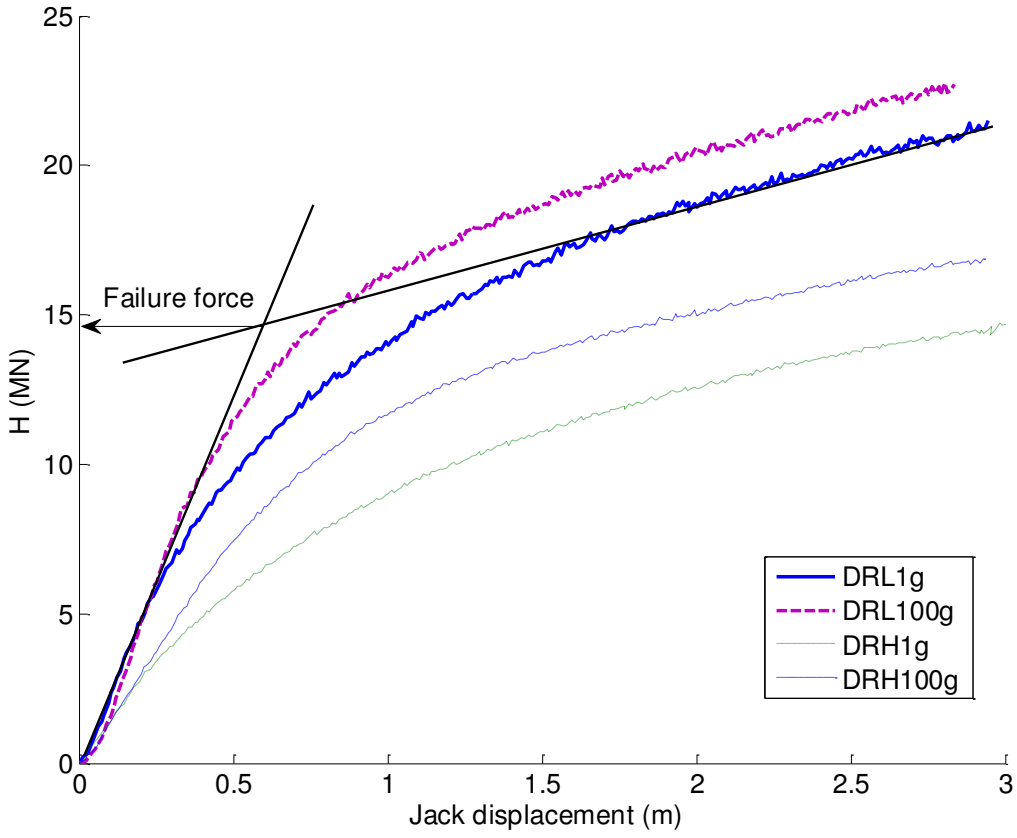

Figure 3-7 : Failure force interpretation

The service load or admissible load used for geotechnical structure design like the superficial foundations and the deep foundations, is directly related to the ultimate load and generally

limited to the third of the soil rupture force (Fond 72 (1972), Rosquoet (2004)). For this reason, the loads applied here for the different load eccentricity configurations and installation methods are compared with the respective ultimate load of the rigid piles (Table 3-6). The higher percentage (37.7%) is reached by DFH1g. All the other piles, on the other hand, present a percentage smaller than the limit suggested by the Fond 72 (1972). This is important to verify that the tested piles are all loaded in service condition.

Table 3-6 : Failure test analysis

Test identification	Failure Force (MN)	Formula Broms'	% of the loading force from the failure force
DRL1g	14.7	19.1	-
DRL100g	15.9	19.1	-
DRH1g	10.6	16.3	-
DFL1g	-	-	34
DFL100g	-	-	31.4
DFH1g	-	-	37.7

3.4.2.2 Flexible pile tests

Once the experimental discrete bending moment profile is obtained (Figure 3-8(c)), fitting these moments using a mathematical function for calculating p and y profiles is necessary. Rosquoet et al. (2010) point out that King (1994) demonstrates that a single polynomial function is not satisfactory to fit the experimental result moments. For this study, a cubic spline is successfully used to fit the moment profiles. Moment fitting is an essential step in result analysis because mathematical processes like integration and derivation can be applied to moment profiles. The force per unit length, p, is determined through the double differentiation of the bending moment profile whereas the lateral displacement y is obtained through the double integration of the curvature M/EI.

Two constants are needed for the double integration to obtain the profile of the lateral displacement. The first one is determined from the experimental measured displacements. The second one is generally the pile head rotation. However, pile head rotation cannot be used here for the second constant because of the lack of accuracy of measurements. The slightest uncertainty between the displacement results measured at the actuator level and the laser results, indeed, generates a systematic divergence as regards the double integration procedure. Rotation measurements are not accurate enough to give satisfactory results. A better option

consists in taking two displacements for integration constants: one on the ground surface and one inside the soil as close as possible of the pile tip. This is why the second constant identification is indirect and consists in determining the pile rotation centre thanks to the soil reaction profile. Two new methods developed for this study are presented and compared below:

(1) The global method: the second integration constant is obtained, by assuming that there is no lateral displacement of the pile if there is no reaction of the soil, i.e., y=0 when P=0 for each loading step (1, 2,…,n loading step) (Figure 3-9(a)). The point depth becomes deeper as loading increases. The method is called "global" because it depends on pile general behaviour and not on loading history. At any time of loading history, the point where p=0 can be extracted and used even if earlier loading steps are unknown.

(2) The incremental method is presented in Figure 3-9(b). Under this method the pile is considered, between two loading increments, to rotate around the point where soil reaction remains constant. If there is no variation of the soil reaction between two loading increments, the pile is assumed not to move horizontally at this depth. The pile, therefore, can be considered as rotating around a peculiar point where $y \neq 0$. This method is called "incremental" because it depends on loading increment. Each step depends on the previous loading steps. P and y profiles of step n-1 are necessary to calculate the constant at step n.

Figure 3-10 displays the depth z, at which y = 0 for test DFL1g using both methods. After comparison, both methods show similar results for the first loading increment. When horizontal loading exceeds 3 MN, each method is starting to produce different results. The incremental method tends to converge with increasing loading whereas the global method tends to diverge. This can be attributed to the fact that, as loading increases, the point where p = 0 is deeper and, consequently, some soil layers initially loaded become then unloaded. In the case of large lateral loading, these same layers may have already caused a plastic deformation, which invalidates the relationship y=0 at p=0. When high lateral loads are concerned, the incremental method must be used.

For the same reason these methods are expected to differ in the case of cyclic loading where the soil is submitted to plastic deformation. The first method is no longer valid and only the second method can be applied. An interesting finding of both methods is the fact that they can be used to build lateral displacement profiles even if only one limit condition can be measured during the test.

Figure 3-11 presents the depths, at which y = 0 obtained during testing. The depth vs. loading curves show a clear convergence with the increase of the loading. These results are in good accordance with the pile general behaviour and the pile displacement results at the sand surface that will be discussed later in this paper: the rotation point then becomes deeper as a function of the increase in the lateral displacement at sand surface.

Figure 3-8(c) presents the experimental moments and the fitting profiles. From these profiles, lateral displacement (Figure 3-8(a)), pile rotation (Figure 3-8(b)), shear force (Figure 3-8(d)) and soil reaction (Figure 3-8(e)) are determined.

The complete analysis of the results obtained in Figure 3-8 provides a clear indication of the pile behaviour. The rotation of the pile is maximum at sand surface then decreases with increasing depth until reaching almost zero at the pile tip. The pile behaviour reveals that the pile can be considered as a flexible pile because its rotation changes according to depth and is not constant. On the other hand, the pile shows to not be fixed at the pile tip and a small displacement is noticed. It confirms the need to use the incremental method discussed above to determine the second integration constant. The pile displacement definitely generates shear forces and soil reactions at pile tip, which, however, cannot be measured precisely because the last gages being placed at a depth of 18 m, the derivation at the pile tip cannot be accurately determined. The pile tip displacement indicates that the pile behaves like a short pile. Although the last gages are located 18 m deep, the moments measured at this depth shows small values, indicating that the pile tip moment is almost zero and that the pile does not behave like a monopile. As a result of this analysis, the pile can be considered as a “short flexible” pile. Unlike long flexible piles, for which no rotation effect is considered, this type of pile, whose performances mostly depend on its flexibility, can initiate a rotation as depth increases.

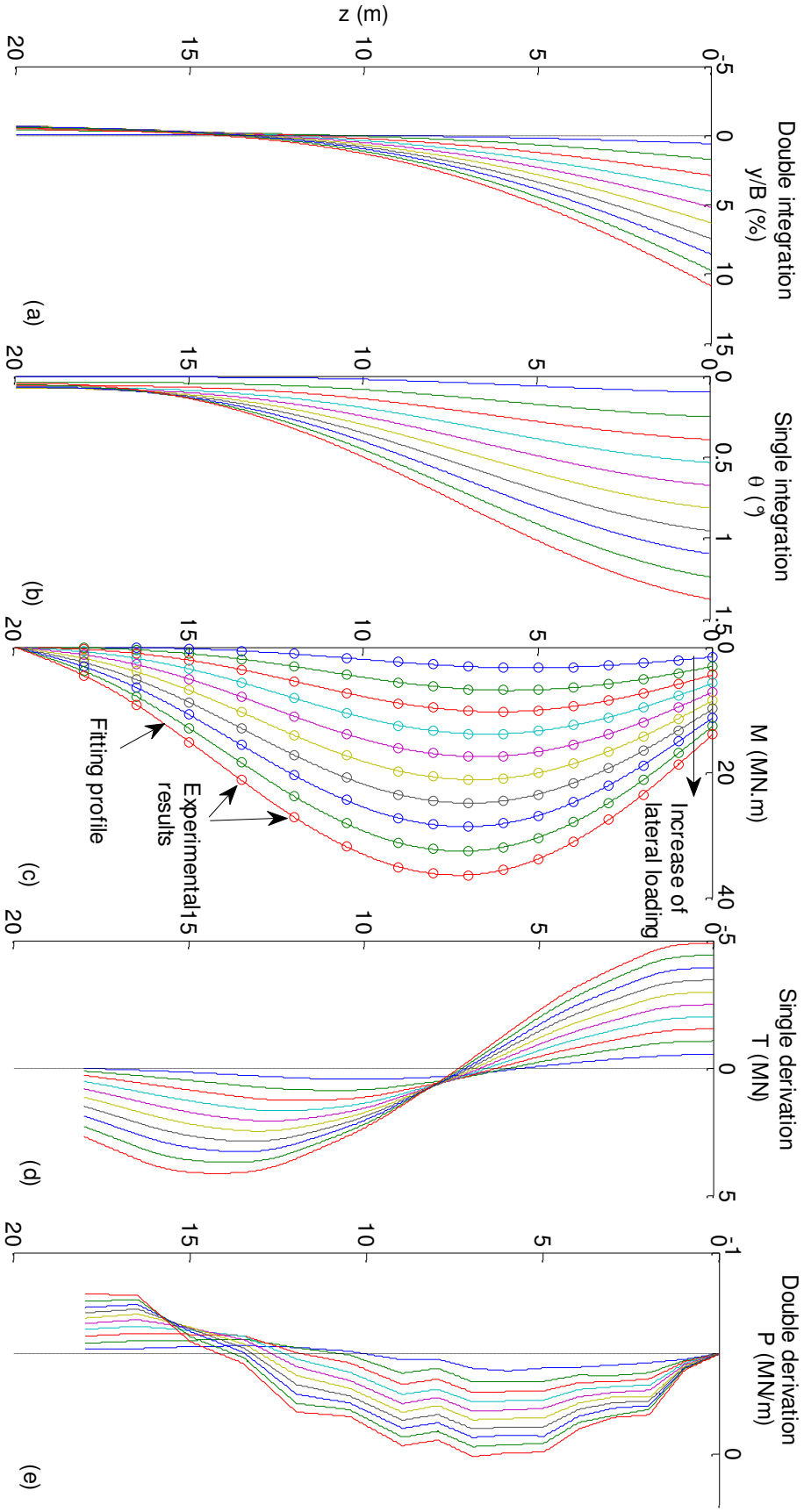

Figure 3-8 : DFL1g: (a) pile deflection (b) pile rotation (c) moment profiles (d) shear force (e) soil reaction

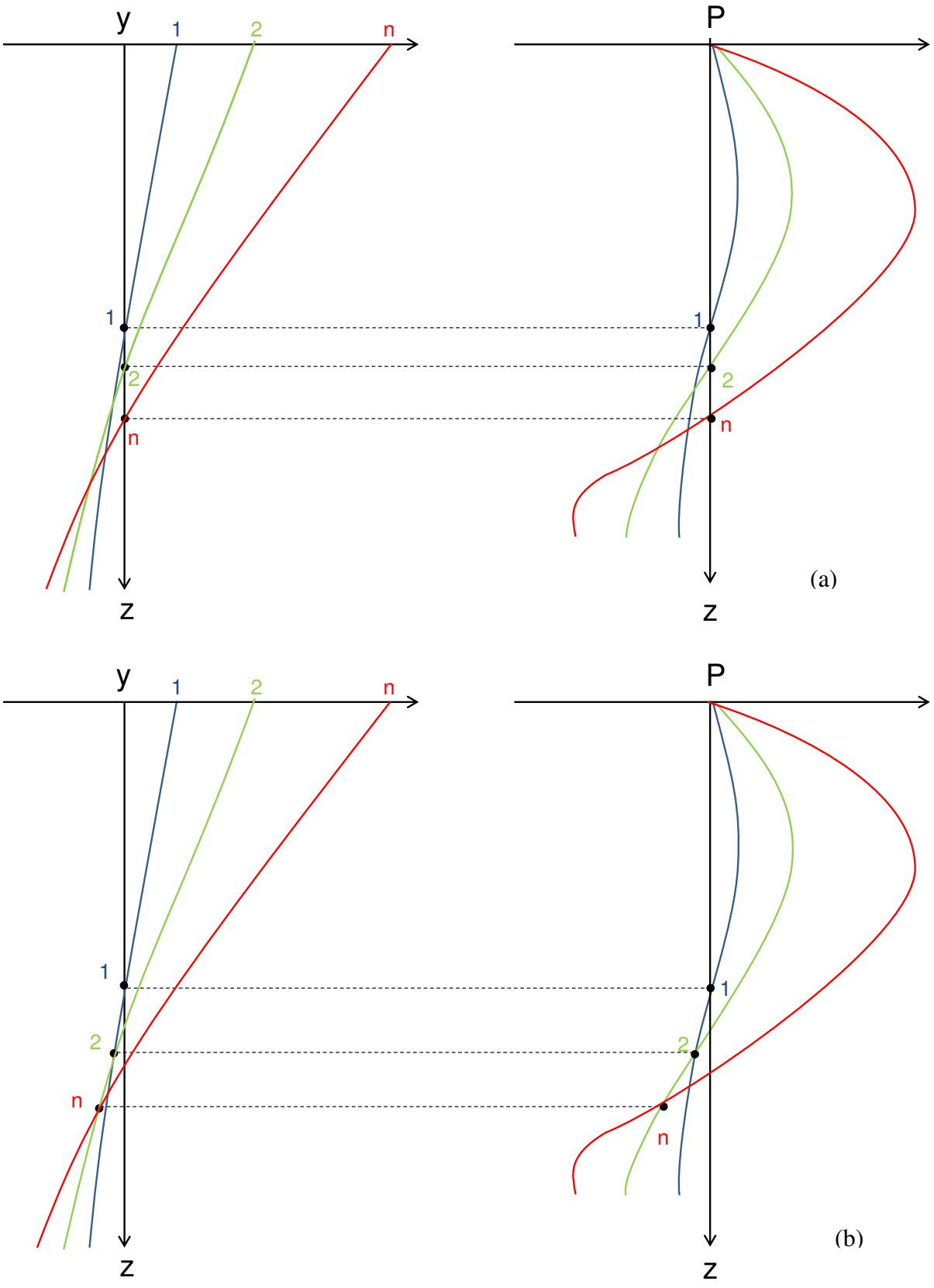

Figure 3-9 : Principle of determination of the second constant for lateral displacement integration

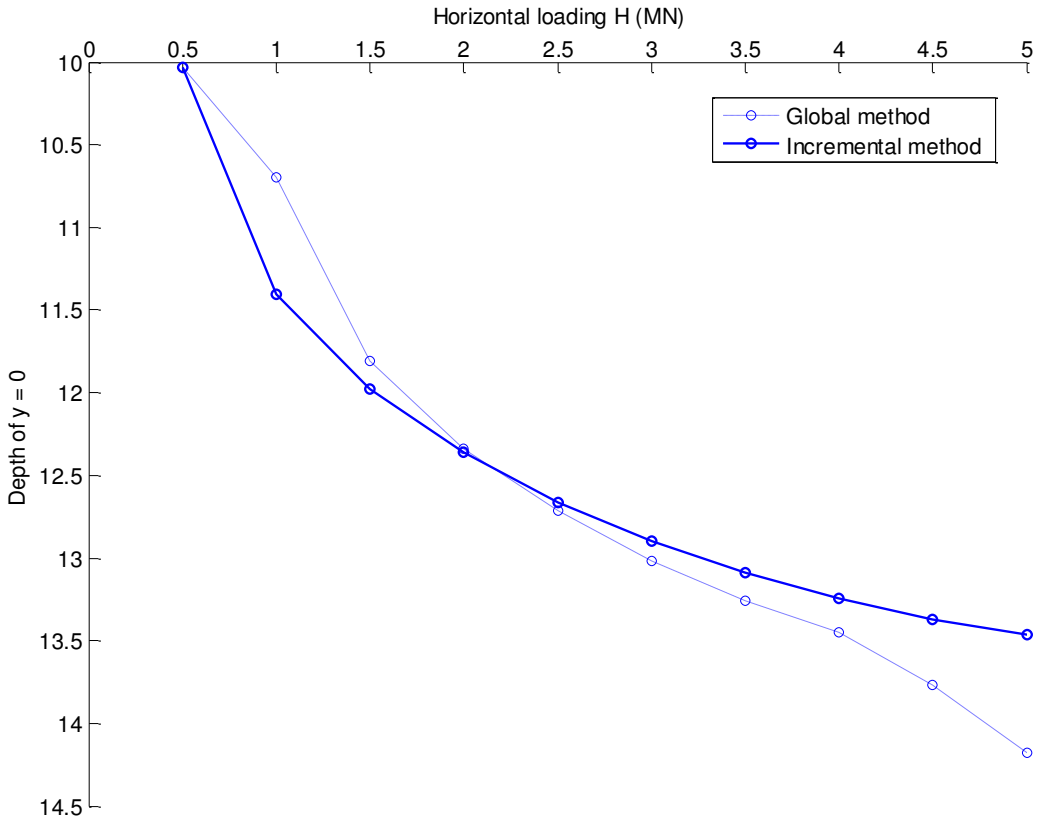

Figure 3-10 : Depth for y=0 using both methods of constant identification for DFL1g

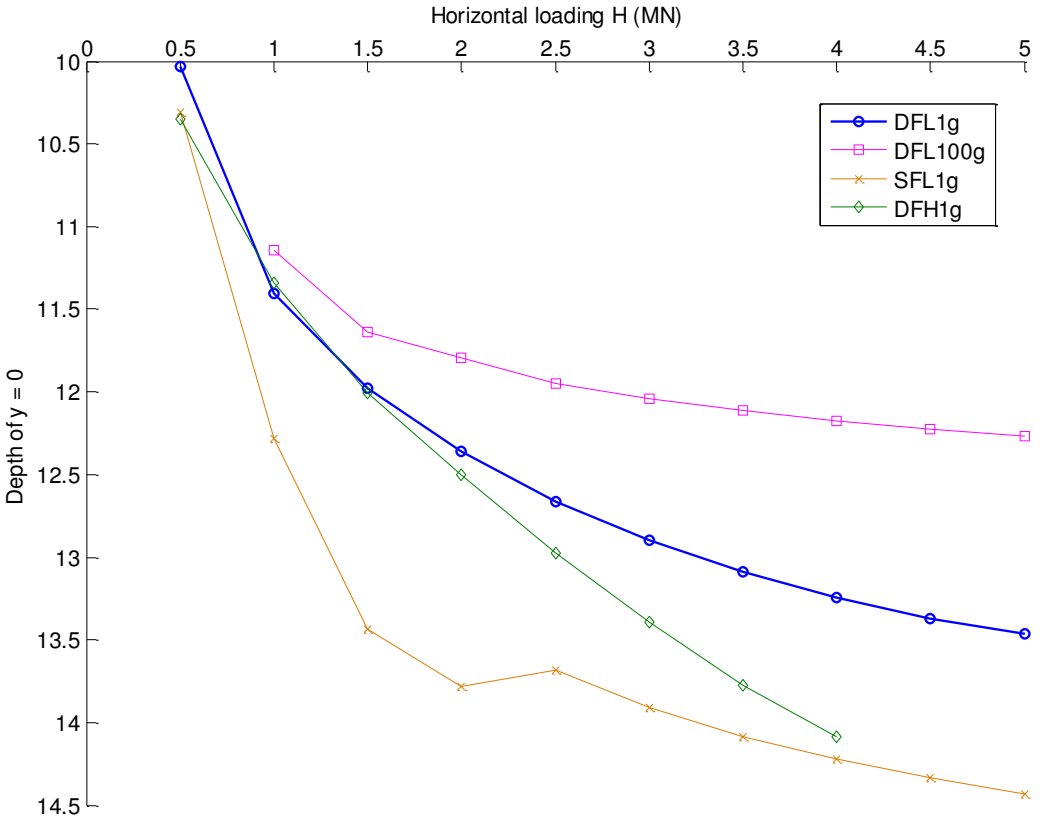

Figure 3-11 : Depth for y=0 using the incremental method

3.4.2.3 Parametric study

A parametric study is conducted to examine i) the effects of the installation methods, ii) load eccentricity and iii) sand saturation on pile horizontal behaviour (bending moment and displacement at sand surface) and on the local behaviour described by p-y curves. Test DFL1g is here considered as reference test. For each parameter studied, some tests are carried out by varying only this parameter at a time compared with the reference test.

3.4.2.3.1 Global study

Figure 3-12 presents the displacements at sand surface of the reference pile DFL1g at the different load steps in comparison with DFL100g, SFL1g and DFH1g. Pile DFL100g installed in flight shows smaller displacements in comparison with the pile installed at 1×g (DFL1g). This can be explained by an increase in sand density at shallow depth and a confining effect around the pile due to its installation at 100×g, which prevent piles from developing extreme displacement.

The saturation of sand (SFL1g) causes a sharp increase in the pile lateral displacement, which can be explained by lateral effective stress decrease. Moreover, eccentricity increase increases lateral displacement because of the moment increase for the same load applied.

The quasi-linear shape of the different loading curves as a function of the lateral displacement makes it possible to quantify the effect of all the lateral displacement parameters. In flight installation reduces pile displacement by approximately 24%. Increasing eccentricity increases lateral displacement by 36% to 46%. Sand saturation constitutes the main parameter, which affects lateral displacement with a raise of up to 57% in the displacement when sand is saturated.

The effects of the studied parameters on the moments at sand surface are presented in Figure 3-13. The curves follow the same trend as in Figure 3-12 for installation method effects and sand saturation. The same reasons explain these results. However, parameters have much less impact on pile rotation than on displacement. In flight installation reduces pile rotation by 14% whereas saturation increases pile rotation by 34%. Increasing eccentricity causes an expected sharp rise in the moment at sand surface for the same load applied due to the increase in lever arm.

The comparison between pile lateral displacement and pile rotation is presented in Figure 3-14 for the different tests. The four tests show a close linear relationship between pile

displacement and rotation. This finding demonstrates that this relationship is highly dependent on pile type and rigidity but not significantly affected by sand and loading conditions and installation method.

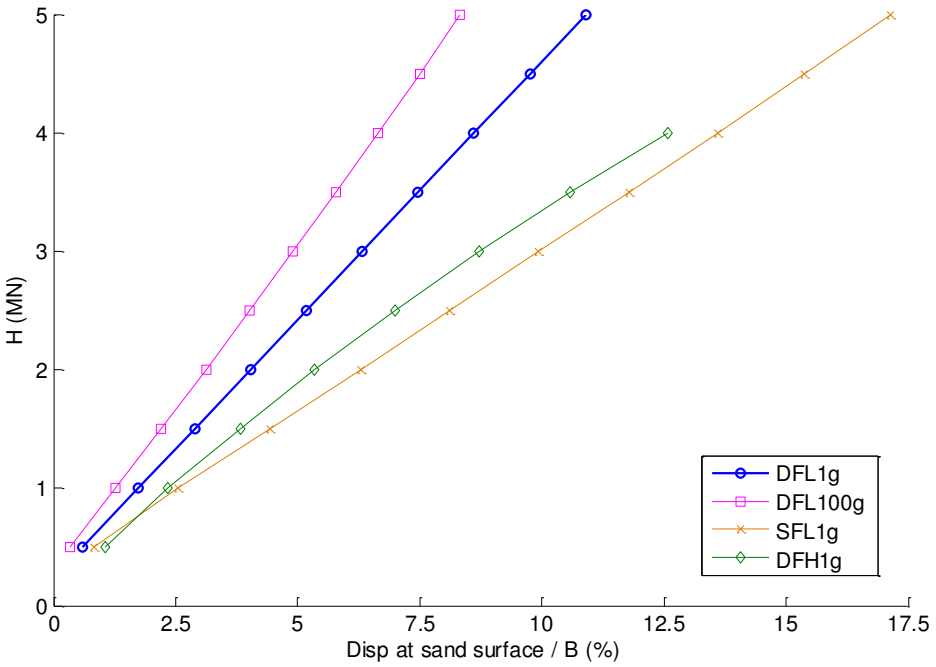

Figure 3-12 : H vs. displacement at sand surface

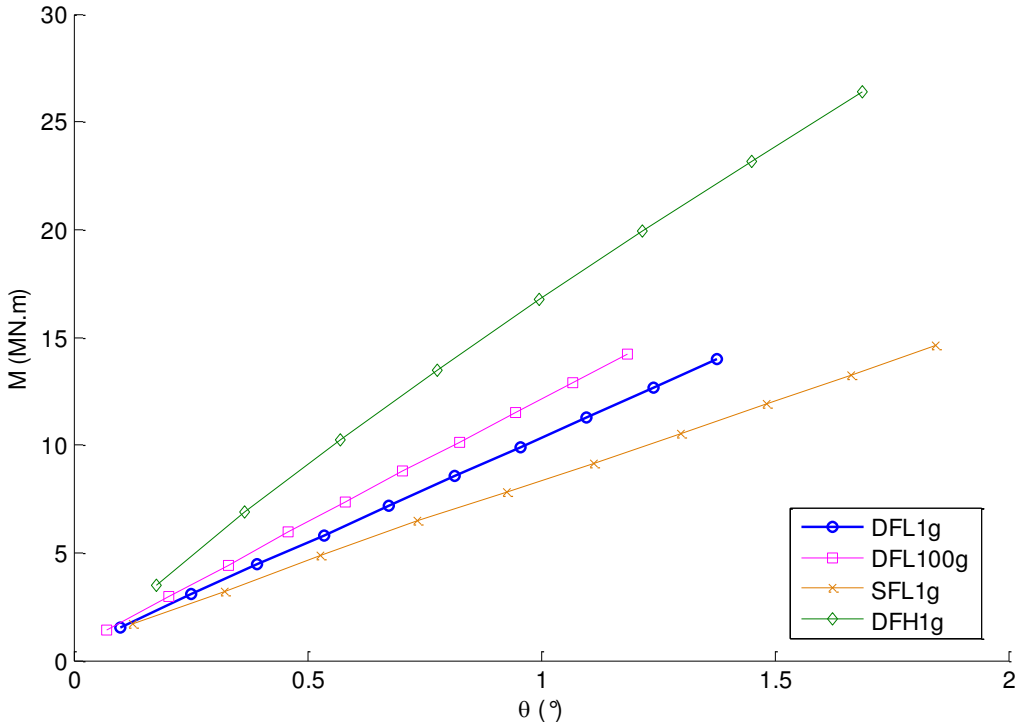

Figure 3-13 : Moment vs. pile rotation at sand surface

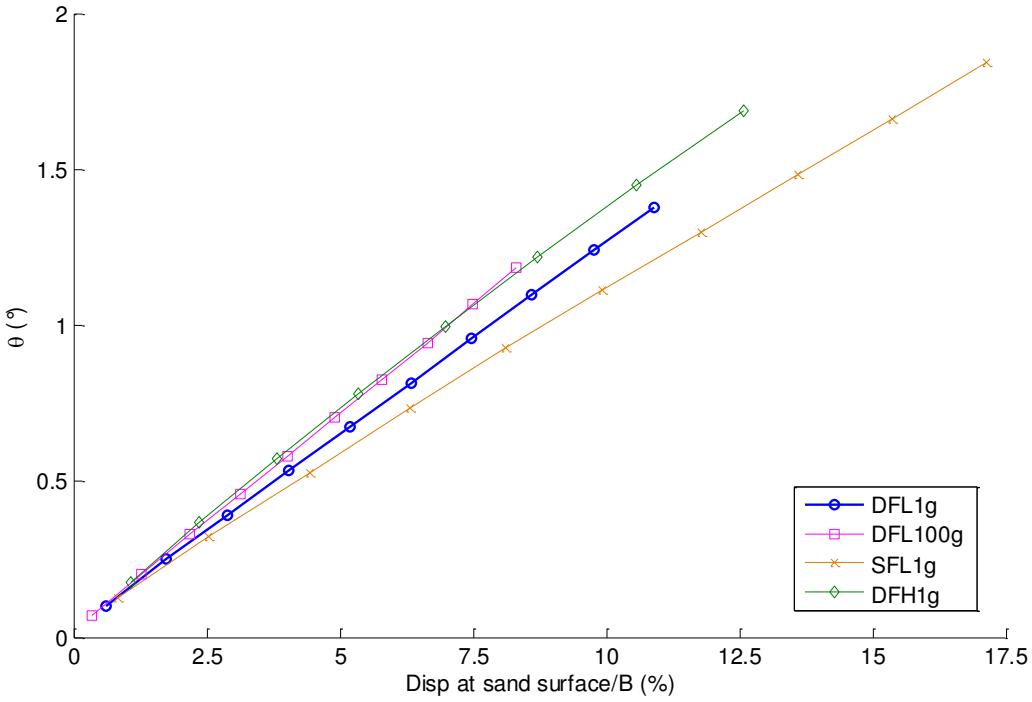

Figure 3-14 : Pile rotation vs. displacement at sand surface

3.4.2.3.2 Moments profiles

The moment profiles of the tested pile at three different loading steps are presented in Figure 3-15. For the piles loaded at 1.67B, the steps chosen correspond to a loading of 1.5, 3.5 and 5 MN, respectively. On the other hand, for the pile loaded at 3.89B the moment profiles correspond to three loading steps, which give the same moment at sand surface than the other tests.

The moment profiles of the two piles installed at 1×g and 100×g, respectively, in medium dense dry sand and loaded with an eccentricity of 1.67B clearly show the influence of the installation method on the maximum moment for the three loading steps (Figure 3-15). DFL100g shows a maximum moment, which is smaller and shallower compared with DFL1g. The depth is about 17% deeper and the maximum moment is 4% greater for the pile installed at 1×g. This may be due to the enhancement of shallow sand properties caused by the pile installation. In flight installation, indeed, produces higher lateral stresses and confining effect on the pile, which results in smaller moments inside the pile.

Sand saturation (SFL1g) generates an increase of about 8% in the maximum moment, which is slightly deeper than the test conducted in dry sand (DFL1g). This can be due, as for lateral displacement, to the effective stress decrease around the pile.

In order to compare the moment profiles of the piles loaded at different eccentricities (DFL1g and DFH1g), the loading steps is chosen so that the moment profiles of both tests have the same moment at the sand surface. The moment profiles of DFH1g correspond to a load of 0.63, 1.47 and 2.08 at 3.89B of eccentricity, respectively. These loading steps have created the same moments at the sand surface compared with DFL1g, but the maximum moment is remarkably smaller and shallower inside the pile.

The maximum moments and their depths obtained at Hmax, which is equal to 5 MN for the tests loaded at 1.67B and 4 MN for the tests loaded at 3.89B, respectively, are presented in Table 3-7. The maximum moment reached during test DFH1g is 43.9 MN.m. This demonstrates the substantial influence that eccentricity increase can have on the maximum moment inside the pile. The study of the maximum moment is always a key factor of pile design to prevent any exceeding pile elastic limit and consequently any plasticity or failure of piles.

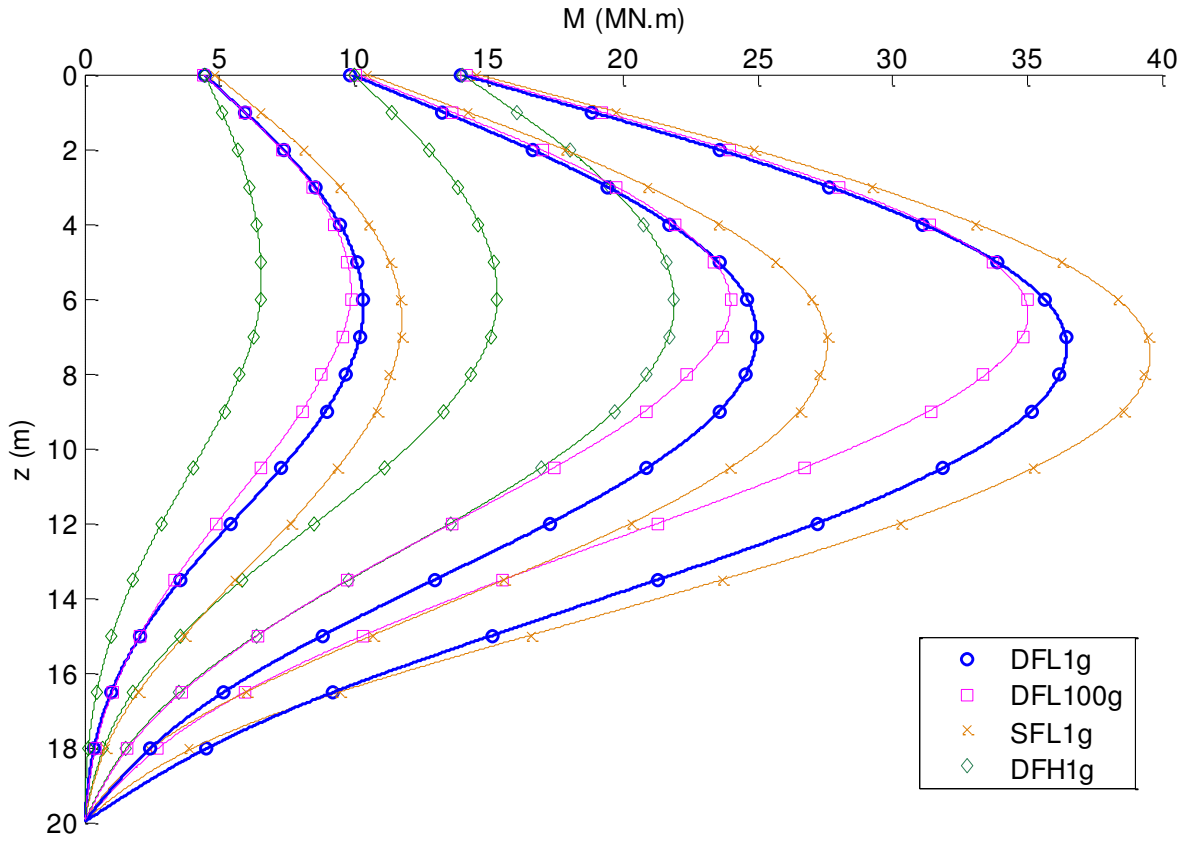

Figure 3-15 : Moment profiles

Table 3-7 : Analysis of the maximum moments for Hmax

Test identification	Maximum moment (MN.m)	Depth of the maximum moment (m)	Depth of the maximum moment/B
DFL1g	36.5	7.2	4
DFL100g	35	6.13	3.4
DFH1g	43.9	6.6	3.67
SFL1g	39.6	7.4	4.12

3.4.2.3.3 Establishment and study of p-y curves

Once the profiles of the lateral displacement and soil reaction at different depths using the method presented in section 3.4.2.2 are obtained, the p-y curves at different depths can be established.

3.4.2.3.3.1 Impact of load eccentricity

The impact of load eccentricity can be studied by the comparison between the tests where the height of the point of application of the load is 1.67B and 3.89B. Figure 3-16 displays the results obtained for the comparison between both tests: the reference pile in medium dense dry sand loaded at 1.67B (DFL1g) and the respective test loaded at 3.89B (DFH1g). While the study is limited to 5B, it is, however, considered sufficient to represent of the upper part of the pile where the most important displacements and can, therefore, be considered as an accurate representation of pile behaviour at large. As expected, the p-y curves of both tests exhibit similar behaviour with, however, DFL1g displaying a more rigid behaviour in some cases. As for the service state considered here, none of the experimental p-y curves reach the values suggested by DNVGL. DNVGL p-y curves present an initial stiffness reaction much higher than the experimental results. DNVGL gives always the same curves regardless of load eccentricity and takes no account of the effects of this parameter.

This finding is in good accordance with the results presented by Yan and Byrne (1992) where the increase in eccentricity generates a softer response of the pile. These results also underline a weakness in Winkler's model and the beam law because, according to those methods, p-y curves, in the same soil, are always identical and do not depend on the loading conditions.

While eccentricity effects in medium dense sand exist but because the differences they cause do not appear to be sufficiently significant, then, for practical applications, the same set of p-y curves might be used to assess pile response when different load eccentricities are applied.

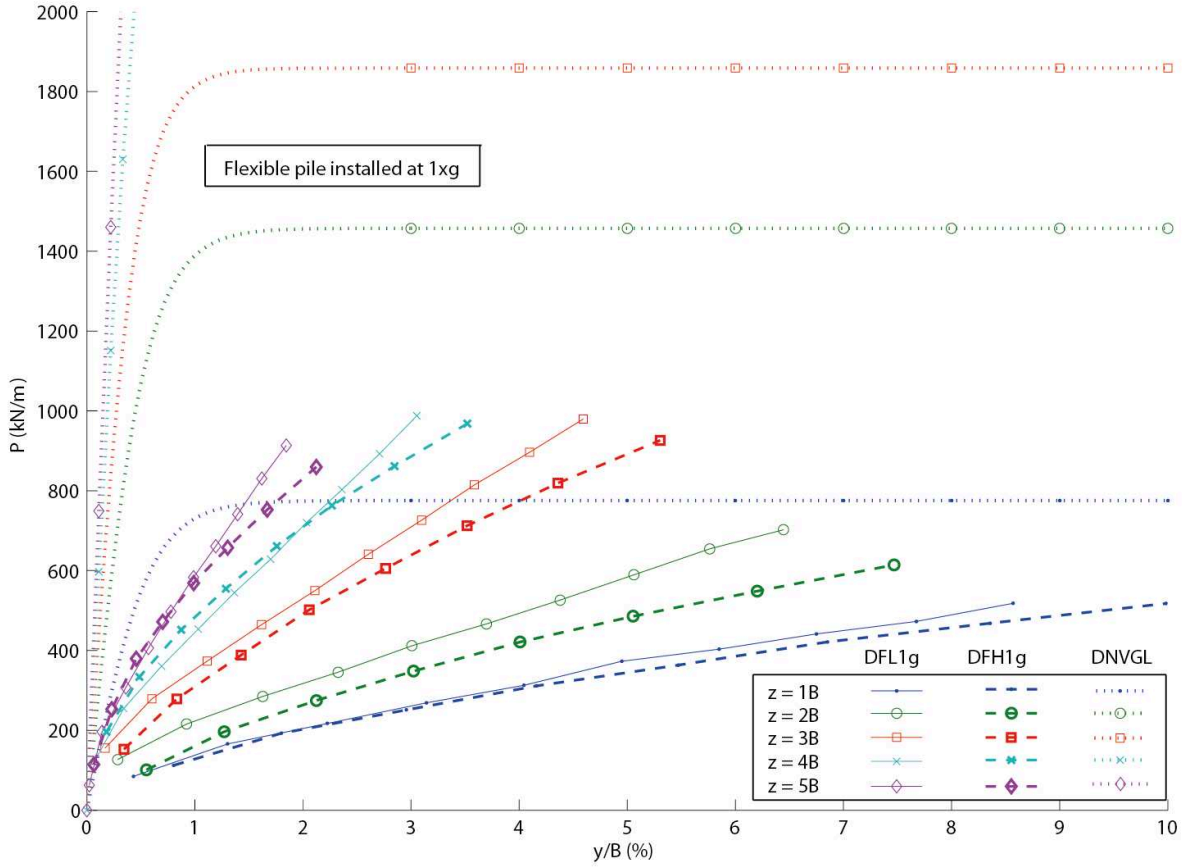

Figure 3-16 : Effect of eccentricity on p-y curves in dry sand (DFL1g vs DFH1g)

3.4.2.3.3.2 Effect of sand saturation on the p-y curves

In design codes, sand saturation is usually considered through the effective stress. Piles in sand are considered loaded under drained conditions without any pressure buildup within the pores. Using effective stress implies that the lateral stresses applied by sand on piles are reduced compared with dry sand. The increase in offshore structure construction involves verifying design codes performances as regards the design of piles installed in saturated sand. Figure 3-17 displays pile performances in dry and saturated sand and compare them with the respective DNVGL code recommendations. SFL1g presents a softer response and a final limit for the p-y curves lower than DFL1g. The DNVGL code presents better performances in saturated sand than dry sand. DNVGL code final limit gives a good representation of the final limit of the experimental p-y curves in saturated sand at shallow depths once convergence is achieved. In some cases, it gives a conservative result like at a depth of 3B. On the other hand, as shown above, in dry sand, DNVGL overestimates the final limit.

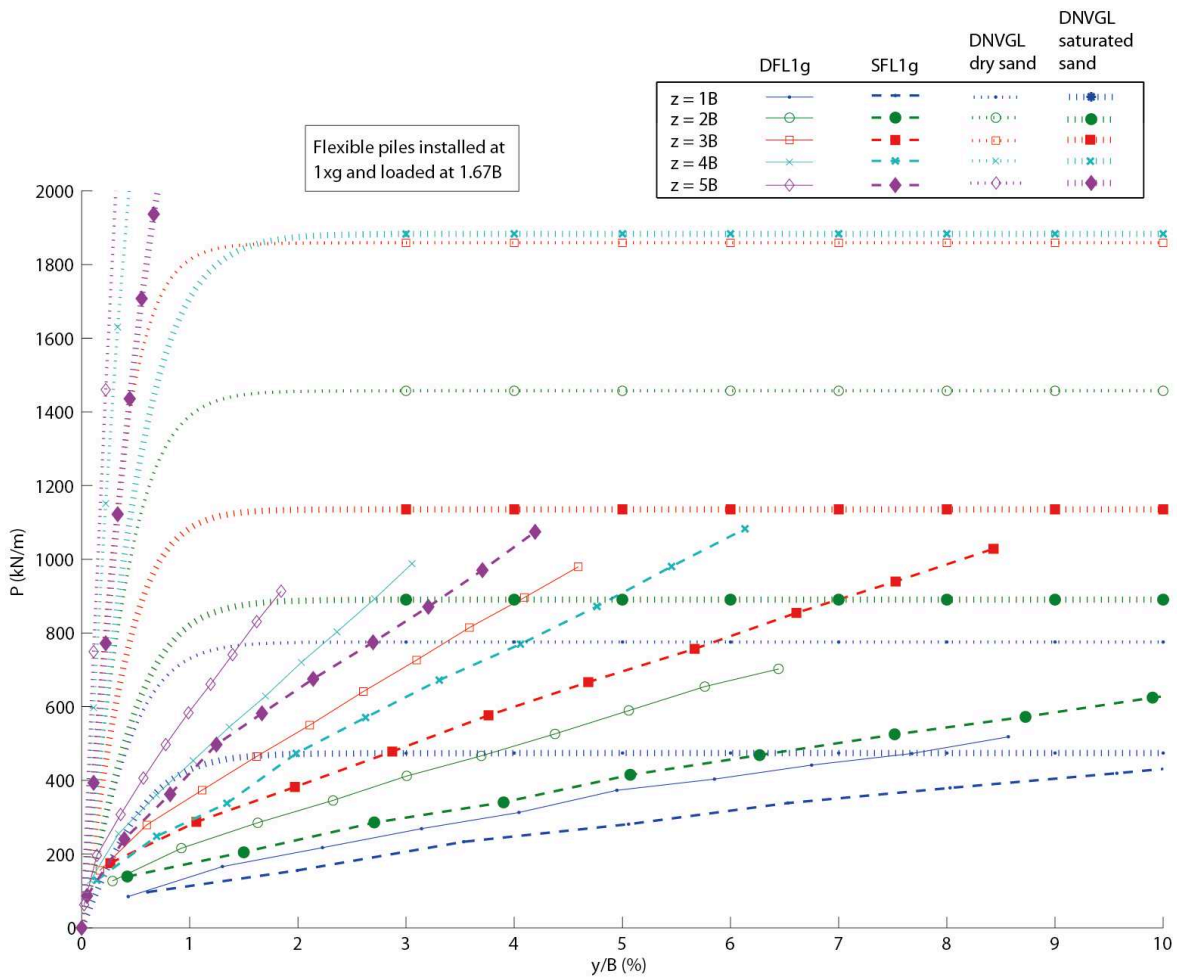

Figure 3-17 : Effect of saturation on p-y curves

3.4.2.3.3.3 Effect of the installation method

The influence of the installation method on the p-y curves of the laterally loaded piles DFL1g and DFL100g at shallow depths (between 1B and 5B) is presented in Figure 3-18. The p-y curves of DFL100g show a stiffer initial response at all the studied depths. Moreover, at depths of 1B and 2B where the p-y curves begin to converge, DFL100g gives a higher final limit than DFL1g. The p-y curves obtained using the DNVGL design code are also plotted in this figure. The DNVGL p-y curves give an initial stiffness reaction much higher than the experimental results. Pile in flight installation appears to reduce the difference between DNVGL and experimental initial stiffness, the DNVGL initial stiffness remaining, however, significantly higher.

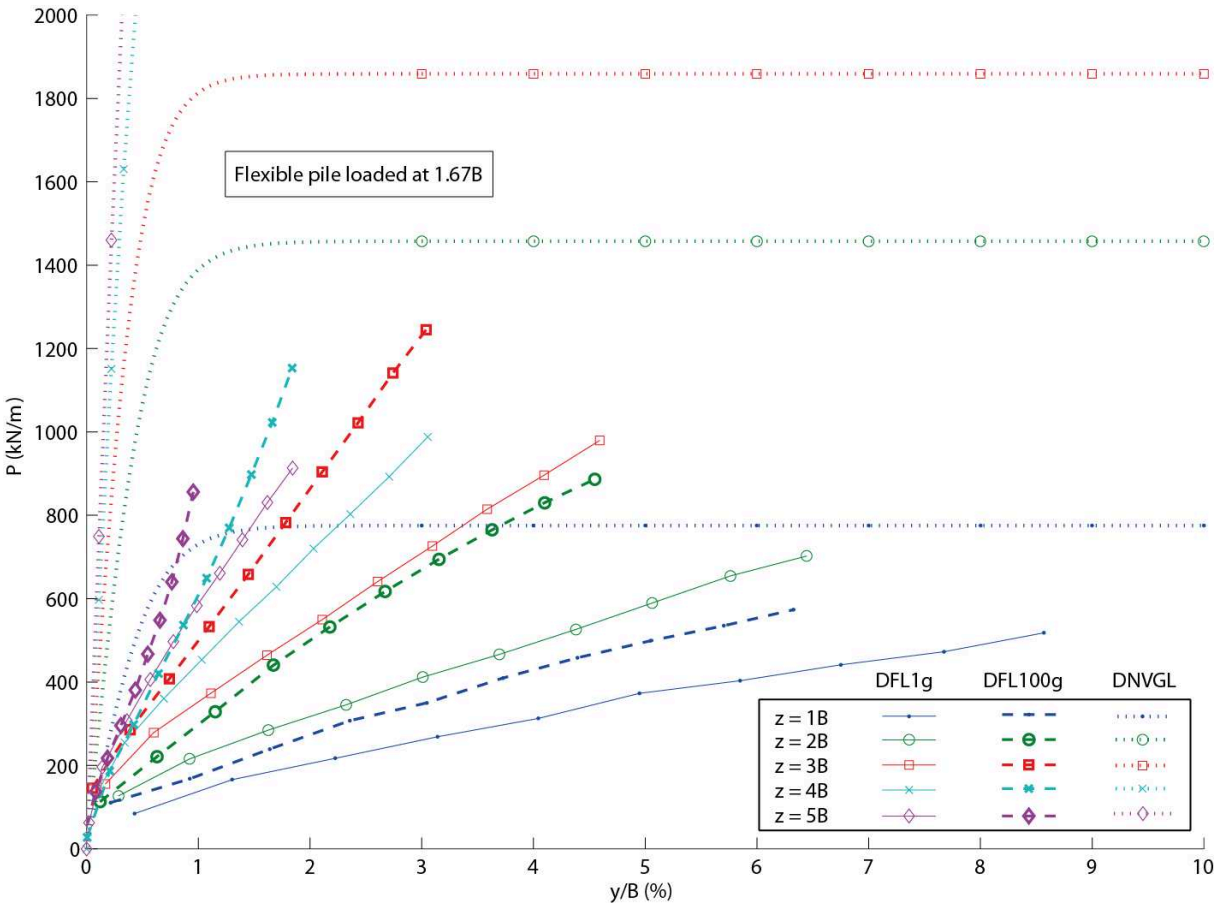

Figure 3-18 : Effect of the installation method on p-y curves (DFL1g vs DFL100g)

These results are in good accordance with the results obtained by Kim et al. (2004) and Dyson and Randolph (2001). Kim et al. (2004) present the load-displacement curves and the p-y curves at 1B, 3B and 6B, respectively, for a preinstalled pile and some piles driven at different driving energies. They show that the lateral pile loading of driven piles is higher than for the preinstalled pile and that it increases as the driving energy increases. They also observe that the soil-pile reactions of the load-transfer curves at a certain depth are larger for driven piles than for the preinstalled pile and that the soil-pile reactions of the driven piles increase as the driving energies increase. On the other hand, Dyson and Randolph (2001) have studied four different installation methods to quantify their influence on the lateral response. They present the pile head load-displacement responses and the load-transfer curves derived from the tests at two depths of 1.3 and 5B, respectively. Pile head load-displacement responses are given in the stiffness order; driven piles, piles jacked at 160×g, 1×g and, finally, preinstalled piles. The stiffness of the load-transfer curves follows the same trends as the pile head response at shallow depths but the differences are substantially reduced with a depth of five diameters. The results presented in the present study confirm the findings of Kim et al. (2004) and Dyson and Randolph (2001) as regards the influence of the installation methods. These findings not

only applied to the cases they studied but can be generalized to all the densities, saturation states and load eccentricities studied in this study. In conclusion, the installation method appears to affect pile response regardless of sand conditions, in which the installation takes places and of the eccentricity of the applied loads.

3.4.2.3.3.4 Effect of the coefficient of the subgrade reaction

The important difference in the initial rigidity of the DNVGL P-y curves and those obtained from the experimental results which doesn't exist in the case of in-situ tests (Byrne et al. (2017)) make necessary to study the reason behind this difference. The equation of the DNVGL P-y curves (equation 29) shows a high influence of the initial coefficient of subgrade reaction on the initial rigidity of these curves. Terzaghi (1955) gives different values of the coefficient of subgrade reaction than those suggested in the method of Reese (1974) on which the DNVGL code is based. Figure 3-19 shows the DNVGL p-y curves obtained using Terzaghi coefficient (k=7.2 MN/m^3) in comparison with the curves obtained using Reese coefficient (k=42 MN/m^3) used normally in the DNVGL code. The use of the coefficient suggested by Terzaghi decreases the difference between the calculated and experimental p-y curves. In order to fully understand the origin of this difference an experimental program must be developed to measure the subgrade reaction inside the centrifuge and to verify if there are any influence of the centrifuge modelling technique on this coefficient. Centrifuge modelling uses clean and homogeneous sand which is different from the in-situ tests where the sand may have been submitted to ageing and cementation phenomena during time which could possibly justify the stiffer initial response of the in-situ soil.

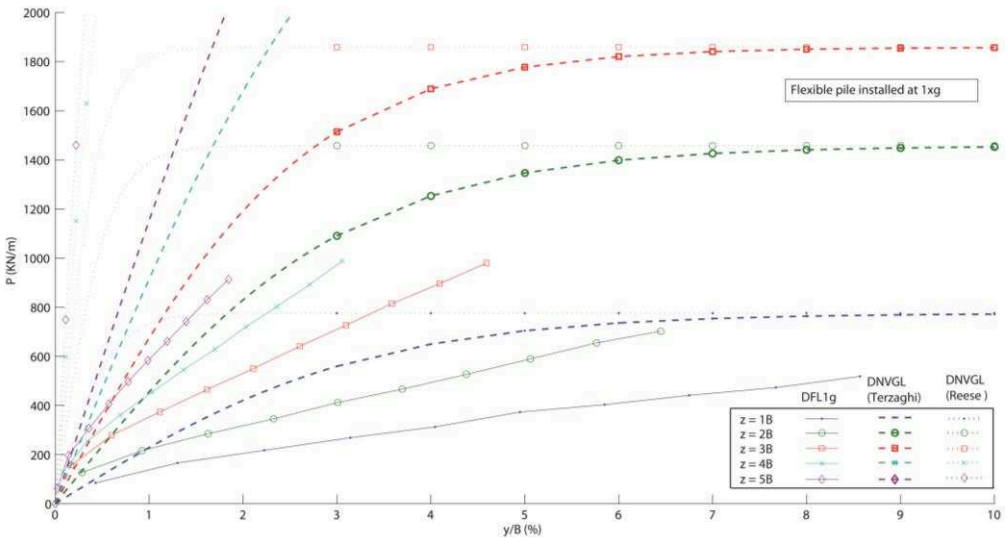

Figure 3-19: DNVGL using Terzaghi or Reese subgrade reaction coefficient

3.4.2.3.3.5 Quantitative comparison

Table 3-8 summarizes the comparison of the test p-y curves at some relative displacements of 1% and 3% at depths ranging from 1B to 5B. Increasing eccentricity causes a mean reduction of about 10% in the p-y curves at the different depths. At some relative displacements of 1% and 3% and for depths within the range 1B-5B, the sand saturation effect reduces the values of the p-y curves by 22% to 35%. Pile in flight installation, on the other hand, produces an increase in the p-y curves of between 30% and 50% at a relative displacement 1%. This increase can reach 70% with a relative displacement of 3%. As regards dry sand, DNVGL gives results five to eight times higher than experimental ones at 1% and three times higher at 3%. As regards saturated sand, DNVGL values are four to six times higher than experimental ones.

Table 3-8 : p-y curve comparison (kN/m)

y/B	1%					3%				
z/B	1B	2B	3B	4B	5B	1B	2B	3B	4B	5B
DFL1g	137	222	352	444	588	260	409	708	971	-
DFL100g	176	297	498	609	908	347	670	1229	-	-
SFL1g	114	174	277	289	420	208	298	491	627	832
DFH1g	128	160	310	483	572	254	346	638	887	-
DNVGL dry sand	775	1456	1851	3081	4602	775	1456	1851	3081	4602
DNVGL saturated sand	478	892	1138	1886	2817	478	892	1138	1886	2817

Stiffnesses at 0.5% of y/B of the studied tests are presented in Table 3-9 . Increasing eccentricity leads to a decrease of 25% in the stiffness at shallow depths but to a small increase at depths of 4B and 5B. Sand saturation affects stiffness by a decrease of up to 40%. In flight installation has an impact on stiffness at shallow depths causing an increase in stiffness of about 45% for z=1B and 15% for z=5B. As regards dry sand, DNVGL stiffness values are seven times higher than experimental ones. As regards saturated sand, however, DNVGL results are four times higher.

These results confirm the previous findings, i.e., the small impact of eccentricity on p-y curves. Sand saturation and installation method, on the other hand, are significant factors that can influence pile capacity.

Consequently, the same p-y curves can be used by the designer when the same range of eccentricities than this study is used. On the other hand, the effects of saturation and installation method must be taken into account. A revision of the DNVGL design code is therefore recommended since the high initial stiffness it uses may underestimate lateral displacement.

Table 3-9 : p-y curve stiffness at 0.5% of y/B (kN/m)

z/B	1B	2B	3B	4B	5B
DFL1g	183	313	500	604	746
DFL100g	268	387	647	682	858
SFL1g	158	288	414	414	541
DFH1g	140	184	384	676	791
DNVGL dry sand	1094	2129	2971	4346	5766
DNVGL saturated sand	600	1178	1677	2407	3137

3.4.3 Cyclic loading tests

In this section the effects of sand saturation, pile installation method and load eccentricities on the lateral behaviour of piles under large number of cycles are discussed.

Table 3-10 shows the new set of names given for the chosen tests to be presented in this section.

Table 3-10 : transition table for tests nomenclature

Test	New name	Dry or saturated sand (D/S)	High or low eccentricity (H/L)	Jacking at 1×g or 100×g (1g or 100g)	H_{min} (N)	H_{max} (N)	Nb of cycles
C11P2FL1G	DL1g	D	L	1g	50	500	200
C11P3FL100G	DL100g	D	L	100g	50	500	1000
C11P4FH1G	DH1g	D	H	1g	40	400	1000
C11P5FH100G	DH100g	D	H	100g	40	400	1000
C12P3FL1G	SL1g	S	L	1g	50	500	1000
C12P4FL100G	SL100g	S	L	100g	50	500	1000
C12P1FH1G	SH1g	S	H	1g	40	400	1000
C12P2FH100G	SH100g	S	H	100g	40	400	1000

3.4.3.1 Pile tests

Once the experimental discrete bending moment profile is obtained (Figure 3-20(c)), fitting these moments using a mathematical function for calculating p and y profiles is necessary. Moment fitting is an essential step in result analysis because mathematical processes like integration and derivation can be applied to moment profiles. The force per unit length, p, is determined through the double differentiation of the bending moment profile whereas the lateral displacement y is obtained through the double integration of the curvature M/EI.

As indicated in the section 3.4.2.2, two constant are needed for the double integration in order to obtain the profile of the lateral displacement. In the case of cyclic loading the second constant is obtained using the incremental method. In this method the pile is considered to rotate around the point where the soil reaction remains constant (Figure 3-21). When the pile changes from the loading to the unloading state or from the unloading to the loading one, if there is no variation of the soil reaction, the pile is assumed not to move horizontally at this depth. The pile, therefore, can be considered as rotating around a particular point where $y \neq 0$. Considering this condition, y at this point can also be assumed to be constant during the loading or unloading steps.

Figure 3-20(c) presents the experimental moments points as well as the fitting profiles. From these profiles, soil reaction (Figure 3-20(e)), shear force (Figure 3-20(d)), pile rotation (Figure 3-20(b)) and lateral displacement (Figure 3-20(a)) are determined.

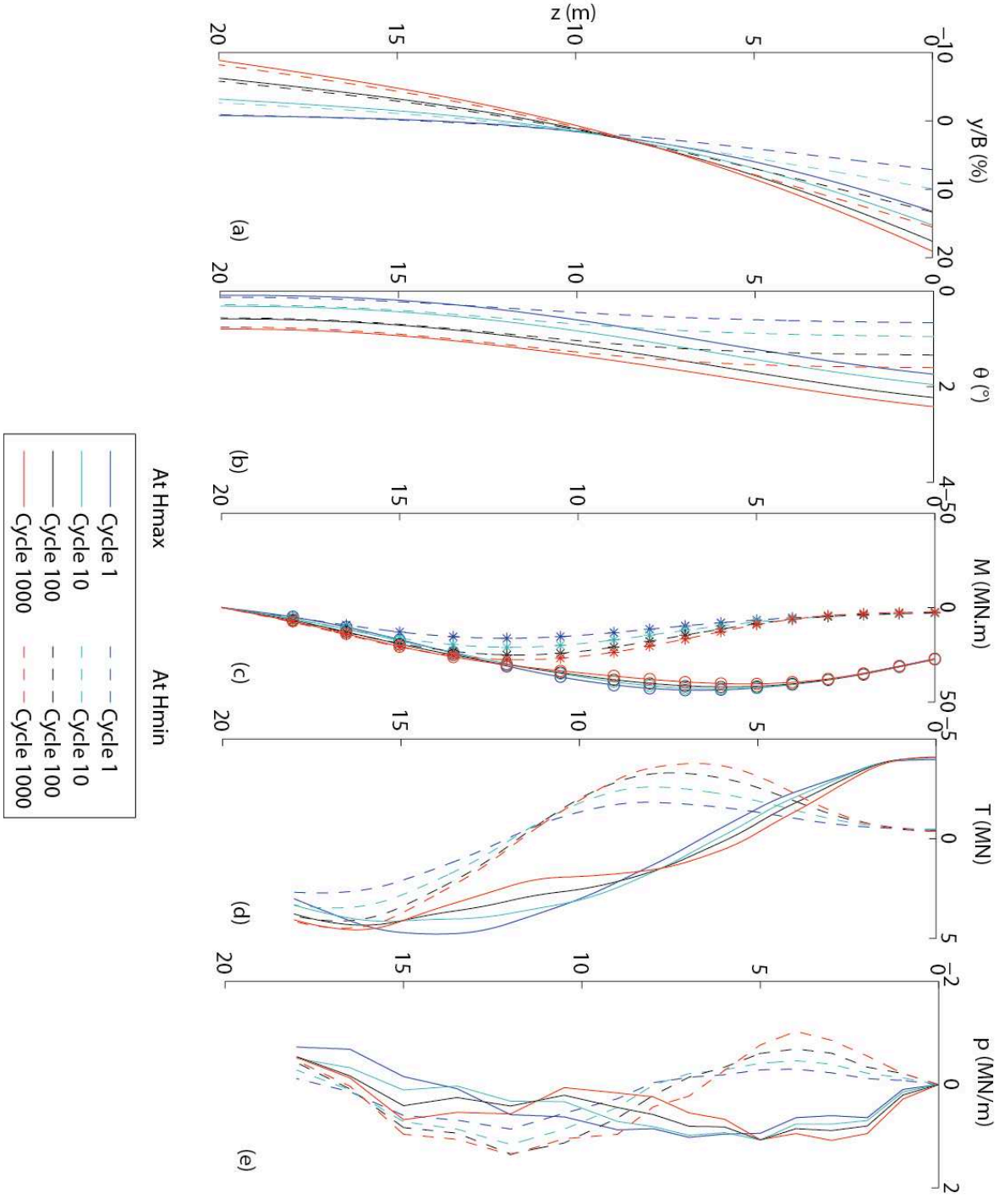

Figure 3-20 : DH1g: (a) pile deflection (b) pile rotation (c) moment profiles (d) shear force (e) soil reaction

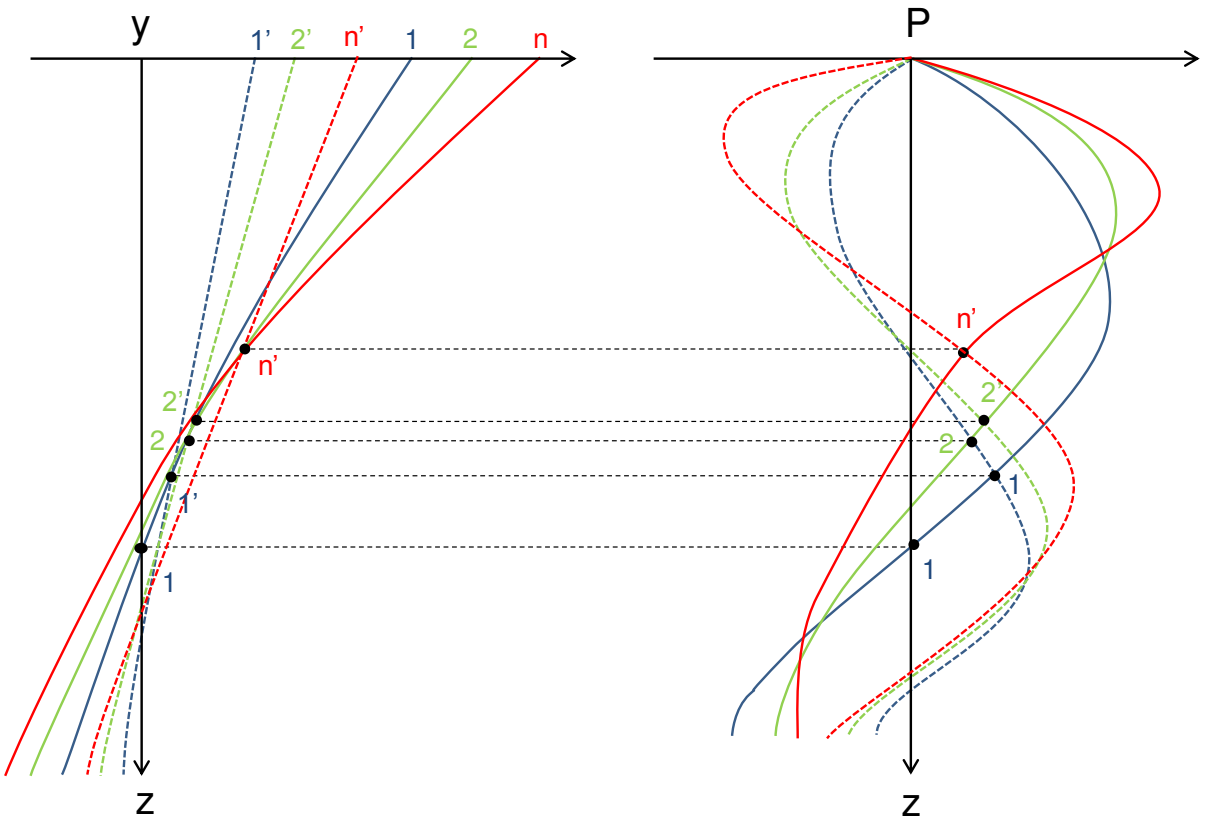

Figure 3-21: Principle of determination of the second constant for lateral displacement integration

Figure 3-20(e) shows the reaction profile of the pile for the cycles 1,10,100 and 1000 at the maximum loading and unloading processes. Once these profiles have been analysed, they can also provide an idea of the pile specific movements during loading and unloading phases. During the first loading phase, the soil reaction is positive up to a depth of 14 m whereas the reaction becomes negative below this depth. This is expected since the pile is rotating and deflecting during monotonic loading. During the first unloading phase, the reaction of the upper part of the pile up to a depth of 8 m is negative. Below this depth, the reaction is positive to a depth of approximately 17m, beyond which the pile is subjected to a weak negative reaction. The negative reaction of the upper part of the pile arises because, during the loading phase, the soil fills the void created behind the pile during displacement and prevents the pile from returning to its original position during the unloading phase. The lower part of the pile hence presents a positive reaction because, when the upper part of the pile cannot return to its initial position, its lower part tends to advance forward and is then subjected to a positive reaction by the soil. With increasing number of cycles the same behaviour is being repeated during the successive loading and unloading phases and an increase in the intensity

of the soil reaction is then observed. This can be explained by the densification of the soil with increasing cycles and the fact that pile displacement also increases, both generating a stronger soil reaction. The tested pile here may not only rotate as the number of cycles increases but also produce a small translation movement. This hypothesis, however, cannot be tested with the current experimental facility.

3.4.3.2 Global study

3.4.3.2.1 Pile displacement at sand surface

The accumulated displacement at sand surface during cyclic loading for Cycle N is normalized through the displacement during the first cycle (displacement at the end of the monotonic loading step) (Figure 3-22). The same is for the displacement of the pile at the cycles 1, 10, 100 and 1000 (Table 3-11). This figure shows also the fitting curves realized with the use of the coefficients (α) presented in Table 3-12 and based on the logarithmic law: $y_N/y_1 = 1+\alpha \ln N$. These coefficients are the degradation factor found in the logarithmic displacement law described above and determined by fitting the logarithmic function with the experimental curves up to 200 cycles. All the fitting curves have a correlation coefficient higher than 98% when compared with the experimental curves up to 200 cycles.

The effect of the load eccentricity on the lateral displacement is observed in Figure 3- on the examples of DL1g and DH1g. A summary of the whole set of tests (Table 3-11) indicates that the accumulation of the lateral displacement of the pile decreases with the increase of the eccentricity.

DL1g and DL100g results (Figure 3-22) show that pile in flight installation decreases the accumulation of the displacement. This is due to the increase in both densification and rigidity of the soil around the pile caused by the in-flight installation method. In sand saturation conditions, accumulated lateral displacement decreases slightly. The comparison of DH1g, DH100g and SH1g presents a performance different from the general trends observed in terms of installation method and eccentricity effects such as described above. Test DH1g is carried out in the strongbox, which has already been used for a series of tests of the campaign and hence has already experienced several increases and decreases in acceleration at the g level as well as another and longer lasting test at 100×g. In this context, the sand of the strongbox may have undergone a densification and, consequently, might have an influence on the decrease in the cumulative displacement of this test. This decrease accounts for DH1g behaviour difference in comparison with DH100g and SH1g.

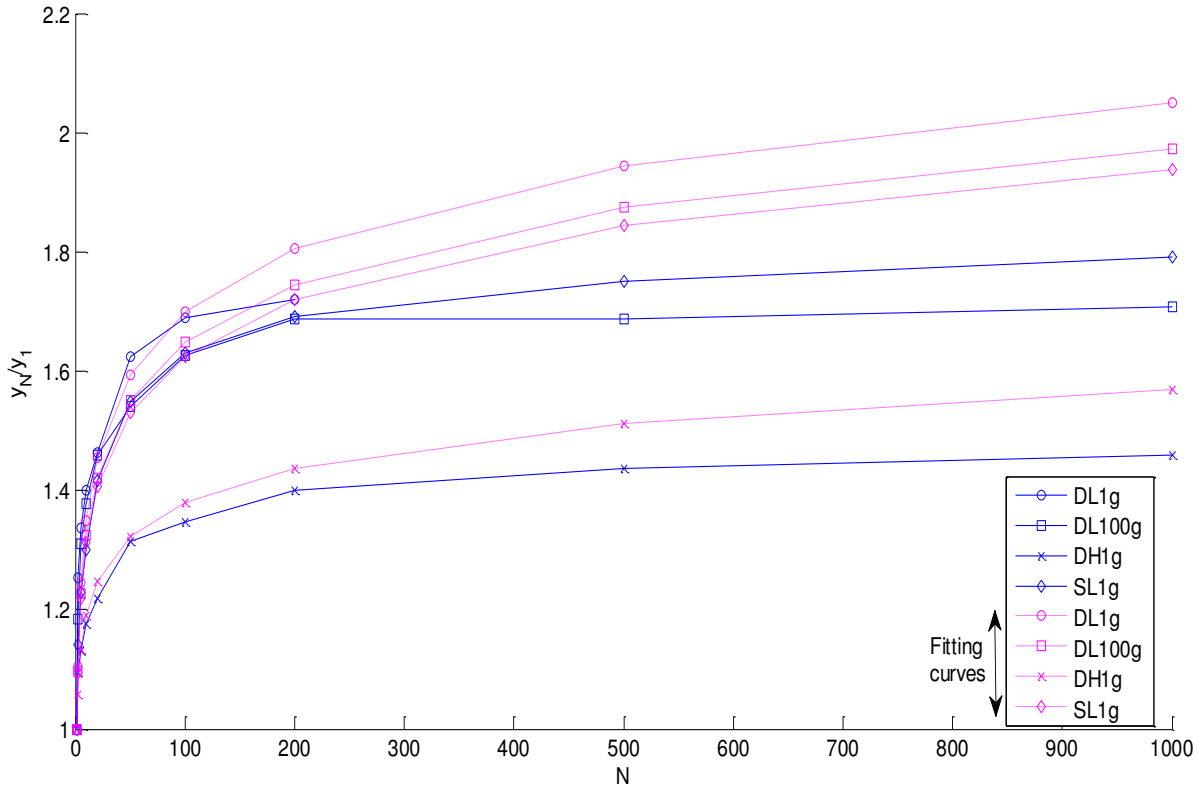

Figure 3-22: Effect of saturation and installation method and eccentricity on the lateral displacement of piles

Table 3-11 : lateral displacement in mm

Test	1	10	100	1000
DL1G	196.1	274.6	331.4	-
DL100G	149.7	206.2	243.7	255.8
DH1G	230.4	273.9	316.3	342.9
DH100G	137.7	178.5	211.2	227.3
SL1G	308.3	401.1	502.7	552.5
SL100G	222.6	271.6	318.6	340.5
SH1G	241.4	290.8	354.2	398.9
SH100G	225.2	271.9	313.9	327.1

The fitting curves obtained using the logarithmic law predict that pile displacement would still increase even after 200 cycles. However, the experimental curves show little increase in the displacement after 200 cycles. The range of coefficient α values, which describes accumulated lateral displacements, presented in Table 3-12 show smaller values than the ranges cited in the work of Bouafia (1994), Li et al. (2010) and Peralta (2010) (Table 3-3). On the other hand, the formula of Verdure et al. (2003) gives a value of 0.162 for the loading condition in the present

study which is similar to the coefficient given by the test DL1g. The coefficient achieved here in dry sand is higher than that proposed by Rosquoet et al. (2017) (α=0.077). This gap is probably explained by the difference in sand density. In the present study, the relative density is 58% but is 86% in Rosquoet et al. 2007. Rakotinindriana (2009) observes two different types of behaviour as regards accumulated displacements: a first one for the cycles up to 100 and the second one beyond 100 cycles when lateral displacement accumulation is represented on a semi-logarithmic scale. These tests have been carried out considering two relative densities (48% and 78%). The α coefficient for the number of cycles smaller than 100 ranges between 0.084 and 0.164 for a relative density of 48% and between 0.0899 and 0.135 for a relative density of 78% depending on the cyclic loading conditions, under which the tests are conducted. In the present study, only one type of cyclic loading is considered because focus is placed on the influence of other parameters (saturation, eccentricity and installation method). However, generally no significant change is observed in lateral displacement accumulation for the present tests.

Table 3-12 : lateral displacement fitting

Test	α	n
DL1G	0.152	0.125
DL100G	0.141	0.11
DH1G	0.082	0.071
DH100G	0.118	0.085
SL1G	0.136	0.124
SL100G	0.093	0.08
SH1G	0.098	0.086
SH100G	0.085	0.072

Figure 3-23 displays the pile rotation accumulated with the cycles and the fitting curves obtained using coefficients (n) described in Table 3-12. The accumulated pile rotation at sand surface exhibits similar overall behaviour as regards the effects of installation method, sand saturation and load eccentricity, as in the case of accumulated pile displacement.

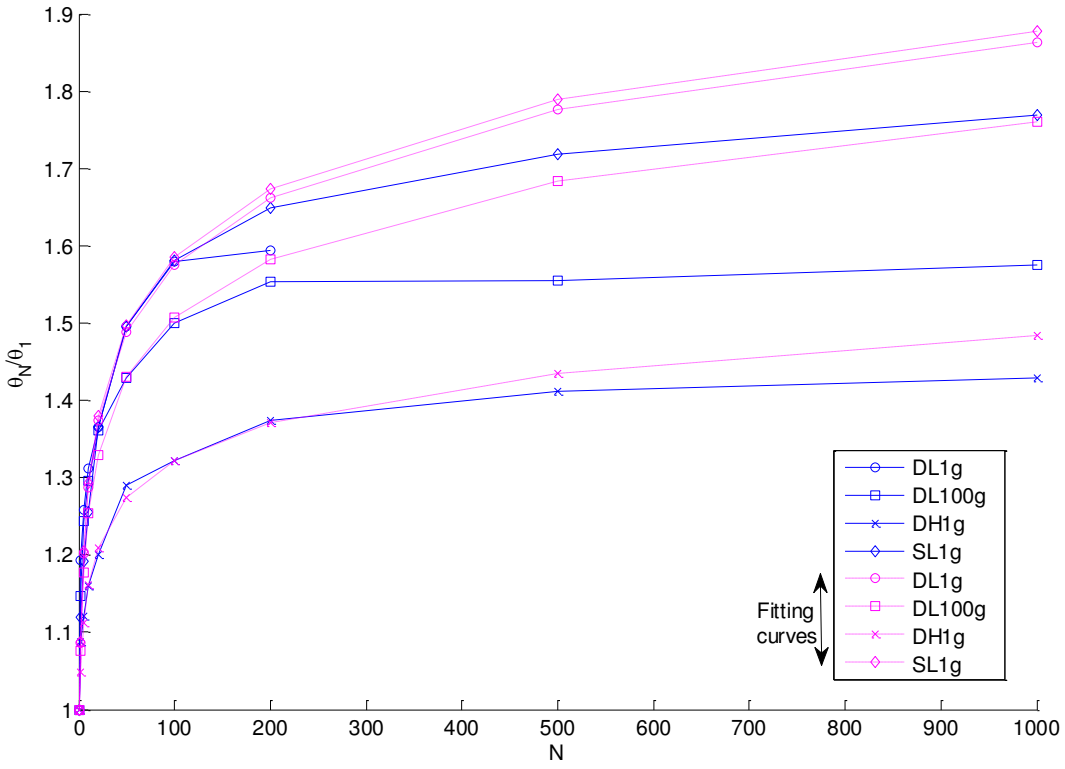

Figure 3-23 : Effect of saturation and installation method and eccentricity on the pile rotation at sand surface

3.4.3.2.2 Maximum moment

The moment profiles of pile DH1g are displayed in Figure 3-20(c) and the maximum moments and it depths for all the tested piles for the cycles 1,10,100 and 1000 are presented in Table 3-13. The maximum moment values and depths decrease as the number of cycles increases. This would be linked to an improvement in the rigidity and density of the soil within the shallower layers. The decreasing trend of the maximum moment is also affected by installation methods. In-flight pile installation increases soil density around the pile. The maximum moment value and depth decrease as a function of increasing cycles is higher for the piles installed at 1×g when compared with 100×g: a decrease of 2 to 9% for the piles installed at 100×g and of up to 16%for the piles installed at 1×g.

This is different from the considered position found in the literature (Rosquoet et al. 2007) where the maximum moment increases with the number of cycles. Rosquoet et al. (2007) observe an increase of 10% for the maximum moment after 40 cycles. However, this increase is strongly dependent on the loading level of the cycles: the smallest the load amplitude, the highest the maximum bending moment variation vs. number of cycles. When the load amplitude is equal to the maximum load, on the other hand, Rosquoet et al. (2007) obtain a

small increase or even a small decrease in one of their tests. In the tests summarized in Table 3-13, the load amplitude is equal to 90% of the maximum load. This high level may account for the increase in both rigidity and density of soil shallow layers and, consequently, for the decrease in the maximum moment observed here.

Table 3-13 : Evolution of the moment with cycles

Cycle number	1		10		100		1000	
Test	Moment (MN)	Depth (m)	Moment (MN)	Depth (m)	Moment (MN)	Depth (m)	Moment (MN)	Depth (m)
DL1G	36.5	7.2	36.1	7.15	35.4	7.1	-	-
DL100G	35	6.13	36.7	6.89	37.03	7.2	36.1	7.6
DH1G	43.9	6.6	43.1	6.2	42.1	5.8	40.5	5.1
DH100G	41.4	5	42.01	5.2	41.6	5.2	40.6	4.98
SL1G	39.6	7.4	38.1	7.2	36.2	7.1	33.4	6.7
SL100G	37.6	6.7	37.9	7.15	37.5	7.3	34.8	7.3
SH1G	44.1	6.1	42.9	5.87	41.6	5.4	38.8	4.6
SH100G	43.5	5.4	43.2	5.6	42.1	5.4	39.6	4.5

3.4.3.3 Cyclic p-y curves

Once the profiles of the lateral displacement and soil reaction at different depths using the method presented in section 3.4.3.1 are obtained, the p-y curves at different depths can be established.

Figure 3-24 presents the monotonic and cyclic p-y curves established for pile DH1g. For each depth, in addition to cycles 1, 10, 100 and 1000, the maximum and minimum cyclic p-y curves are plotted. The cyclic p-y curves of depths ranging from 1B to 3B (Figure 3-24(a)) exhibit similar behaviour: the p-y cyclic curves behave as an extension of the monotonic curves and the soil reaction increases with the number of cycles. This behaviour is also observed for all the minimum cyclic p-y curves at these depths. As regards cycle number, the difference between ymin and ymax during each cycle decreases as the number of cycles increases. This confirms that pile displacement during one cycle decreases with the number of cycles as well as the amplitude of the pile displacement cycles. Combined with increasing soil reaction in terms of cycles, this can be justified by the densification and the increase of the rigidity of the soil around the pile as the number of cycles increases. Soil behaviour, therefore,

is enhanced and the amplitude of the pile displacement during one cycle decreases. The depths between 4B and 6B (Figure 3-24(b)) correspond to a soil layer where pile displacement is very small. Consequently, the pile behavior during the cycles is unclear. Moreover, at such depths, the soil reaction profiles during the loading and the unloading phases cross and the presence of the pile rotation points is observed. It should be noted, however, that at depths of 4B and 5B, the maximum soil reaction decreases sharply as the number of cycles increases while the minimum soil reaction increases significantly. As mentioned before, this is due to the presence of the rotation points in this layers and to the fact that, with increasing cycles, the soil upper (loading phase) and lower (unloading phase) layers are increasingly mobilized. At depths between 7B and 10B, the soil reaction during the loading phase decreases slowly with the increase in the number of cycles whereas, during the unloading phase it increases slowly with the number of cycles. Consequently, the difference between Pmin and Pmax at all depths, with the exception of 7B, decreases as the number of cycles increases. Soil reaction during the unloading phase is even higher than during the loading phase for depths from 7B to 9B. This demonstrates that, at these depths, soil mobilization is turned towards preventing pile displacement during the unloading phase rather than during the loading phase, the upper soil layers playing the most important role in this case.

These findings are similar to those usually found in the literature (Rosquoet 2004), but with a difference as regards the shallower layers: in the literature, cyclic p-y curves normally deteriorate within the first layers in relation to the cycle number. In the present study, however, the first layers up to a depth of 2B show an improvement of the soil reaction with increasing number of cycles. This difference is probably explained by the high rigidity of the piles used compared with the normal flexible piles. This results in piles exhibiting significant rotation in addition to deflection. This would cause substantial mobilization and possible densification of the shallower soil layers. The effect is even stronger if coupled with a high cyclic loading level as discussed above in the section of the maximum moments.

Table 3-14 presents the stiffness values obtained during cycles 1, 10, 100 and 1000 at depths of 1B, 2B and 3B, at which pile lateral displacement is the greatest. The results show a sharp increase in the stiffness values of the cycles with increasing number of cycles. Between the first cycle and cycle 1000 the stiffness has increased four to five times. The clear stiffness increase confirms previous findings on the improvement of the sand shallower layers and increase in both rigidity and density of these layers.

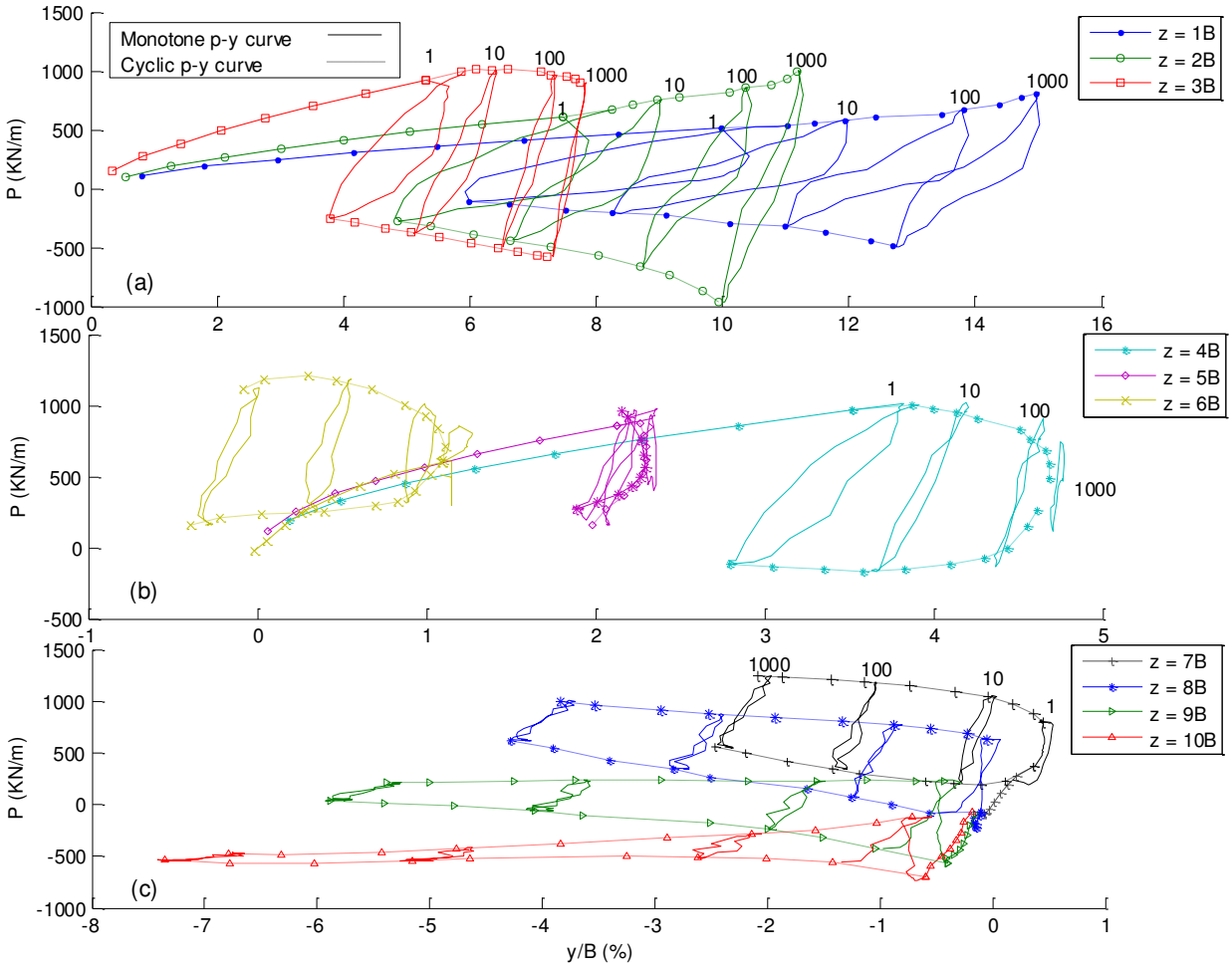

Figure 3-24 : Cyclic p-y curves DH1g

Table 3-14 : stiffness in MN/m

	1	10	100	1000
1B	8.2	11.89	19.59	32.01
2B	17.62	28.66	50.76	88.16
3B	39.95	59.72	99.08	158.17

3.4.3.3.1 Cylic p-y curves comparison

The influence of the installation method on the cyclic p-y curves is shown in Figure 3-25. During monotonic loading, pile in flight installation increases the initial rigidity of the p-y curves.). At the end of the monotonic phase, piles installed in flight present a higher level of soil reaction. During cyclic loading, soil reaction enhancement is greater at shallow depths for the piles installed at 1×g than for the piles installed in flight. At deeper depths, Pile DH100g

displays a degradation rate during the cycles higher than DH1g. At the end of the cycles, the level of the soil reaction at the different depths is similar for the piles installed at 1×g or at 100×g. This initial soil reaction difference between both piles, which originates in shallow layers during monotonic loading, is compensated whereas, at deeper layers, DH100g higher degradation rate causes the pile soil reaction to display results similar to DH1g ones. The initial gap between both piles observed during monotonic loading is due to the surrounding soil enhancement generated by pile in flight installation. With increasing number of cycles, the soil around pile DH1g becomes stiffer and the gap initially caused by the installation method is quickly compensated.

Figure 3-26 presents the influence of eccentricity on the cyclic p-y curves for the first 200 cycles (beyond that threshold, the laser results are not reliable). As with the monotonic p-y curves, load eccentricity does not affect the cyclic p-y curves.

Finally, the influence of saturation on the cyclic p-y curves is shown in Figure 3-27. Under monotonic loading conditions, the piles installed in dry sand present a stiffer response. Consequently, at the end of the monotonic loading step, Pile DL100g displacement values are smaller than Pile SL100g. However, both piles reach approximately similar levels of reaction (difference less than 15%). During cyclic loading, the similarity between the two piles continues to be observed with both piles showing approximately the same soil reaction level at the end of the cycles.

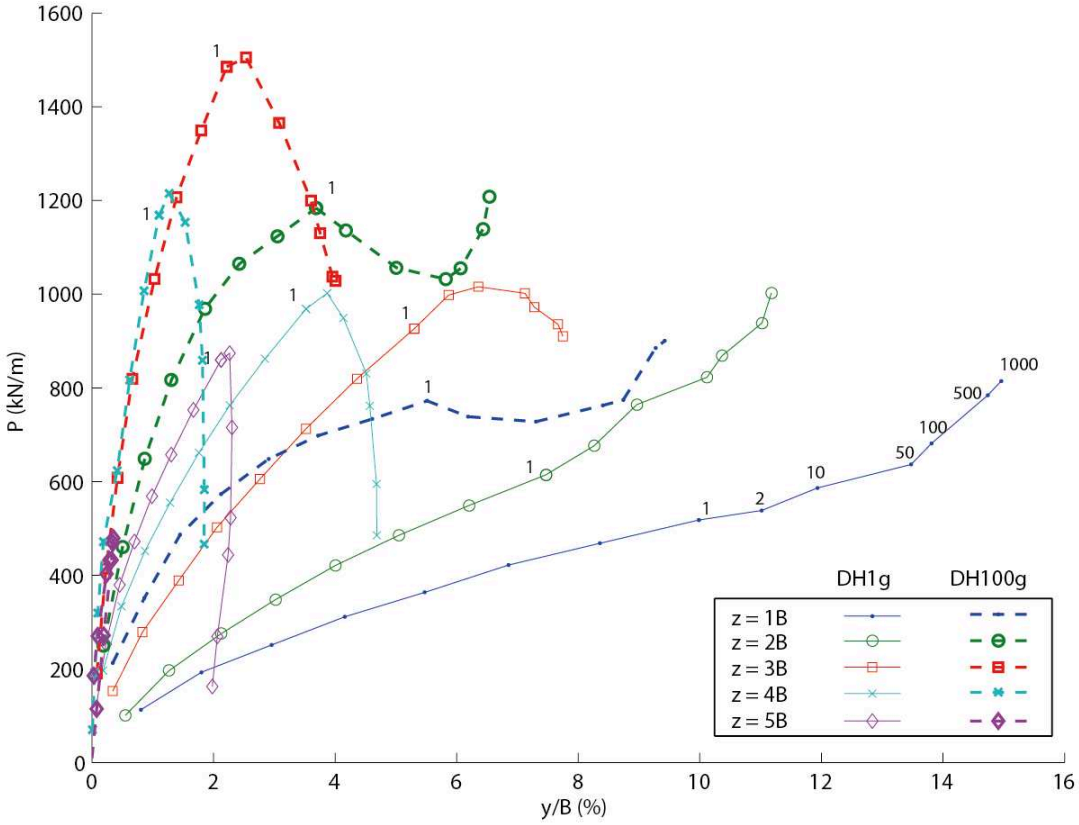

Figure 3-25: Effect of the installation method on cyclic p-y curves

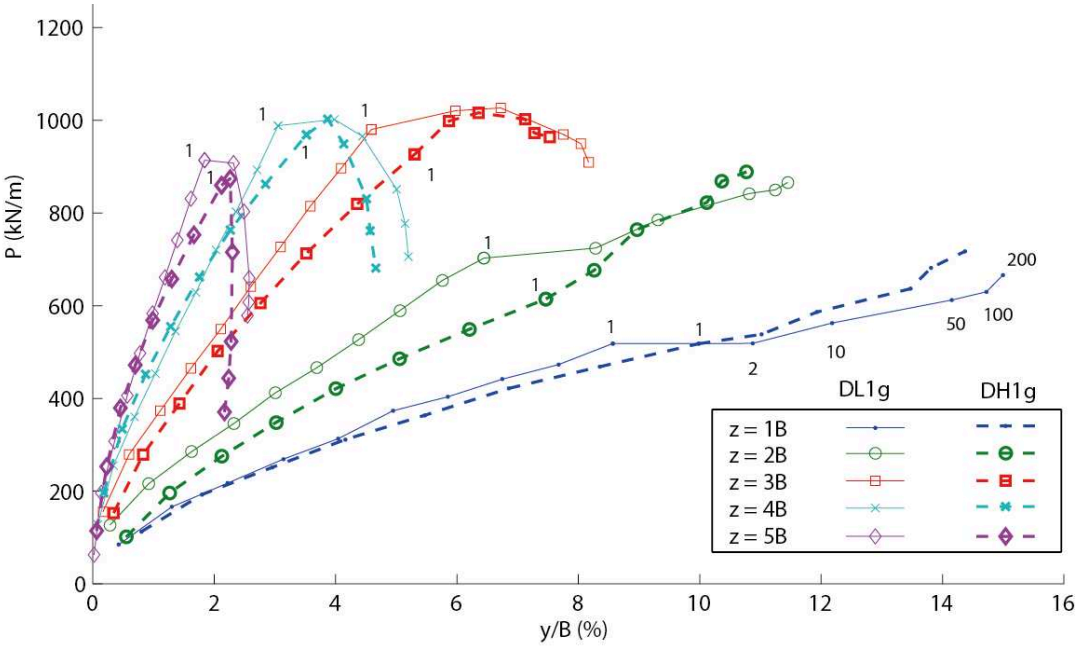

Figure 3-26: Effect of the eccentricity on cyclic p-y curves

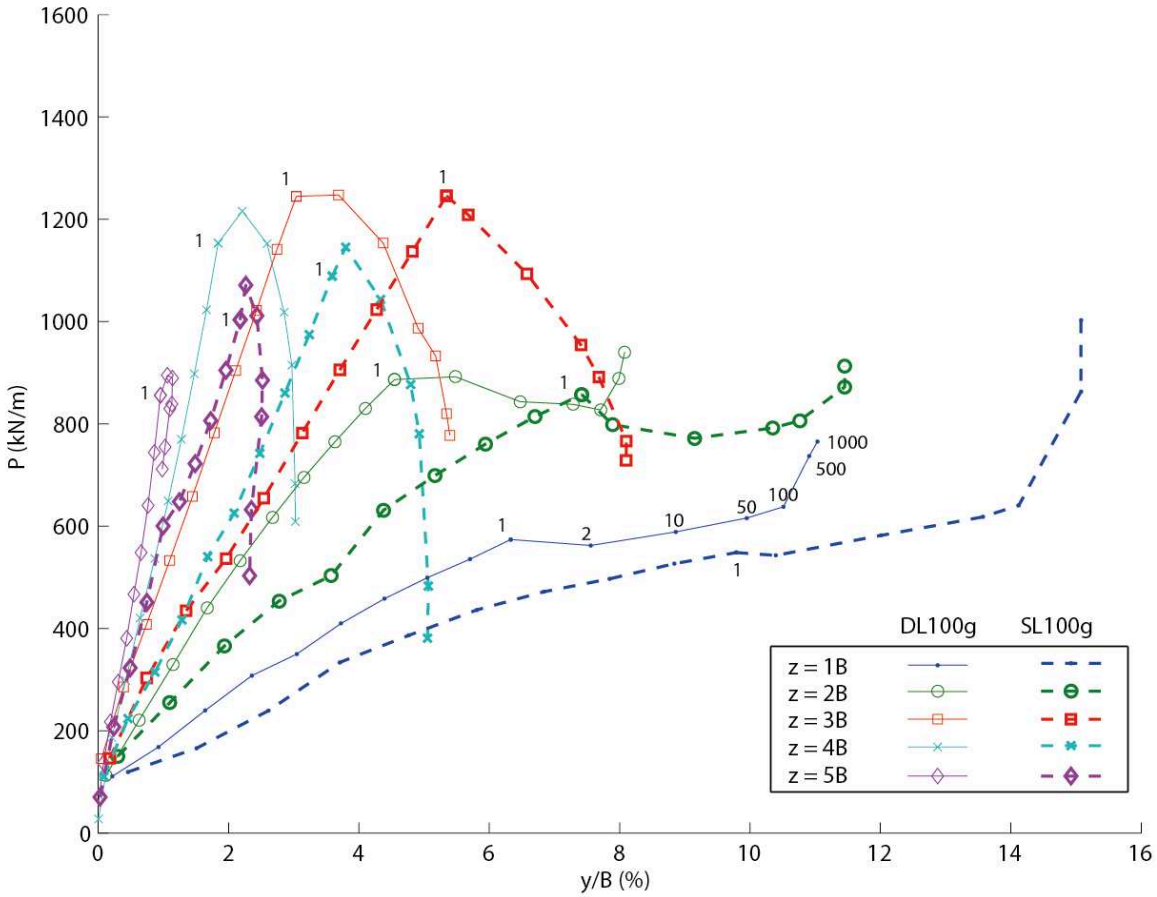

Figure 3-27: Effect of saturation on cyclic p-y curves

3.5 Conclusion

An instrumented model pile with 16 levels of gages at scales 1/100 with an embedment depth of 200 mm have been tested, using geotechnical centrifuge at 100×g, in order to determine the effects of the installation method, load eccentricity and sand saturation on the lateral behaviour of single pile under monotonic and cyclic loading.

The failure force, identified on rigid pile with the double-tangent approach, is higher: 1) in the case of piles installed at 100×g in comparison with the piles installed at 1×g 2) When the eccentricity of the load is lower.

A new method is developed for the determination of the constants required for the integration procedure used to determine the pile lateral displacement profile. The identification of the second constant consists in determining the pile rotation centre using the soil reaction profile. A full discussion of the method and of its benefits is also proposed. This method, called incremental method, allows for the establishment of the p-y curves of tests conducted on instrumented piles even if only one limit condition can be measured reliably during testing.

After the identification of the method of the double integration, the effects of the installation method, load eccentricity and sand saturation on the global (pile displacement and moments) and local (p-y curves) behaviour of piles are determined.

A. For the **monotonic loading** analysis:

1. Increasing **load eccentricity** produces softer response of the p-y curves. DNVGL does not take the effect of this parameter into account. Because load eccentricity effects are not very significant and for practical reasons, we suggest using the same set of p-y curves to assess pile response when different load eccentricities are applied.
2. The **sand saturation** proved to be an important parameter: 1) it can affect lateral displacement with an increase up to 57% of the displacement compared to dry sand. 2) the saturation of the medium dense sand led to about 40 % softer response of the p-y curves in comparison with dry sand.
3. Pile **in-flight installation** causes a decrease of 24% in the lateral displacement of the piles at sand surface. They have also maximum moment values smaller and shallower than the maximum moments of the piles jacked at 1×g. The previous results can be attributed to the densification of the shallow sand depth. The p-y curves corresponding to these piles display a final threshold of up to 70% higher and an initial response of up to 45% stiffer than the piles installed at 1×g.

The comparison with the p-y curves of the DNVGL code showed that the design code doesn't take into consideration the effect of eccentricity and installation method on the p-y curves. For dry sand the DNVGL showed stiffness's 7 times higher than the experimental ones. On the other hand, for saturated sand the DNVGL was 4 times higher.

B. For the **cyclic loading** (up to 1000 cycles) analysis:

The maximum moment in the pile during the cycles is analyzed and showed to decrease in value and become shallower with the increase of the cycles. The displacement at sand surface is also presented. A detailed examination and interpretation of the cyclic p-y curves of a test is then presented for the different layers of the soils.

1. The accumulation of the lateral displacement of the pile decreases with the increase of **the eccentricity** but the load eccentricity didn't show to have an important effect on the development of cyclic p-y curves.

2. The **sand saturation** shows a little decrease in the accumulation of lateral displacement but didn't show to have an important effect on the development of cyclic p-y curves.
3. The **installation of the pile in flight** induces generally a decrease of the accumulation of the displacement. Concerning the p-y curves, the shallow depths showed an improvement of the soil reaction at a better rate for the pile installed at 1×g in comparison with the pile installed at flight. On the other hand in the deeper depths the pile installed at flight show a higher degradation rate during the cycles than the pile installed at 1×g.

4 Conclusion and perspectives

A parametric study, on centrifuge small-scale model pile at 100×g, was realized in order to study the different parameters that can affect the axial and lateral behaviour of piles.

The **axial capacity** is studied using different type of model piles installed in homogenous Fontainebleau sand prepared by air pluviation technic in order to obtain two relative densities (58% and 99%). Each pile had an embedded depth of 25 cm at 100×g which represent a prototype pile of 25 m of depth.

The **effect of installation method** is studied using a rigid rough 18 mm pile instrumented at the tip. The pile was installed monotonically at 1×g, monotonically at 100×g or cyclically at 100×g. The pull out capacity of the piles showed a clear tendency to increase with the increasing number of the installation strokes. The results show a pull out capacity gain of up to 67% with increasing cyclic installation strokes. The explanation discussed in this thesis has proposed that a possible relationship may exist between the gain in the capacity and the dilation and crushing of sand usually observed in cases where rough surfaces are in contact with dense sand.

The effect of **pile diameter**, **pile tip geometry**, **sand density** and **sand saturation** is then presented using piles with different diameter and different tip conditions (open or closed-ended). The main results that can be exploited from this study are the followings:

- The saturation of dense sand has significant influences on plug creation during pile installation.
- The displacement until tension failure differs depending on the density and water content conditions. Its values does not always equal the conventional value of 10% of B.
- The initial stiffness increases with sand density being, however, lower in saturated sand than in dry sand.
- A linear relationship between the jacking load and the embedded volume of the tested piles is described.
- The decrease in pile diameter enhances plug formation in open-ended piles.
- Open-ended piles showed greater tension capacities than closed ones.
- The ratio of the tension to the compression capacity is systematically larger for open-ended piles than for closed-ended piles.

The last parameter studied for the axial loading is the **pile roughness** which is realized by comparing the capacities of a smooth and a rough pile and give as results:

- The increase of roughness show that the pull out shaft resistance increases by 36% in dense sand and by 57% in medium sand. The push-in shaft friction, moreover, triples as roughness increases.
- Rough piles, indeed, present push-in and pull-out shaft resistances three times higher in dense sand than in medium sand. Smooth piles, moreover, reveal some push-in and pull-out shaft resistances four times higher in dense sand than in medium sand.

In all the cases a comparison between the experimental results and the capacities given by the design codes is realized. In compression, the design codes are generally conservative in comparison with the experimental results. In tension mode, ICP performance is good in dense sand. However, both ICP and NF provide a large overestimate of the pile tension capacities in medium dense sand. API and DNVGL also overestimate the tension capacity in medium dense sand while underestimating it in dense sand.

The second part of this report discusses the study realized on the **lateral behaviour** of piles. Several tests were realized using a 16 levels instrumented pile from inside installed in medium dense Fontainebleau sand in order to determine the effects of the installation method, load eccentricity and sand saturation on the lateral behaviour of single pile under monotonic and cyclic loading. The model pile at 100×g represents a prototype pile of 20 m of depth, 1.8 m of diameter and a bending stiffness of 19.74 GN.m^2.

The failure force, identified on rigid pile with the double-tangent approach, is higher: 1) in the case of piles installed at 100×g in comparison with the piles installed at 1×g 2) When the eccentricity of the load is lower.

A new method is developed for the determination of the constants required for the integration procedure used to determine the pile lateral displacement profile. The identification of the second constant consists in determining the pile rotation centre using the soil reaction profile. A full discussion of the method and of its benefits is also proposed. This method, called incremental method, allows for the establishment of the p-y curves of tests conducted on instrumented piles even if only one limit condition can be measured reliably during testing.

After the identification of the method of the double integration, the effects of the installation method, load eccentricity and sand saturation on the global (pile displacement and bending moments) and local (p-y curves) behaviour of piles are determined.

For the **monotonic loading** analysis:

- Increasing **load eccentricity** within sand produces softer response of the p-y curves.
- The **sand saturation** proved to be an important parameter: 1) it can affect lateral displacement with an increase up to 57% of the displacement compared to dry sand. 2) the saturation of the medium dense sand led to about 40 % softer response of the p-y curves in comparison with dry sand.
- Pile **in-flight installation** causes a decrease of 24% in the lateral displacement of the piles at sand surface. The p-y curves corresponding to these piles display a final threshold of up to 70% higher and an initial response of up to 45% stiffer than the piles installed at 1×g.

The comparison with the p-y curves of the DNVGL code showed that the design code doesn't take into consideration the effect of eccentricity and installation method on the p-y curves. For dry sand the DNVGL showed stiffness' 7 times higher than the experimental ones. On the other hand, for saturated sand the DNVGL was 4 times higher.

For the **cyclic loading** (up to 1000 cycles) analysis:

- The accumulation of the lateral displacement of the pile decreases with the increase of **the eccentricity** but the load eccentricity didn't show to have an important effect on the development of cyclic p-y curves.
- The **sand saturation** shows a little decrease in the accumulation of lateral displacement but didn't show to have an important effect on the development of cyclic p-y curves.
- The **installation of the pile in flight** induces generally a decrease of the accumulation of the displacement. Concerning the p-y curves, the shallow depths showed an improvement of the soil reaction at a better rate for the pile installed at 1×g in comparison with the pile installed at flight. On the other hand in the deeper depths the pile installed in flight displays a higher degradation rate during the cycles than the pile installed at 1×g.

The perspectives and the continuation of this work could follow several approached:

- Studying the effect of the sand density on the lateral behavior of piles. A number of tests have been realized in this study in very dense sand but not fully analyzed. A comparison with the obtained results and with additional tests in loose sand could be made.
- Analyzing the strain gauges response during the installation of the piles. The use of the quarter-bridge gauges gives the possibility to study the shaft friction of the pile during its installation.
- Pile driving. In the present study two installations methods were used (jacking at 1×g or 100×g) but the offshore piles are driven in situ. The development of an adequate in-flight hammer for driving model piles could model more precisely the reality.
- Using inclined load. All the tests realized were under horizontal or vertical loading. The use of inclined load can be important to verify the hypothesis of its decomposition in lateral and vertical loadings.
- Using fiber optic. With the development of the instrumentation techniques, it is possible nowadays to use fiber optics inside model piles, which gives the opportunity, in comparison with strain gauges, to reduce considerably the wiring harness, and then to work on small-scale model open-ended piles.
- The present study treated the case of an intermediate pile between a monopile and a long flexible pile. It should be interesting to study the effects of the studied parameters of this thesis in the case of shorter monopiles.
- The highly controlled data obtained on physical models, constitutes a database that could be more coupled with numerical modelling, including particularly the effect of the installation method, with modern approaches such as the Material Point Method (MPM).

5 References

[1] Achmus, M., Kuo, Y.S. & Abdel-Rahman, K. (2009). Behavior of monopile foundations under cylic lateral load. Computers and Geotechnics. **36**: 725-735.

[2] Aksoy, H.S., Inal, E. & Gor, M. (2016). Skin friction between soil and pile materials. ASCE 2016. 12th international congress on advances in civil engineering. Istanbul/ Turkey.

[3] Alawneh, A.S., Malkawi, A.I.H. & Al-Deeky, H. (1999). Tension tests on smooth and rough model piles in dry sand. Can.Geotech. J. **36**: 746-753.

[4] Alizadeh, M. & Davisson, M.T. (1970). Lateral load test on piles Arkansas River project. J. Soil Mech. And Found. Engrg. Div. ASCE. **96**(5): 1583-1604.

[5] Altuhafi, F.N., Jardine,R.J., Georgiannou, V.N. & Moinet, W.W. (2018). Effects of particle breakage and stress reversal on the behaviour of sand around displacements piles. Géotechnique. **68**(6):546-555.

[6] API 1993. Recommended practice for planning, designing, and constructing fixed offshore platforms: working stress design, RP2A-WSD, 20th edn. Washington, DC: American Petroleum Institute.

[7] API (American Petroleum Institute) (2011). API RP 2GEO: geotechnical and foundation design considerations. American Petroleum Institute, Washington, DC, USA.

[8] Biarez, J. & Gresillon, J. (1972). Essais et suggestions pour le calcul de la force portante des pieux en milieu pulvérulent. Geotechnique **22**(2) : 433-450.

[9] Blanc, M. & Thorel, L. (2016). Effects of cyclic axial loading sequences on piles in sand. Géotechniques Letters **6**:1-5.

[10] Bouafia, A. (1994). Etude experimental du chargement lateral cyclique repeté des pieux isolés dans le sable en centrifugeuse. Can.Geotech. J. **31**(5):740-748.

[11] Broms, B. (1964). Lateral resistance of piles in cohesionless soils. J. Soil Mech and Found. Engrg. ASCE. **90**(3): 123-156.

[12] Bustamante, M. & Gianeselli, L. (1982). Pile bearing capacity by means of static penetrometer CPT. 2nd Eur.Symp. on penetration testing. Amesterdam.493-500.

[13] Byrne, B.W., McAdam, R.A., Burd, H.J. Houlsby, G.T., Martin, C.M. Beuckelaers, W.J.A.P, Zdravkovic, L., Taborda, D.M.G, Potts, D.M., Jardine, R.J, Ushev, E., Liu, T.F., Abadias, D., Gavin, K., Igoe, D., Doherty, P., Skov Gretlund, J., Pacheco Andrade, M., Muir Wood, A., Schroeder, F.C, Turner, S and Plummer, M. (2017) PISA: New Design Methods for Offshore Wind Turbine Monopiles. Keynote. Proc 8th Int. Conf. on Offshore Site Investigations and Geotechnics, SUT London. Vol. 1, p. 142-161. doi:10.3723/OSIG17.142 https://www.ingentaconnect.com/content/sut/1hzvzd

[14] Chang, C.S. & Whitman, R.V. (1988). Drained permanent deformation of sand due to cyclic loading. Journal of Geotechnical Engineering. ASCE. **96**(5): 1605-1627.

[15] Clausen, C. J. F., Aas, P. M. & Karlsrud, K. (2005). Bearing capacity of driven piles in sand, the NGI approach. In Frontiers in offshore geotechnics (eds S. Gourvenec & M. Cassidy), pp. 677–681. London: Taylor & Francis.

[16] Davisson, M.T. & Salley, J.R. (1968). Lateral load tests on drilled piers. ASTM Symp. On Deep Found. West Conshohocken. 68-83.

[17] Deeks, A.D., White, D.J. & Bolton, M.D. (2005). A comparison of jacked, driven and bored piles in sand. Proc. 16th Int. Conf. on Soil Mechanics and Geotechnical Engineering. Vol 16, AA Baleka, Osaka, Japan, 2103-2106.

[18] De Nicola, A. & Randolph, M.F. (1994). Tensile and compressive shaft capacity of piles in sand. Journal of Geotechnical Engineering, ASCE **119**(12):1952-1973.

[19] De Nicola, A. & Randolph, M.F. (1999). Centrifuge modeling of pipes piles in sand under axial loads. Géotechnique **49**(3): 295-318.

[20] DNV (1977). Rules for the design, construction and inspection of offshore strcutures. Hovek, Norway: Det Norske Veritas.

[21] DNV (2004). Offshore standard: Design of offshore wind turbine structures, DNV-OS-J101. Hellerup, Denmark: Det Norske Veritas.

[22] DNVGL-ST-0126 (2016). Support structures for wind turbines. Appendix F pile resistance and load-displacement relationships.168p.

[23] Duncan, J.M., Evans Jr., L.T. & Ooi, P.S.K. (1994). Lateral load analysis of single piles and drilled shafts. J. Geotech and Geoenvron Eng. **120**(6):1018-1033.

[24] Dyson, G .J. & Randolph, M.F. (2001). Monotonic lateral loading of piles in calcareous sand. J. Geotech. Geoenviron. Eng. **127**(4):346-352.

[25] El haffar, I., Blanc, M., Thorel, L. (2017). Impact of pile installation method on the axial capacity in sand. Géotechnique Letters. **7**:260-265.

[26] Eurocode 7. (2005). Geotechnical design – Part 1 general rules (NF EN 1997). 145p.

[27] Eurocode 3 (2002) DD ENV 1993-5:1998. Design of steel structures, chapter 5, piling.

[28] Fellenius, B. & Altaee, A. (1995). Critical depth: How it came into being and why it does not exist. Proceedings of the ICE-Geotechnical.

[29] Fisher, D.J., O'Neill, M.W. & Contreras, J.C. (1995). DS^2: Drilled shaft decision support system. J. Constr. Eng. Manage. **121**(1):86-94.

[30] Fond 72. (1972). Fondations courantes d'ouvrages d'art. LCPC SETRA, Ministere de l'Amenagement du Territoire, de l'equipement, du Logement et du Tourisme. Fascicule 5.

[31] Foray, P., Colliat J-L. & Nauroy, J-F. (1993). Bearing capacity of driven model piles in dense sands from calibration chamber tests. Proceedings 25th Offshore Technology Conference, Houston, Tex., May 1993, OTC Paper 7194, **2**: 655-665.

[32] Foray, P., Balachowski, L. & Colliat J-L. (1998). Bearing capacity of model piles driven into dense overconsolidated sands. Can. Geotech. J. **35**:374-385.

[33] Frank, R. (1999). Calcul des fondations superficielles et profondes, Techniques de l'ingénieur, Presses de l'Ecole Nationale des ponts et chaussées.141pages.

[34] Gaaver, K.E. (2013). Uplift capacity of single piles and pile groups embedded in cohesionless soil. Alexandria Engineering Journal. **52**: 365-372.

[35] Garnier, J. & Konig, D. (1998). Scale effects in piles and nail loading tests in sand. Proceedings International Conference Centrifuge 98. Tokyo. Vol. 1. pp. 205-210.

[36] Garnier, J. (2001). « Modèles physiques en géotechnique. Partie I : Evolution des techniques expérimentales et des domaines d'application ». Révue française de géotechnique, Paris, France, **97**(4), 3-29.

[37] Garnier, J. (2002). « Modèles physiques en géotechnique. Partie II : Evolution des techniques expérimentales et des domaines d'application ». Révue française de géotechnique, **98**(1), 5-28.

[38] Garnier, J., Gaudin, C., Springman, S.M., Culligan, P.J., Goodings, D., Konig, D., Kutter, B., Phillips, R., Randolph, M.F., & Thorel, L. 2007. Catalogue of scaling laws and similitude questions in geotechnical centrifuge modelling. International Journal of Physical Modelling in Geotechnics. **7**(3): 01-23.

[39] Gavin, K., Lgoe, D. & Doherty, P. (2011). Piles for offshore wind turbines: a state-of-the-art review. Geotechnical Engineering. **164**: 245-256.

[40] Guefrech A., Rault G.,Chenaf N., Thorel L., Garnier J., Puech A. (2012). Stability of cast in place piles in sand under axial cyclic loading . 7th Int. Conf. Offshore Site investigation and Geotechnics. London. 12-14 sept. pp.329-334.

[41] Hadjadji, T., Frank, R. & Degny, E. (2002). Analyse du comportement expérimental de pieux sous chargements horizontaux, Rapport de recherché serie Géotechnique et Risques Naturels. No. GT-74. May 2002.

[42] Hanna, T.H. & Tan, R.H.S. (1973). The behaviour of long piles under compressive loads in sand. Canadian Geotechnical Journal **10**(3): 311-340.

[43] Hansen, B. (1961). The ultimate resistance of rigid piles against transversal force. Bulletin n°12. The Danish Geotechnical Institut. Copenhaguen. Pp.1-9.

[44] Henke, S. &Grabe, J. (2008). Numerical investigation of soil plugging inside open-ended piles with respect to the installation method. Acta Geotechnica. **3**:215-223.

[45] Hokmabadi, A.S., Fakher, A., Fatahi & B. 2012. Full scale lateral behavior of monopoles in granular marine soils. Marine structures **29**. 198-210.

[46] Hossain, M.K. & Briaud, J.L. (1993). Improved soil characterization for piles in sand in API RP-2A. Proceedings of the 23rd Annual Offshore Technology Conference, Houston, OTC paper 7193: 637-654.

[47] Huang, A.B., Hsueh, C.K., O'Neill, M.W., Chern, S. & Chen, C. (2001). Effects of construction on laterally loaded pile groups. J. Geotech. Geoenviron. Eng.**127**(5): 385-397.

[48] Iskander, M. (2010). Behavior of Pipe Piles in Sand. Pp 25-33.

[49] Jamiolkowski, M., Ladd, C.C., Germain, J.T. & Lancellotta, R. (2003). Evaluation of relative density and shear strength of sands from CPT and DMT. Proc Soil Behavior and Soft Ground Construction, J.T. Germaine, T.C. Sheahan, and R.V. Whiteman, eds ASCE New York, 201-238.

[50] Jardine, R.J., Lehane B.M.& Everton, S.J. (1993). Friction coefficients for piles in sands and silts. Offshore Site Investigation and Foundation Behaviour **28**: 661-677.

[51] Jardine R.J. & F.C. Chow. (1996). New Design Methods for Offshore Piles. Marine Technology Directorate Ltd., Publication MTD 96/103, London 1996. ISBN 1 870553 31 4.

[52] Jardine, R., Overy, R. & Chow, F. (1998). Axial capacity of offshore piles in dense North Sea sands. J.of Geotech. Geoenviron. Engng, ASCE, **124**(2):171-178.

[53] Jardine, R., Chow, F., Overy, R. & Standing, J. (2005). ICP design methods for driven piles in sands and clays.Thomas Telford, London.

[54] Kerisel, J. (1961). Fondations profondes en milieu sableux. In Proceedings of the fifth International conference Soil Mechnics. Pp. 73-83.

[55] Khemakhem, M. (2012). Etude expérimental de la réponse aux charges latérales monotones et cycliques d'un pieu fore dans l'argile. PhD thesis. Ecole Centrale de Nantes.

[56] King, G.J.W. (1994). The interpretation of data from tests on laterally loaded piles. In Leung, C.F., Lee, F.H. & Tan, T.S. (eds). Centrifuge 94. Pp. 515-520. Rotterdam: Balkema.

[57] Klinkvort, R.T. (2012). Centrifuge modelling of drained lateral pile-soil response. PhD Thesis. DTU. Technical University of Denmark.

[58] Kim, B.T., Kim, N.K., Lee, W.J. & Kim, Y.S. (2004). Experimental load-transfer curves of laterally loaded piles in Nak-Dong River sand. J. Geotech. Geoenviron. Eng. **130**(4): 416-425.

[59] Kim, J. H., Choo, Y.W., Kim, D.J. & Kim, D.S. (2016). Miniature cone tip resistance on sand in a centrifuge. J.of Geotech. Geoenviron. Engng, ASCE, **142**(3): 04015090.

[60] Kishida, H. & Uesugi, M. (1987). Tests of the interface between sand and steel in the simple shear apparatus. Geotechnique **37**(1):45-52.

[61] Ko, H.Y., Atkinson, R.H., Globe, G.G. & Ealy, C.D. (1984). Centrifuge Modelling Of Piles Foundations, Analysis and Design Of Piles Foundations, J.R. Meyer, Ed., ASCE, New York: 21-40.

[62] Ko, J. & Jeong, S. (2015). Plugging effect of open-ended piles in sandy soil. Can Geotech.J. **52**: 535-547.

[63] Kolk, H. J., Baaijens, A. E., and Senders, M.(2005). Design criteria for pipe piles in silica sands. Proc., Int. Symp. on Frontiers in Offshore Geomechanics, ISFOG, Taylor & Francis, London, 711–716.

[64] Kong, L.G. & Zhang, L.M. (2007). Rate-controlled lateral-load pile tests using a robotic manipulator in centrifuge. Geotechnical Testing Journal. **30**(3):192-201.

[65] Kondner R.L. (1963). Hyperbolic stress-strain response: cohesive soils. J. Soil Mech. And Fund. Div. **89**(1):115-144. ASCE.

[66] Kraft, L.M. (1990). Computing axial pile capacity in sands for offshore conditions. Marine Geosources & Geotechnology **9**(1):61-92.

[67] Kraft, L.M. (1991). Performance of axially loaded pipe piles in sand. Journal of Geotechnical Engineering **117**(2), 272-296.

[68] Kramer, S.L. & Heavey, E.J. (1988). Lateral load analysis of nonlinear piles. Journal Geotech. Eng. ASCE. **114**(9): 1045-1049.

[69] Kulhawy, F.H. (1984). Limiting Tip and Side Resistance-Fact or Fallacy? In Foundation Engineering in the Face of Uncertainty@ sHonoring Fred H. Kulhawy. Pp18-36. ASCE.

[70] Kumara, J.J., Kikuchi, Y. & Kurashina. (2016). The effectiveness of thickened wall at the pile base of open-ended piles in increasing soil plugging. Japanese Geotechnical Society Special Publication **4(6)**: 138-143.

[71] Leblanc, C., Byrne, B.W., Houlsby, G.T. (2010a). Response of stiff piles to random two-way lateral loading. Géotechnique. **60**(9): 715-721.

[72] Leblanc, C., Houlsby, G.T. & Byrne, B.W. (2010b). Response of stiff piles in sand to long-term cyclic lateral loading. Géotechnique. **60**(2): 79-90.

[73] Lee, J., Salgado, R. & Paik, K . (2003). Estimation of Load Capacity of Pipe Piles in Sand Based on Cone Penetration Test Results. J. Geotech. Geoenviron. Engng. **129**(5): 391-403.

[74] Lehane, B.M. & Gavin, K.G. (2001). Base Resistance of Jacked Pipe Piles In Sand. J. Geotech. Geoenviron. Engng. **127**(6): 473-480.

[75] Lehane, B.M. & Randolph, M.F. (2002). Evaluation of a minimum base resistance for driven piles in siliceous sand. J. Geotech. Geoenviron. Engng. **128**(3): 198-205.

[76] Lehane,B.M. & White,D.J. (2005). Lateral stress changes and shaft friction for model displacement piles in sand. Can. Geotech.J. **42**:1039-1052.

[77] Lehane, B.M., Lim, J.K., Carotenuto, P., Nadim F., Lacasse, S., Jardine, R.J. and Dijk, B.F.J. (2017). Characteristics of unified databases for driven piles. Keynote. Proc 8th Int. Conf. on Offshore Site Investigations and Geotechnics, SUT London. SUT London. Vol. 1, p. 162-194. doi:10.3723/OSIG17.162 https://www.ingentaconnect.com/content/sut/1hzvzd

[78] Li, Z., Haigh, S.K., Bolton, M.D. (2010). Centrifuge modelling of mono-pile under cylic lateral loads. 7th International conference on physical modelling in Geotechnics. ICPMG. Zurich. Vol. 2: 965-970.

[79] Lin S.S., Liao, J.C. (1999). Permanent strains of piles in sand due to cyclic lateral loads. Journal of Geotechnical and Geoenvironmental Engineering. **125**(9):798-802.

[80] Lings, ML. (1985). The Skin Friction of Driven Piles in Sand. MSc thesis, University of London (Imperial College), UK.

[81] Lings, M.L. & Dietz, M.S. (2005). The peak strength of sand-steel interfaces and the role of dilation. Soils and Foundations **45**(6): 1-14.

[82] Little, R.L. & Briaud, J.L. (1988). Full scale cyclic lateral load tests on six single piles in sand. Paper GL-88-27. Geotechnical Div., Texas A & M Univ., College station, Texas 30p.

[83] Long, J. & Vanneste, G. (1994). Effects of cyclic lateral loads on pile in sand. J. Geotech. Engrg. **120**(1): 225-244.

[84] Matlock H. (1970). Correlations for design of laterally loaded piles in soft clay. In : Proc. 2nd Ann. Offshore Tech. Conf.Houston, Texax . Pp 577-594.

[85] McVay, M., Bloomquist, D.A., Vender-line, D. and Clause, J. (1994). Centrifuge modeling of laterally loaded pile groups in sands. ASTM. Geotechnical Testing Journal. **17**:129-137.

[86] Meimon, Y., Baguelin, F., Jezequel, J.F. (1986). Pile group behaviour under long time lateral monotonic and cyclic loading. 3rd Int. Conf. on numerical methods in offshore piling. Pp. 285-302. Nantes.

[87] Menard, L., Bourdon, G & Gambin, M. (1969). Methode générale de calcul d'un Rideau ou d'un pieu sollicité horeizentalement en fonctiondes résultats préssiométriques. Sols-Soils. 22-23:16-29.

[88] Meyerhof, G. (1976). Bearing capacity and settlement of pile foundations. Journal of Geotechnical and Geoenvironmental Engineering 102 (ASCE# 11962).

[89] Mezazigh, S. (1995). Etude experimentale de pieux chargés latéralement : proximité d'un talus et effet de groupe. Université de Nantes.

[90] Mezazigh, S., Garnier, J., Favraud, C. & Levacher, D. (1994). Effect of slope and sand density on p-y reaction curves for piles in sand. In Leung, C.F. Lee, F.H. & Tan, T.S. (eds). Centrifuge 94. Pp. 101-108. Rotterdam: Balkema.

[91] Moss, R.E.S., Caliendo, J.A. & Anderson, L.R. (1998). Investigation of a cyclic laterally loaded model pile group. Soil Dynamics and Earthquake Engineering. 17:519-523.

[92] Murchison J.M. & O'Neill, M.W. (1984). Evaluation of p-y relationships in cohesionless soil. In: Analysis and design of piles foundations. New York: ASCE. p.174-191.

[93] NF EN ISO 4287 (1998). Geometrical Product Specifications (GPS) - Surface texture : profile method - Terms, definitions and surface texture parameters. 58p.

[94] NF P 94-059 (2000). Sols: Reconnaissance et essais – Détermination des masses volumiques minimale et maximale des sols non cohérents.

[95] NFP 94 262 (2012). Justification of geotechnical work - National application standards for the implementation of Eurocode 7 - Deep foundations, 206p.

[96] Norme francaise (2012). Justification des ouvrages géotechniques-*Norme d'application nationale de l'Eurocode 7.* NF P 94-262.

[97] Norwegian Geotechnical Institute (2001). Bearing Capacity of Driven Piles, Piles in Sand. Internal report no. 525211-2, 21 January 2001.

[98] O'Neill, M.W. & Murchison, J.M. (1983). An evaluation of p-y relationships in sands, Research Rep. No. GT-DF02-83. Department of Civil Engineering, University of Houston, TX.

[99] Paik, K. & Salgado, R. (2003). Determination of Bearing Capacity of Open – Ended piles in Sand. J. Geotech. Geoenviron. Engng. **129**(1): 46-57.

[100] Paik, K., Salgado, R., Lee, J. & Kim, B. (2003). Behavior of Open- and Closed-Ended Piles Driven Into Sands. J. Geotech. Geoenviron. Engng. **129**(4): 296-306.

[101] Paikowsky, S.G. & Whiteman, R.V. (1990). The effects of plugging on pile performance and design. Can Geotech. J. **27**: 429-440.

[102] Petek, K., Felice, C.W. & Holtz, R.D. (2002). Capacity analysis of drilled shafts with defetcs. International Deep foundations Congress: An international perspective on theory, design, construction, and performance, Geotechnical special publication. M.W. O'Neill and F.C. Townsend,eds, ASCE, Reston, VA., 1120-1135.

[103] Phanikanth, V.S., Choudhury, D. & Reddy G.R. (2010). Response of single pile inder lateral loads in cohesionless soils. Electronic Journal of Geotechnical Engineering. **15**: 813-830.

[104] Potyondy, J.G. (1961). Skin friction between various soils and construction materials. Geotechnique **11**(4): 339-353.

[105] Poulos, H.G. (1971). Behaviour of laterally loaded piles : 1 –single pile. Journal of Geotechnical Engineering, A.S.C.E., **101**(SM5): 733-751.

[106] Poulos, H.G. & Davis, E.H. (1980). Pile Foundations, Analysis and design. First edi. John Wiley and sons. New York.

[107] Prakash, S. (1962). Behavior of pile groups subjected to lateral loads. PhD dissertation. University of Illinois. Urbana. III.

[108] Pra-ai, S. (2013). Behaviour of soil-structure interfaces subjected to a large number of cycles. Applications to piles. Ph. D. thesis. Université de Grenoble.

[109] Puech, A. (2013). Advances in axial cyclic pile design: Contribution of the SOLCYP project. Proceedings of TC 209 Workshop – 18th ICSMGE, Paris 4 september 2013. Design for cylic loading: Piles and other foundations. 45-57.

[110] Puech, A. & Benzaria, O. (2013). Effects of installation method on the static behaviour of piles in highly overconsolidated Flanders clay. Proceedings of TC 209 Workshop – 18th ICSMGE, Paris 4 september 2013. Design for cylic loading: Piles and other foundations, pp. 69-72.

[111] Poulos, H.G. & Davis, E.H. (1980). Pile foundation analysis and design. Number Monograph.

[112] Puech, A. & Benzaria, O. (2013). Effects of installation method on the static behaviour of piles in highly overconsolidated Flanders clay. Proceedings of TC 209 Workshop – 18th ICSMGE, Paris 4 september 2013. Design for cylic loading: Piles and other foundations, pp. 69-72.

[113] Rakotonindriana, J. (2009). Comportement des pieux et des groups de pieux sous chargement lateral cyclique. PhD thesis. Ecole national des Ponts et Chaussées.

[114] Rao, K.S.S. & Venkatesh, K.H. (1985). Uplift behaviour of short piles in uniform sand. Soils and Foundations **25**(4): 1-7.

[115] Randolph, M. F., Dolwin, J. & Beck, R. (1994). Design of driven piles in sand. Géotechnique **44**(3): 427-448.

[116] Reese LC, Cox WR, Koop FD. (1974). Analysis of laterally loaded piles in sand. In: Proc. 6th Ann. Offshore Tech. Conf. Austin, Texas. P. 473-485.

[117] Robinsky, E.I., Sagar, W.L. & Morrison, C.F. (1964). Effect of shape and volume of the capacity of model piles in sand. Canad. Geotech. J. **1**(4).

[118] Rosquoet F. (2004). Pieux sous charge latérale cyclique. PhD thesis. Ecole centrale et Université de Nantes.

[119] Rosquoet, F., Thorel, L., Garnier, J. & Canepa, Y. (2007). Lateral cyclic loading of sand-installed piles. Soils & Foundations. **47**(5): 821-832.

[120] Rosquoet, F., Thorel, L., Garnier, J. & Khemakhem, M. (2010). P-y curves on model piles: Uncertainty identification. Physical modelling in Geotechnics – Springman, Laue & Seward (eds). Taylor & Francis Group, London.

[121] Schneider, J.A., Xu, Xiangtao & Lehane, B.M. (2008). Database Assessment of CPT-Based Design Methods for Axial Capacity of Driven Piles in Siliceous Sands. J. of Geotech. Geoenviron. Engng. 1227-1244.

[122] Scott R.F. (1980). Analysis of centrifuge pile tests: simulation of pile driving. Res. Rep. OSAPR Project 13. Washington, D.C: Amercian Petroleum Institute.

[123] Scott, R.F. (1981). Pile testing in centrifuge. Proceedings of the Xth International Conference on Soil Mechanics and Foundation Engineering, Stockholm, **2**: 839-842.

[124] Silva, M. (2014). Experimental study of ageing and axial cyclic loading effect on shaft friction along driven piles in sands. Ph. D. thesis. Université de Grenoble.

[125] Solcyp recommendation. (2017). Design of piles under cyclic loading. ISTE Ltd and John Wiley & Sons.

[126] Swan, C.C. Changes in soil during pile driving. 59:139 Foundation Engineering. University of lowa.

[127] Tejchman, J. & Wu, W. (1995). Experimental and numerical study of sand-steel interfaces. International journal for numerical and analytical methods in geomechanics **19**: 513-536.

[128] Terzaghi, O. (1955). Evaluation of the coefficient of sub grade reaction. Géotechnique. **5** :297-326.

[129] Thorel, L., et Garnier, J. (2002). Des « G » aux techniques de modèles. Production LCPC. Vidéo de 19 min.

[130] Tiwari, B. & Al-Adhadh, A.R. (2014). Influence of relative density on static soil-structure frictional resistance of dry and saturated sand. Geotechnical Geological Engineering **32**: 411-427.

[131] Toolan, F.E., Lings, M.L., Bristol, U. & Mirza, U.A. (1990). An appraisal of API RP2A recommendations for determining skin friction of piles in sand. In proceedings of the 22nd Annual Offshore Technology Conference, May 7-10, Houston, Texas, pp.33-42.

[132] Uesugi, M. & Kishida, H. (1986a). Influential factors of friction between steel and dry sands. Soils and Foundations. **26**(2): 33-46.

[133] Uesugi, M. & Kishida, H. (1986b).Frictional resistance at yield between dry sand and mild steel. Soils and Foundations. **26**(4): 139-149.

[134] Uesugi, M., Kishida, H. & Tsubakihara, Y. (1988). Behaviour of sand particles in sand-steel friction. Soils and Foundations **28**(1): 107-118.

[135] Verdure, L. Garnier, J. & Levacher, D. (2003). Lateral cyclic loading of single piles in sand. International Journal of Physical Modelling in Geotechnics. IJPMG. 3:17-28.

[136] Vesic, A. (1970). Tests on instrumented piles, Ogeeche River site. Journal of Soil Mechanics & Foundations Division **96**(SM2): 561-584.

[137] Wesselink B.D., Murff J.D., Randolph M.F., Nunez IL, Hyden AM. (1988). Analysis of centrifuge model test data from laterally loaded piles in calcareous sand. In: Engineering for calcareous sediments, Vol. 1. Rotterdam, The Netherlands, Balkema. p. 261-270.

[138] White, D., Finlay, T., Bolton, M. & Bearss, G. (2002). Press-in piling: Ground vibration and noise during pile installation. Proceedings of the International Deep Foundations Congress. Orlando, USA. ASCE Special Publication 116, pp 363-371.

[139] White, D.J. & Bolton, M.D. (2005). Comparing CPT and pile base resistance in sand. Geotechnical Engineering **158**: 3-14.

[140] Yajima, J., Konishi, T., Uesugi, M. & Kishida, H. (1984). Influence of surface roughness on friction between steel and Toyoura sand. Proc. The annual meeting of kantoh branch, Architectural Institute of Japan, 5-8 (in Japanese).

[141] Yan, L., Byrne, P.M. (1992). Lateral pile response to monotonic pile head loading. Can. Geotech. J. **29**. 955-970.

[142] Yang, J., Tham, L.G., Lee, P.K.K., Chan, S.T. & Yu, F. (2006a). Behaviour of jacked and driven piles in sandy soil. Géotechnique **56**(4): 245-259.

[143] Yang, J., Tham, L.G., Lee, P.K.K., & Yu, F. (2006b). Observed performance of long steel H-piles jacked inti sandy soils. J. Geotech. Geoenviron. Eng. **132**(1): 24-35.

[144] Yang, Z.X., Jardine, R.J., ZHU, B.T., Foray, P. & Tsuha, C.H.C. (2010). Sand grain crushing and interface shearing during displacement pile installation in sand. Géotechnique **60**(6): 469-482.

[145] Yang, Z. X., Guo, W.B., Jardine, R. J. and Chow, F. C. (2017). Design method reliability assessment from an extended database of axial load tests on piles driven in sand. Canadian Geotechnical Journal. Can. Geotech. J. 54: 59–74 dx.doi.org/10.1139/cgj-2015-0518

[146] Yoshimi, Y. & Kishida, T. (1981). Friction between sand and a metal surface. Proc. 10th ICSMFE,**1**:831-834.

[147] Yu, F., Kou, H., Liu, J., Yang, Y. (2012). Jacking Installation of Displacement Piles : from Empiricism toward Scientism. EJGE **17** ,Bund. J ., 1381-1390.

[148] Zarrabi, M., & Eslami, A. (2016). Behavior of piles under different installaction effects by physical modelling. Int. J. Geomech. **16**(5).

[149] Zhang, C., White, D.D. & Randolph, M. (2011). Centrifuge modelling of the cyclic lateral response of a rigid pile in soft clay. Journal of Geotechnical and Geoenvironmental Engineering. **137**(7): 717-729.

Appendix 1 : Summary of the realized tests

Strongbox C1

D_r = 58%

Model pile : pile 3

Test : C1P1S18O100G

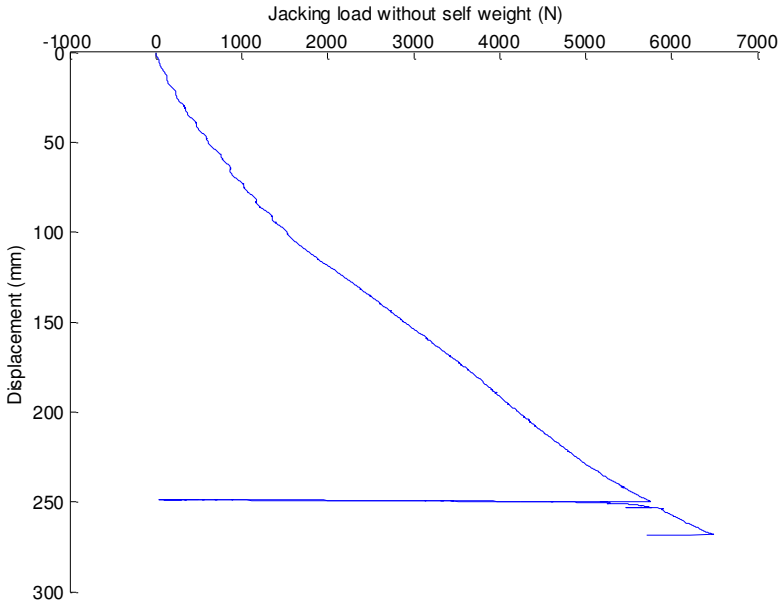

Figure A1-1 : C1P1S18O100G head force sensor

Model pile: pile 2

Test : C1P2S18C100G

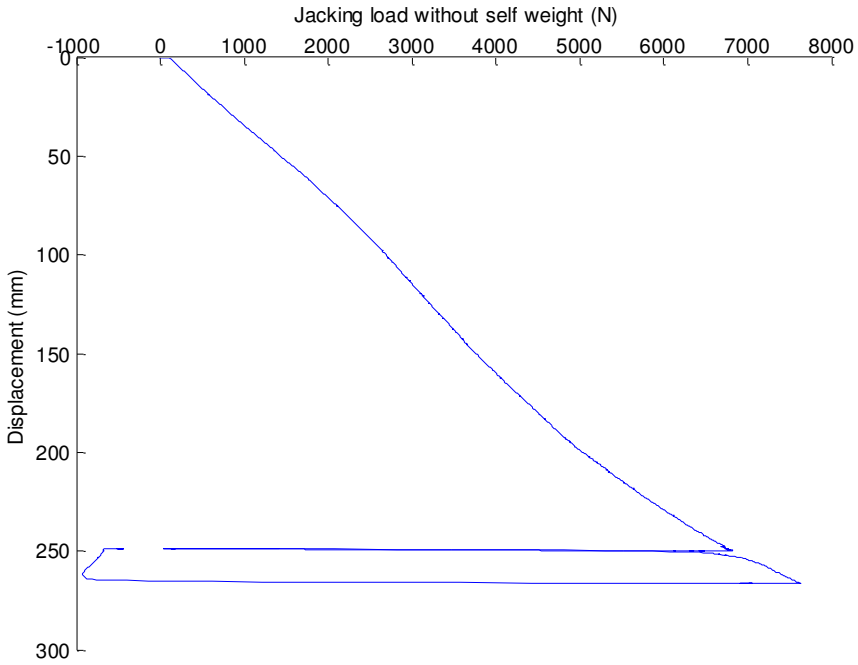

Figure A1-2: C1P2S18C100G head force sensor

Model pile : pile 1

Test : C1P3R18C100G

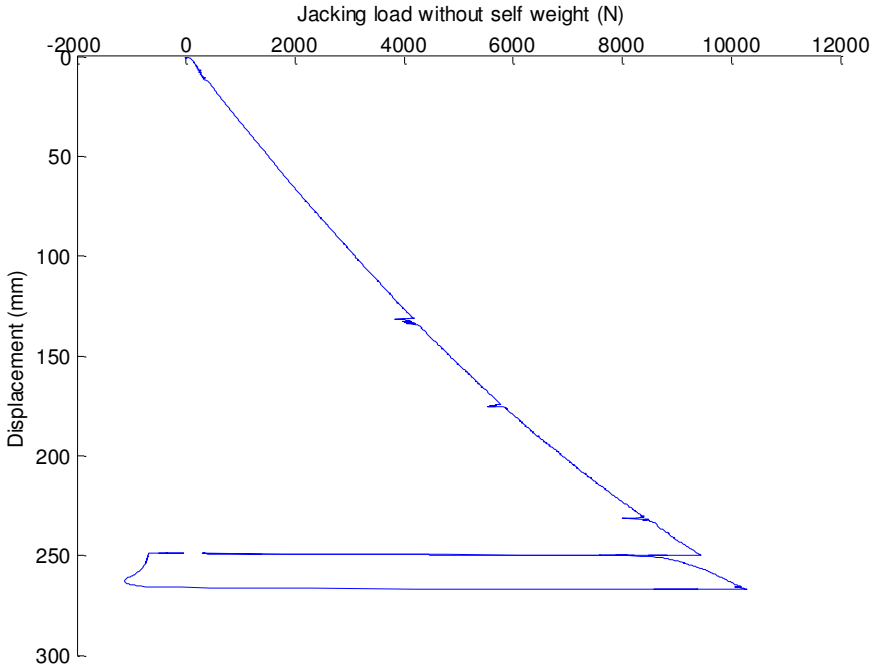

Figure A1-3: C1P3R18C100G head force sensor

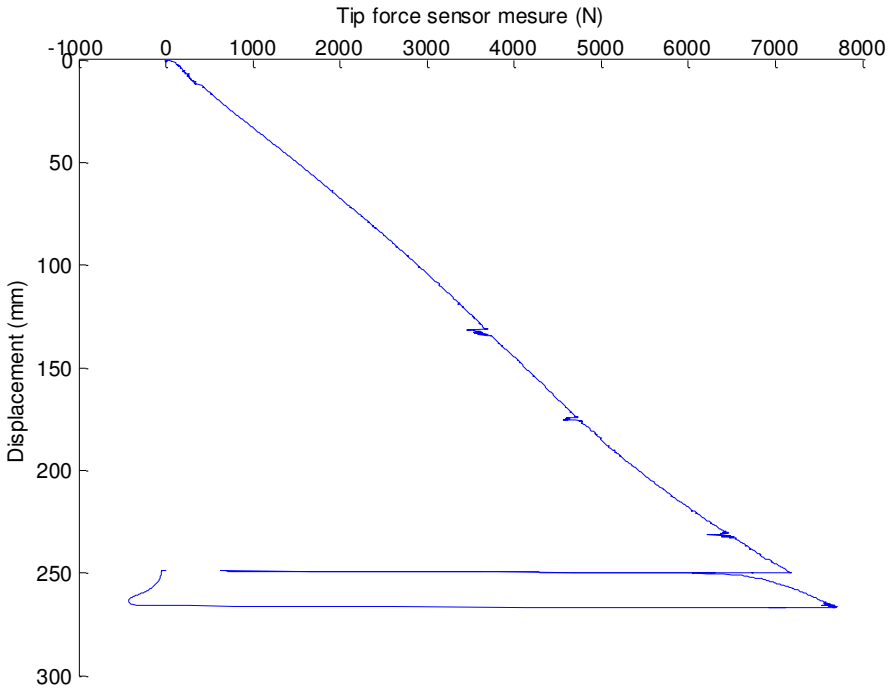

Figure A1-4: C1P3R18C100G tip force sensor

Model pile : pile 2

Test : C1P5S18C100G

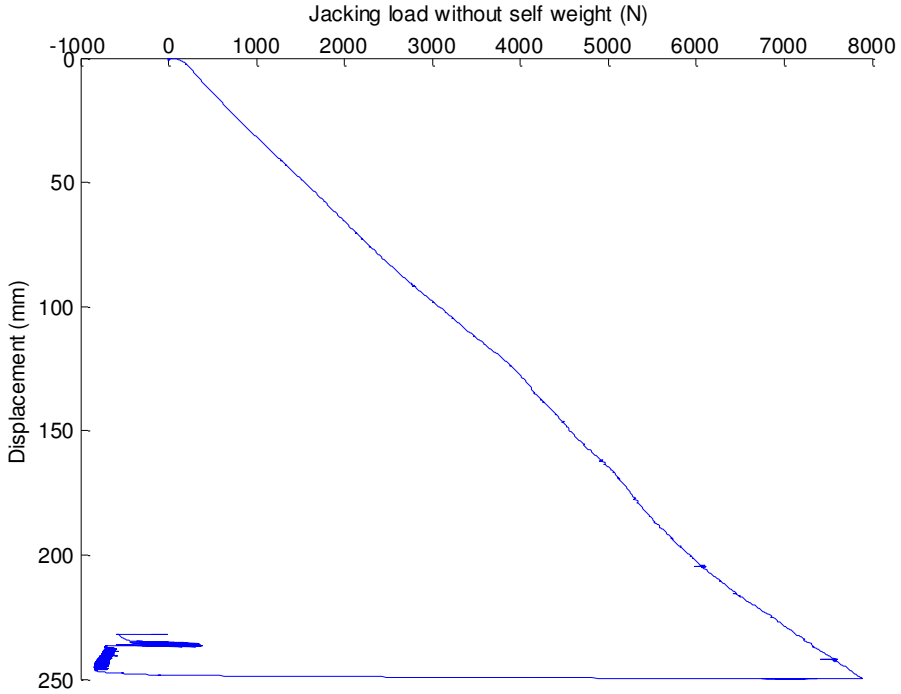

Figure A1-5 : C1P5S18C100G head force sensor

Model pile : pile 3

Test : C1P6S18O100G

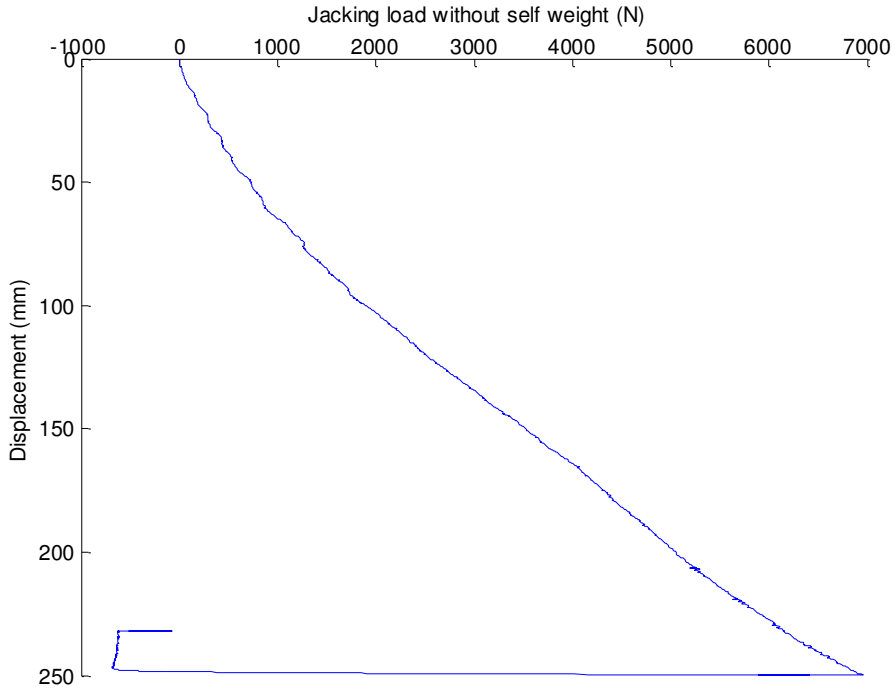

Figure A1-6: C1P6S18O100G head force sensor

Strongbox C2

D_r = 99%

Model pile : pile 1

Test : C2P1R18C100G

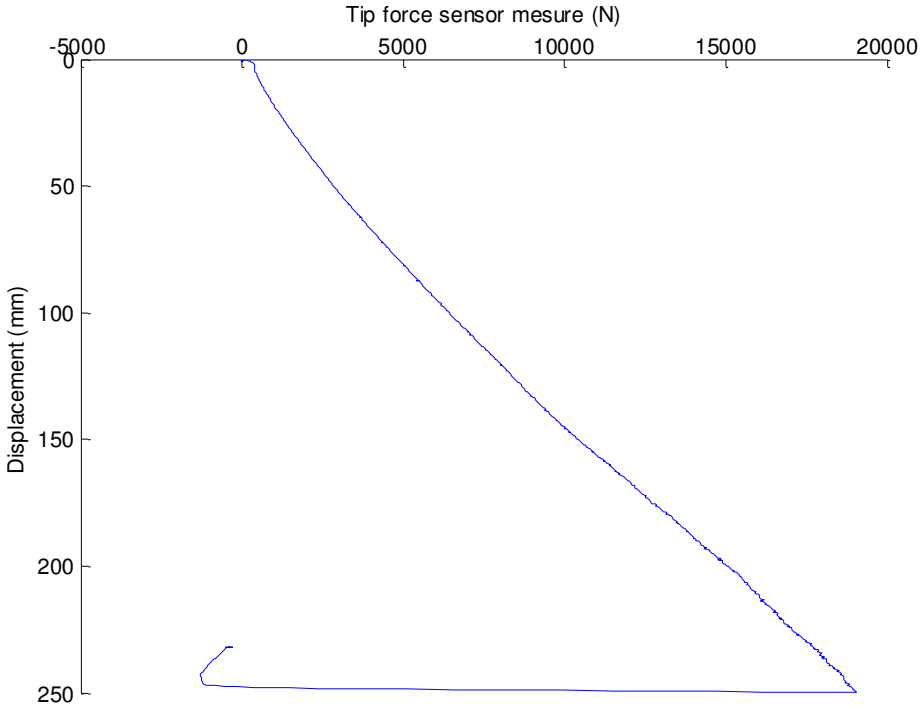

Figure A1-7: C2P1R18C100G head force sensor

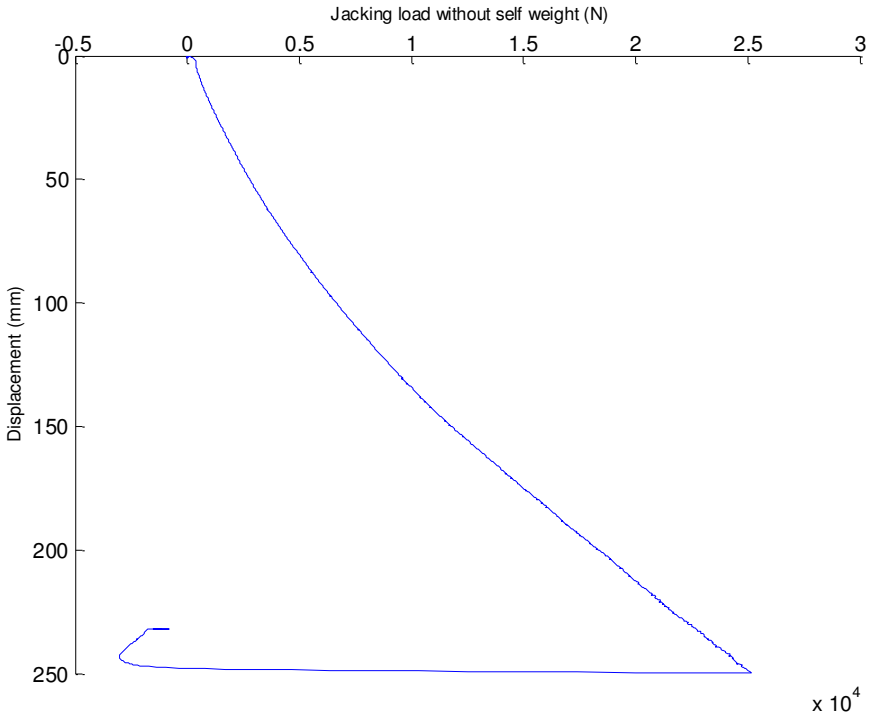

Figure A1-8: C2P1R18C100G tip force sensor

Model pile : pile 1

Test : C2P3R18C25

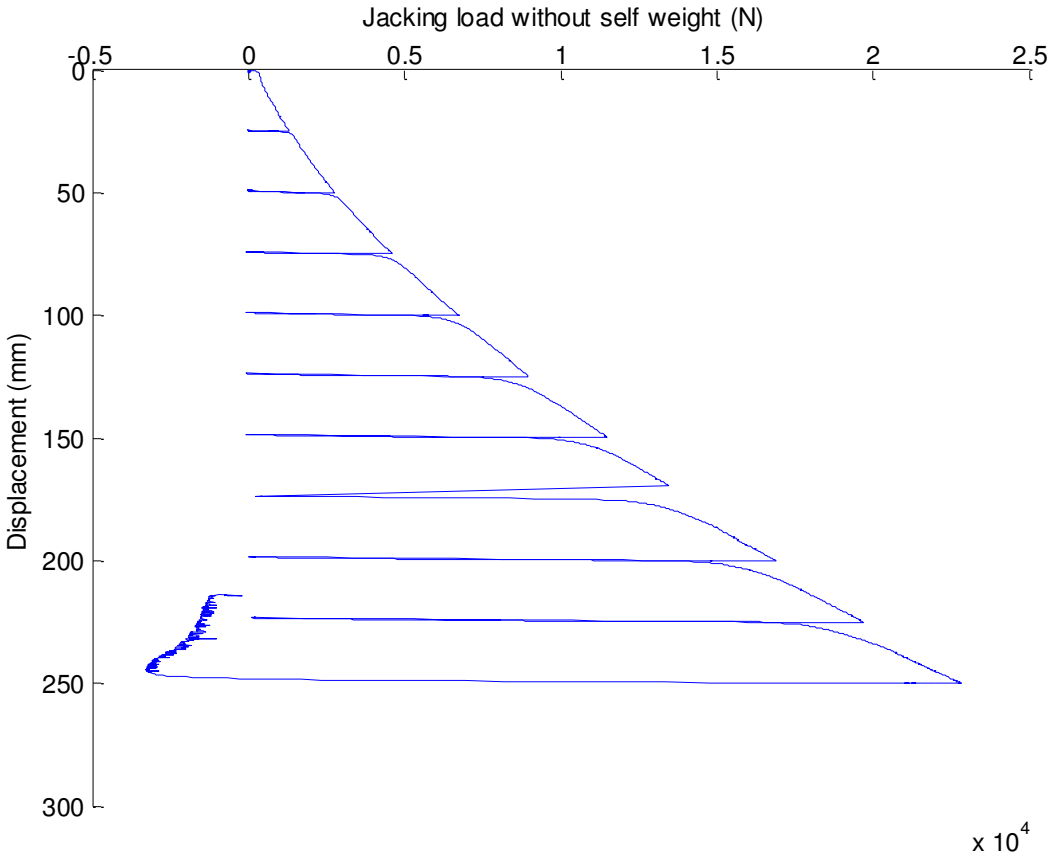

Figure A1-9: C2P3R18C25 head force sensor

Model pile : pile 1

Test : C2P4R18C25

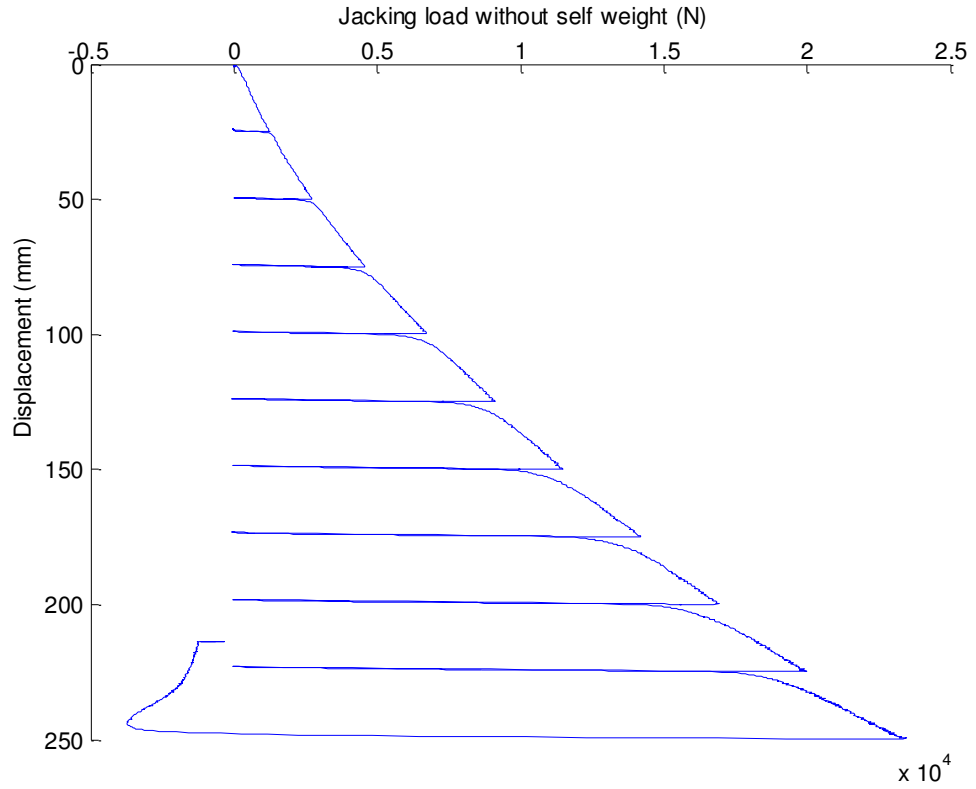

Figure A1-10: C2P4R18C25 head force sensor

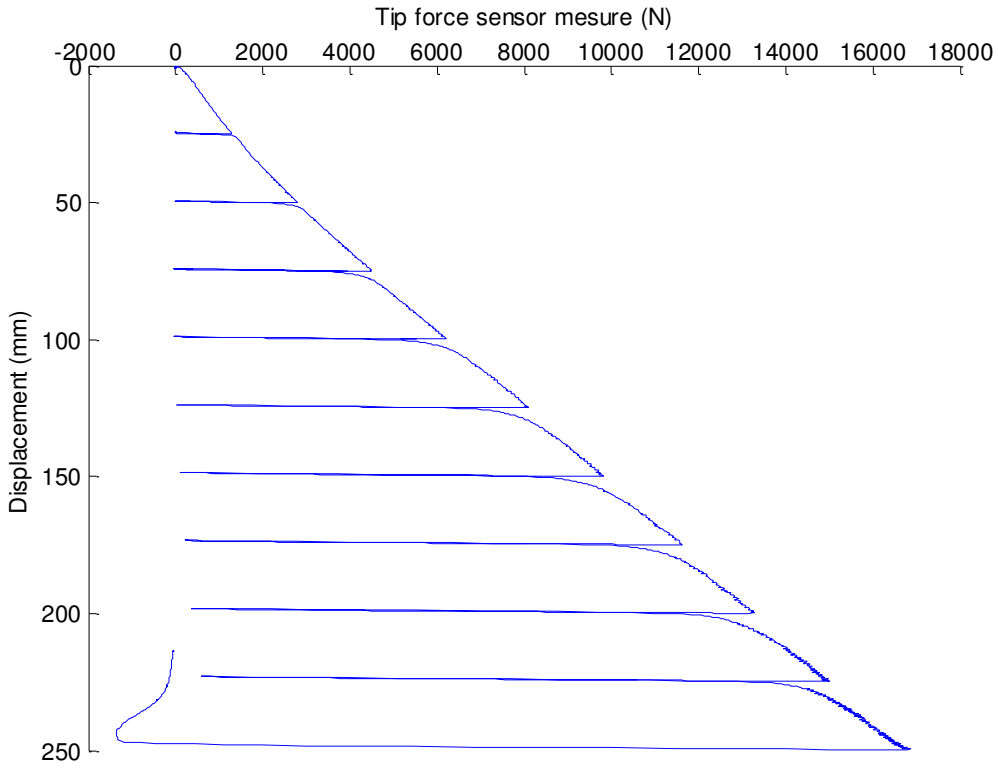

Figure A1-11: C2P4R18C25 tip force sensor

Model pile : pile 1

Test : C2P6R18C10

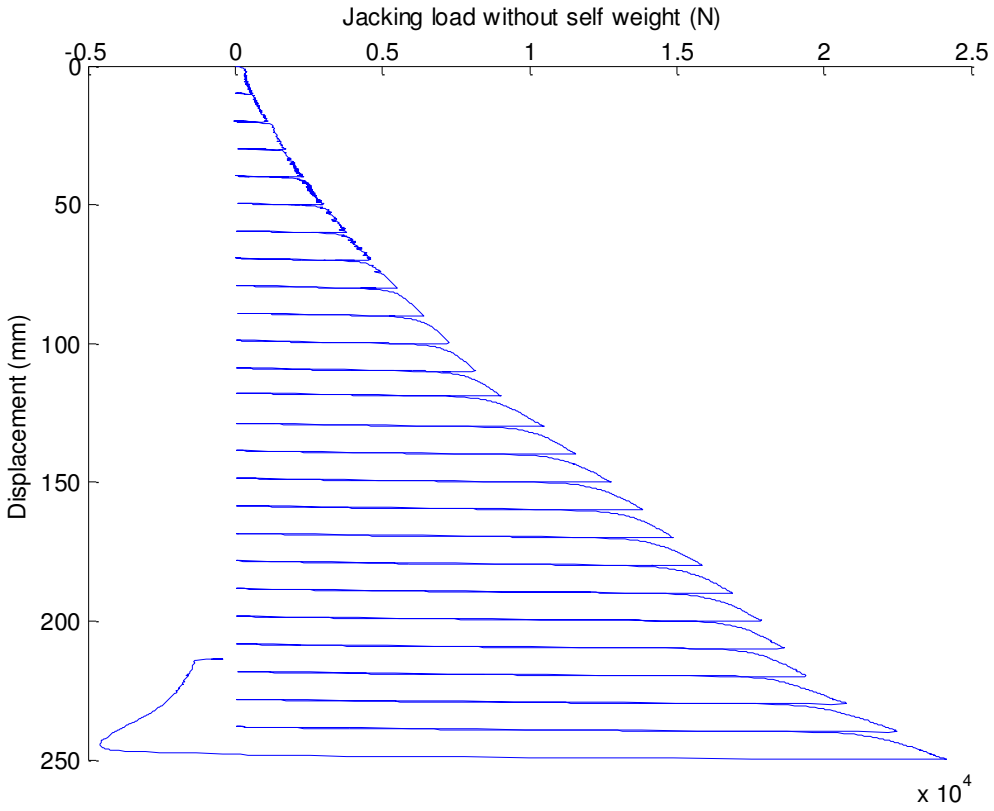

Figure A1-12: C2P6R18C10 head force sensor

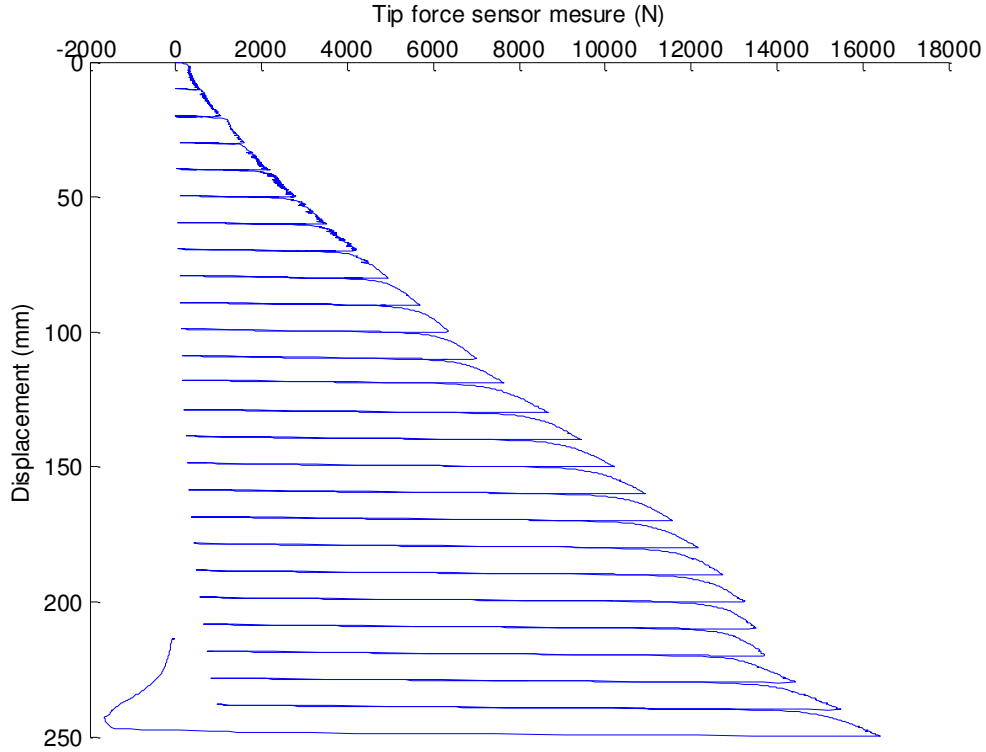

Figure A1-13: C2P6R18C10 tip force sensor

Strongbox C3

D_r = 99%

Model pile : pile 1

Test : C3P1R18C1G

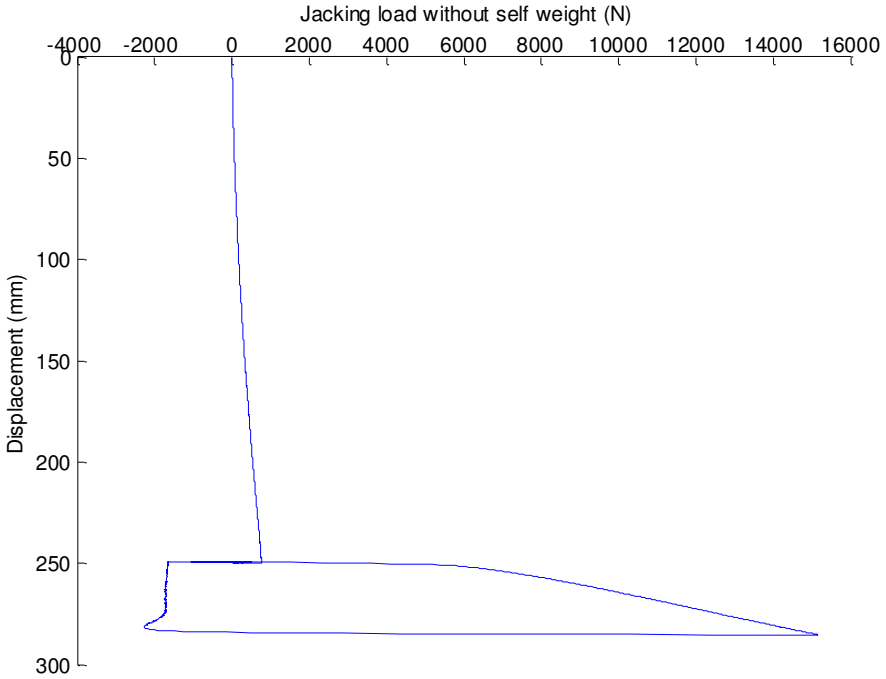

Figure A1-14 : C3P1R18C1G head force sensor

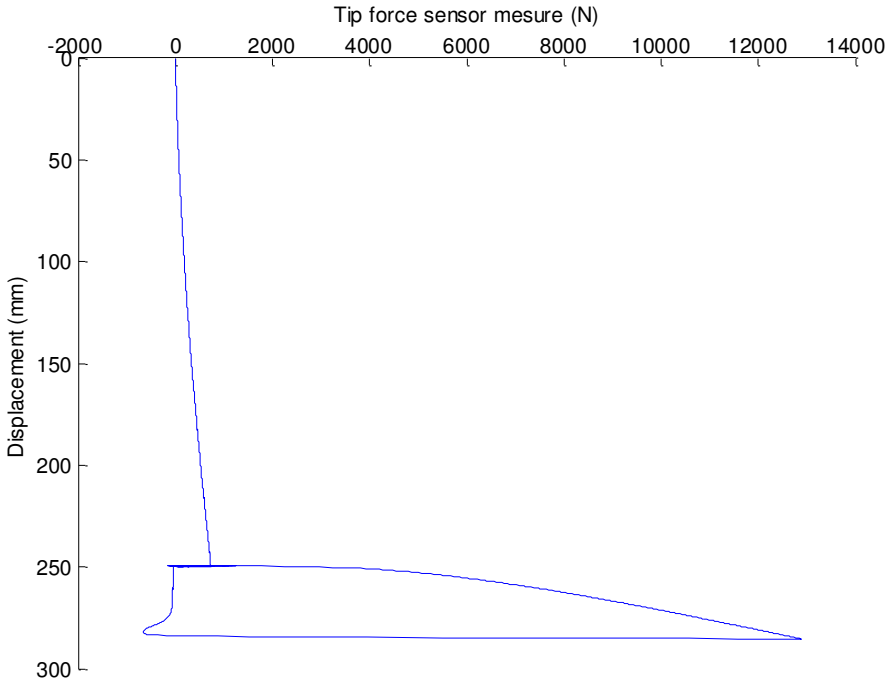

Figure A1-15: C3P1R18C1G tip force sensor

Model pile : pile 1

Test : C3P2R18C1G

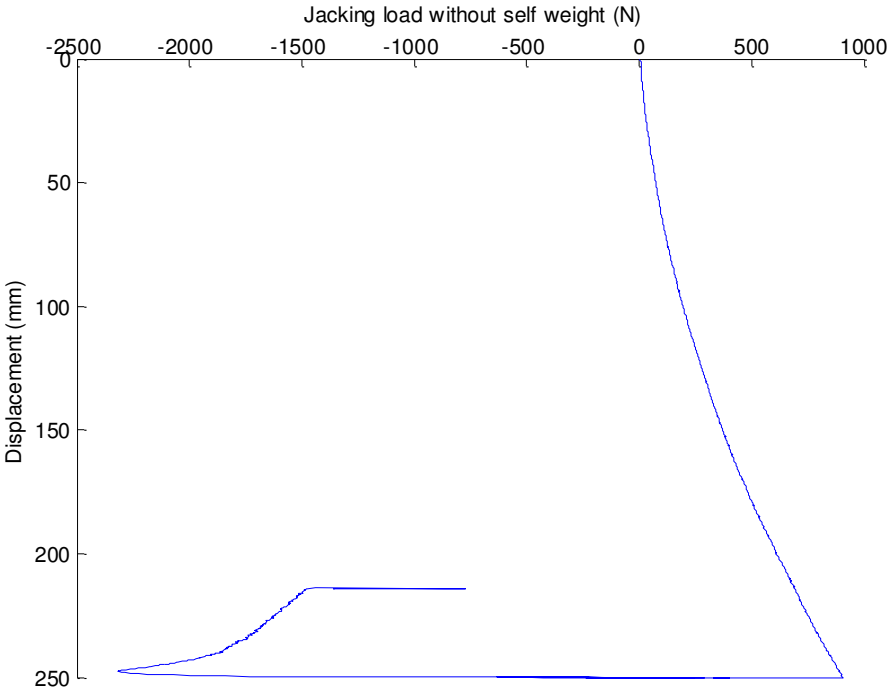

Figure A1-16: C3P2R18C1G head load sensor

Model pile : pile 1

Test : C3P4R18C1G

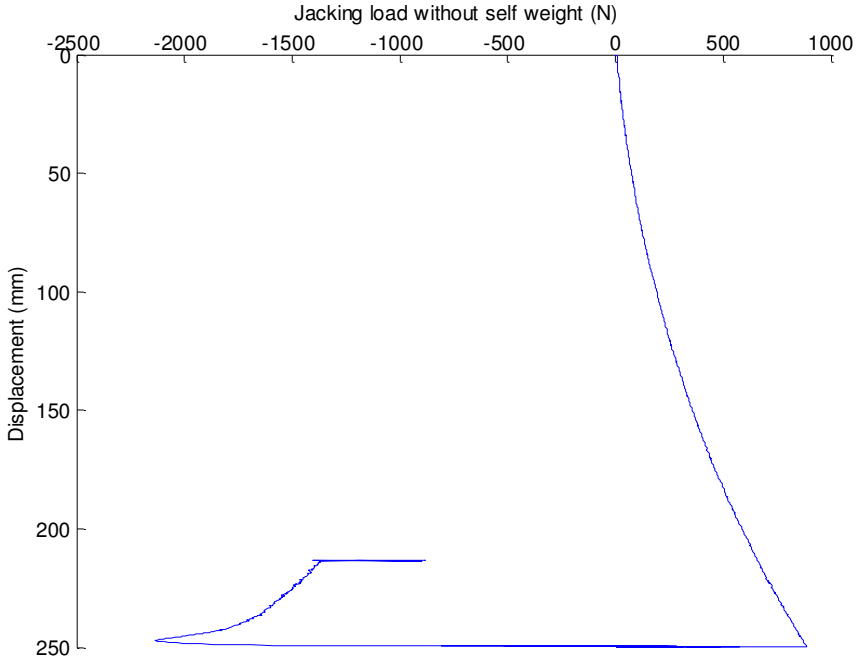

Figure A1-17: C3P4R18C1G head load sensor

Model pile : pile 1

Test : C3P5R18C10

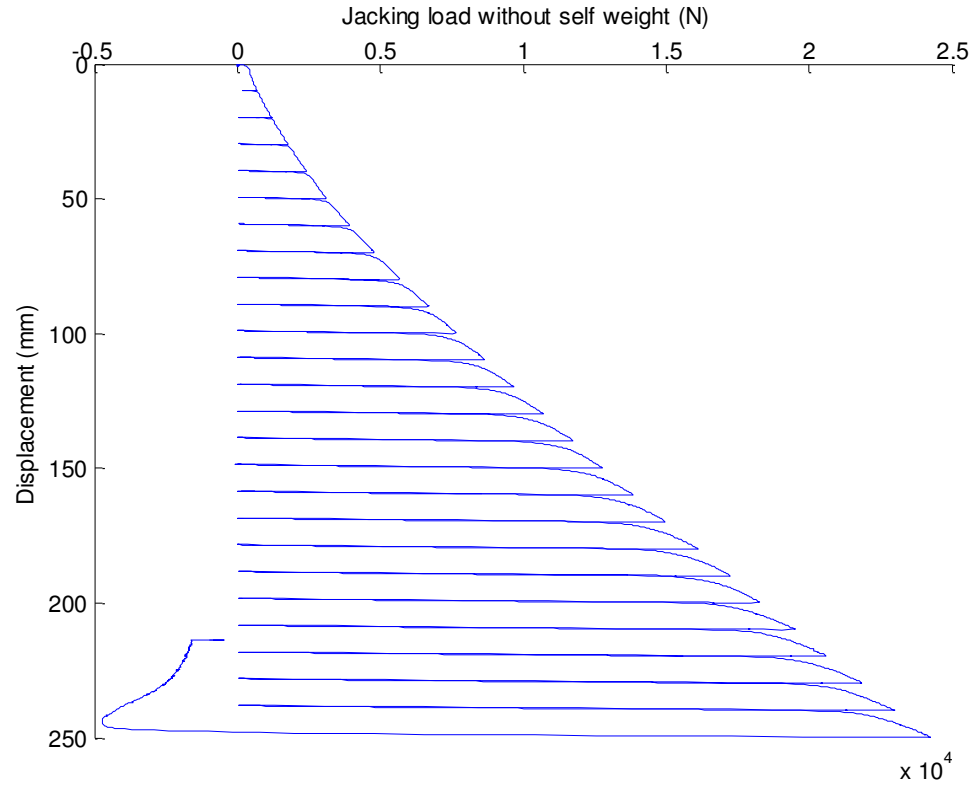

Figure A1-18: C3P5R18C10 head load sensor

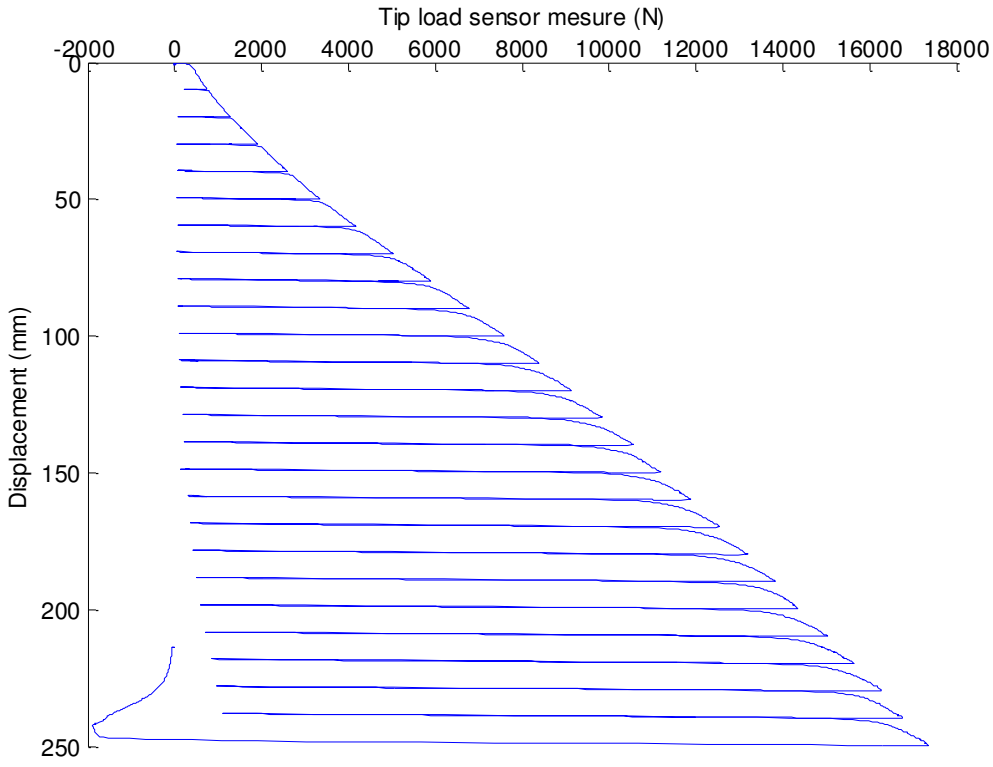

Figure A1-19: C3P5R18C10 tip load sensor

Model pile : pile 1

Test : C3P6R18C100G

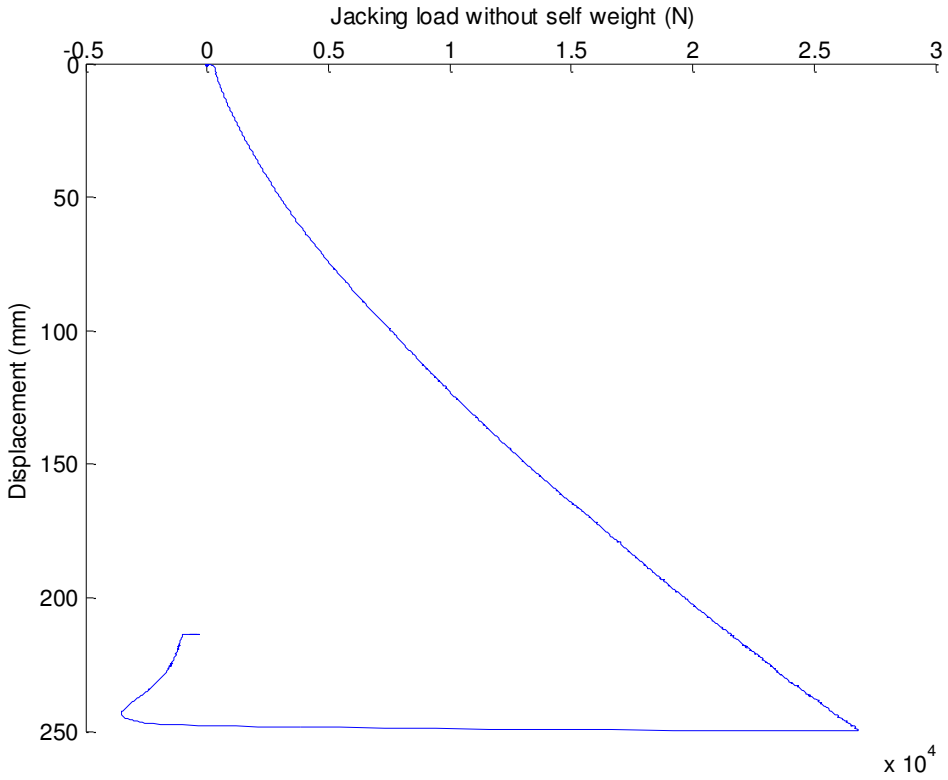

Figure A1-20: C3P6R18C100G head load sensor

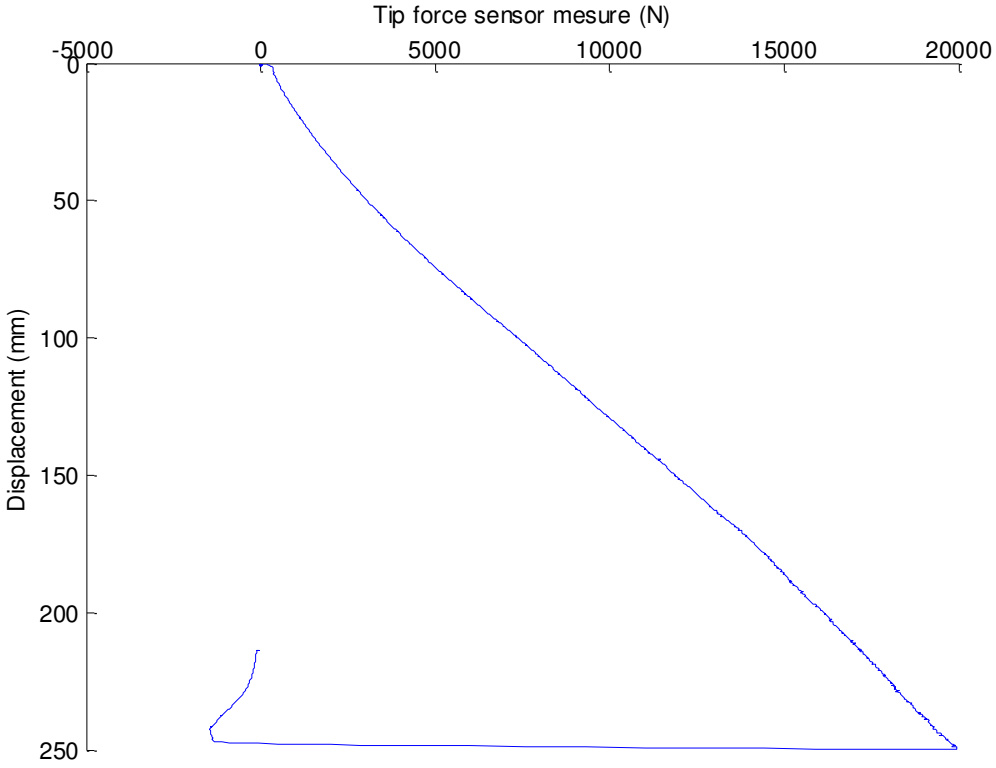

Figure A1-21: C3P6R18C100G tip load sensor

Strongbox C4

D_r = 99%

Model pile : pile 1

Test : C4P1R18C50

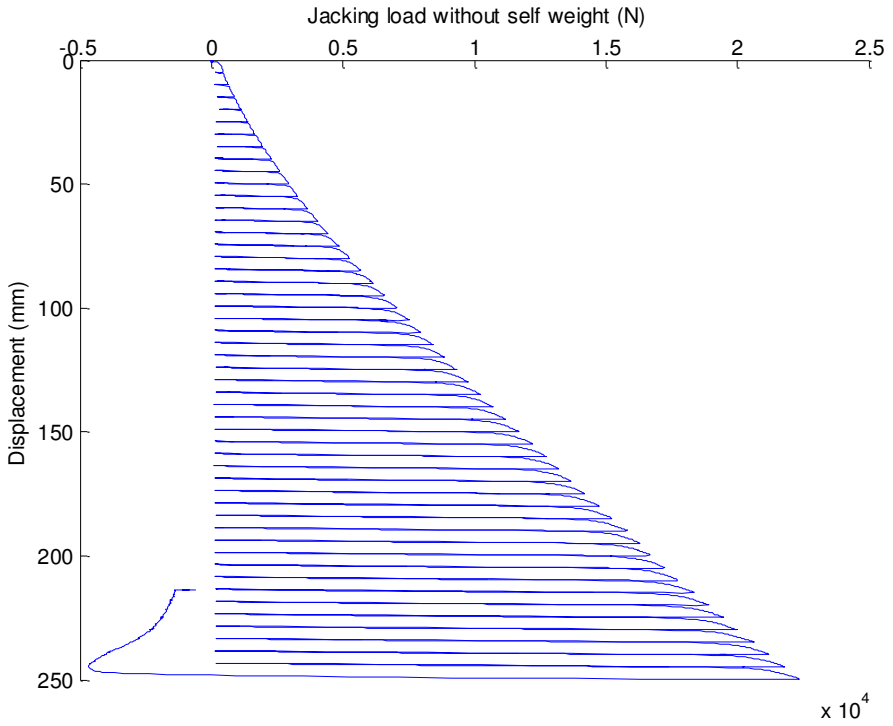

Figure A1-22: C4P1R18C50 head load sensor

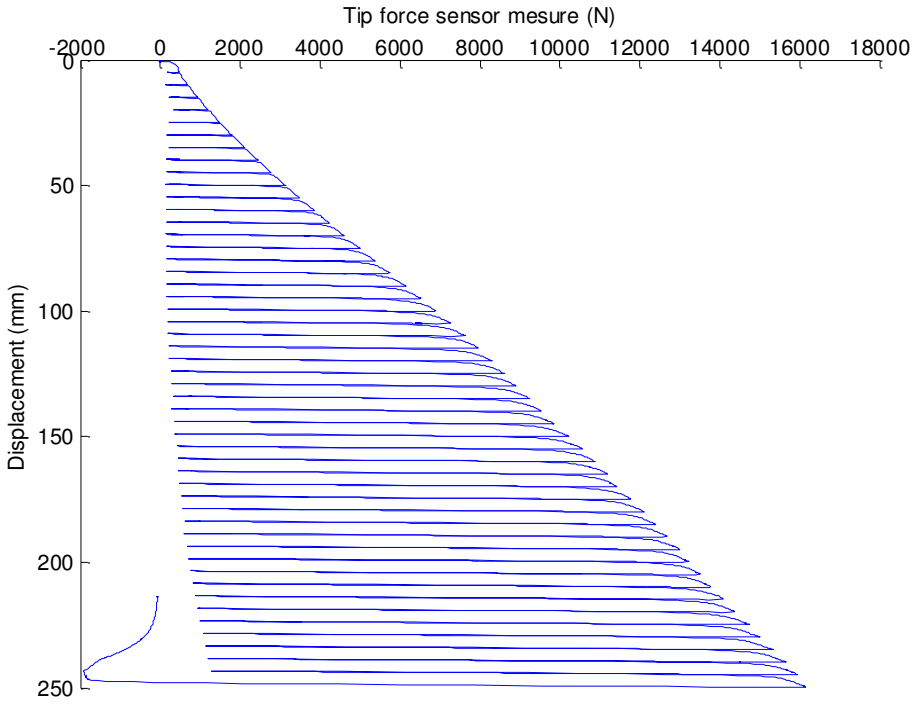

Figure A1-23: C4P1R18C50 tip load sensor

Model pile : pile 1

Test : C4P2R18C100

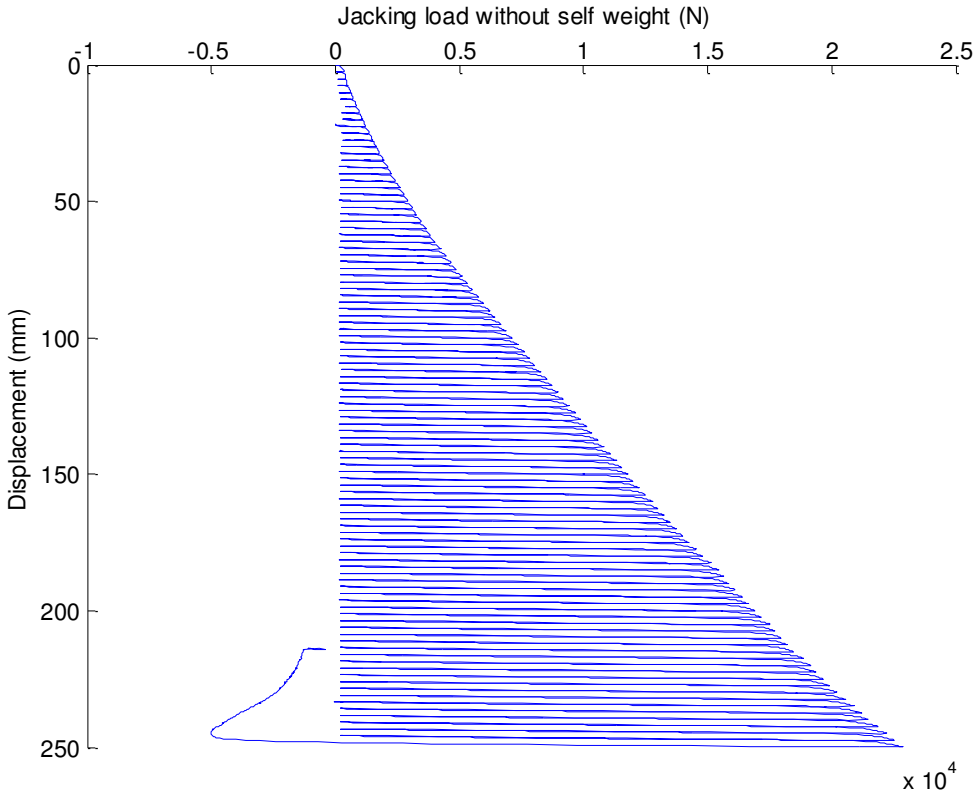

Figure A1-24: C4P2R18C100 head load sensor

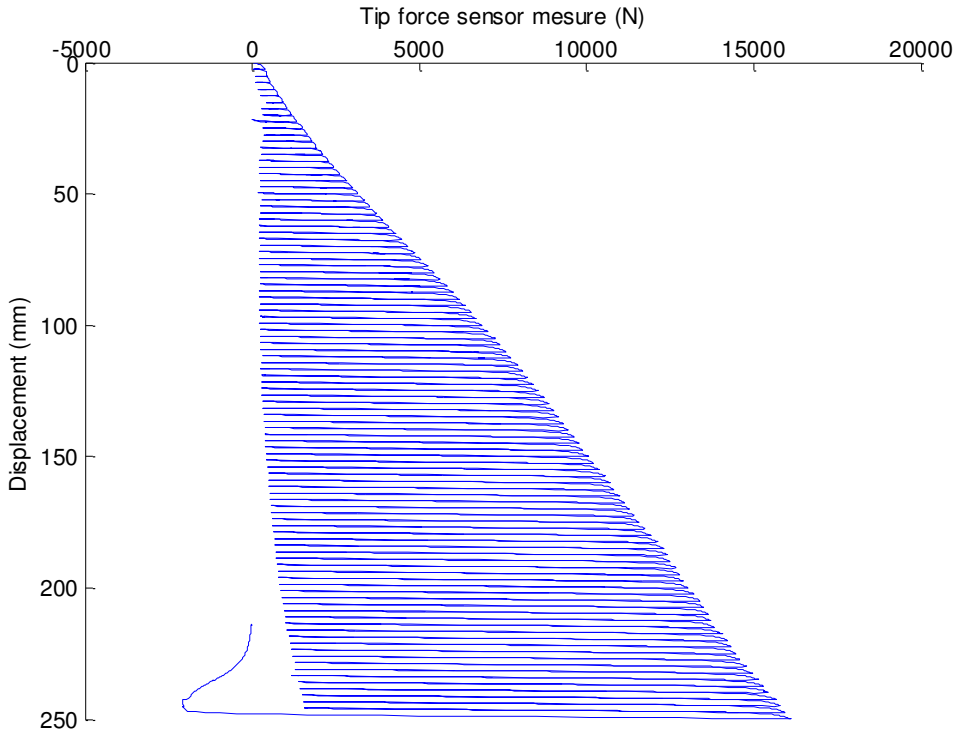

Figure A1-25: C4P2R18C100 head load sensor

Strongbox C5

D_r = 99%

Model pile : pile 3

Test : C5P3S18O100G

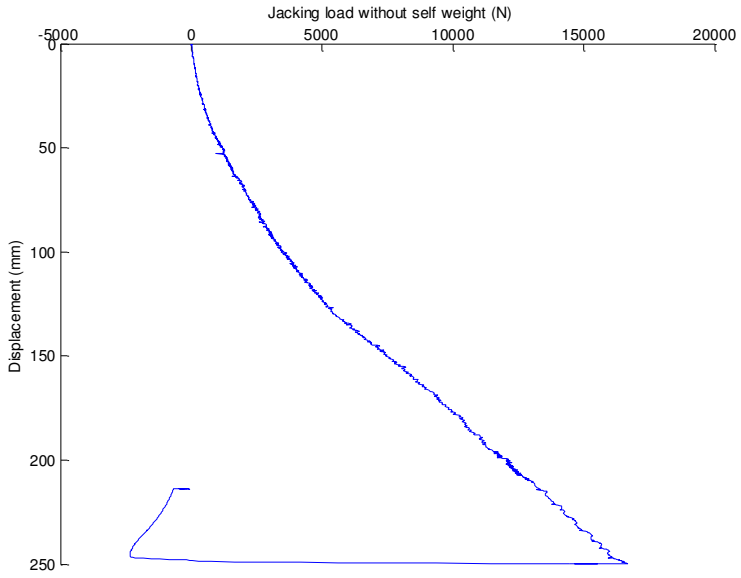

Figure A1-26: C5P3S18O100G head load sensor

Model pile : pile 2

Test : C5P4S18C100G

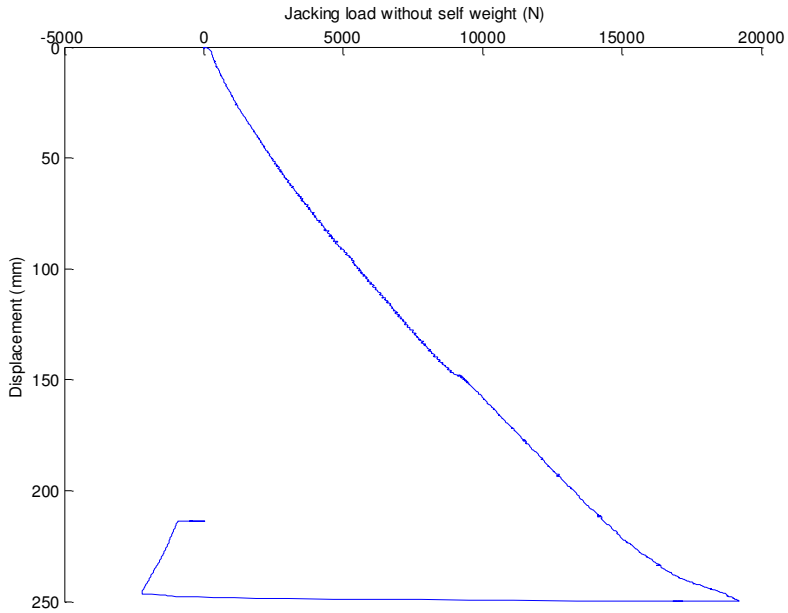

Figure A1-27: C5P4S18C100G head load sensor

Model pile : pile 7

Test : C5P5S14O100G

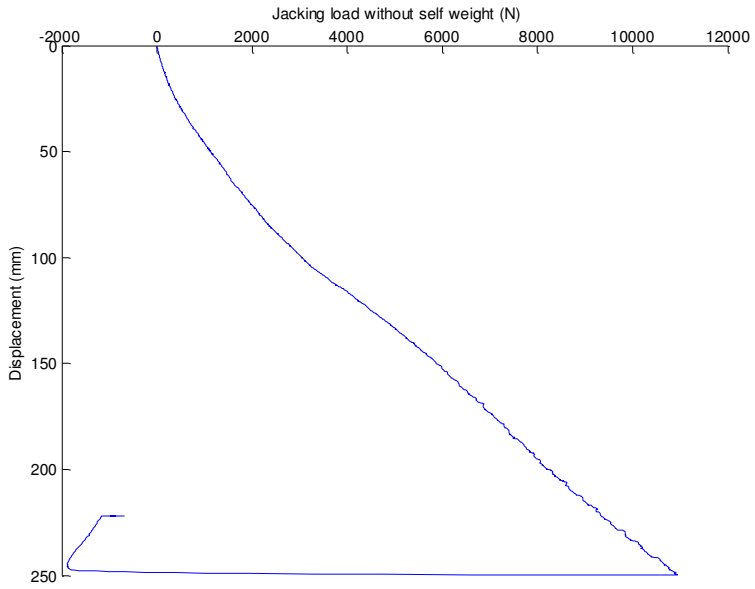

Figure A1-28: C5P5S14O100G head load sensor

Model pile : pile 6

Test : C5P6S14C100G

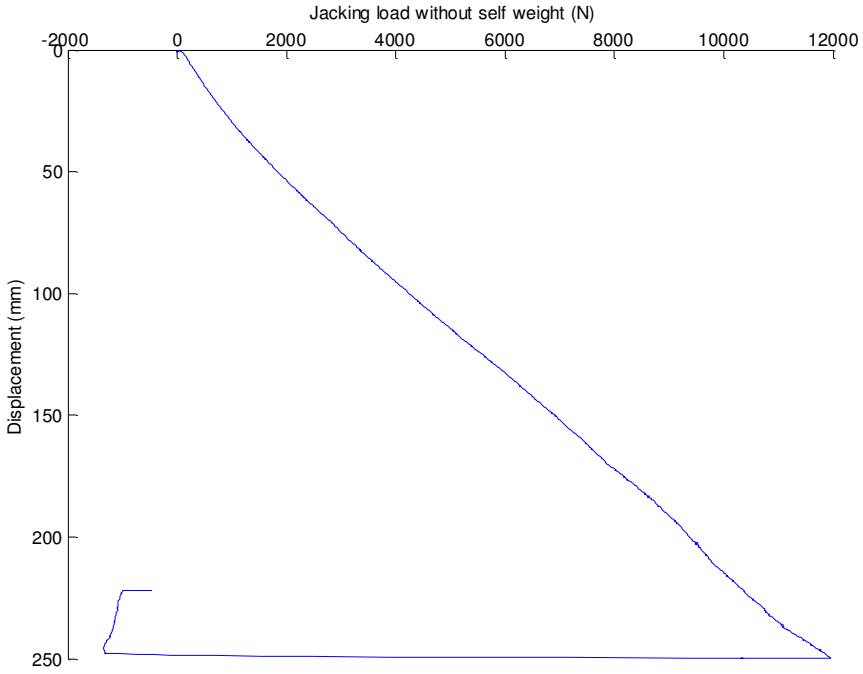

Figure A1-29: C5P6S14C100G head load sensor

Model pile : pile 5

Test : C5P7S16O100G

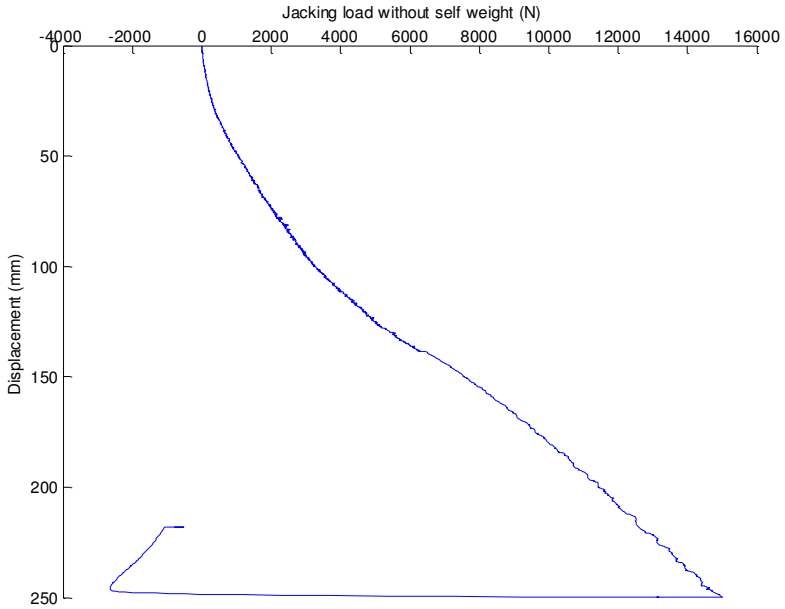

Figure A1-30: C5P7S16O100G head load sensor

Model pile : pile 4

Test : C5P8S16C100G

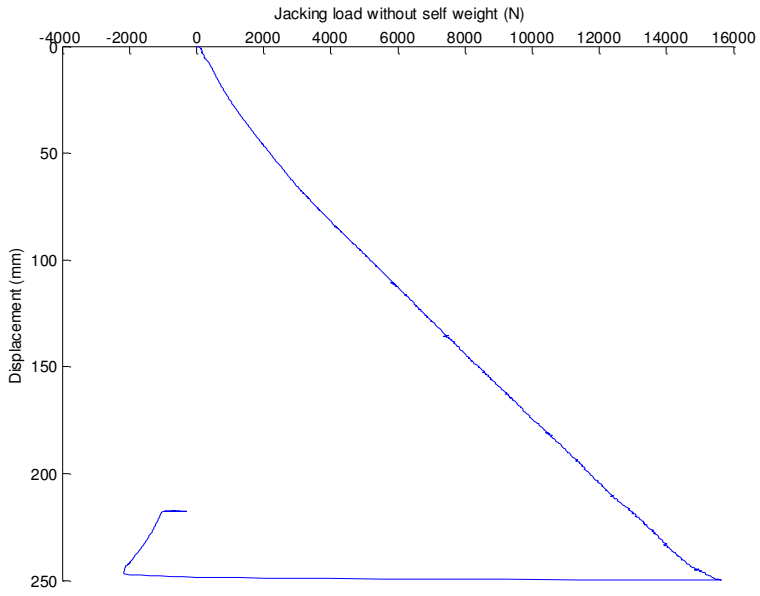

Figure A1-31: C5P8S16C100G head load sensor

Strongbox C6

D_r = 58%

Model pile : pile 3

Test : C6P1S18O100G

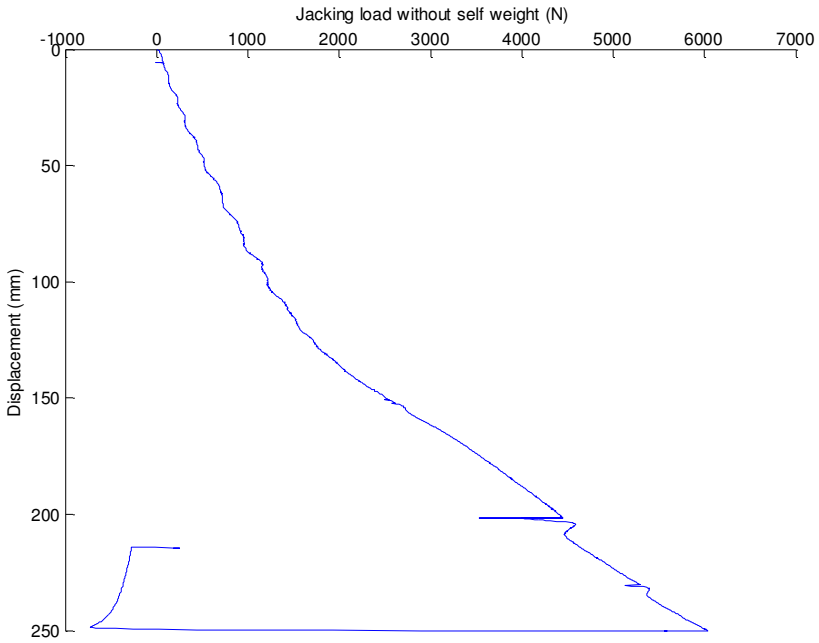

Figure A1-32: C6P1S18O100G head load sensor

Model pile : pile 2

Test : C6P2S18C100G

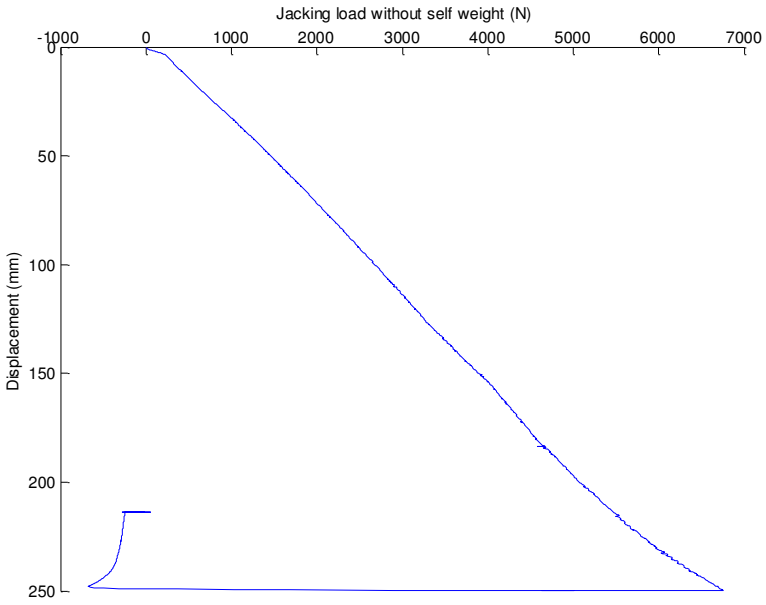

Figure A1-33: C6P2S18C100G head load sensor

Model pile : pile 5

Test : C6P3S16O100G

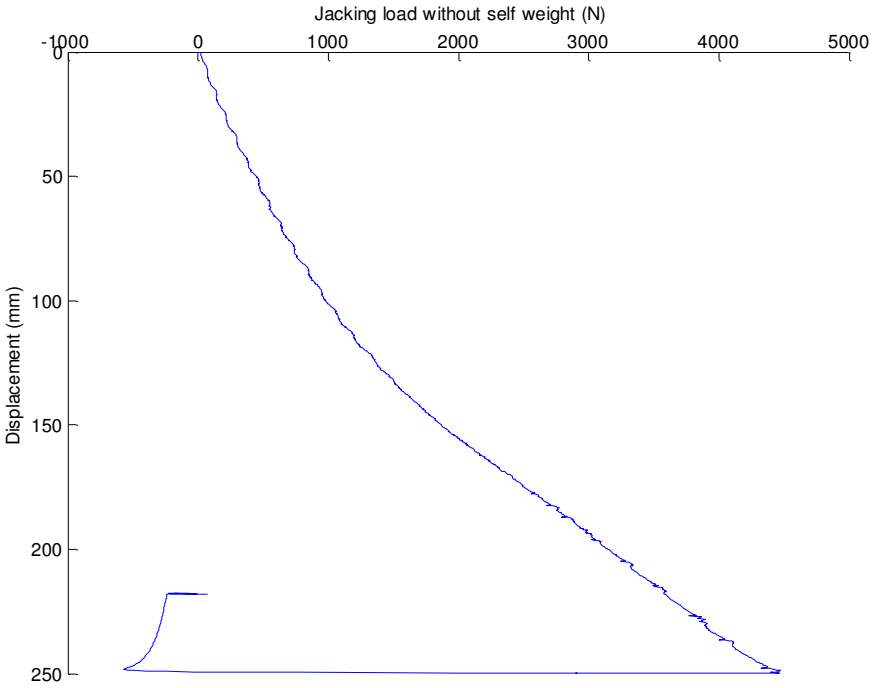

Figure A1-34: C6P3S16O100G head load sensor

Model pile : pile 4

Test : C6P4S16C100G

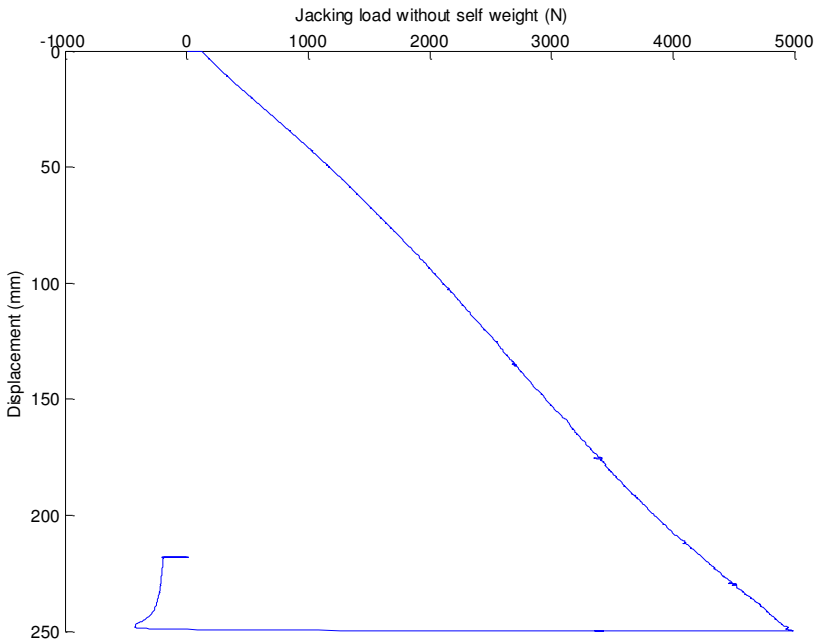

Figure A1-35: C6P4S16C100G head load sensor

Model pile : pile 4

Test : C6P4S16C100G

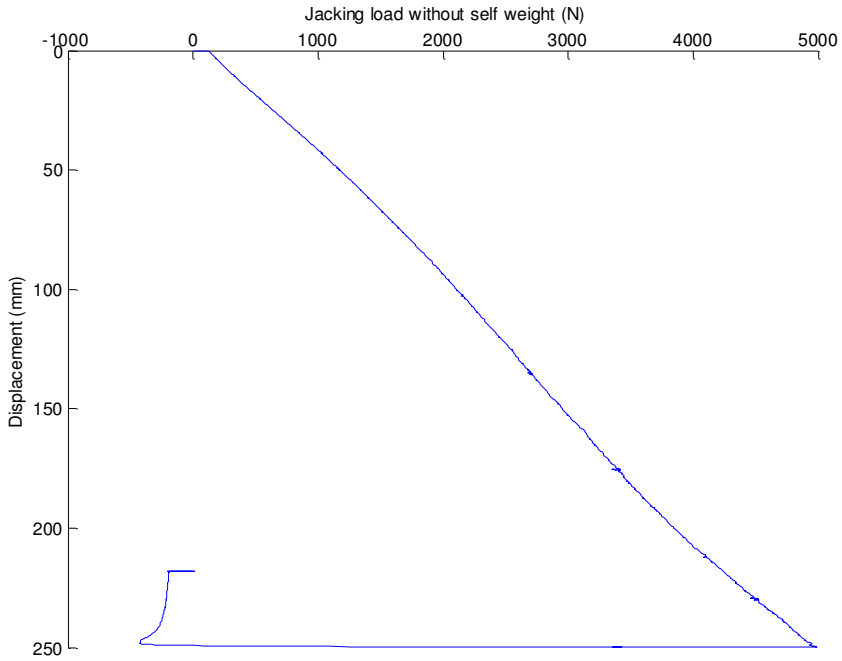

Figure A1-36: C6P4S16C100G head load sensor

Model pile : pile 7

Test : C6P5S14O100G

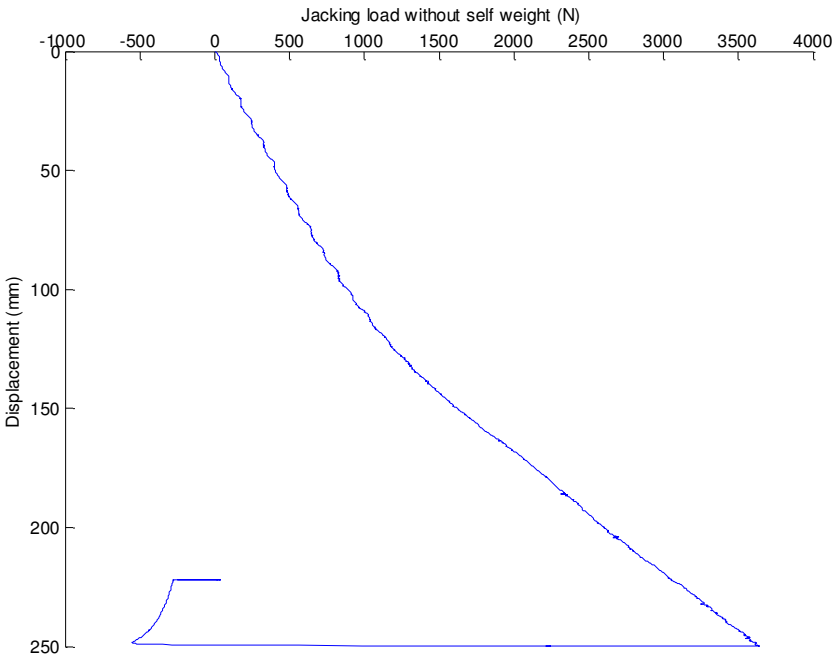

Figure A1-37: C6P5S14O100G head load sensor

Model pile : pile 6

Test : C6P6S14C100G

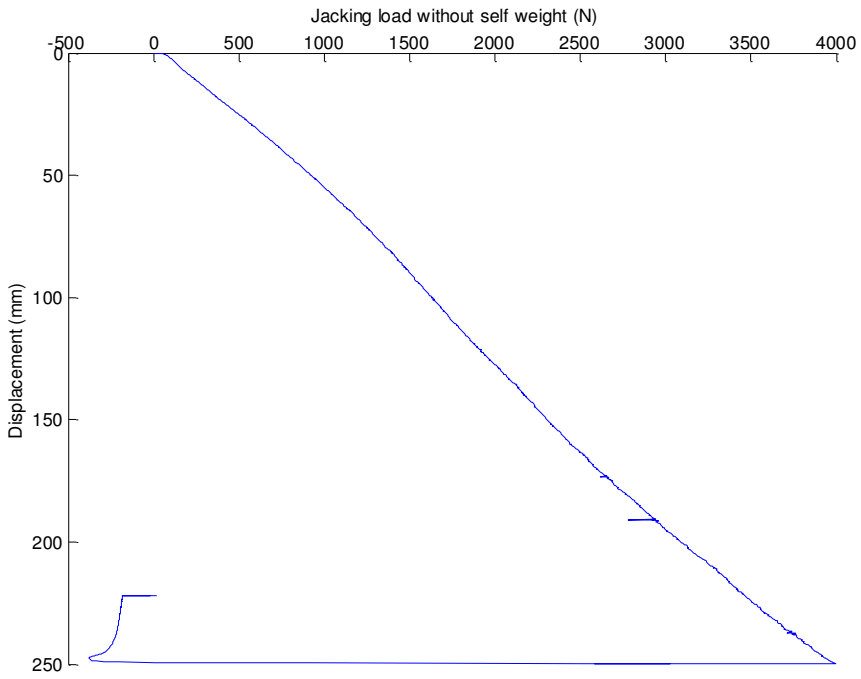

Figure A1-38: C6P6S14C100G head load sensor

Model pile : pile 9

Test : C6P7S12O100G

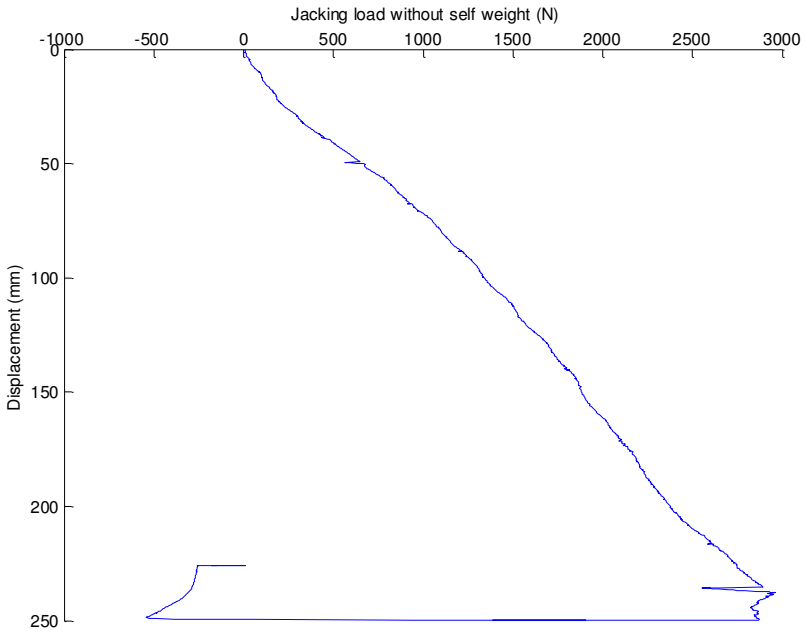

Figure A1-39: C6P7S12O100G head load sensor

Model pile : pile 8

Test : C6P8S12C100G

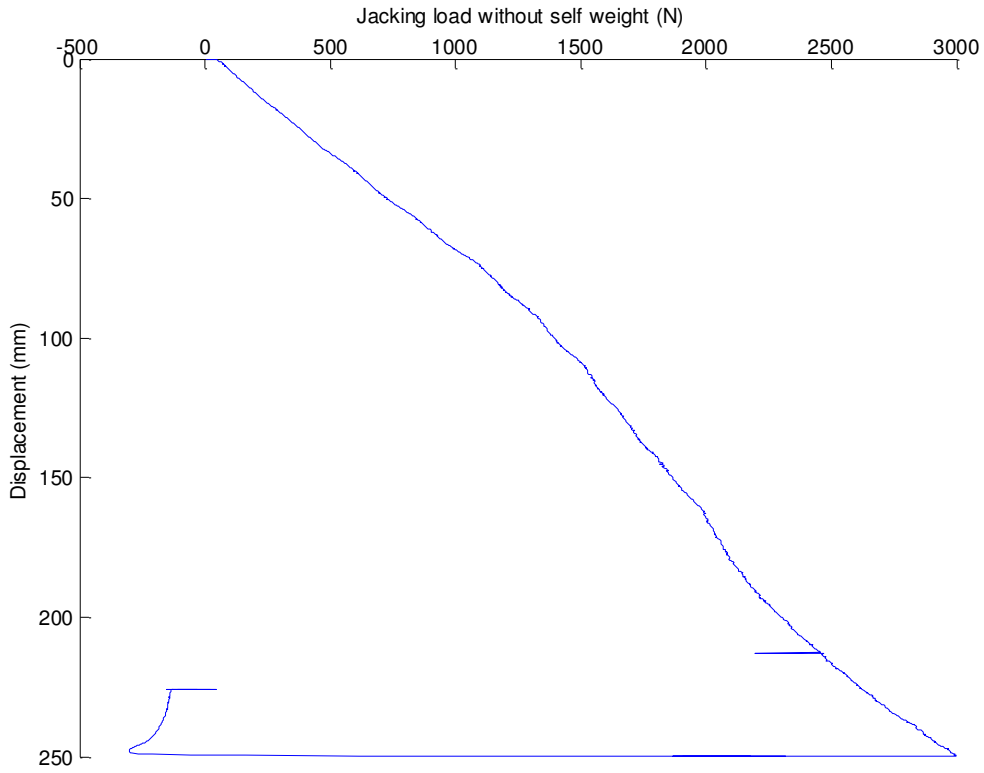

Figure A1-40: C6P8S12C100G head load sensor

Strongbox C7

D_r = 58%

Model pile : pile 3

Test : C7P1S18O100G

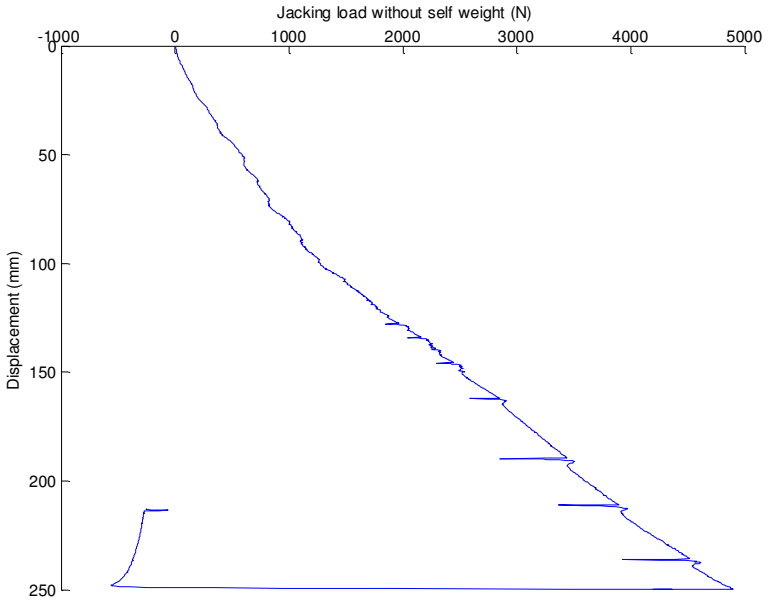

Figure A1-41: C7P1S18O100G head load sensor

Model pile : pile 2

Test : C7P2S18C100G

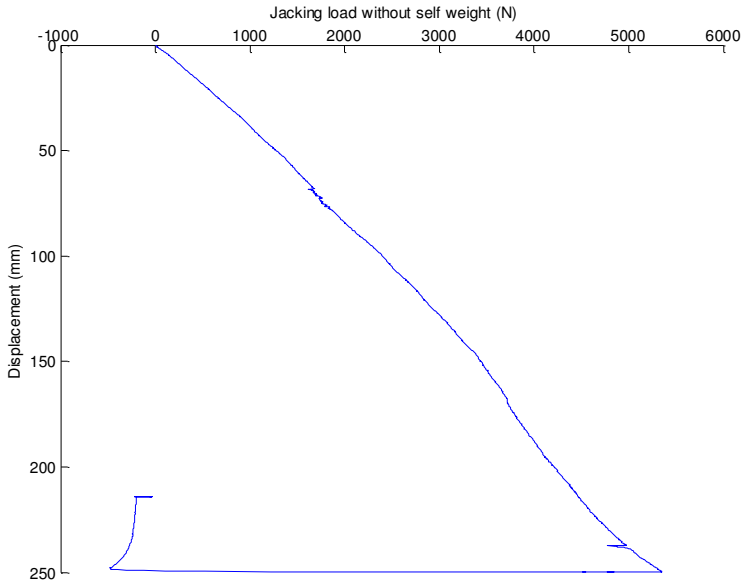

Figure A1-42: C7P2S18C100G head load sensor

Model pile : pile 5

Test : C7P3S16O100G

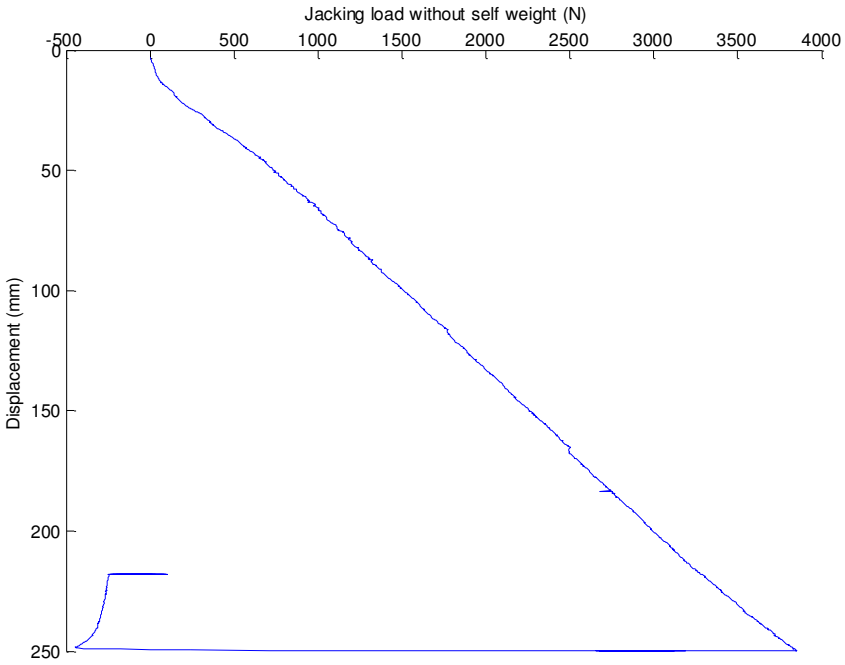

Figure A1-43: C7P3S16O100G head load sensor

Model pile : pile 4

Test : C7P4S16C100G

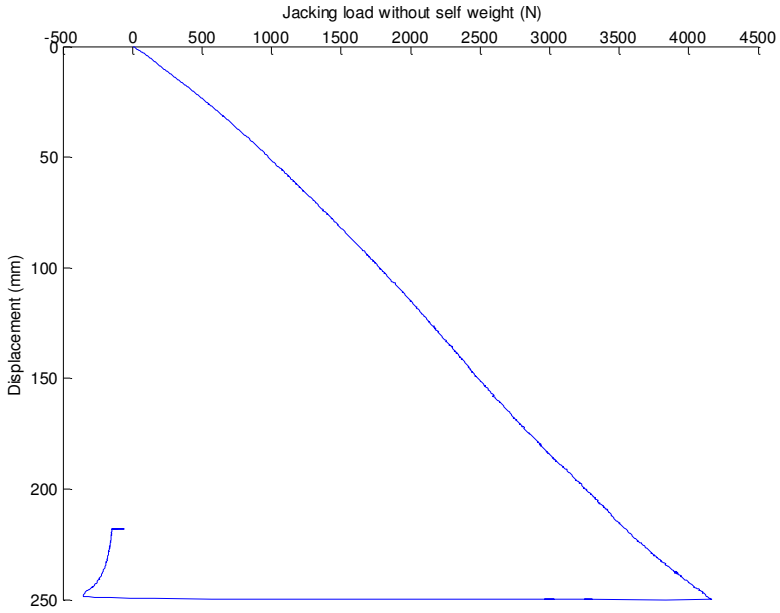

Figure A1-44: C7P4S16C100G head load sensor

Model pile : pile 7

Test : C7P5S14O100G

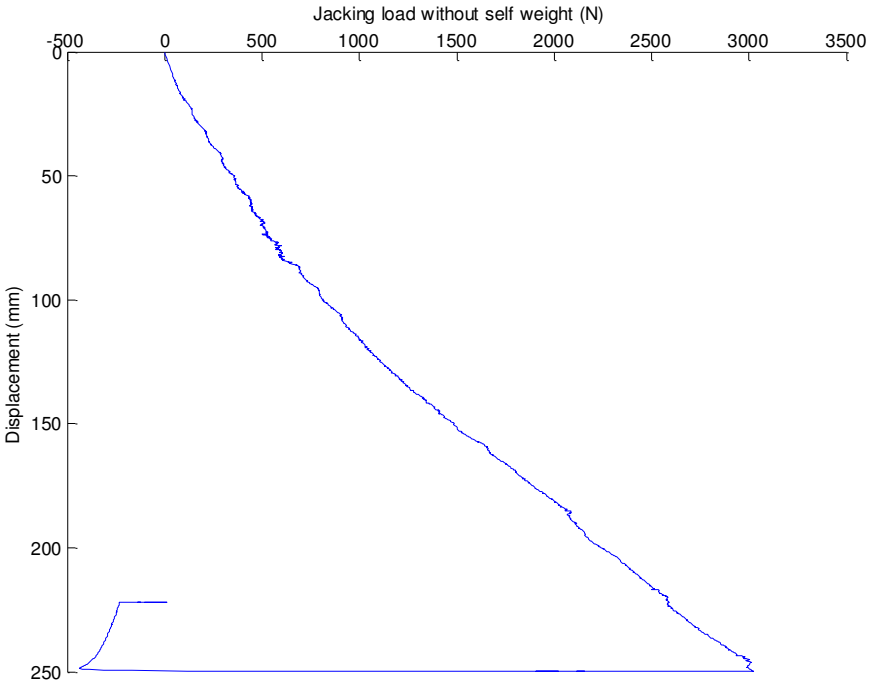

Figure A1-45: C7P5S14O100G head load sensor

Model pile : pile 6

Test : C7P6S14C100G

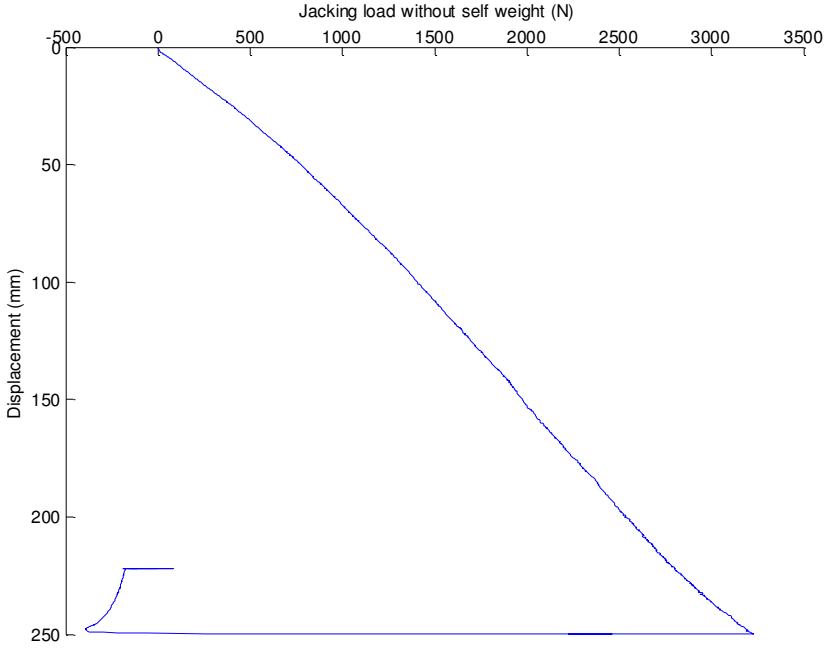

Figure A1-46: C7P6S14C100G head load sensor

Model pile : pile 9

Test : C7P7S12O100G

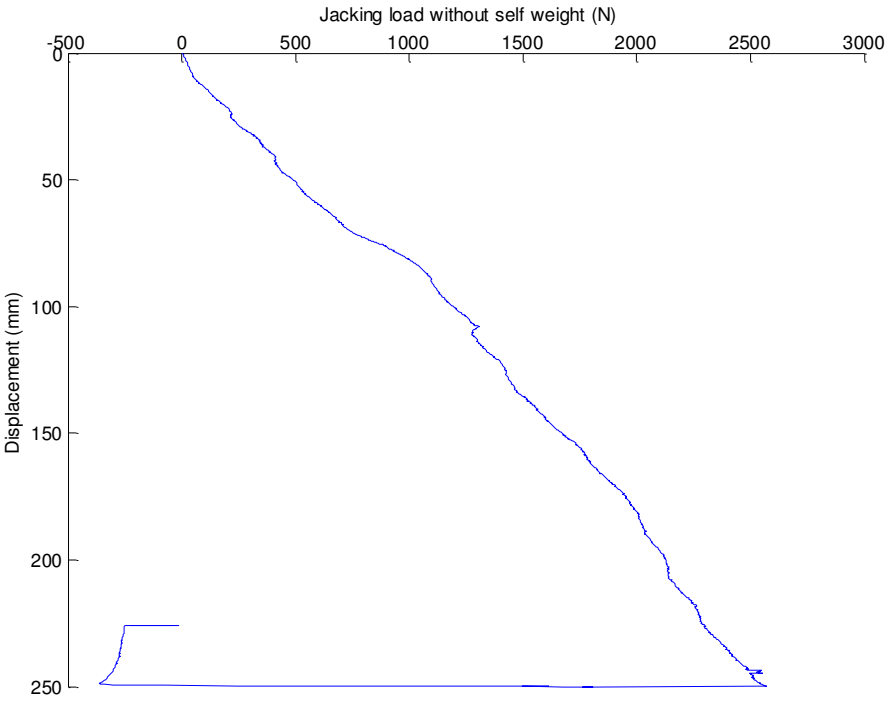

Figure A1-47: C7P7S12O100G head load sensor

Model pile : pile 8

Test : C7P8S12C100G

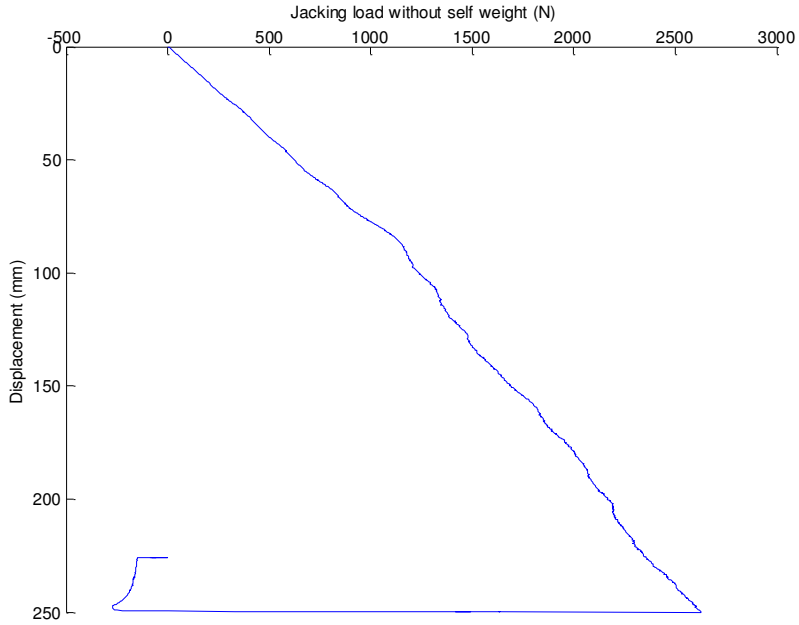

Figure A1-48: C7P8S12C100G head load sensor

Strongbox C8

D_r = 99%

Model pile : pile 3

Test : C8P1S18O100G

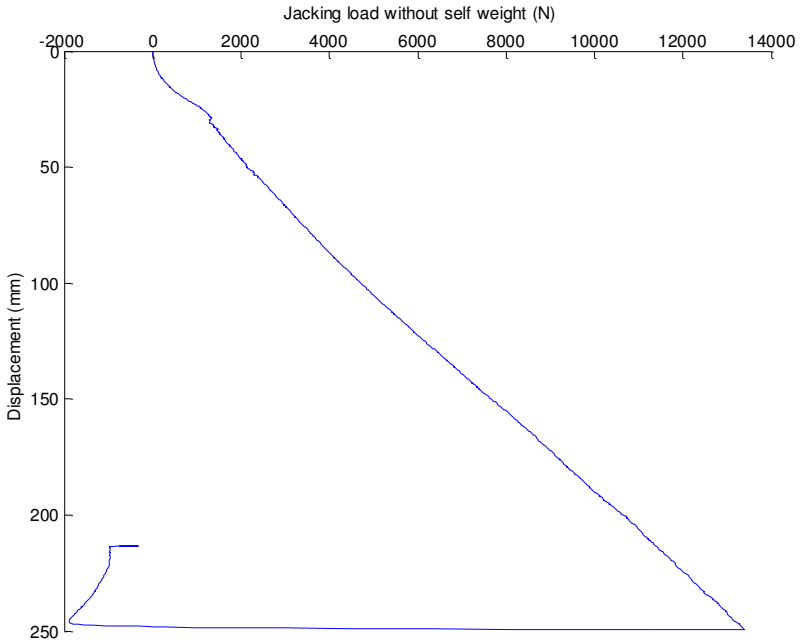

Figure A1-49: C8P1S18O100G head load sensor

Model pile : pile 2

Test : C8P2S18C100G

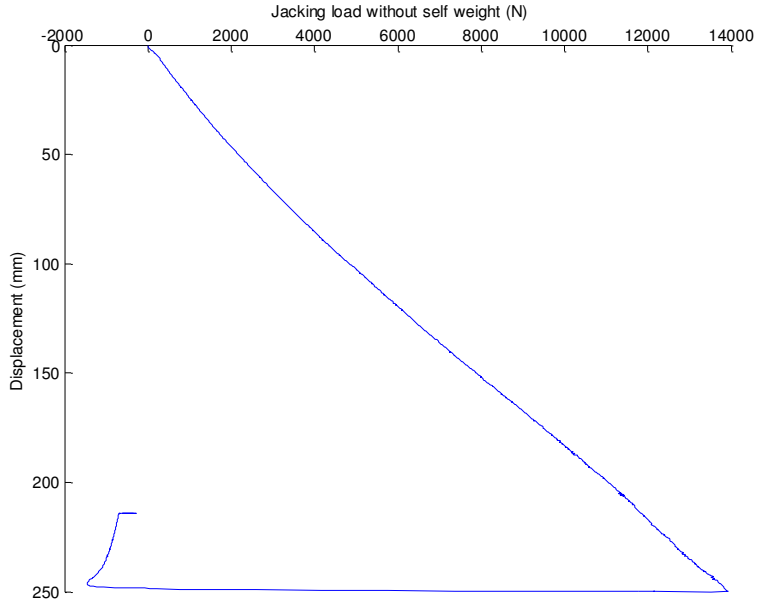

Figure A1-50: C8P2S18C100G head load sensor

Model pile : pile 5

Test : C8P3S16O100G

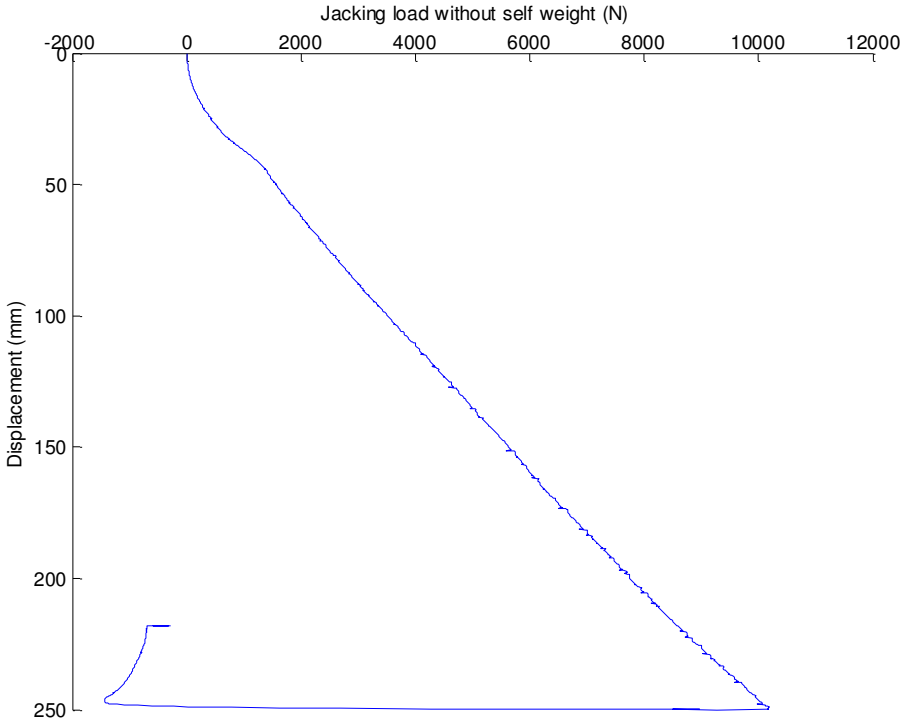

Figure A1-51: C8P3S16O100G head load sensor

Model pile : pile 4

Test : C8P4S16C100G

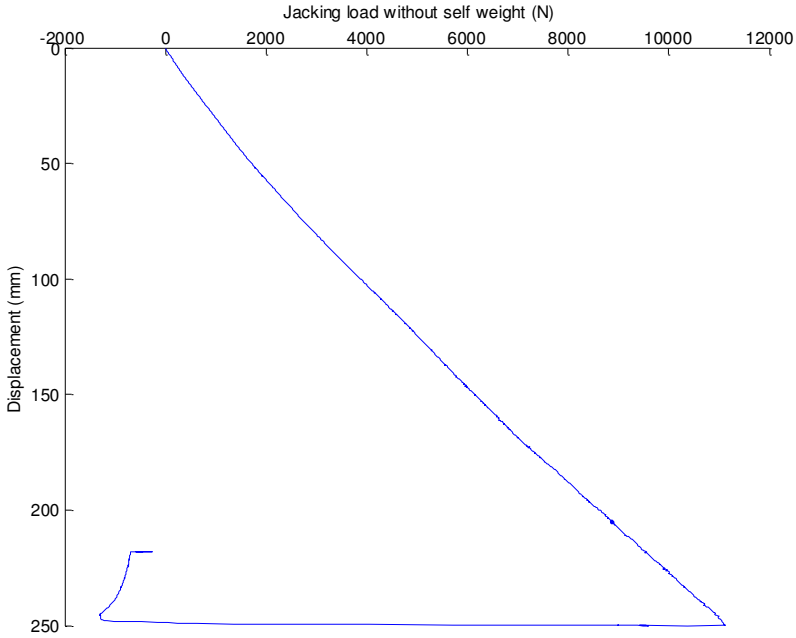

Figure A1-52: C8P4S16C100G head load sensor

Model pile : pile 7

Test : C8P5S14O100G

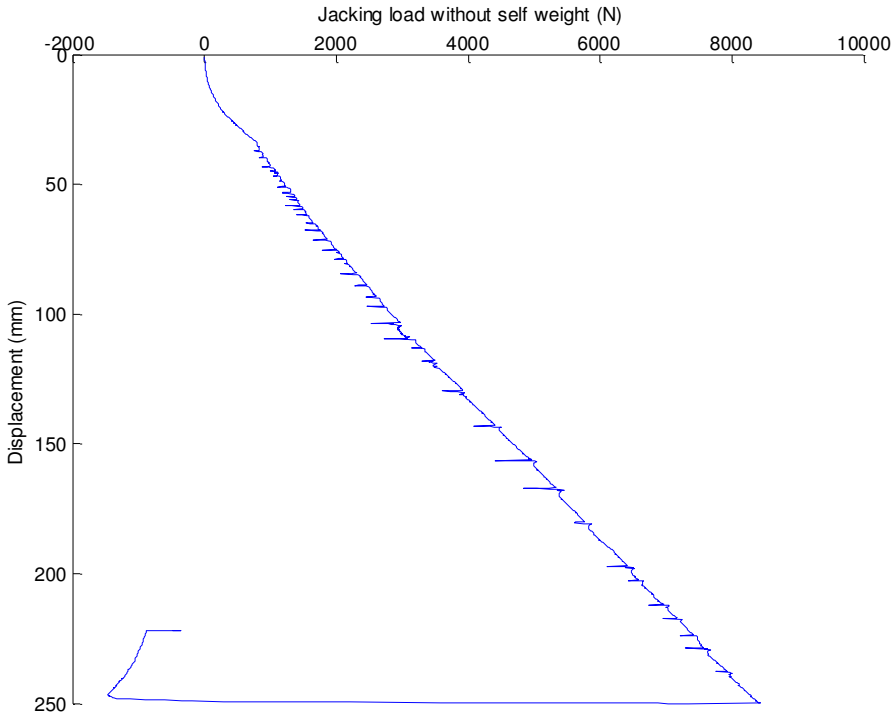

Figure A1-53: C8P5S14O100G head load sensor

Model pile : pile 6

Test : C8P6S14C100G

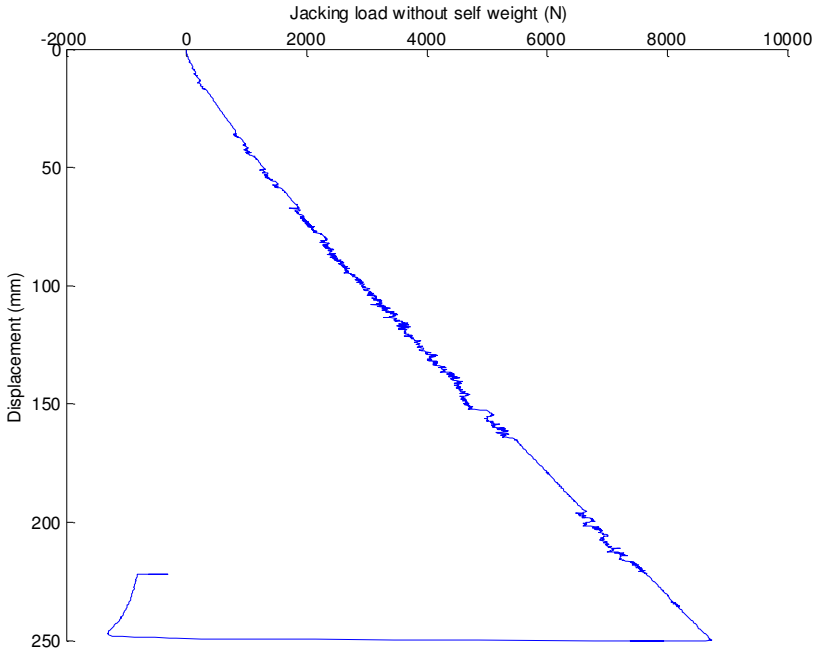

Figure A1-54: C8P6S14C100G head load sensor

Model pile : pile 9

Test : C8P7S12O100G

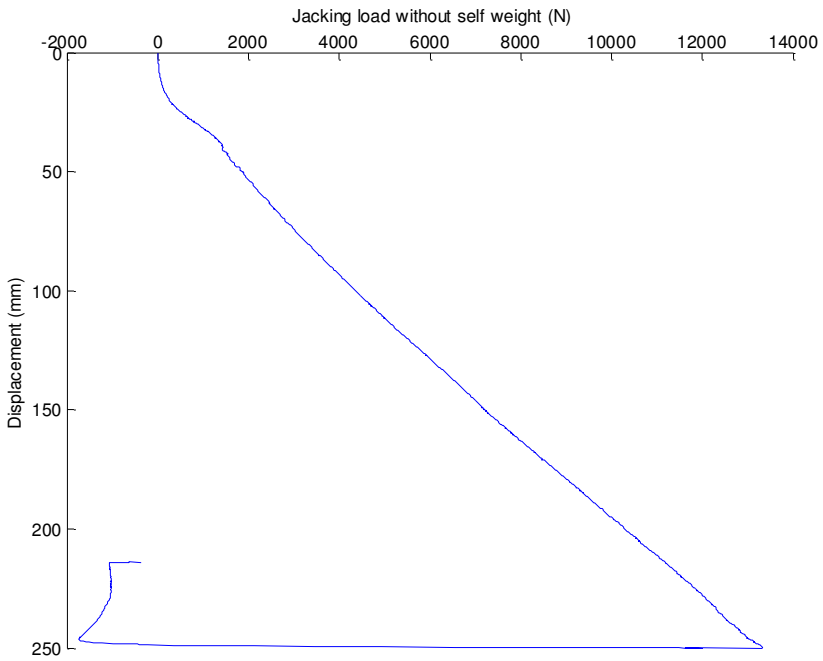

Figure A1-55: C8P7S12O100G head load sensor

Model pile : pile 8

Test : C8P8S12C100G

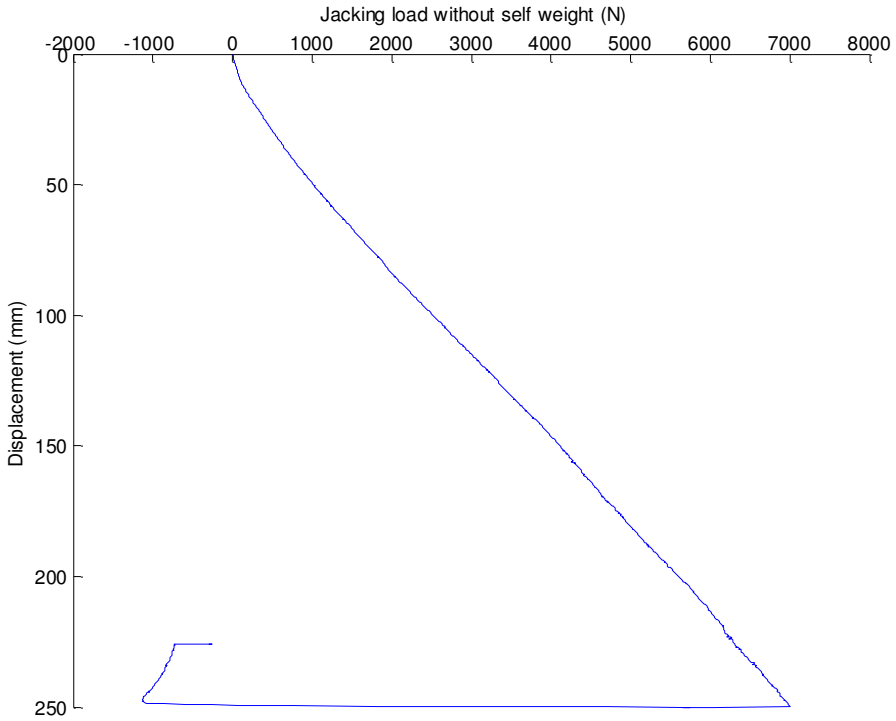

Figure A1-56: C8P8S12C100G head load sensor

Strongbox C9

D_r = 58%

Model pile : rigid pile

Test : C9P1RL100G

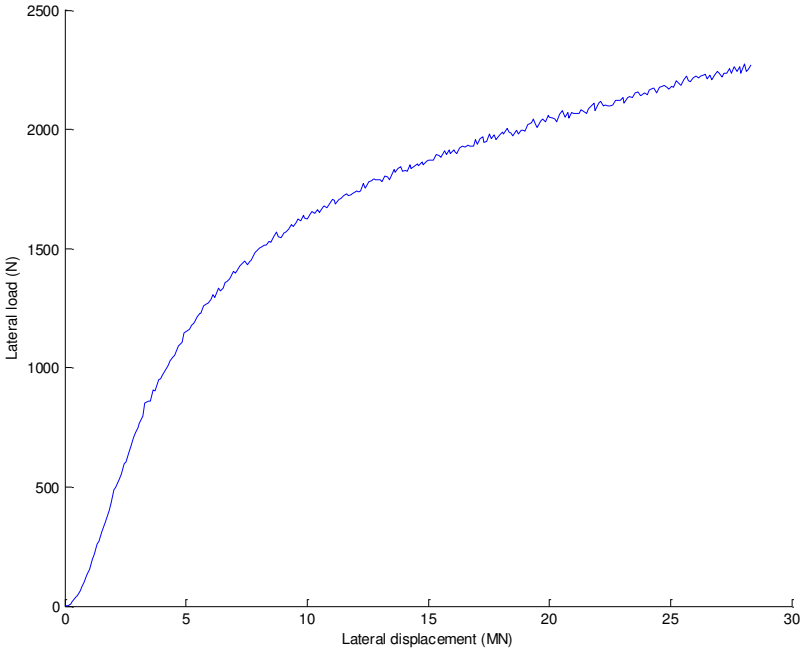

Figure A1-57: C9P1RL100G lateral load sensor

Model pile : rigid pile

Test : C9P2RL1G

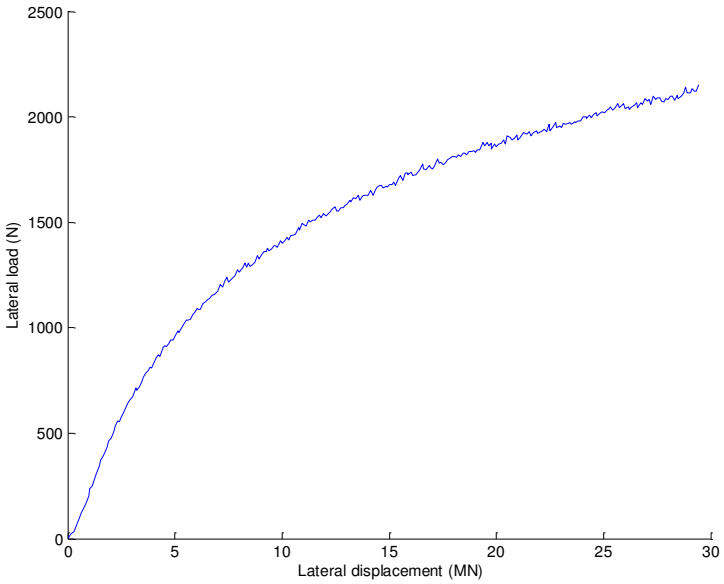

Figure A1-58: C9P2RL1G lateral load sensor

Model pile : rigid pile

Test : C9P3RH100G

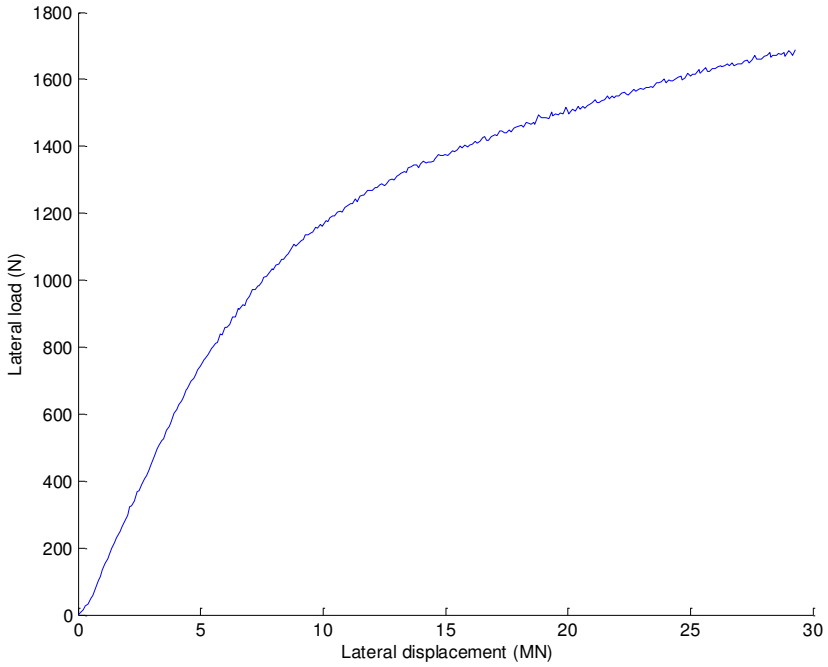

Figure A1-59: C9P3RH100G lateral load sensor

Model pile : rigid pile

Test : C9P4RH1G

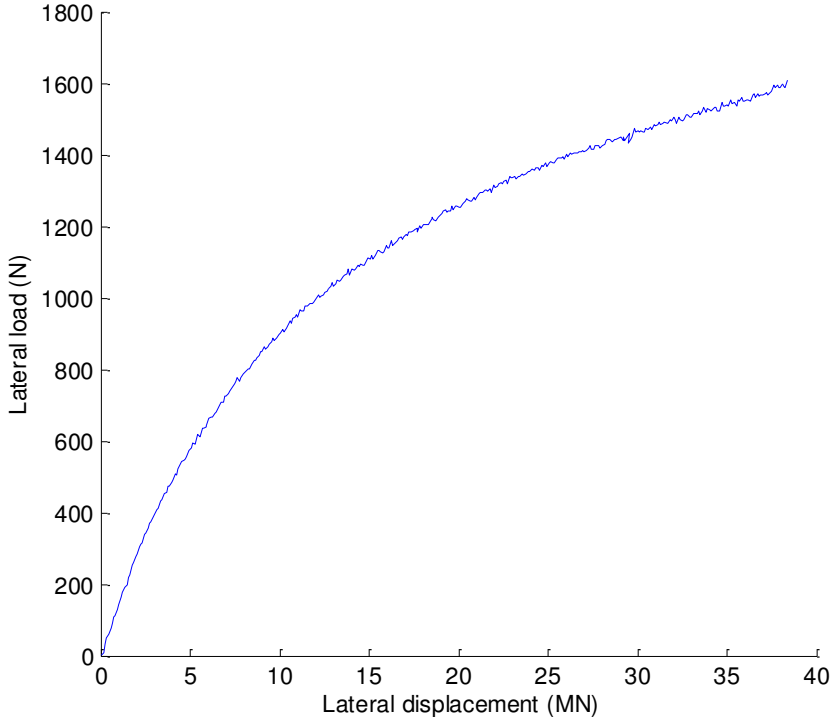

Figure A1-60: C9P4RH1G lateral load sensor

Conteneur C10

D_r = 99%

Model pile : rigid pile

Test : C10P1RH100G

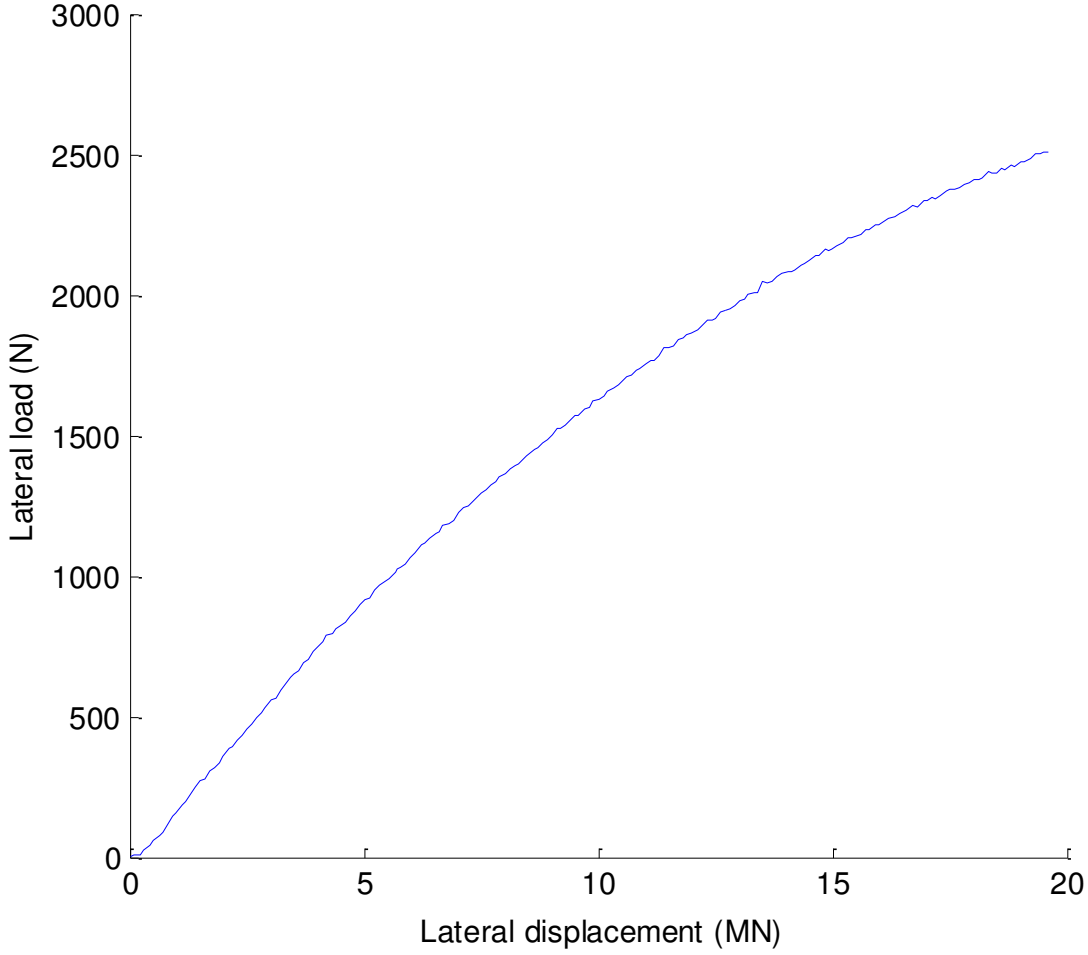

Figure A1-61: C10P1RH100G lateral load sensor

Model pile : rigid pile

Test : C10P2RH100G

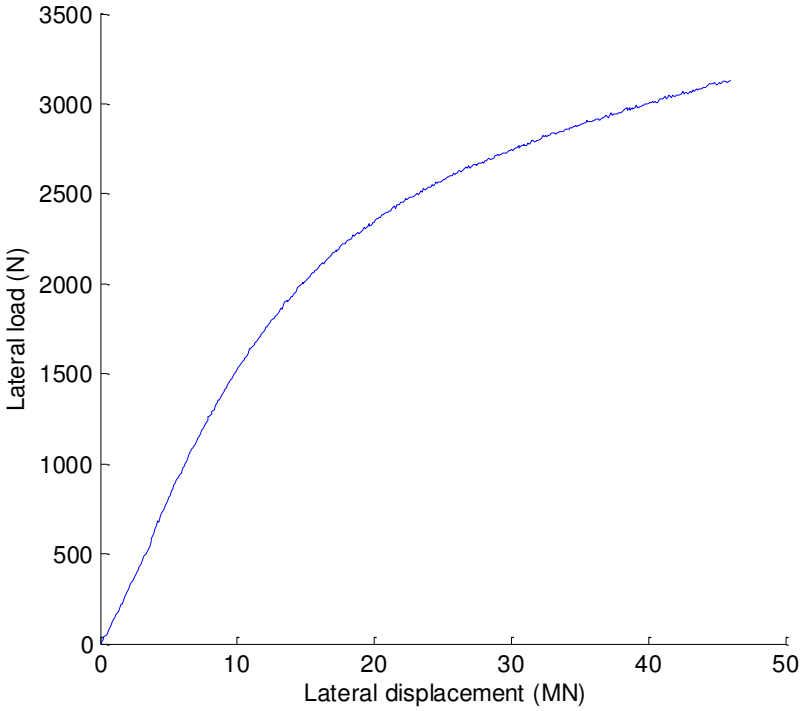

Figure A1-62: C10P2RH100G lateral load sensor

Model pile : rigid pile

Test : C10P3RH1G

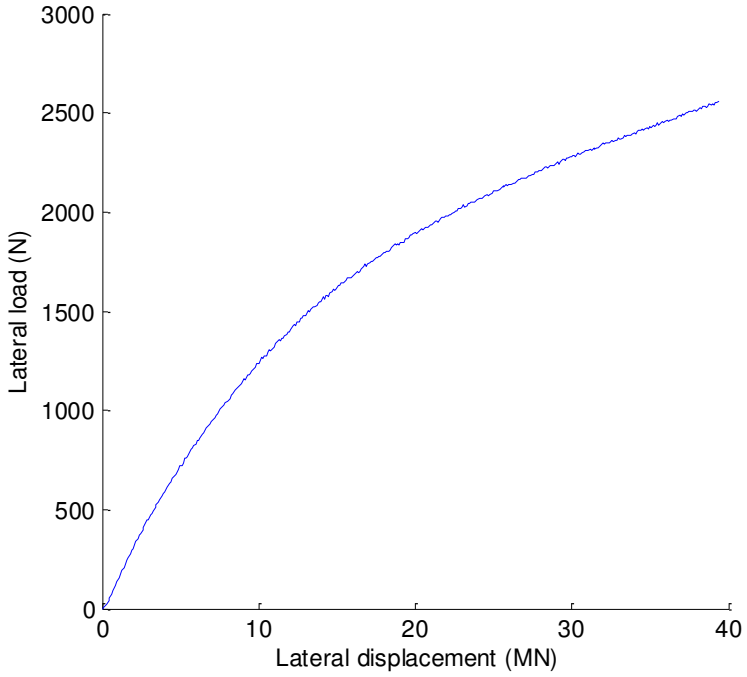

Figure A1-63: C10P3RH1G lateral load sensor

Model pile : rigid pile

Test : C10P4RL1G

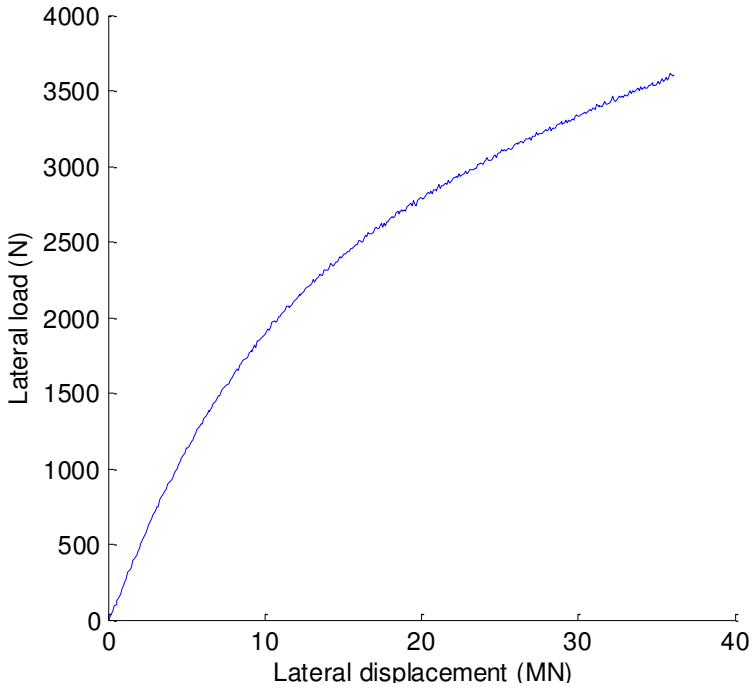

Figure A1-64: C10P4RL1G lateral load sensor

Model pile : rigid pile

Test : C10P5RL100G

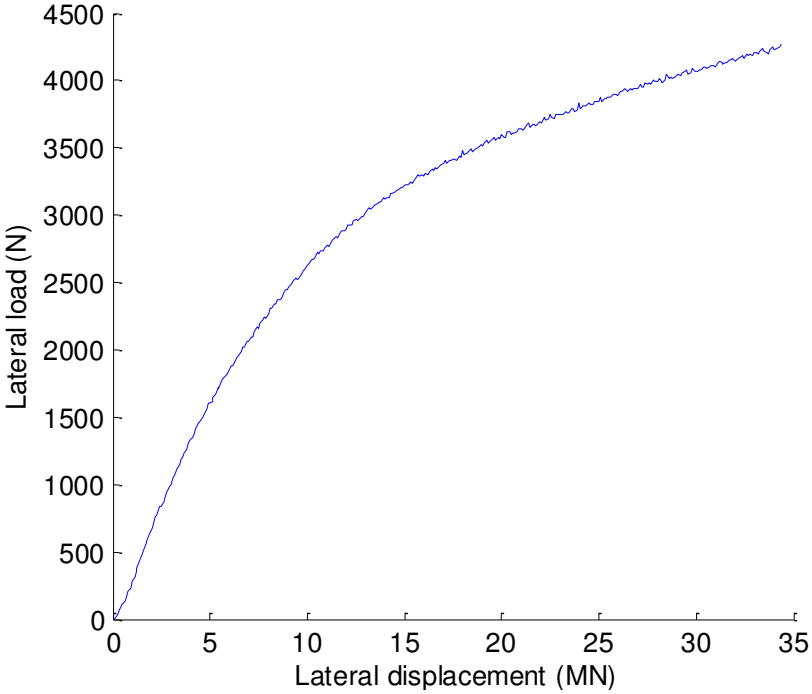

Figure A1-65: C10P5RL100G lateral load sensor

Strongbox C11 D_r = 58% (Dry)

Model pile : instrumented pile

Test : C11P2FL1G (Monotonic loading)

The figures represent the increase of the lateral loading with step of 50 N

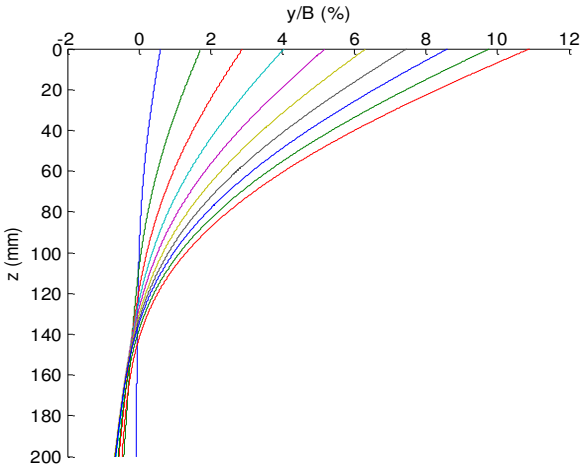

Figure A1-66 : lateral displacement vs depth

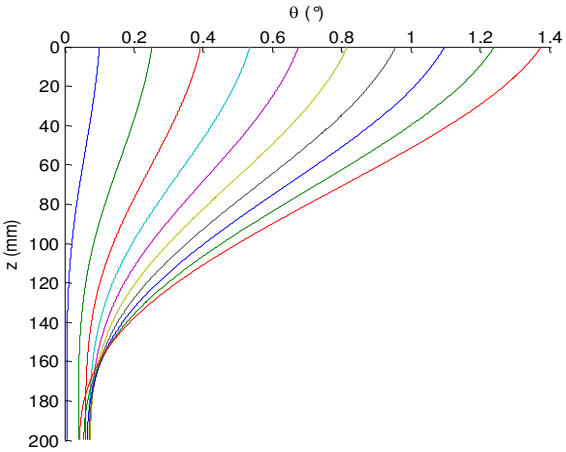

Figure A1-67: rotation vs depth

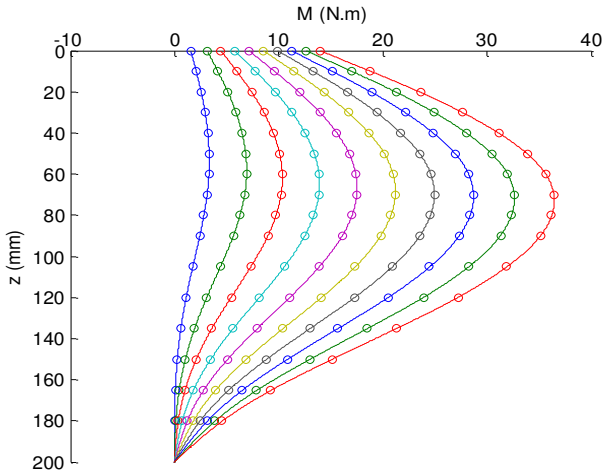

Figure A1-68: moment vs depth

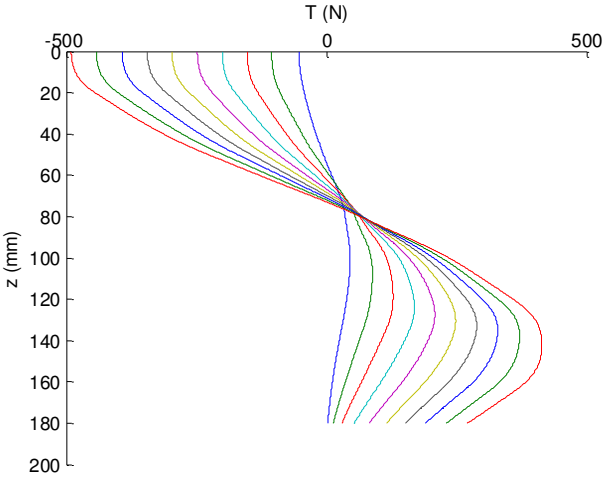

Figure A1-69: shear force vs depth

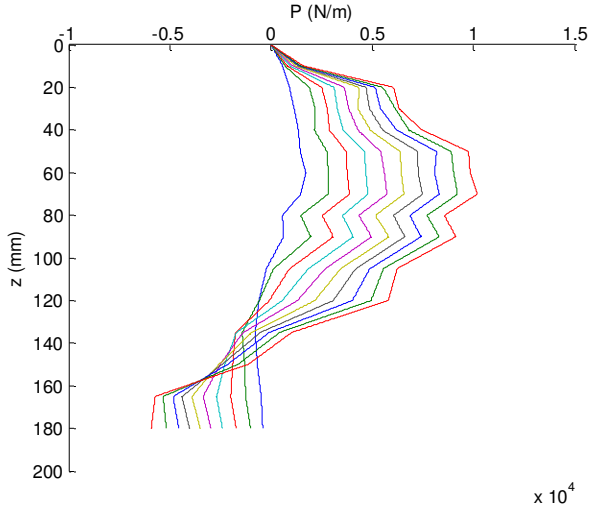

Figure A1-70: Soil reaction vs depth

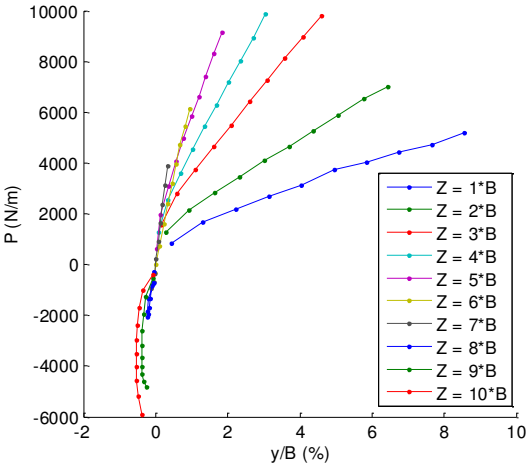

Figure A1-71: monotonic p-y curves

Test : C11P2FL1G (Cyclic loading)

The figures represent the cycles 1, 10, 100, 200

Loading line complete and unloading hatched line

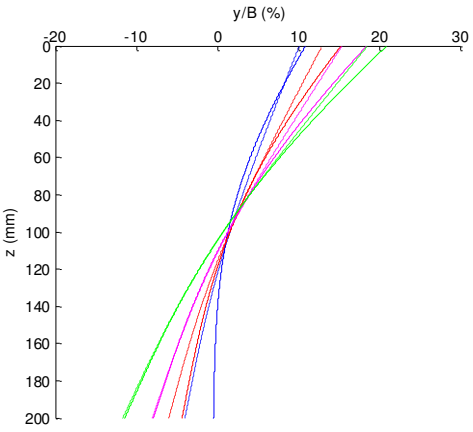

Figure A1-72: lateral displacement vs depth

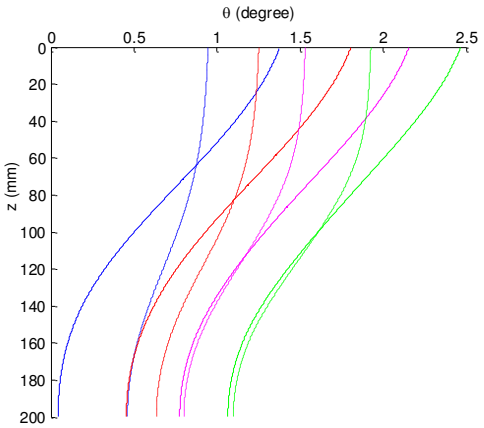

Figure A1-73: rotation vs depth

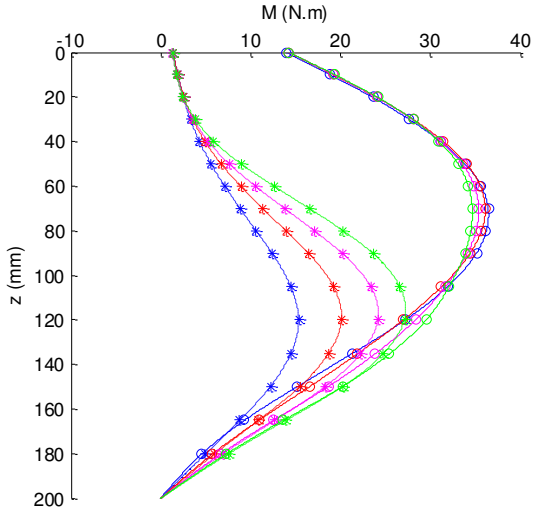

Figure A1-74: moment vs depth

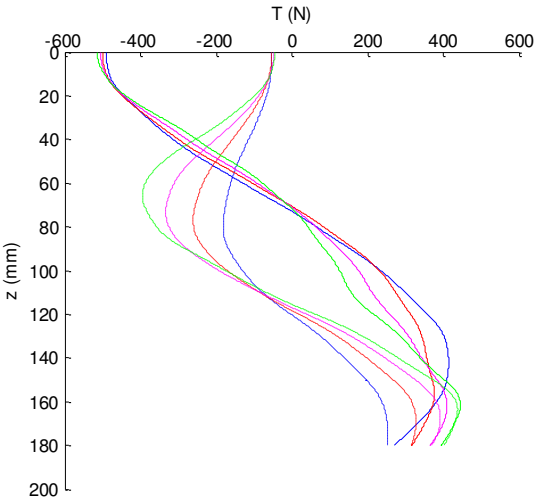

Figure A1-75: shear force vs depth

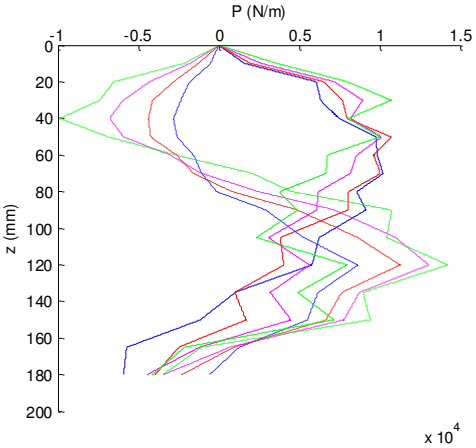

Figure A1-76: Soil reaction vs depth

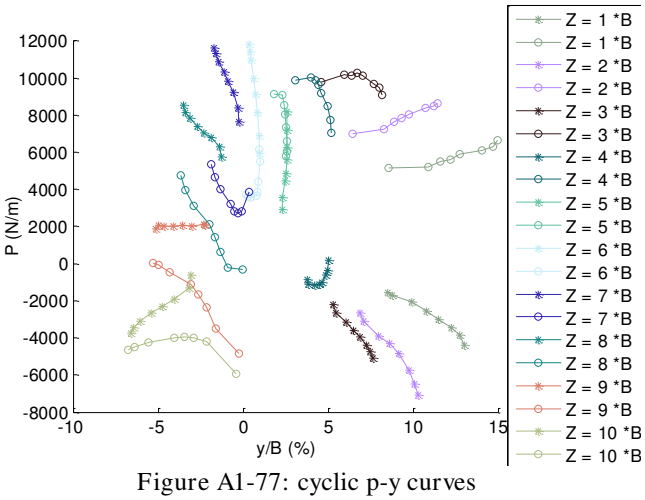

Figure A1-77: cyclic p-y curves

Model pile : instrumented pile

Test : C11P3FL100G (Monotonic loading)

The figures represent the increase of the lateral loading with step of 50 N

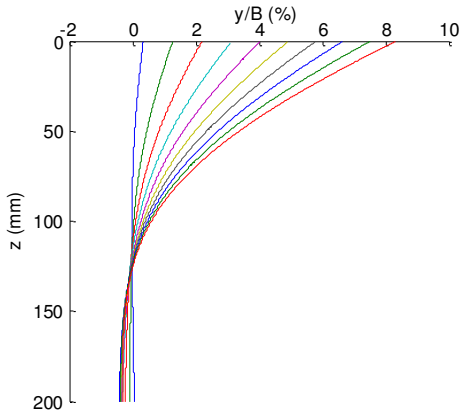

Figure A1-78 : lateral displacement vs depth

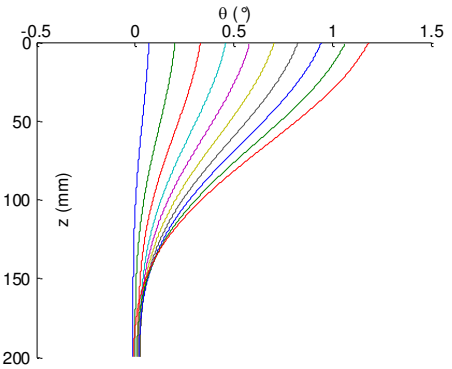

Figure A1-79 : rotation vs depth

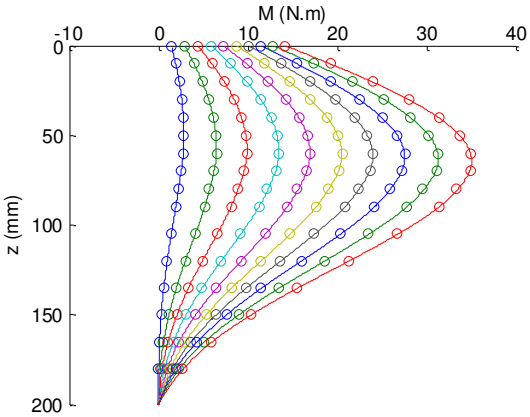

Figure A1 -80 : moment vs depth

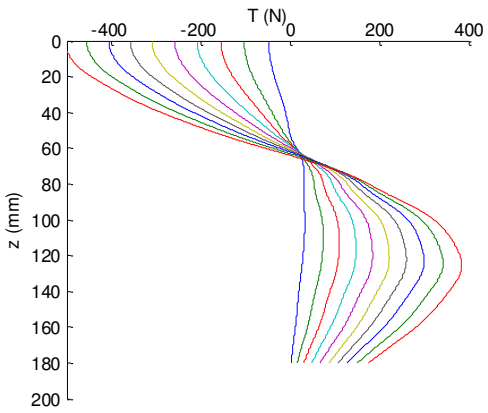

Figure A1-81 : shear force vs depth

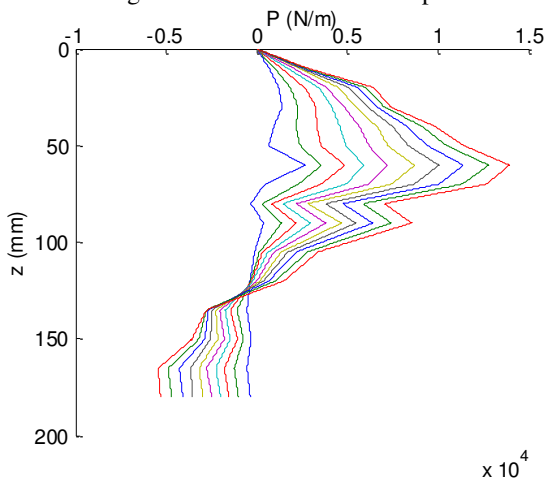

Figure A1-82 : Soil reaction vs depth

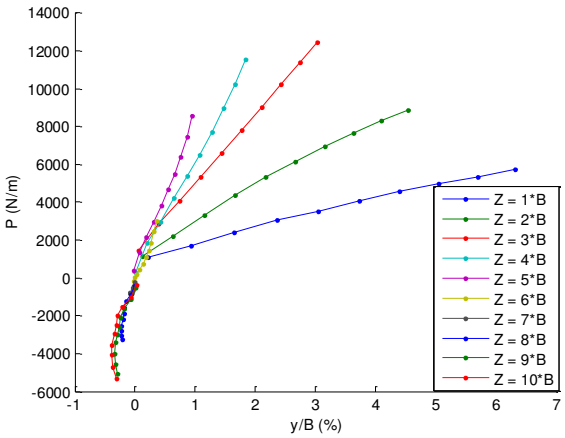

Figure A1-83 : monotonic p-y curves

Test : C11P3FL100G (Cyclic loading)

The figures represent the cycles 1, 10, 100, 1000

Loading line complete and unloading hatched line

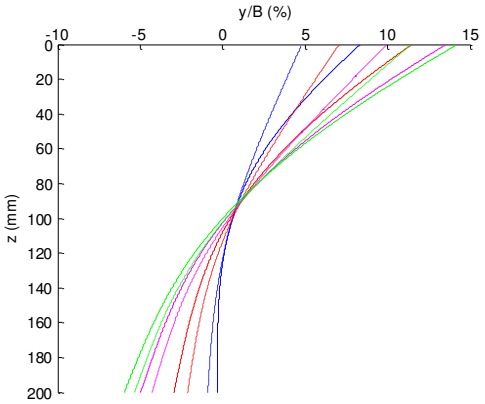

Figure A1-84 : lateral displacement vs depth

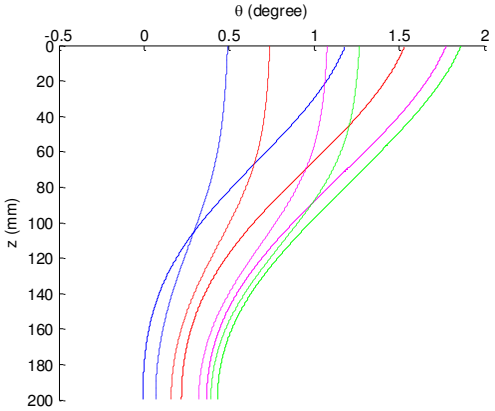

Figure A1 -85 : rotation vs depth

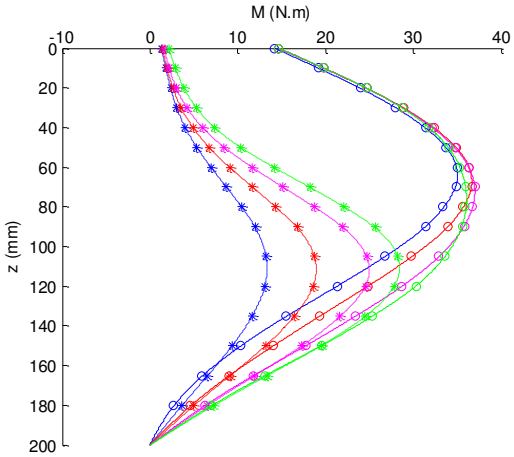

Figure A1-86 : moment vs depth

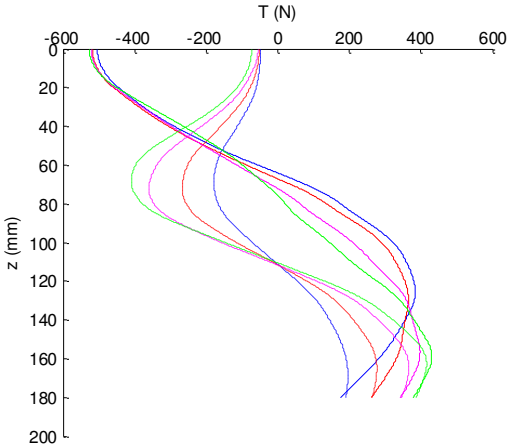

Figure A1-87 : shear force vs depth

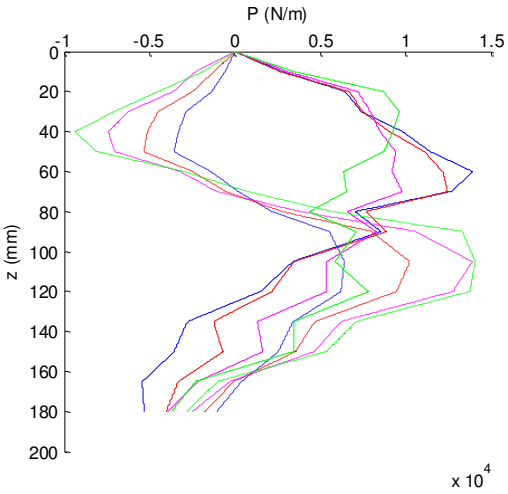

Figure A1-88 : Soil reaction vs depth

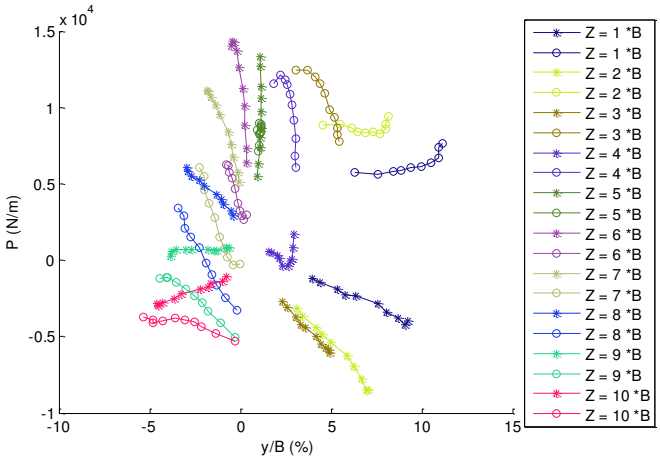

Figure A1-89 : cyclic p-y curves

Model pile : instrumented pile

Test : C11P4FH1G (Monotonic loading)

The figures represent the increase of the lateral loading with step of 50 N

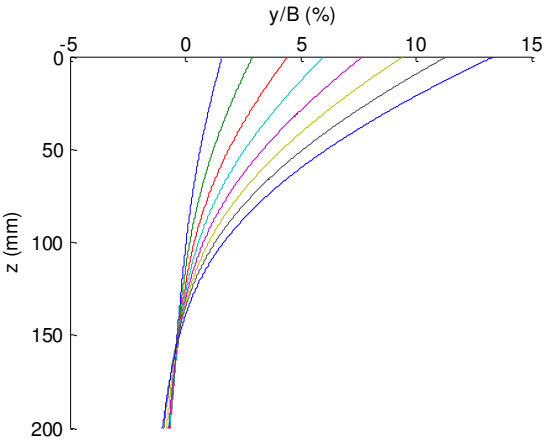

Figure A1-90 : lateral displacement vs depth

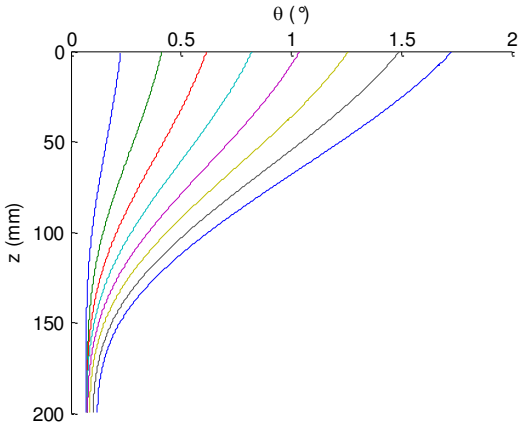

Figure A1-91 : rotation vs depth

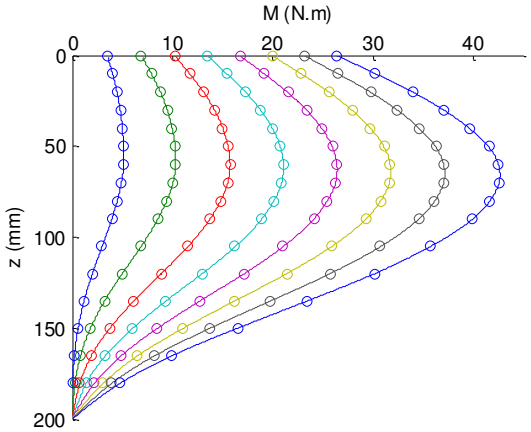

Figure A1-92 : moment vs depth

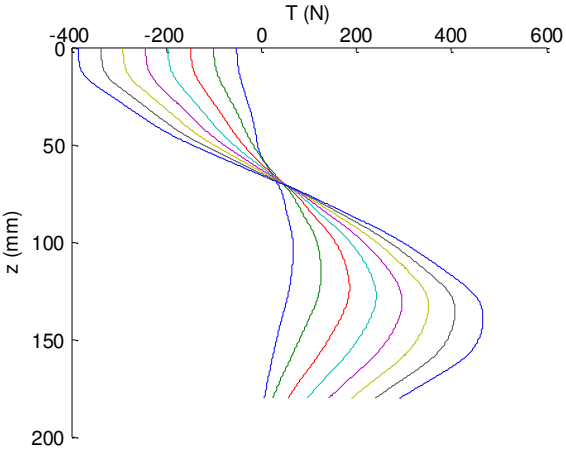

Figure A1-93 : shear force vs depth

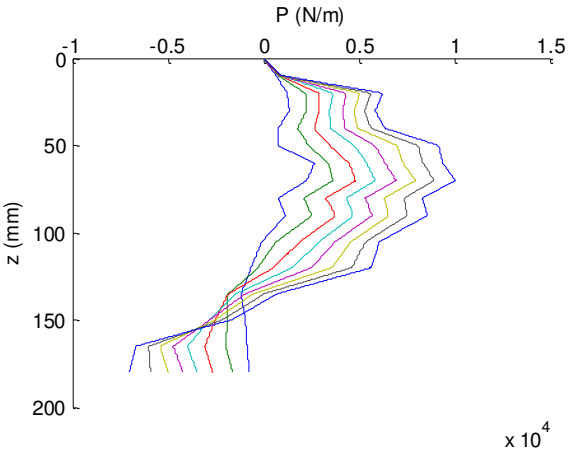

Figure A1-94 : Soil reaction vs depth

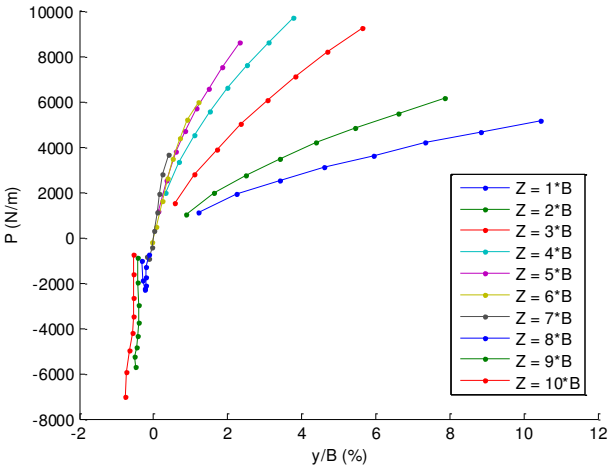

Figure A1-95 : monotonic p-y curves

Test : C11P4FH1G (Cyclic loading)

The figures represent the cycles 1, 10, 100, 1000

Loading line complete and unloading hatched line

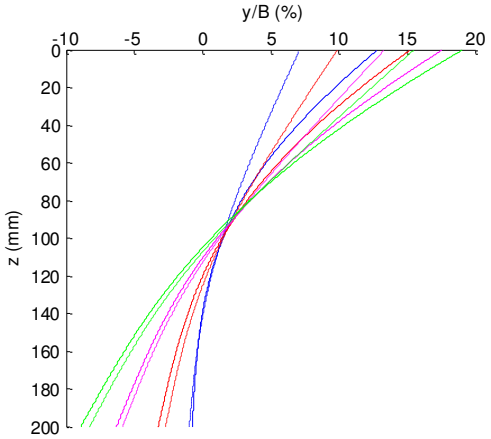

Figure A1-96 : lateral displacement vs depth

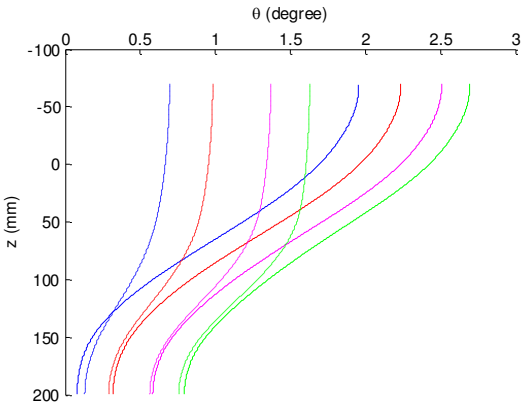

Figure A1-97 : rotation vs depth

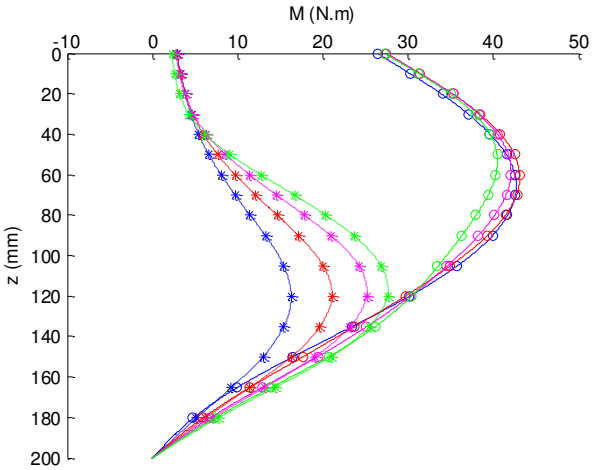

Figure A1-98 : moment vs depth

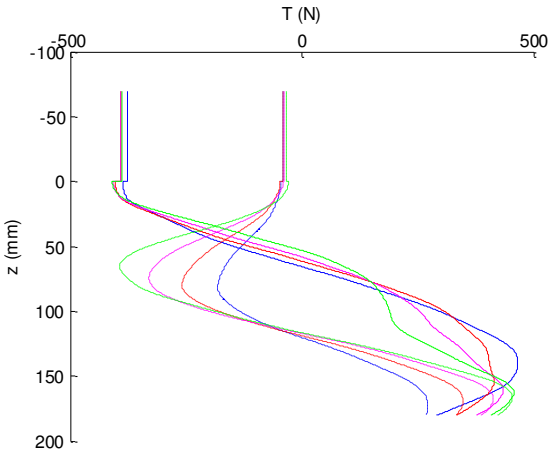

Figure A1-99 : shear force vs depth

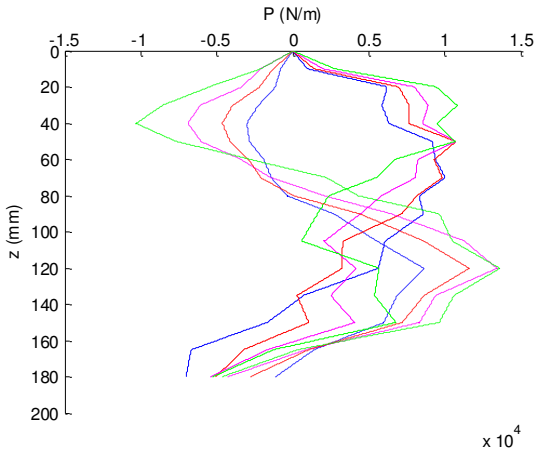

Figure A1-100 : Soil reaction vs depth

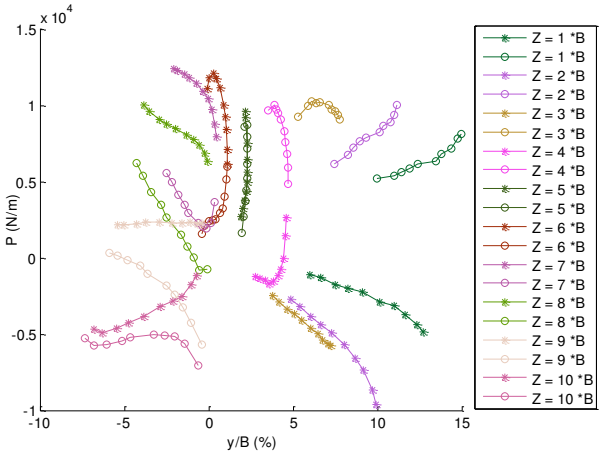

Figure A1-101 : cyclic p-y curves

Model pile : instrumented pile

Test : C11P5FH100G (Monotonic loading)

The figures represent the increase of the lateral loading with step of 50 N

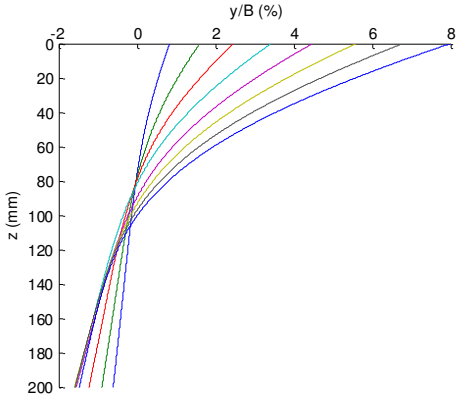

Figure A1-102 : lateral displacement vs depth

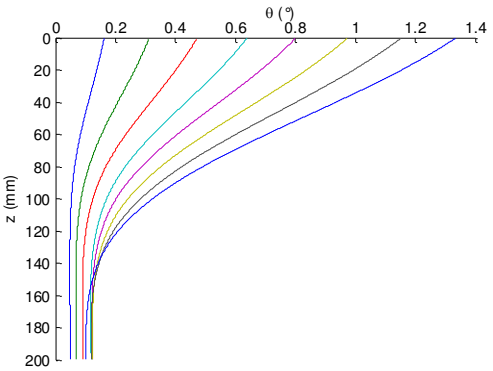

Figure A1-103 : rotation vs depth

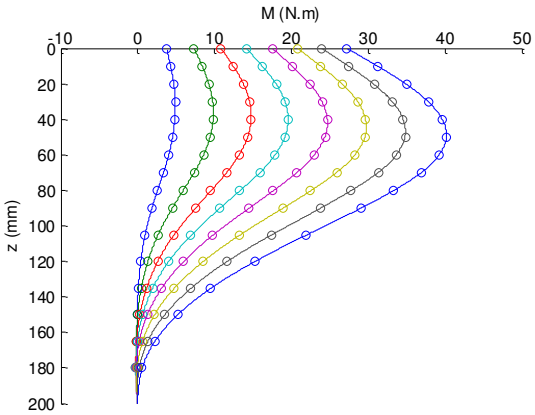

Figure A1-104 moment vs depth

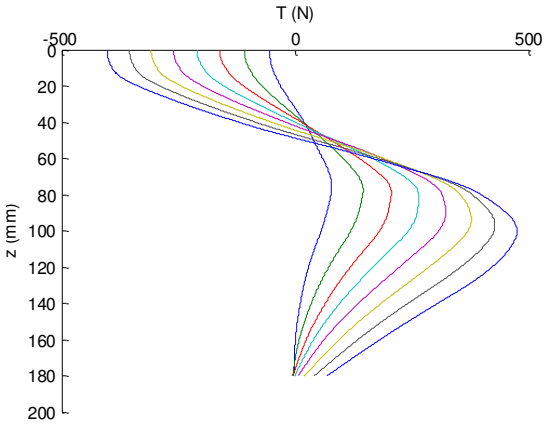

Figure A1-105 : shear force vs depth

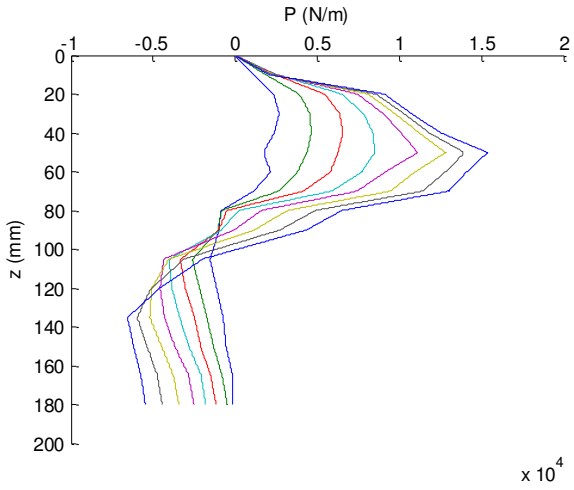

Figure A1-106 : Soil reaction vs depth

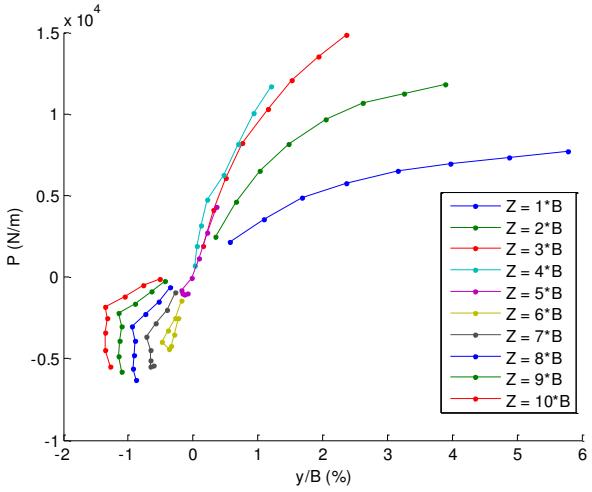

Figure A1-107 : cyclic p-y curves

Test : C11P5FH100G (Cyclic loading)

The figures represent the cycles 1, 10, 100, 1000

Loading line complete and unloading hatched line

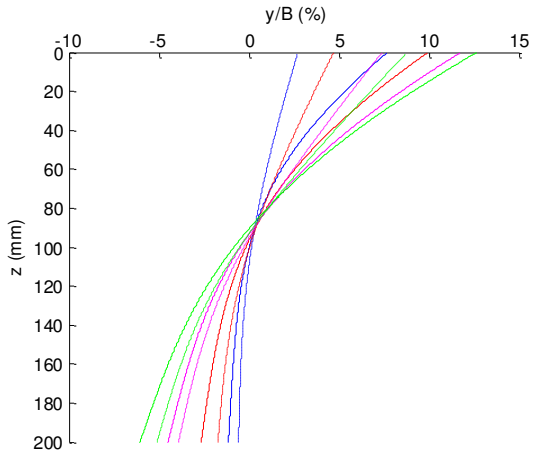

Figure A1-108 : lateral displacement vs depth

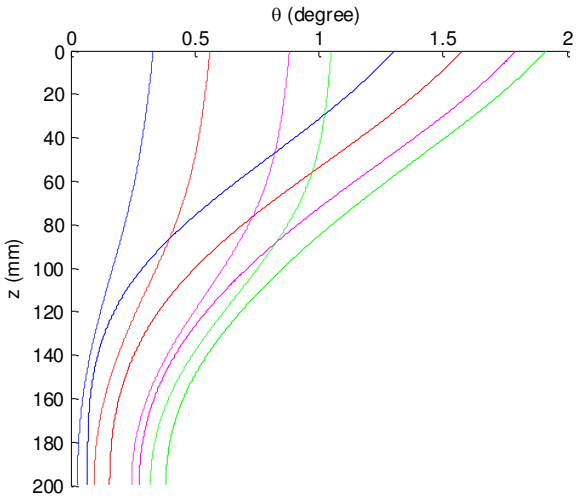

Figure A1-109 : rotation vs depth

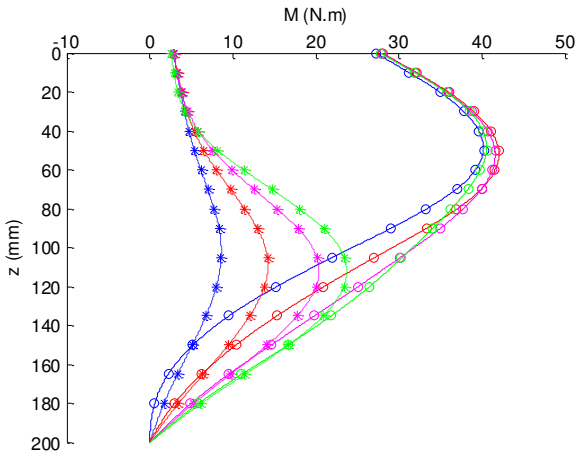

Figure A1-110 : moment vs depth

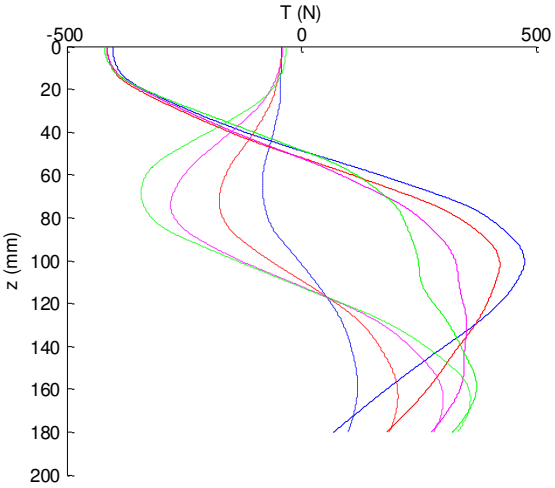

Figure A1-111 : shear force vs depth

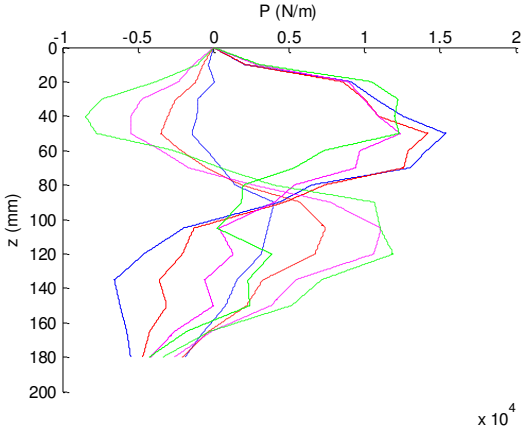

Figure A1-112 : Soil reaction vs depth

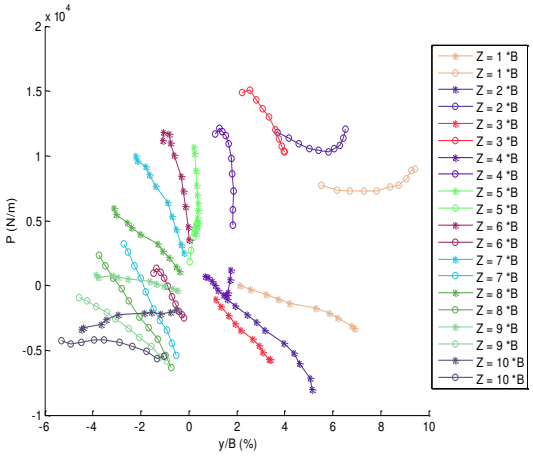

Figure A1-113 : cyclic p-y curves

Strongbox C12 D_r = 58% (Saturated)

Model pile : instrumented pile

Test : C12P1FH1G (Monotonic loading)

The figures represent the increase of the lateral loading with step of 50 N

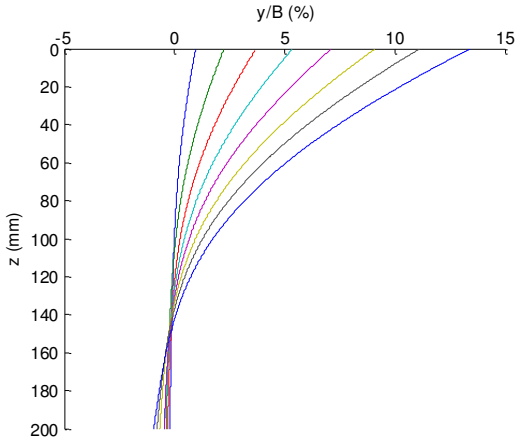

Figure A1-114 : lateral displacement vs depth

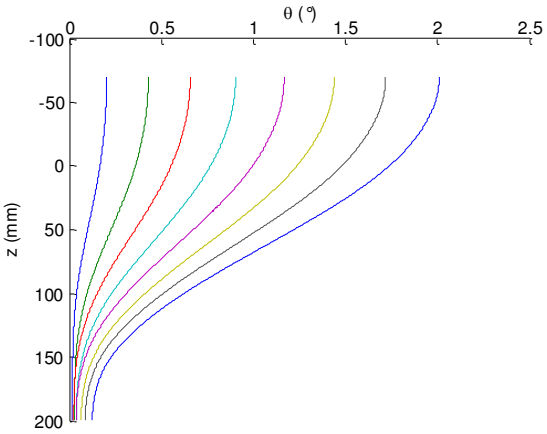

Figure A1-115 : rotation vs depth

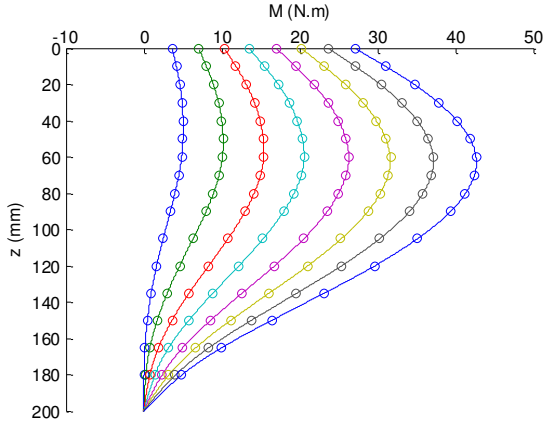

Figure A1-116 : moment vs depth

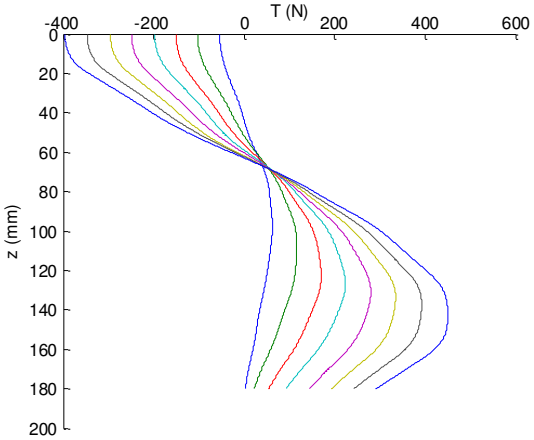

Figure A1-117 : shear force vs depth

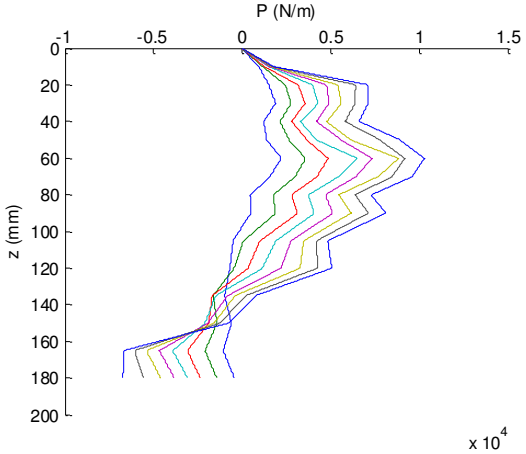

Figure A1-118 : Soil reaction vs depth

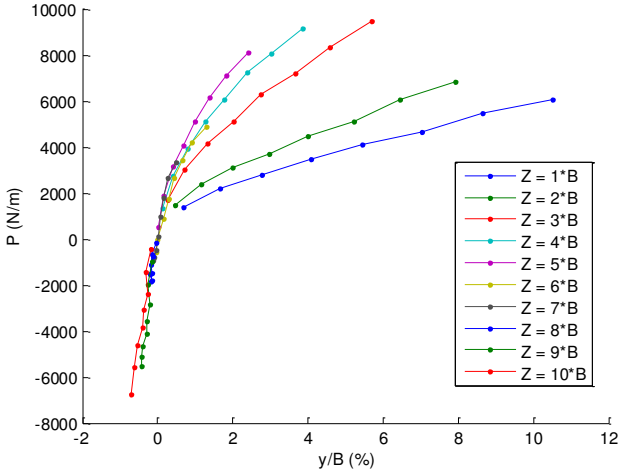

Figure A1-119 : monotonic p-y curves

Test : C12P1FH1G (Cyclic loading)

The figures represent the cycles 1, 10, 100, 1000

Loading line complete and unloading hatched line

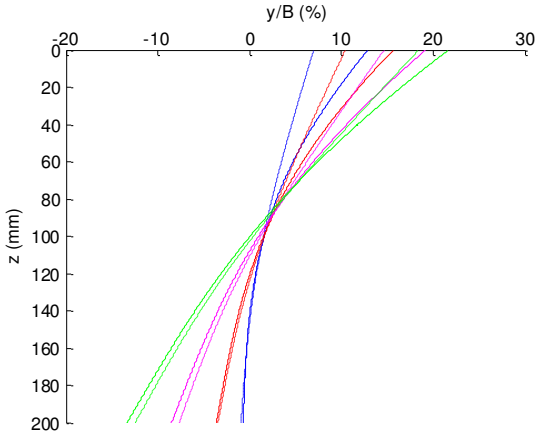

Figure A1-120 : lateral displacement vs depth

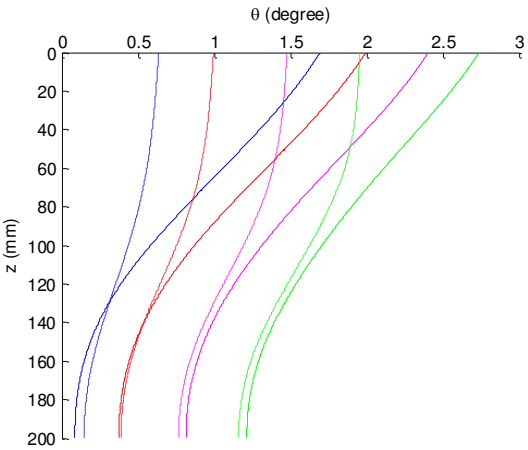

Figure A1-121 : rotation vs depth

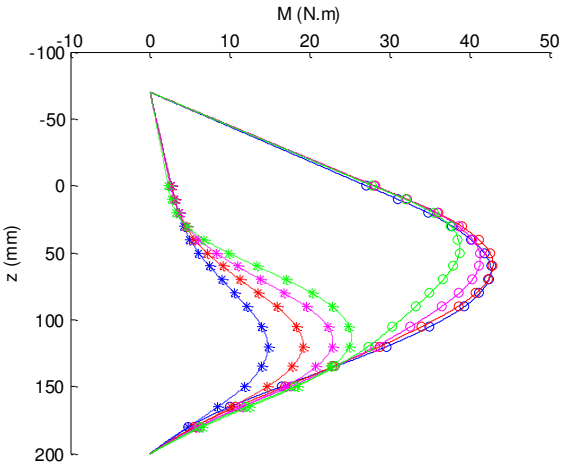

Figure A1-122 : moment vs depth

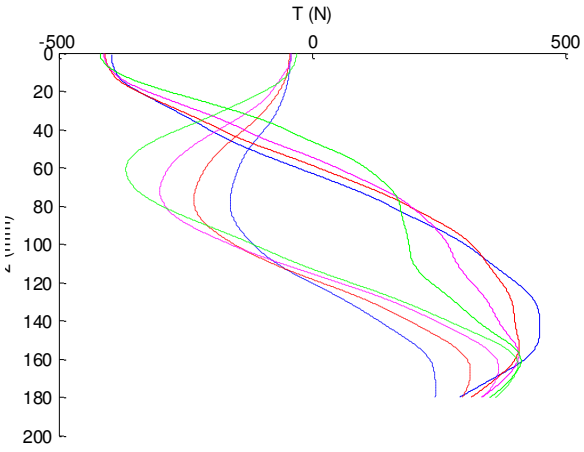

Figure A1-123 : shear force vs depth

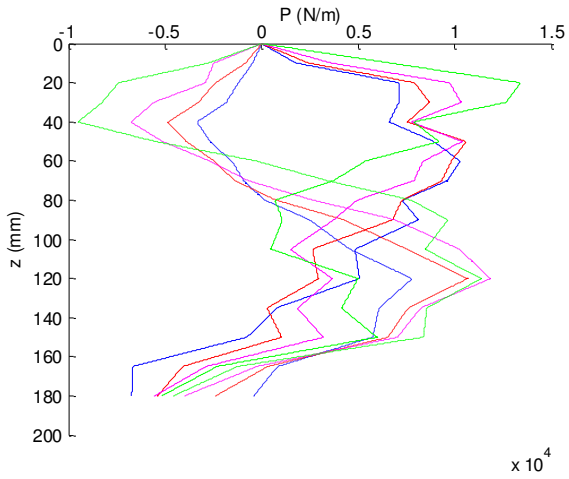

Figure A1-124 : Soil reaction vs depth

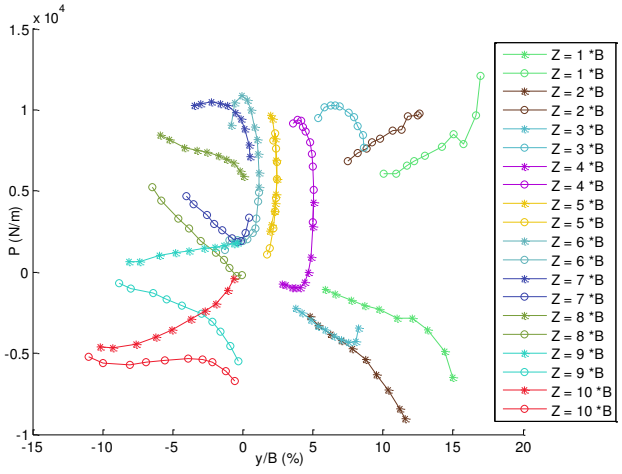

Figure A1-125 : cyclic p-y curves

Model pile : instrumented pile

Test : C12P2FH100G (Monotonic loading)

The figures represent the increase of the lateral loading with step of 50 N

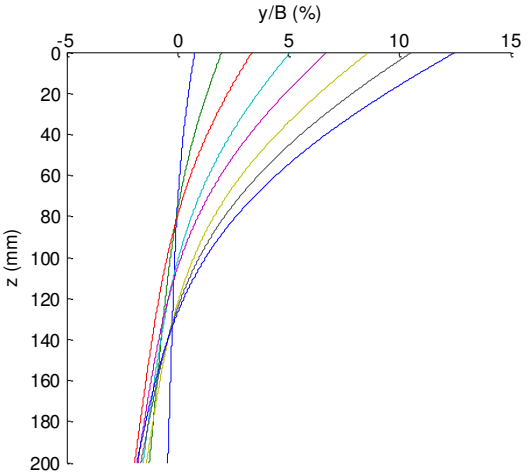

Figure A1-126 : lateral displacement vs depth

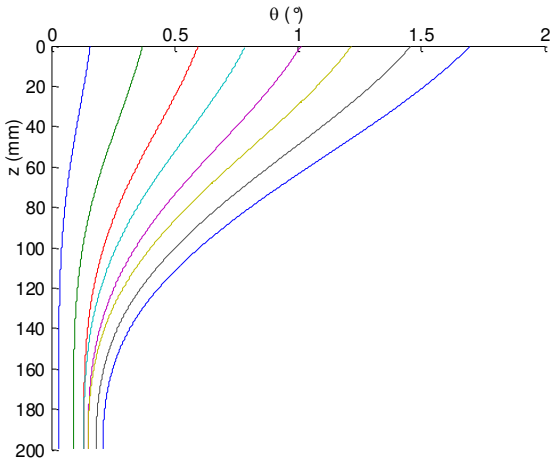

Figure A1-127 : rotation vs depth

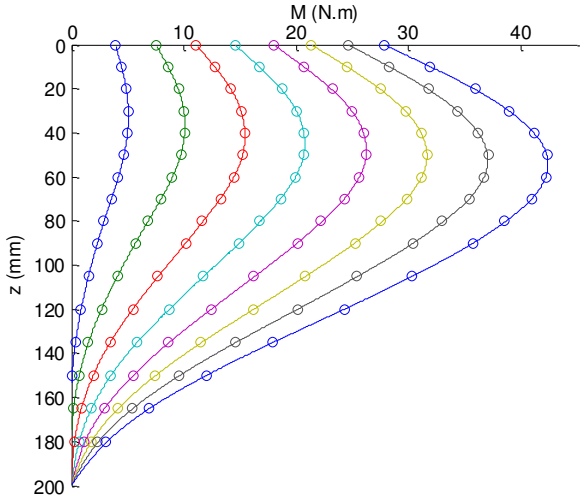

Figure A1-128 : moment vs depth

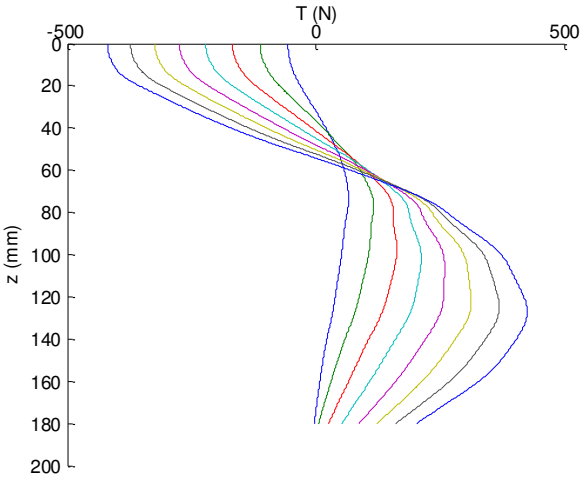

Figure A1-129 : shear force vs depth

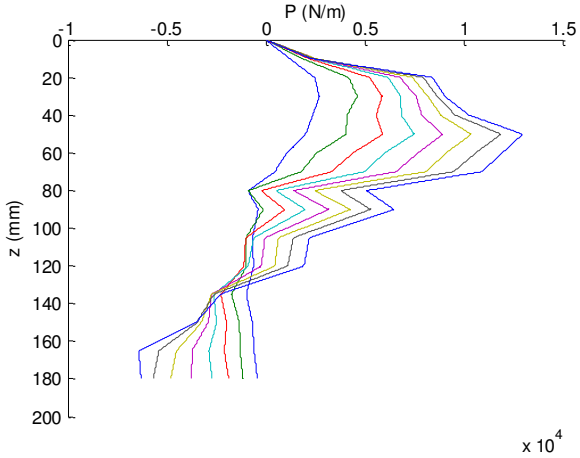

Figure A1-130 : Soil reaction vs depth

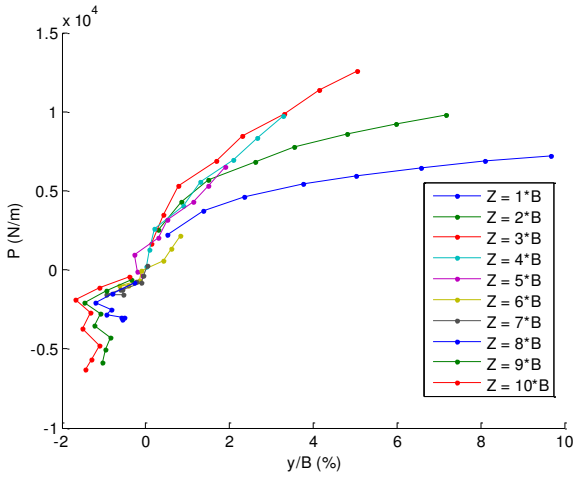

Figure A1-131 : monotonic p-y curves

Test : C12P2FH100G (Cyclic loading)

The figures represent the cycles 1, 10, 100, 1000

Loading line complete and unloading hatched line

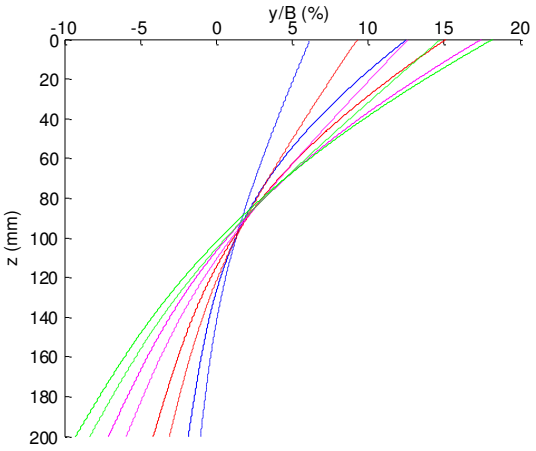

Figure A1-132 : lateral displacement vs depth

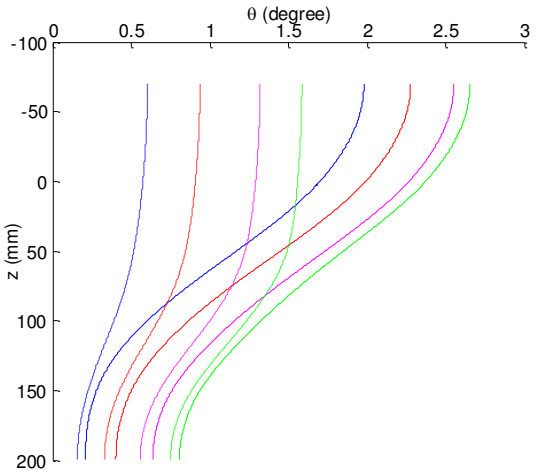

Figure A1-133 : rotation vs depth

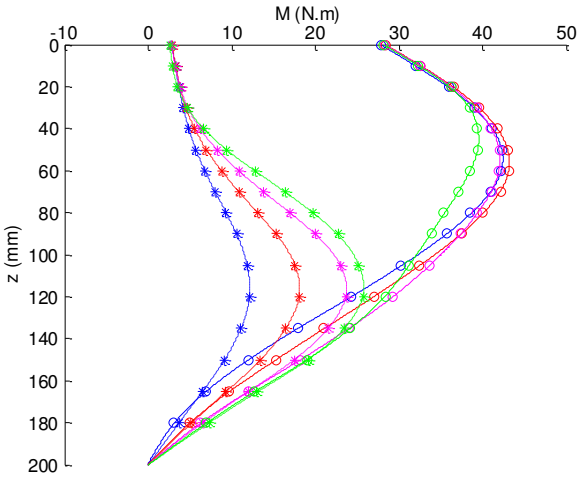

Figure A1-134 : moment vs depth

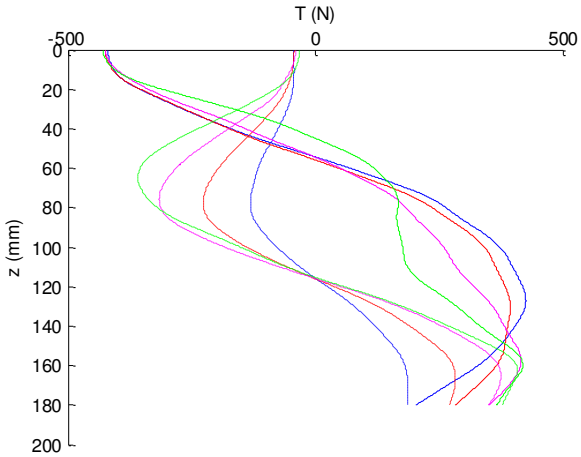

Figure A1-135 : shear force vs depth

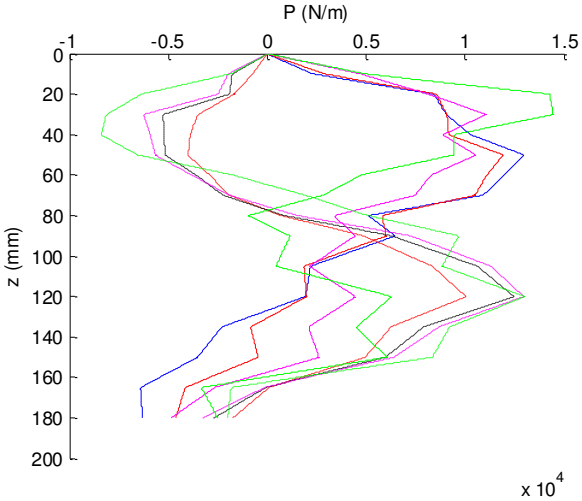

Figure A1-136 : Soil reaction vs depth

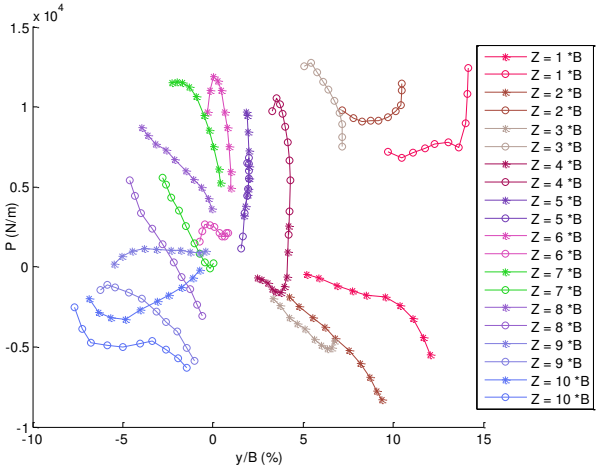

Figure A1-137 : cyclic p-y curves

Model pile : instrumented pile

Test : C12P3FL1G (Monotonic loading)

The figures represent the increase of the lateral loading with step of 50 N

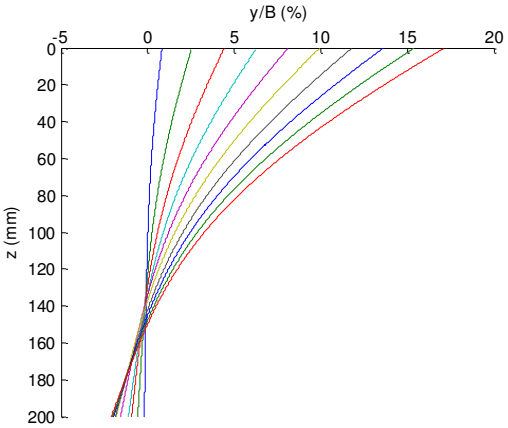

Figure A1-138 : lateral displacement vs depth

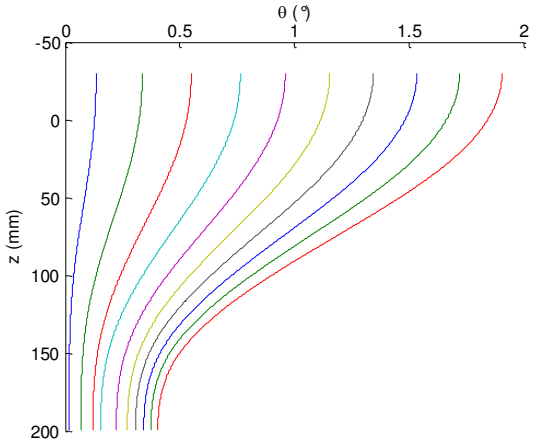

Figure A1-139 : rotation vs depth

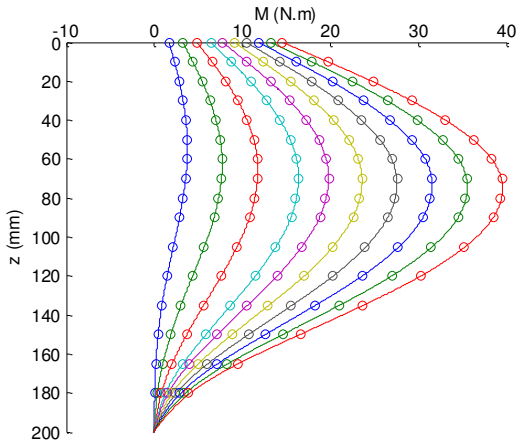

Figure A1-140 : moment vs depth

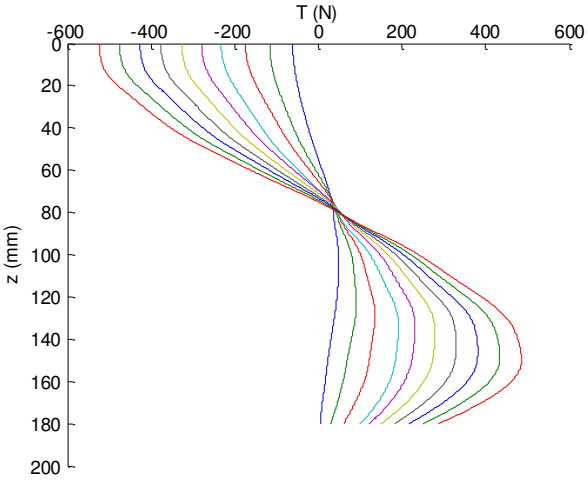

Figure A1-141 : shear force vs depth

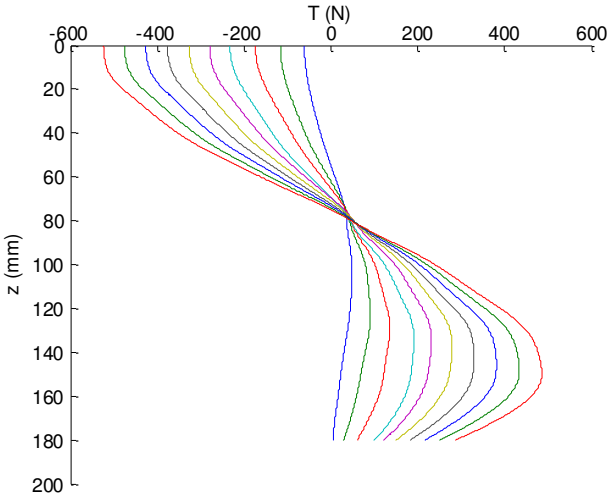

Figure A1-142 : Soil reaction vs depth

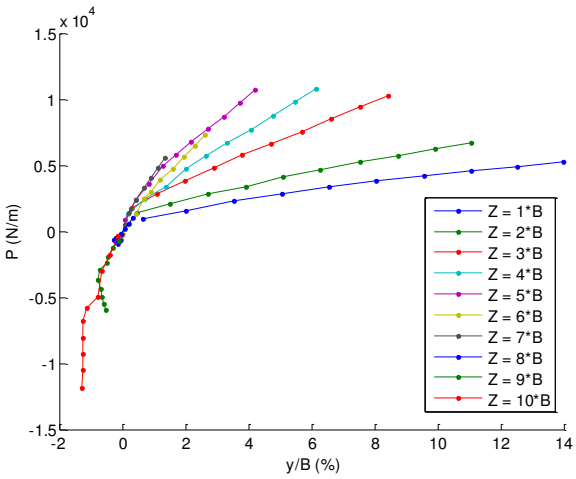

Figure A1-143 : monotonic p-y curves

Test : C12P3FL1G (Cyclic loading)

The figures represent the cycles 1, 10, 100, 1000

Loading line complete and unloading hatched line

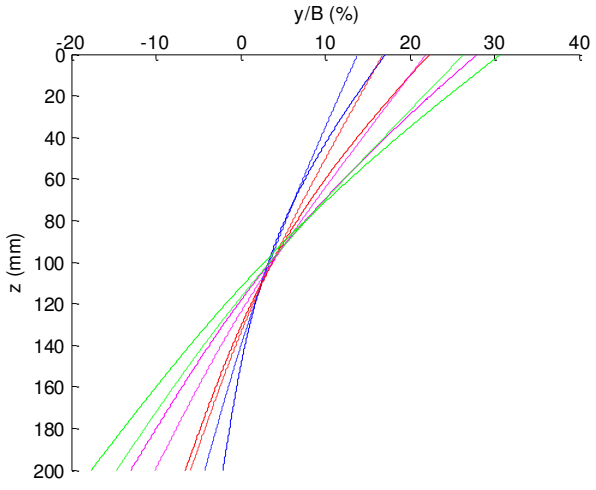

Figure A1-144 : lateral displacement vs depth

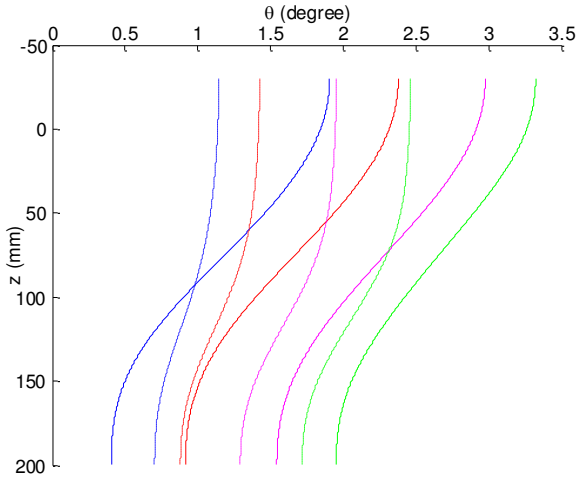

Figure A1-145 : rotation vs depth

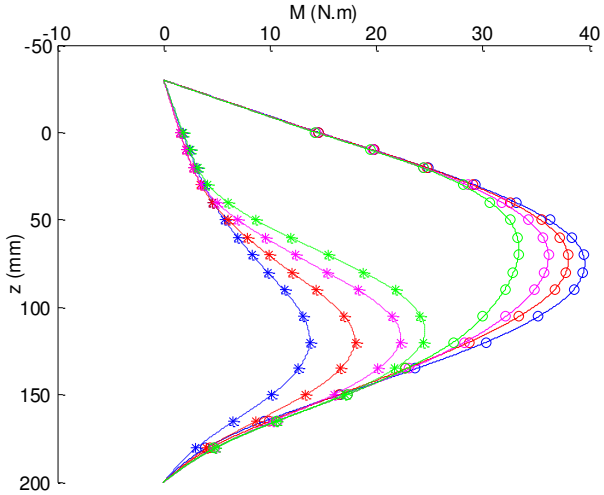

Figure A1-146 : moment vs depth

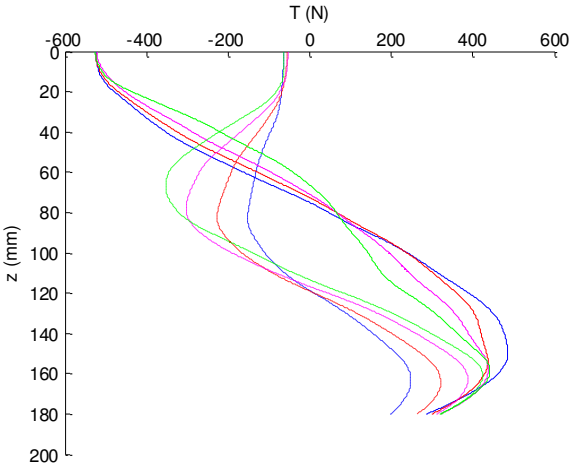

Figure A1-147 : shear force vs depth

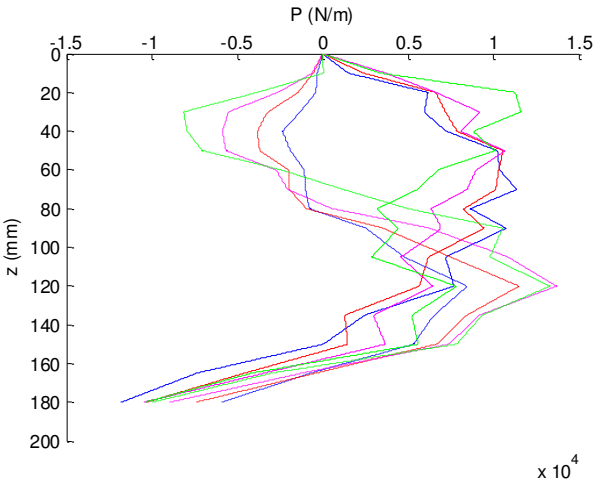

Figure A1-148 : Soil reaction vs depth

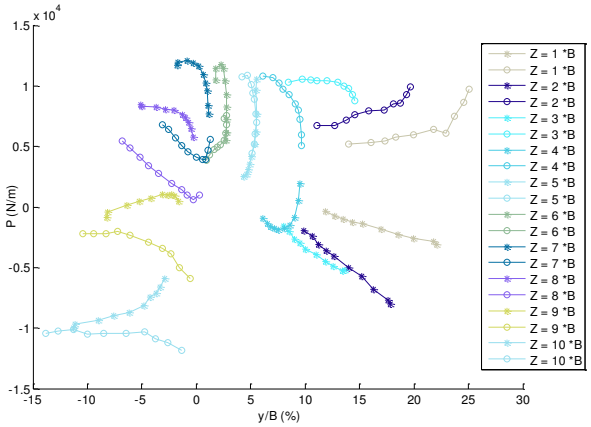

Figure A1-149 : cyclic p-y curves

Model pile : instrumented pile

Test : C12P4FL100G (Monotonic loading)

The figures represent the increase of the lateral loading with step of 50 N

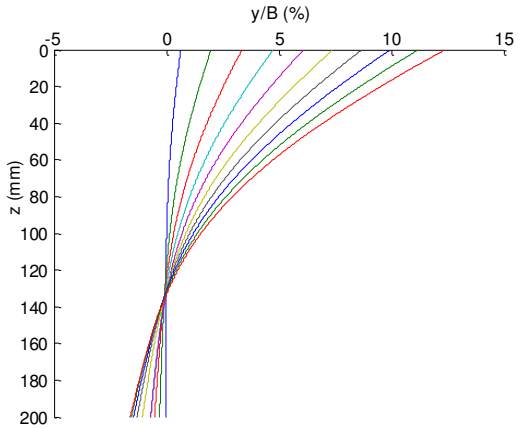

Figure A1-150 : lateral displacement vs depth

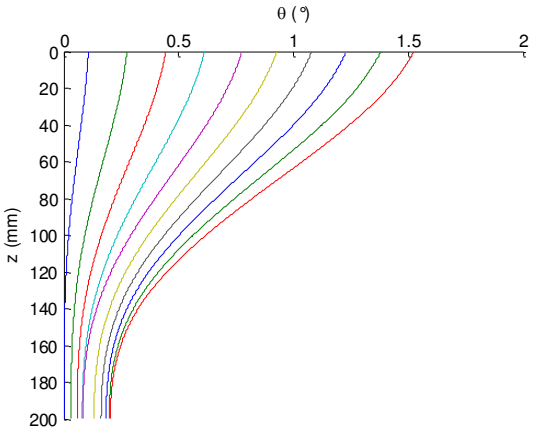

Figure A1-151 : rotation vs depth

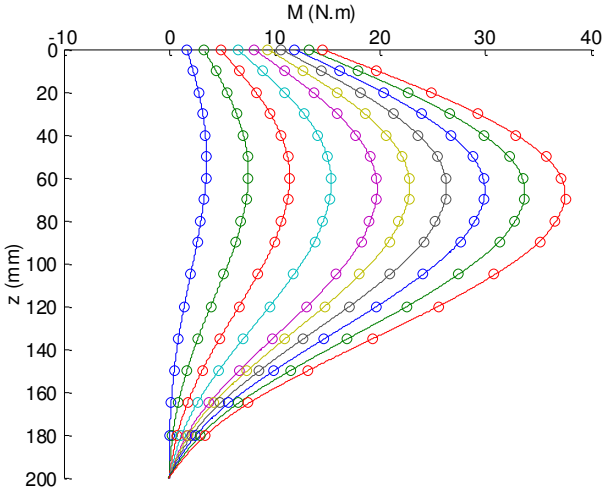

Figure A1-152 : moment vs depth

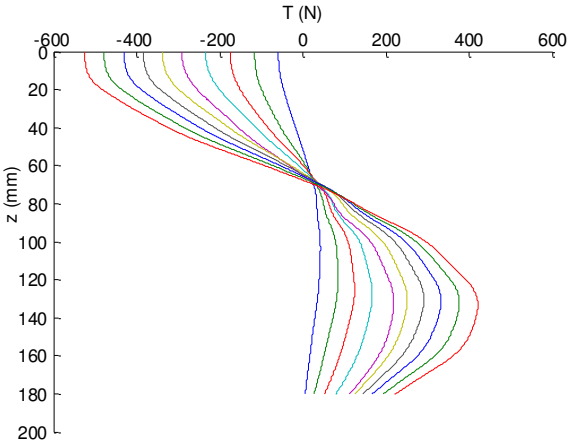

Figure A1-153 : shear force vs depth

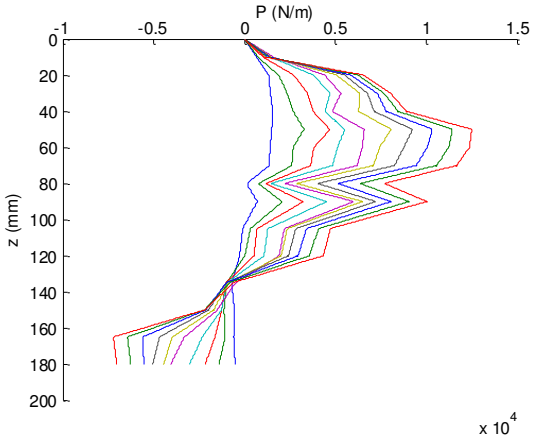

Figure A1-154 : Soil reaction vs depth

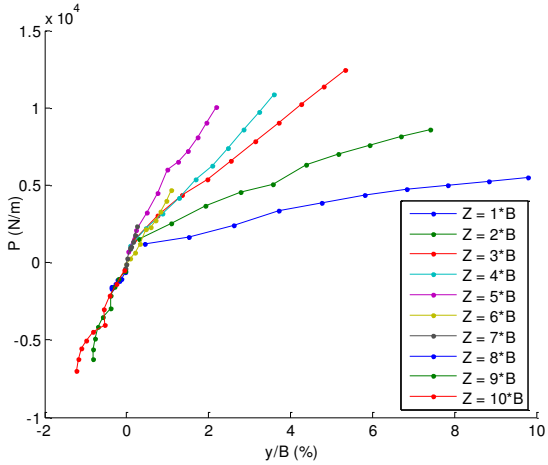

Figure A1-155 : monotonic p-y curves

Test : C12P4FL100G (Cyclic loading)

The figures represent the cycles 1, 10, 100, 1000

Loading line complete and unloading hatched line

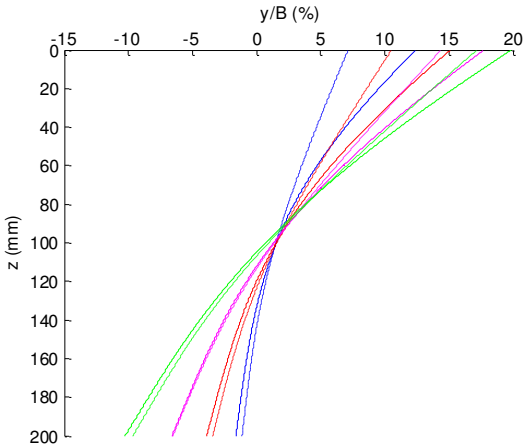

Figure A1-156 : lateral displacement vs depth

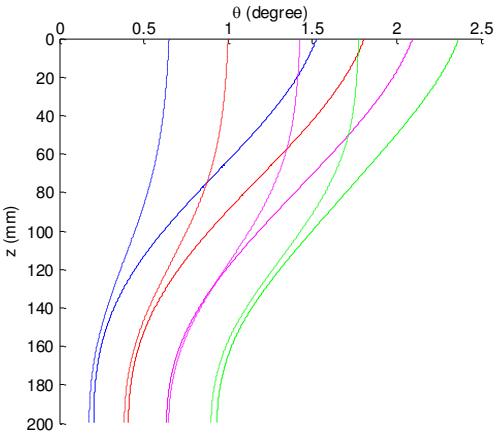

Figure A1-157 : rotation vs depth

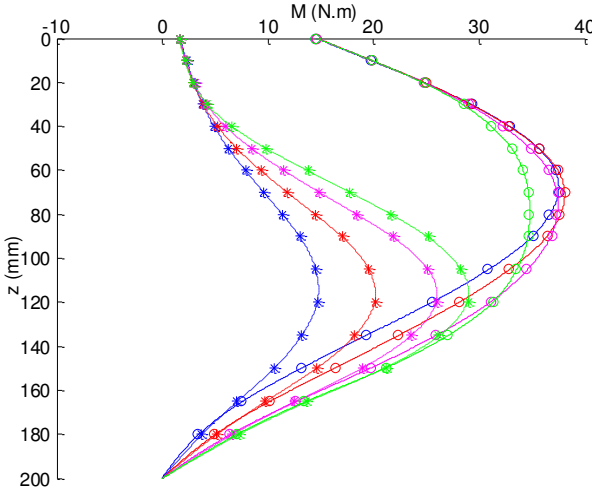

Figure A1-158 : moment vs depth

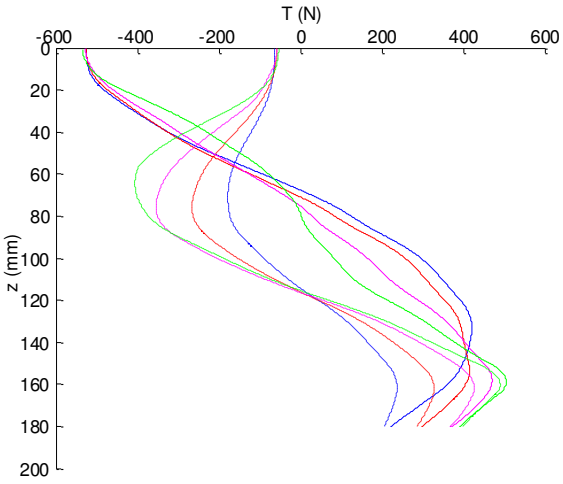

Figure A1-159 : shear force vs depth

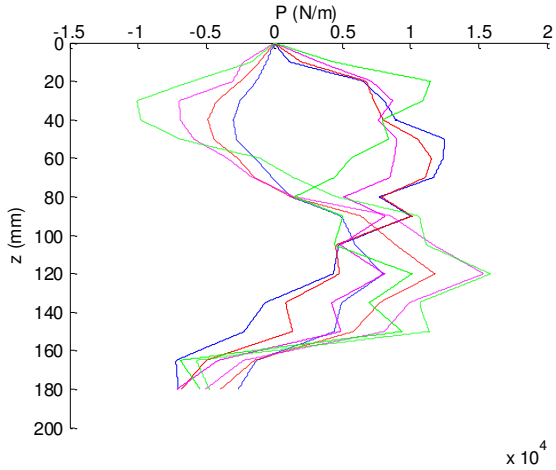

Figure A1-160 : Soil reaction vs depth

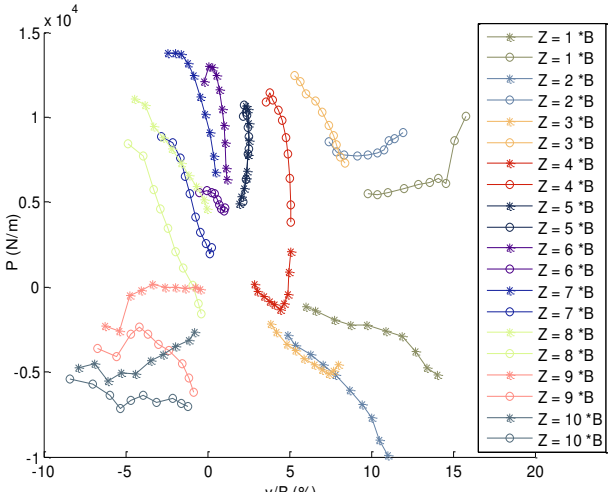

Figure A1-161 : cyclic p-y curves

Model pile : instrumented pile

Test : C12P5FL1G (Monotonic loading)

The figures represent the increase of the lateral loading with step of 50 N

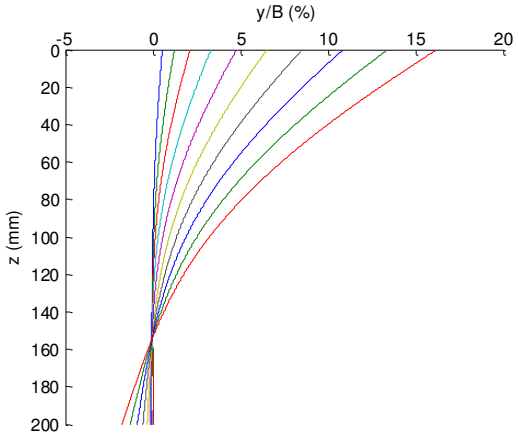

Figure A1-162 : lateral displacement vs depth

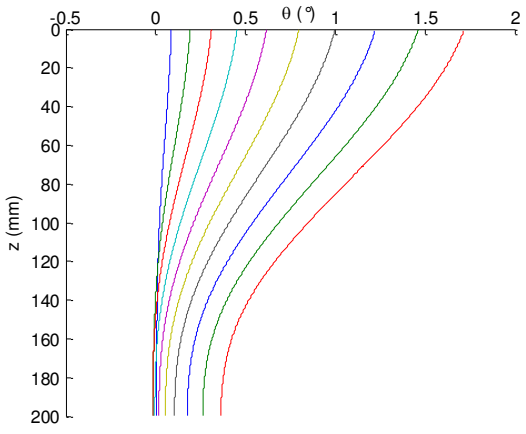

Figure A1-163 : rotation vs depth

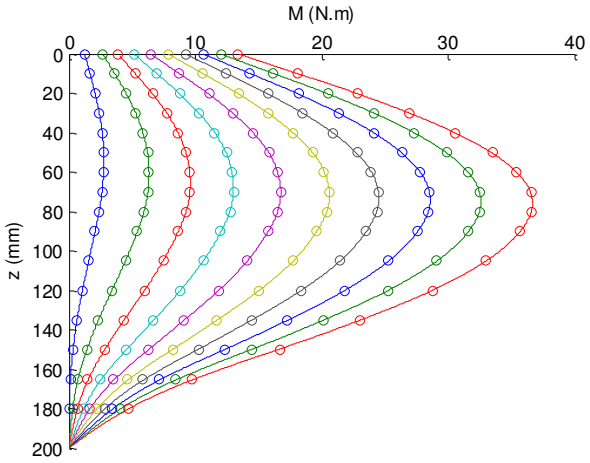

Figure A1-164 : moment vs depth

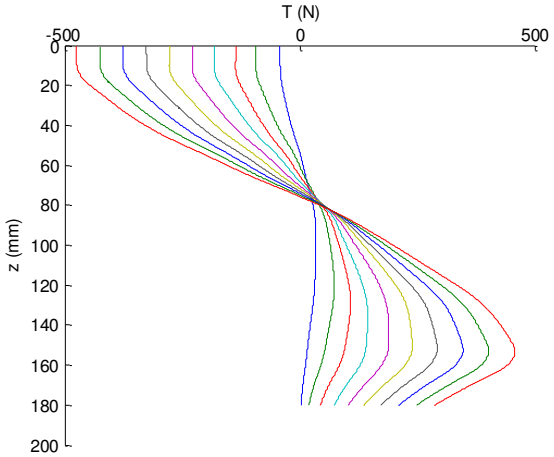

Figure A1-165 : shear force vs depth

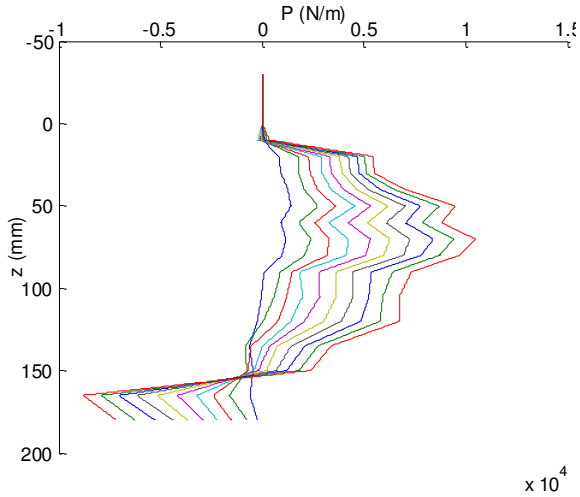

Figure A1-166 : Soil reaction vs depth

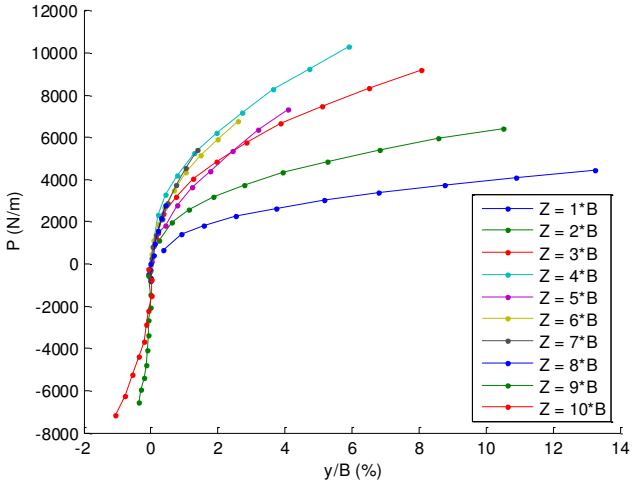

Figure A1-167 : monotonic p-y curves

Strongbox C13 D_r = 99% (Saturated)

Model pile : instrumented pile

Test : C13P1FL1G (Monotonic loading)

The figures represent the increase of the lateral loading with step of 50 N

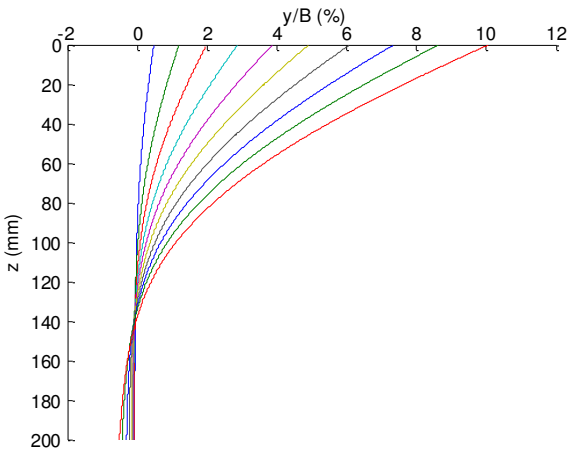

Figure A1-168 : lateral displacement vs depth

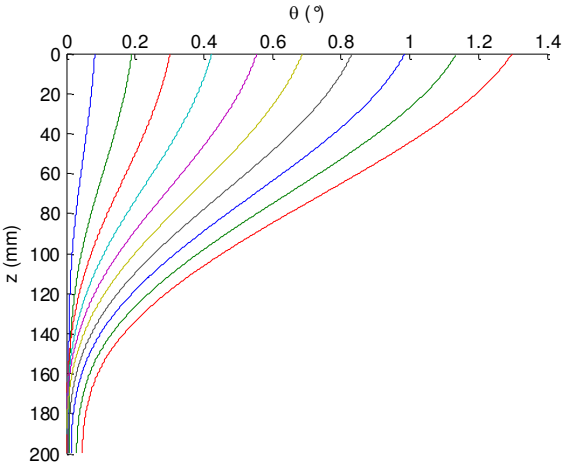

Figure A1-169: rotation vs depth

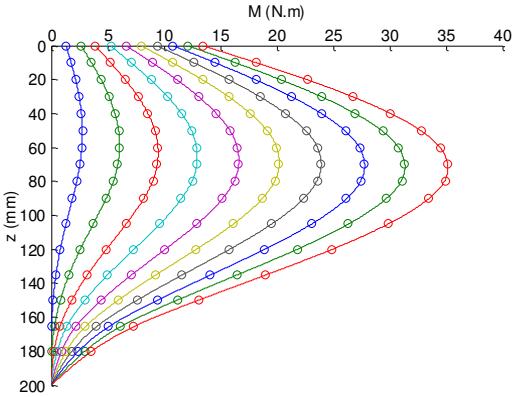

Figure A1-170 : moment vs depth

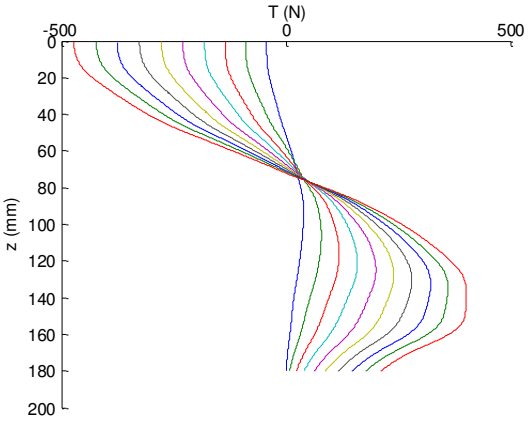

Figure A1-171 : shear force vs depth

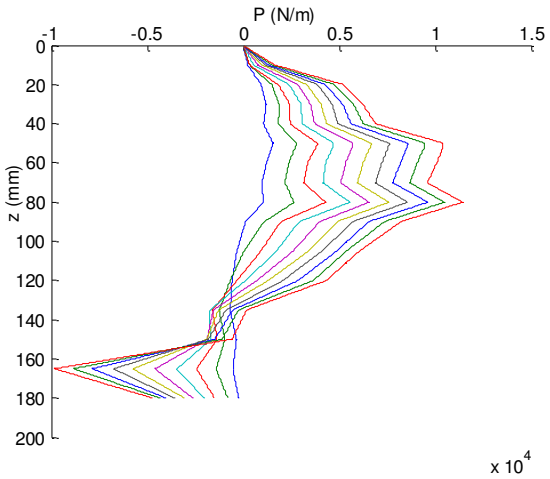

Figure A1-172 : Soil reaction vs depth

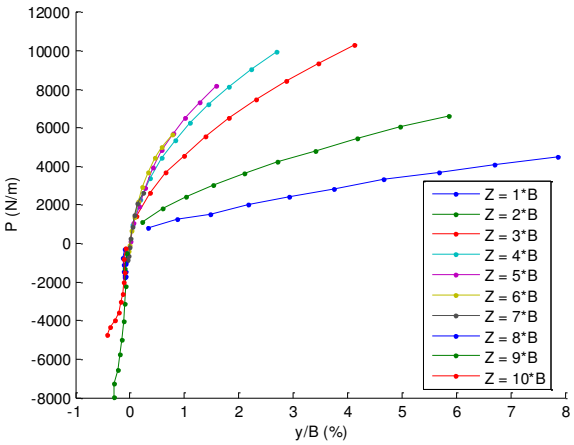

Figure A1-173 : monotonic p-y curves

Test : C13P1FL1G (Cyclic loading)

The figures represent the cycles 1, 10, 100, 1000

Loading line complete and unloading hatched line

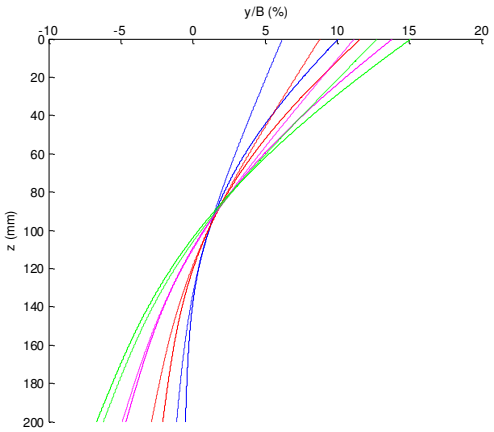

Figure A1-174 : lateral displacement vs depth

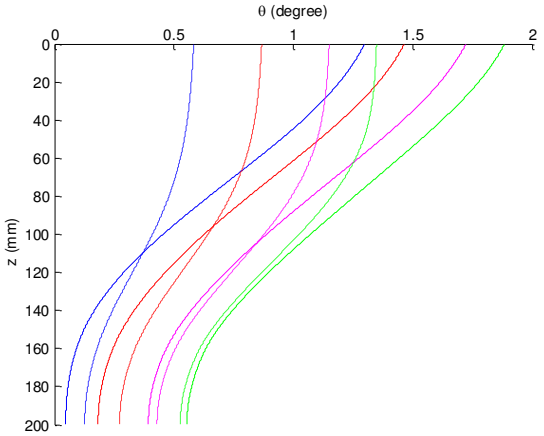

Figure A1-175: rotation vs depth

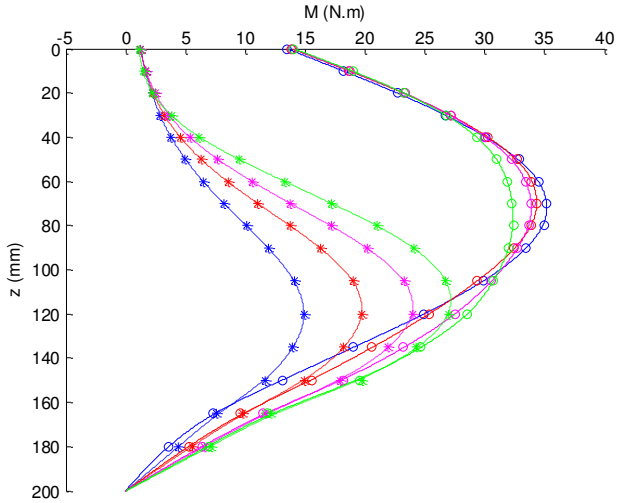

Figure A1-176: moment vs depth

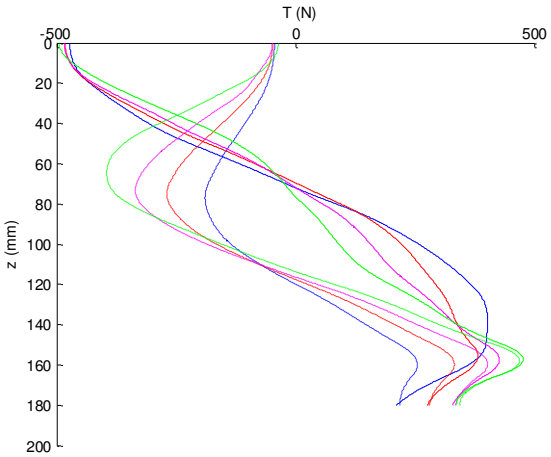

Figure A1-177: shear force vs depth

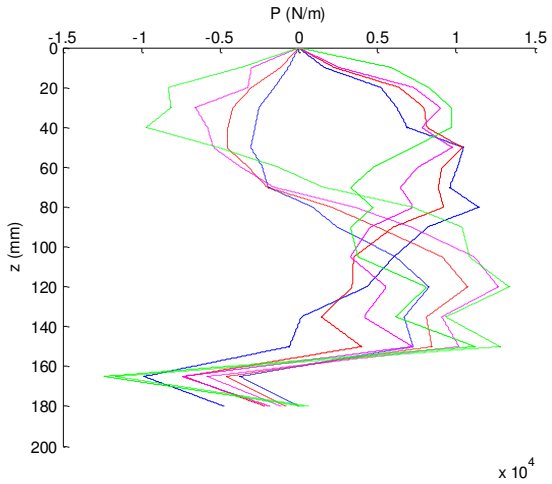

Figure A1-178 : Soil reaction vs depth

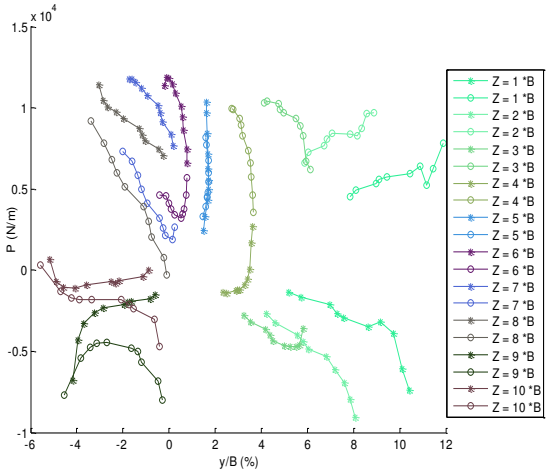

Figure A1-179 : cyclic p-y curves

Model pile : instrumented pile

Test : C13P2FL100G (Monotonic loading)

The figures represent the increase of the lateral loading with step of 50 N

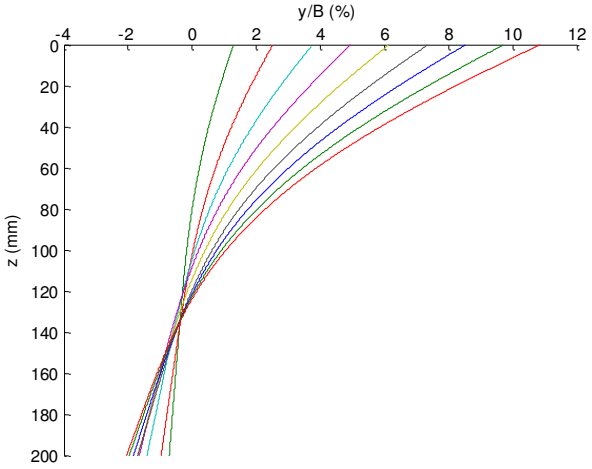

Figure A1-180 : lateral displacement vs depth

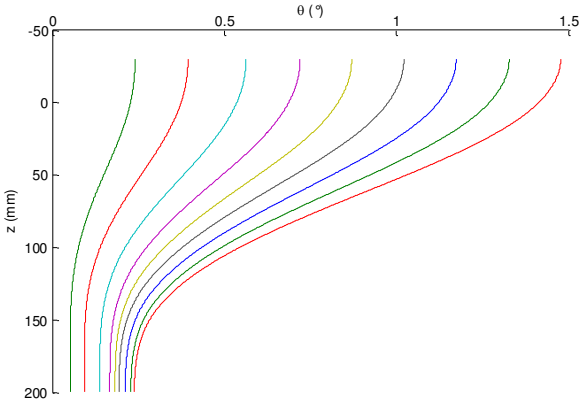

Figure A1-181: rotation vs depth

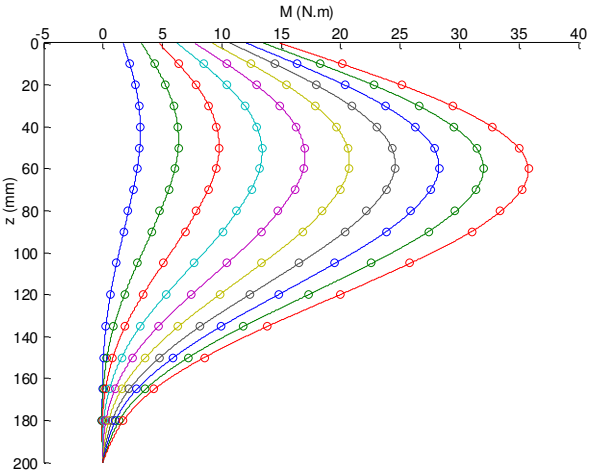

Figure A1-182: moment vs depth

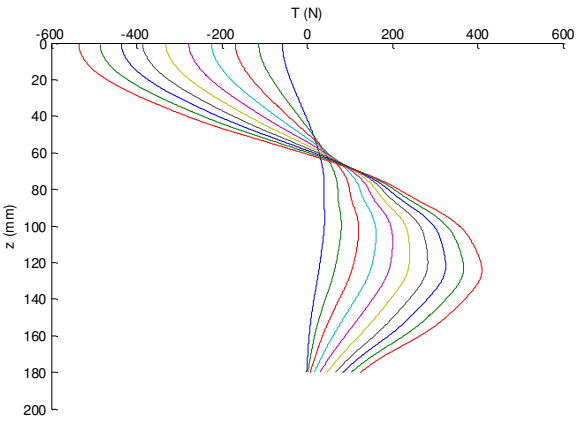

Figure A1-183 : shear force vs depth

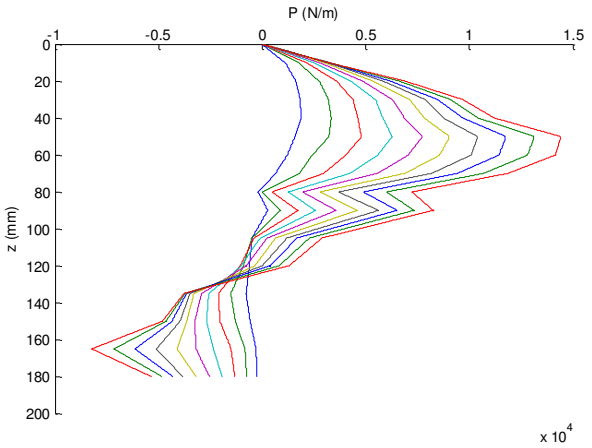

Figure A1-184 : Soil reaction vs depth

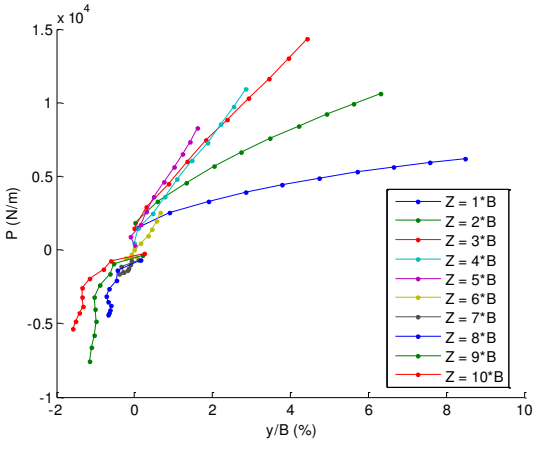

Figure A1-185: monotonic p-y curves

Model pile : instrumented pile

Test : C13P3FH1G (Monotonic loading)

The figures represent the increase of the lateral loading with step of 50 N

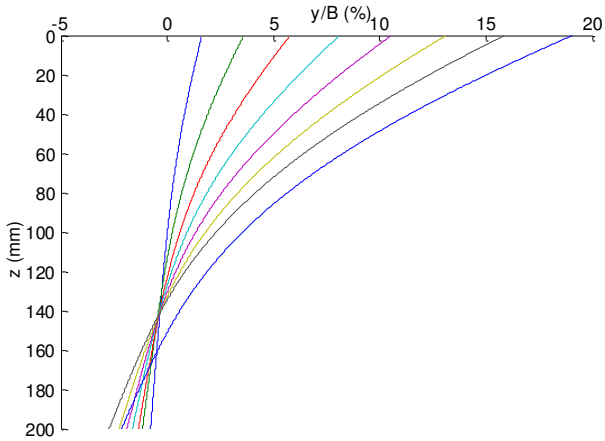

Figure A1-186 : lateral displacement vs depth

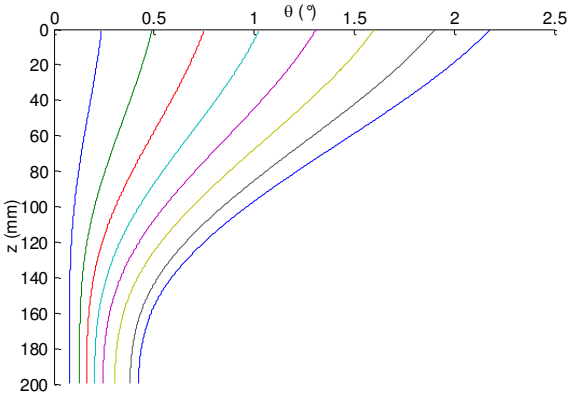

Figure A1-187: rotation vs depth

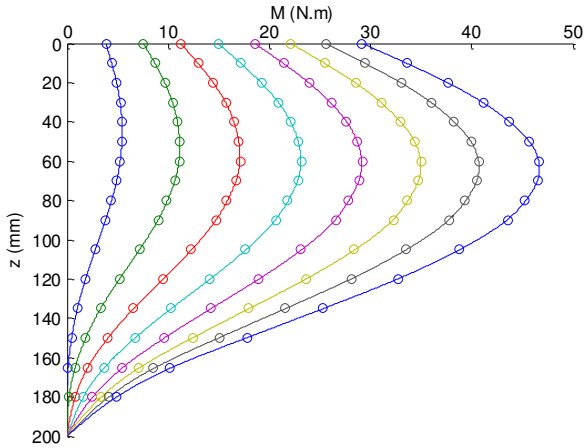

Figure A1-188: moment vs depth

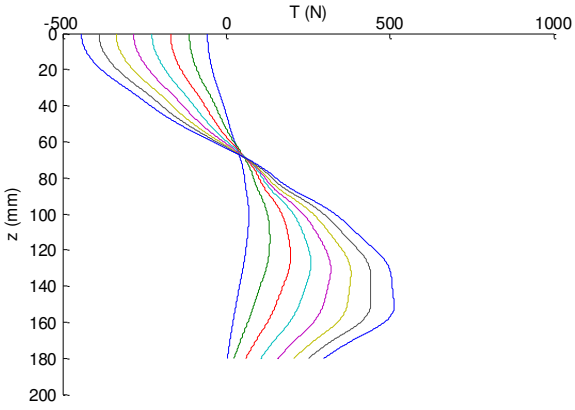

Figure A1-189 : shear force vs depth

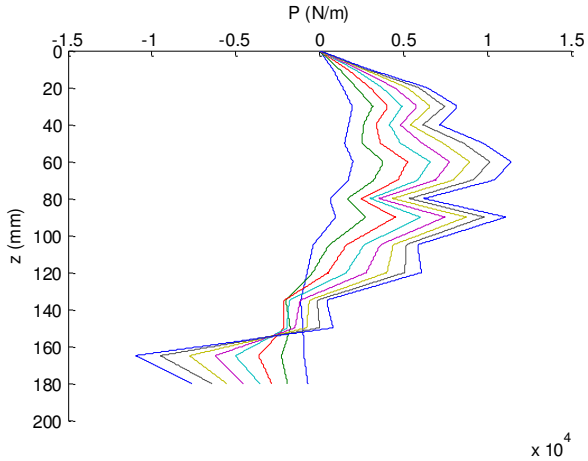

Figure A1-190: Soil reaction vs depth

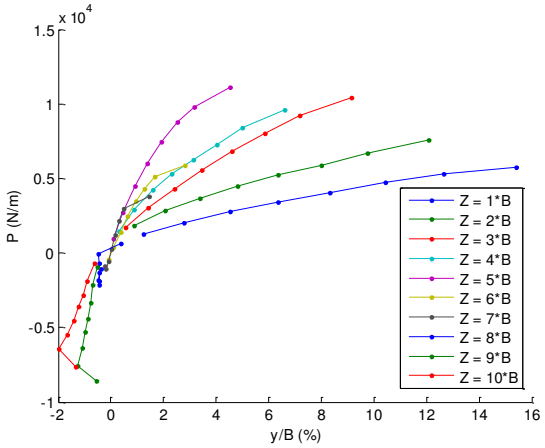

Figure A1-191: monotonic p-y curves

Test : C13P3FH1G (Cyclic loading)

The figures represent the cycles 1, 10, 100, 1000

Loading line complete and unloading hatched line

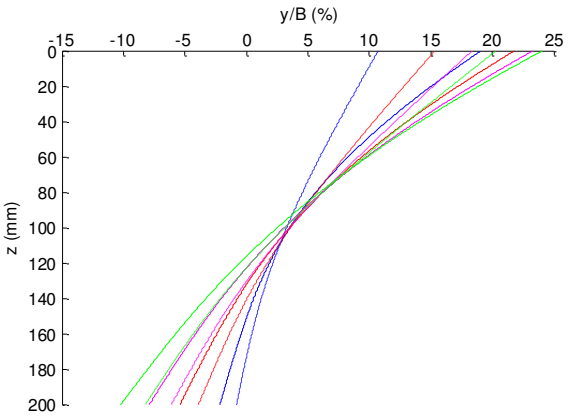

Figure A1-192 : lateral displacement vs depth

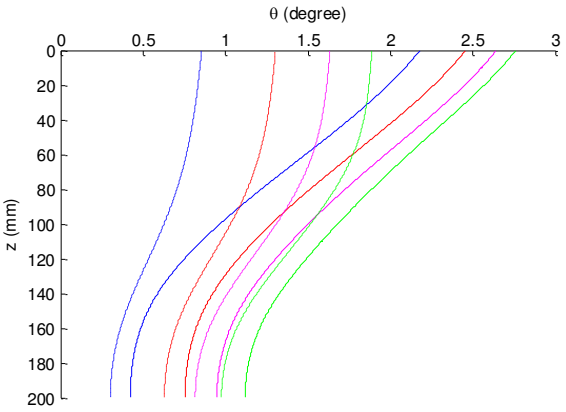

Figure A1-193: rotation vs depth

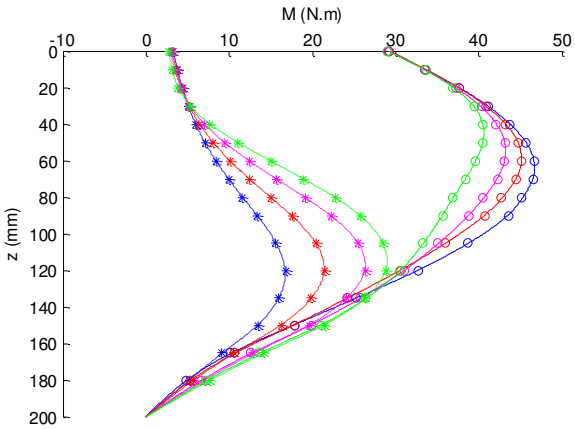

Figure A1-194: moment vs depth

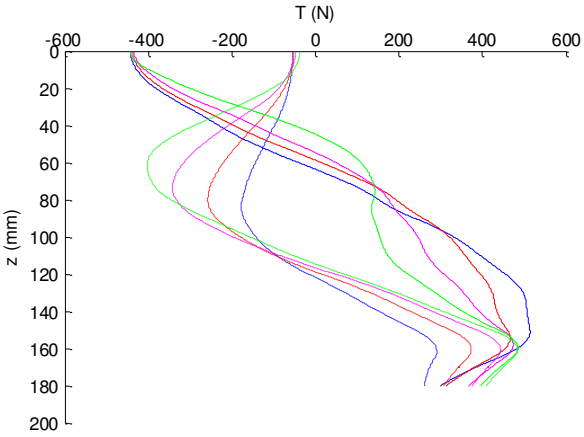

Figure A1-195: shear force vs depth

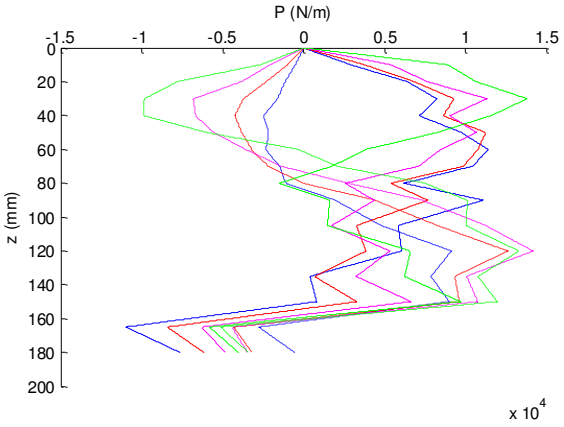

Figure A1-196 Soil reaction vs depth

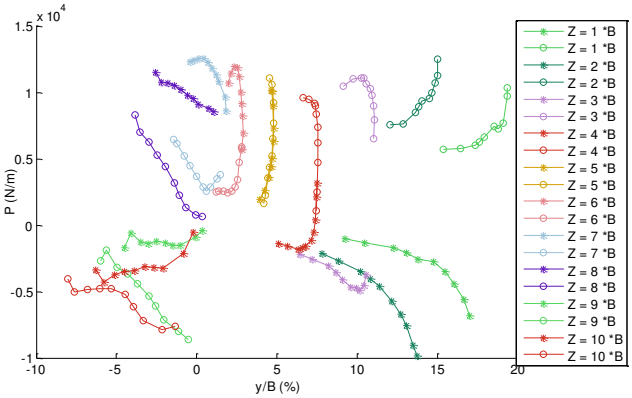

Figure A1-197: cyclic p-y curves

Model pile : instrumented pile

Test : C13P4FH100G (Monotonic loading)

The figures represent the increase of the lateral loading with step of 50 N

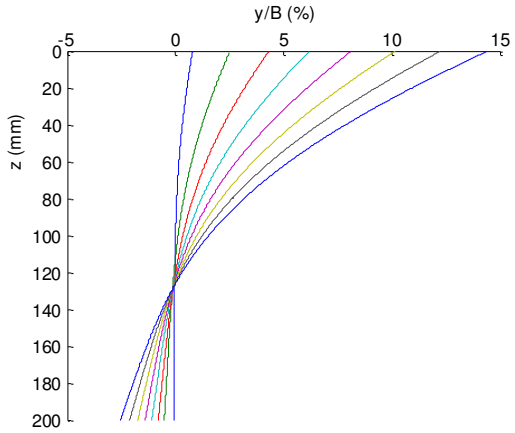

Figure A1-198 : lateral displacement vs depth

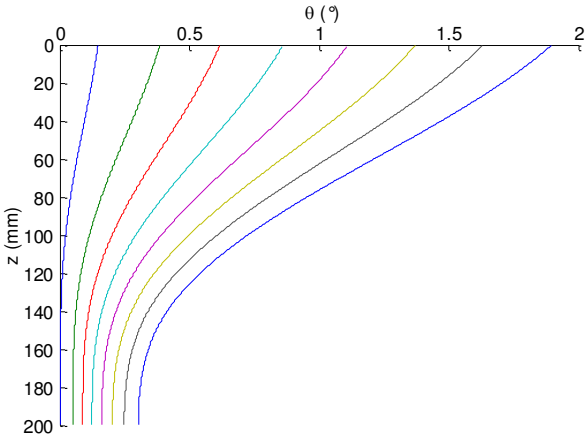

Figure A1-199: rotation vs depth

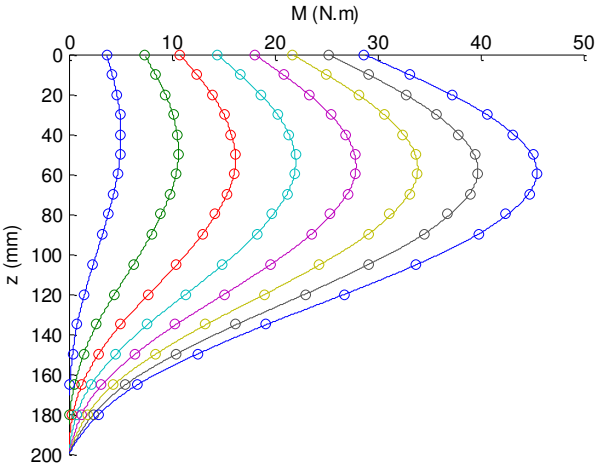

Figure A1-200: moment vs depth

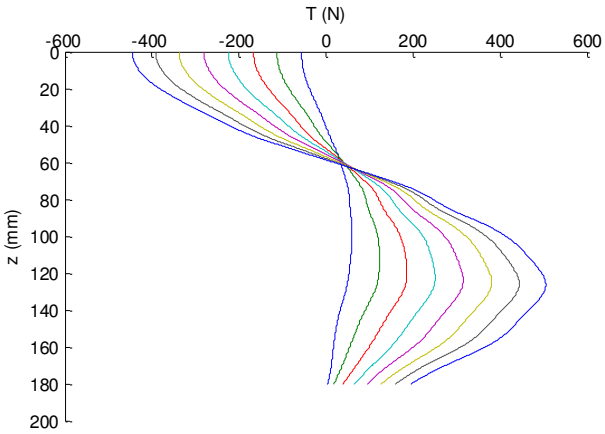

Figure A1-201: shear force vs depth

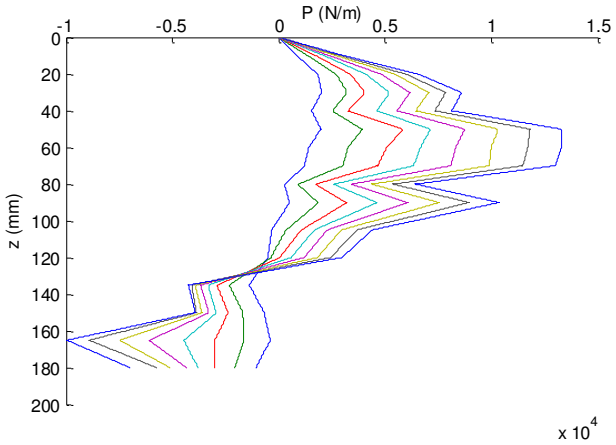

Figure A1-202: Soil reaction vs depth

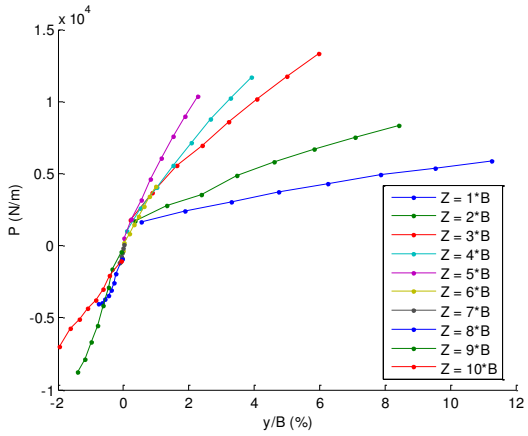

Figure A1-203: monotonic p-y curves

Test : C13P4FH100G (Cyclic loading)

The figures represent the cycles 1, 10, 100, 1000

Loading line complete and unloading hatched line

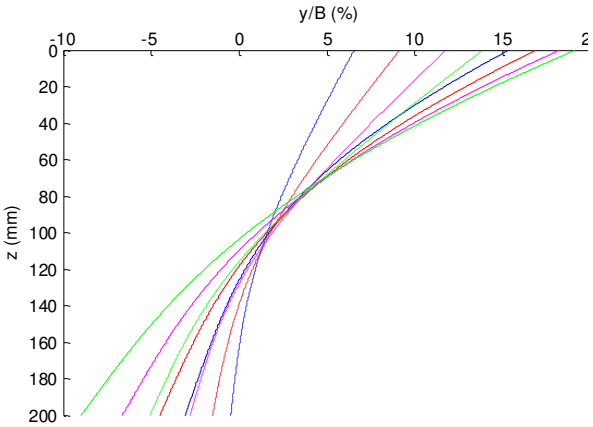

Figure A1-204 : lateral displacement vs depth

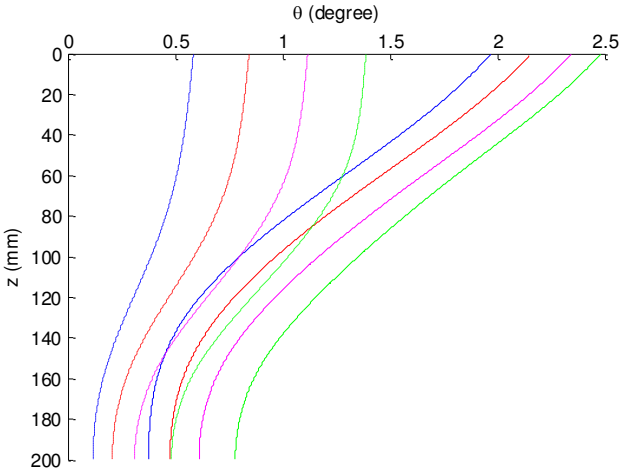

Figure A1-205 : rotation vs depth

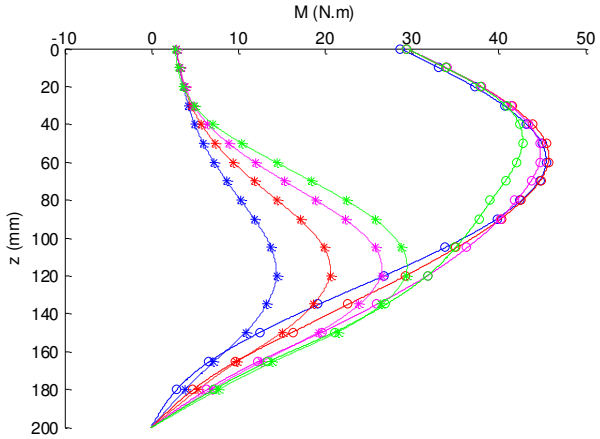

Figure A1-206: moment vs depth

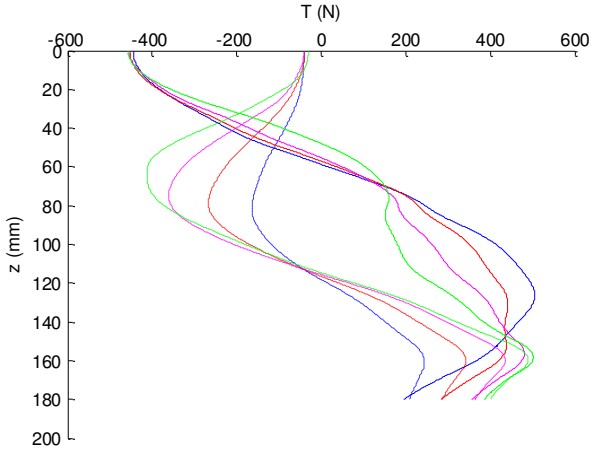

Figure A1-207: shear force vs depth

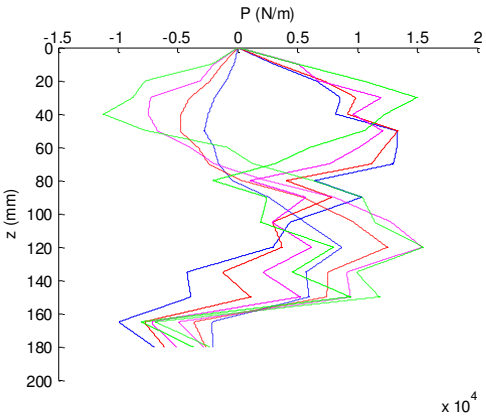

Figure A1-208: Soil reaction vs depth

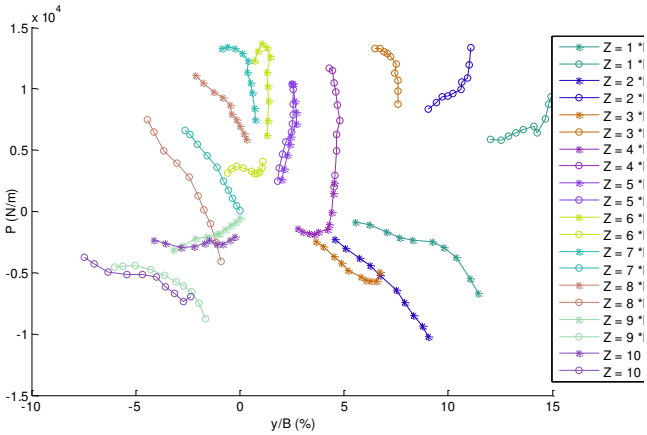

Figure A1-209: cyclic p-y curves

Model pile : instrumented pile

Test : C13P5FL1G (Monotonic loading)

The figures represent the increase of the lateral loading with step of 50 N

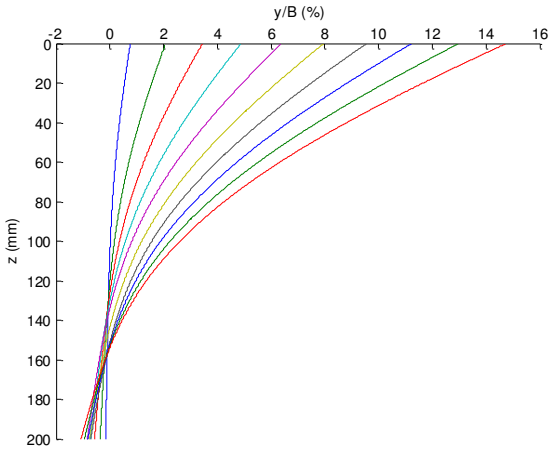

Figure A1-211 : lateral displacement vs depth

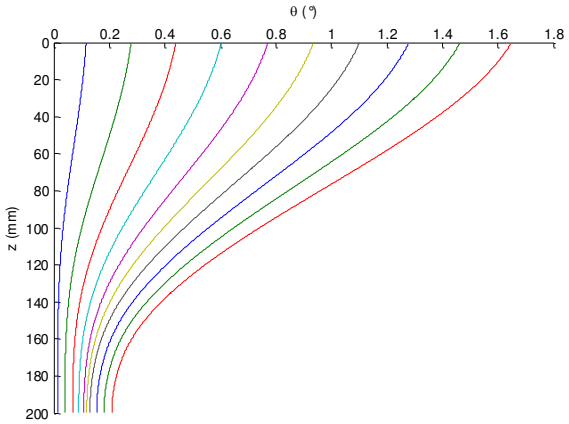

Figure A1-212: rotation vs depth

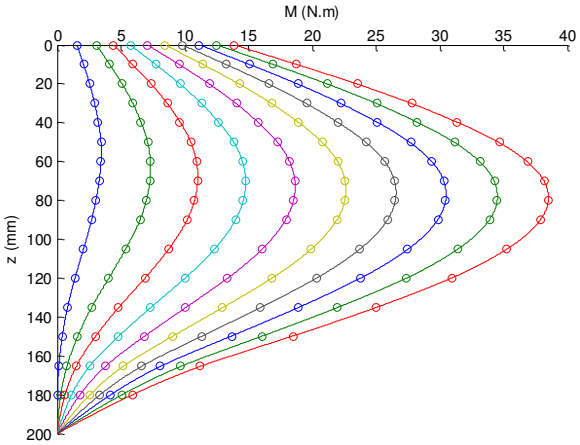

Figure A1- 213: moment vs depth

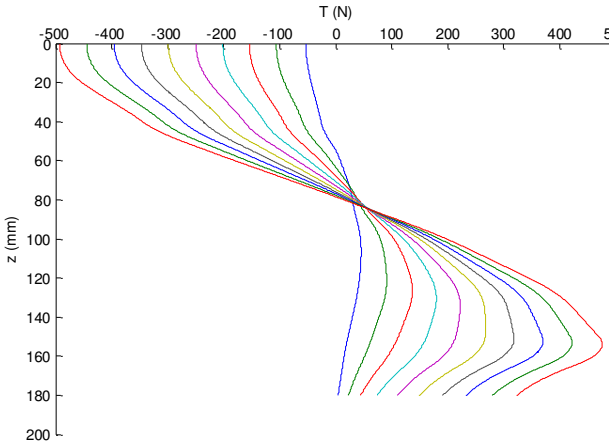

Figure A1-214: shear force vs depth

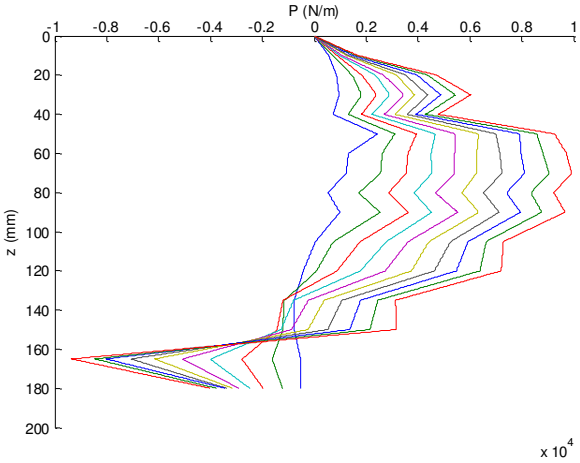

Figure A1-215: Soil reaction vs depth

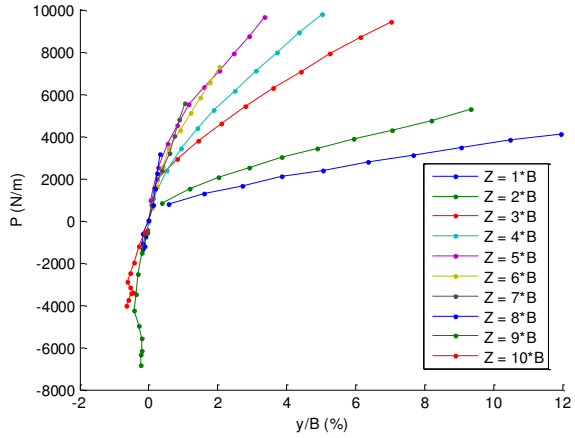

Figure A1-216: monotonic p-y curves

Test : C13P5FL1G (Cyclic loading)

The figures represent the cycles 1, 10, 100, 1000

Loading line complete and unloading hatched line

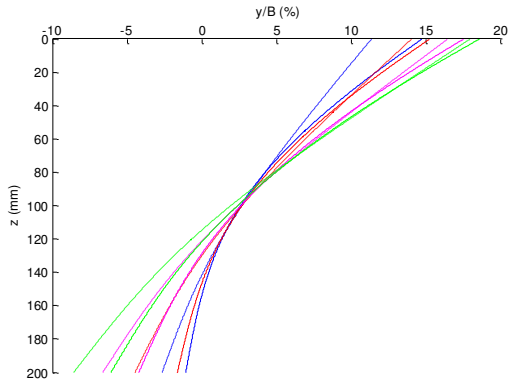

Figure A1-217 : lateral displacement vs depth

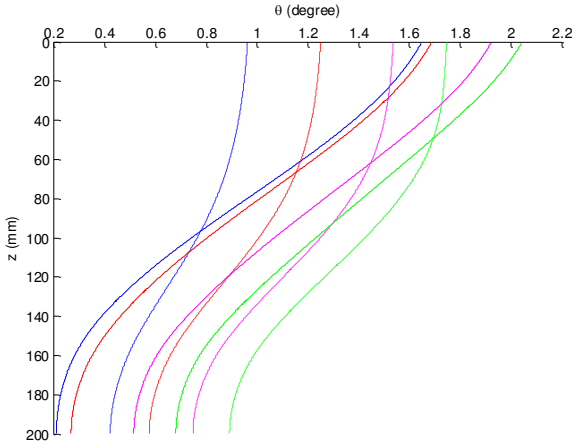

Figure A1-218: rotation vs depth

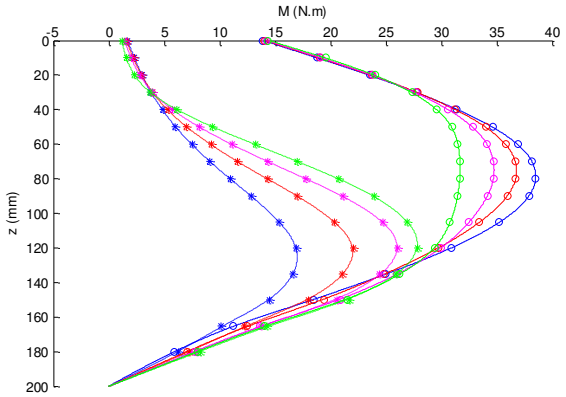

Figure A1-219: moment vs depth

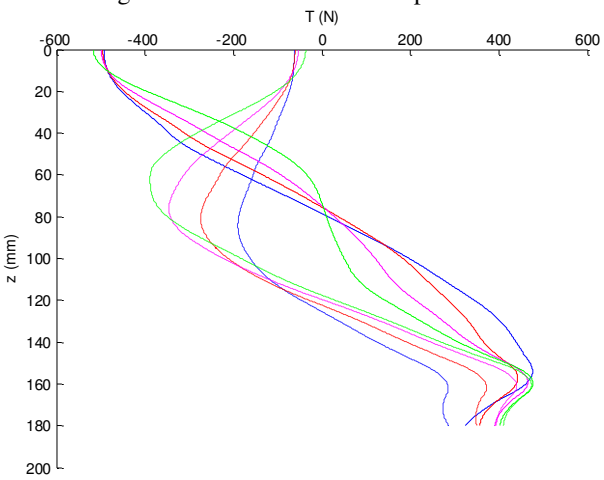

Figure A1-220: shear force vs depth

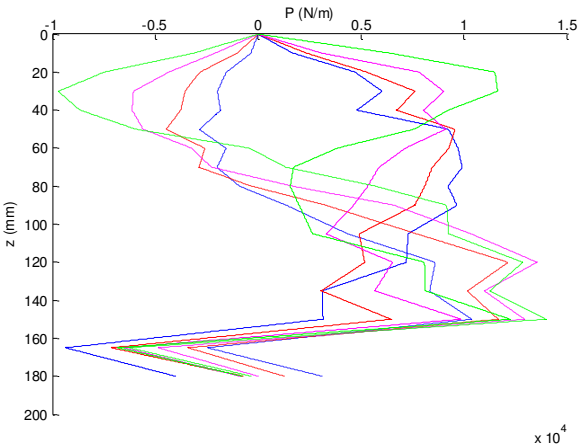

Figure A1-221: Soil reaction vs depth

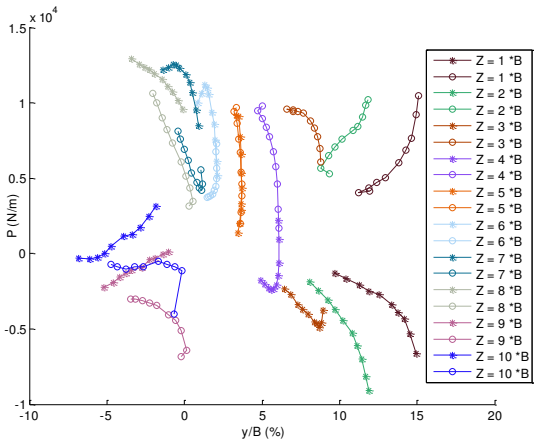

Figure A1-222: cyclic p-y curves

Model pile : instrumented pile

Test : C13P6FL1G (Monotonic loading)

The figures represent the increase of the lateral loading with step of 50 N

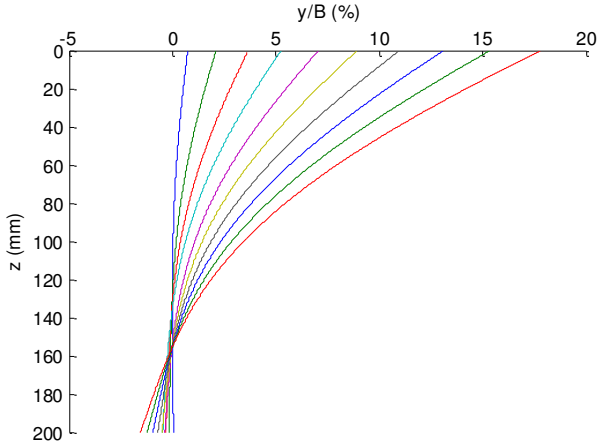

Figure A1-223 : lateral displacement vs depth

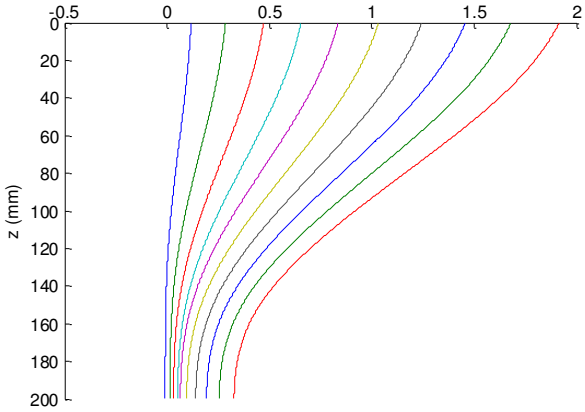

Figure A1-224: rotation vs depth

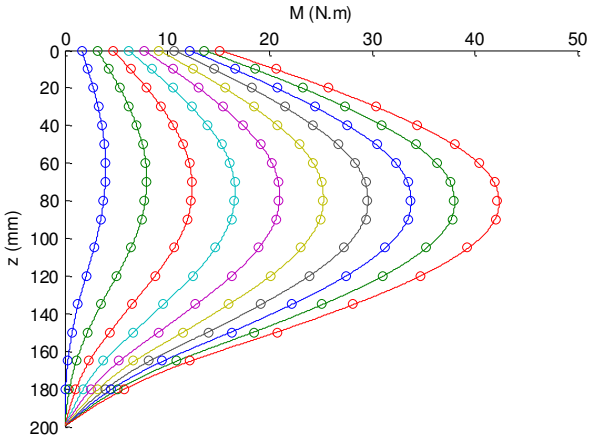

Figure A1-225: moment vs depth

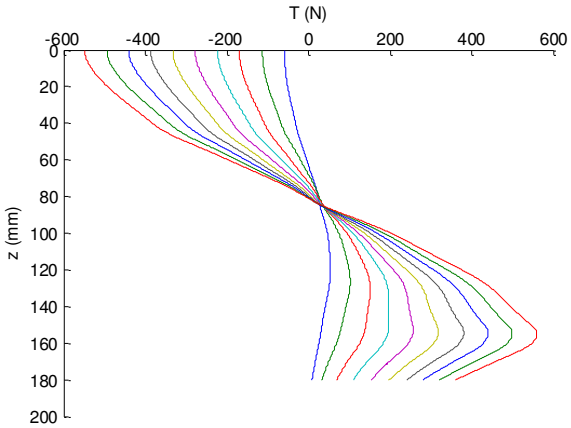

Figure A1-226: shear force vs depth

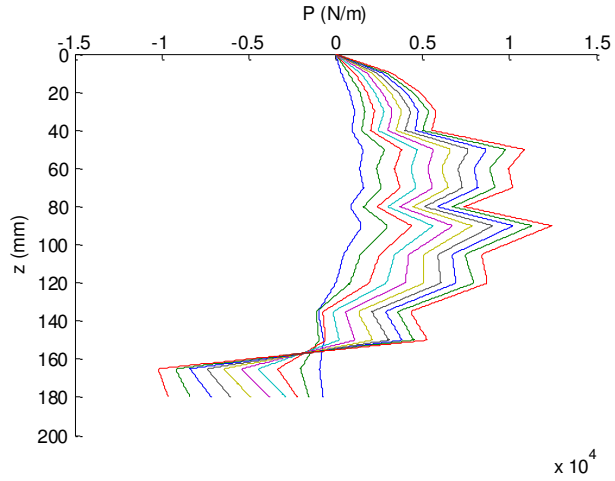

Figure A1-227: Soil reaction vs depth

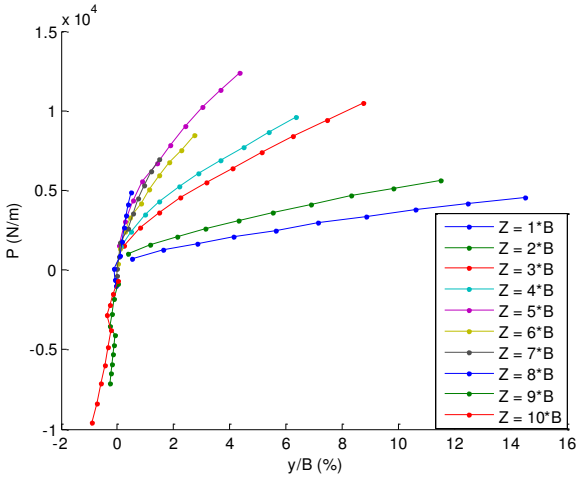

Figure A1-228: monotonic p-y curves

Test : C13P6FL1G (Cyclic loading)

The figures represent the cycles 1, 10, 100, 1000

Loading : line complete and unloading : hatched line

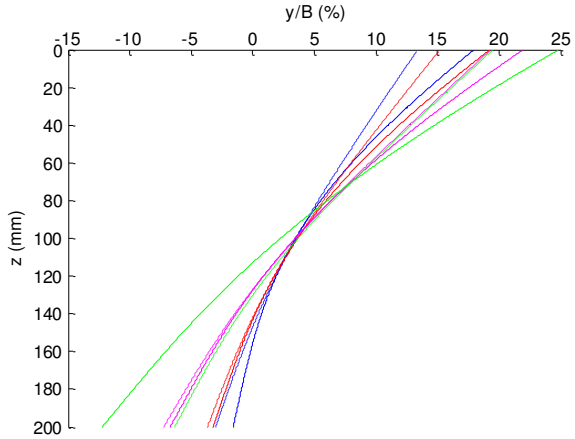

Figure A1-229 : lateral displacement vs depth

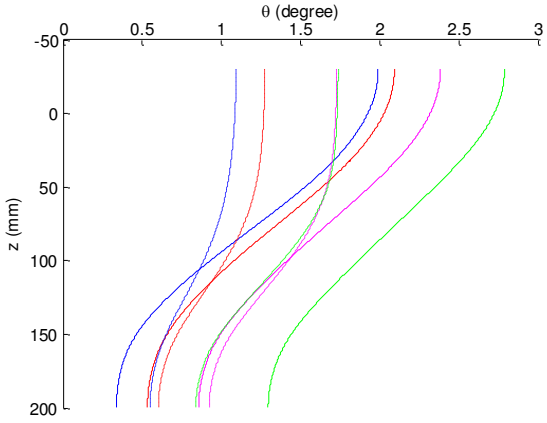

Figure A1-230: rotation vs depth

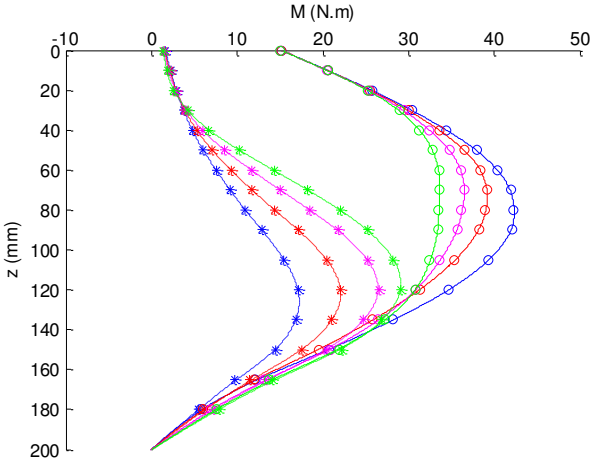

Figure A1-231: moment vs depth

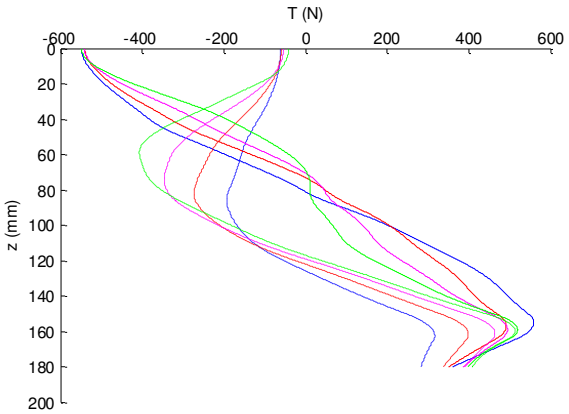

Figure A1-232: shear force vs depth

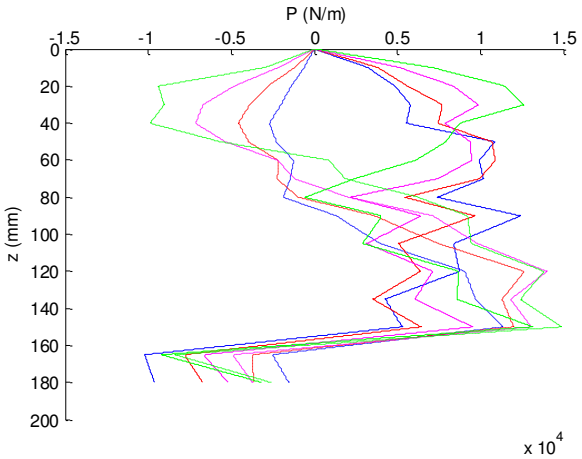

Figure A1-233: Soil reaction vs depth

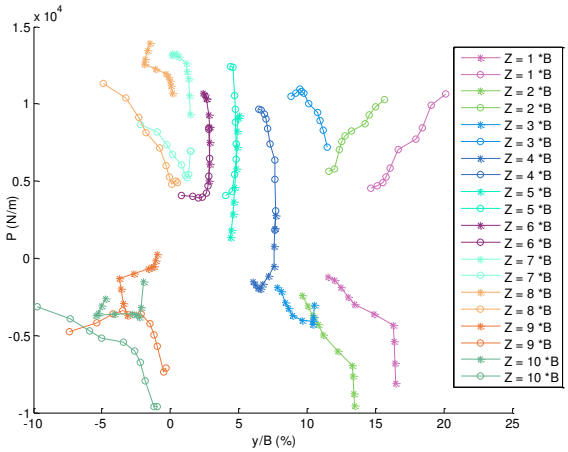

Figure A1-234: cyclic p-y curves

Model pile : instrumented pile

Test : C13P7FL1G (Monotonic loading)

The figures represent the increase of the lateral loading with step of 50 N

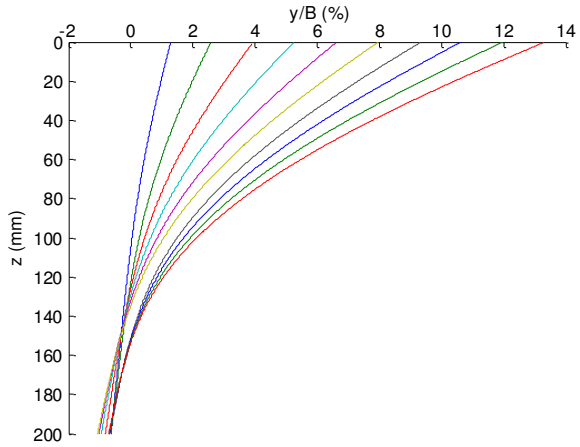

Figure A1-235 : lateral displacement vs depth

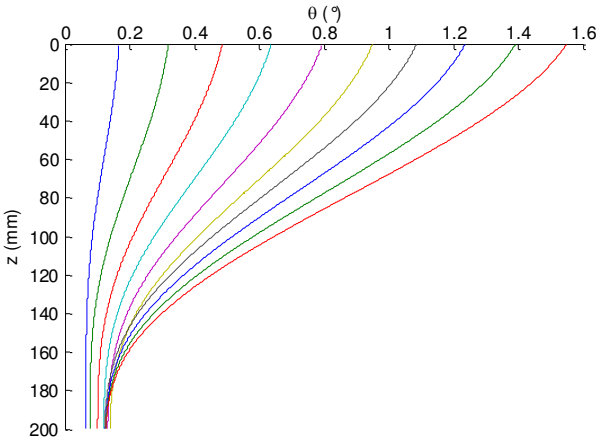

Figure A1-236 :rotation vs depth

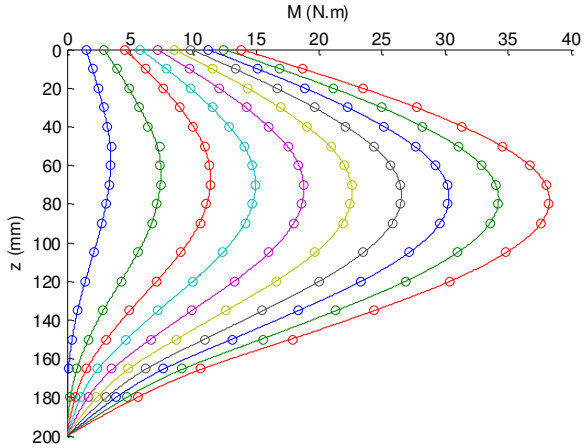

Figure A1-237: moment vs depth

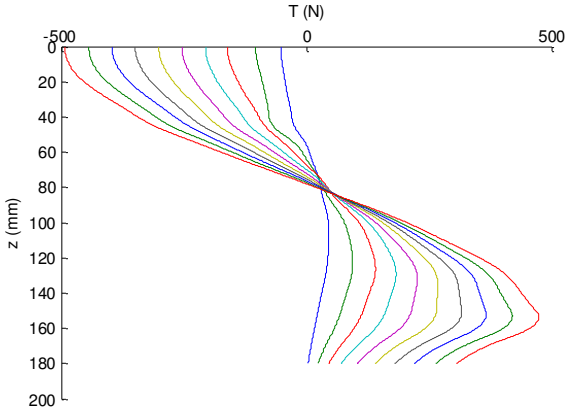

Figure A1-238: shear force vs depth

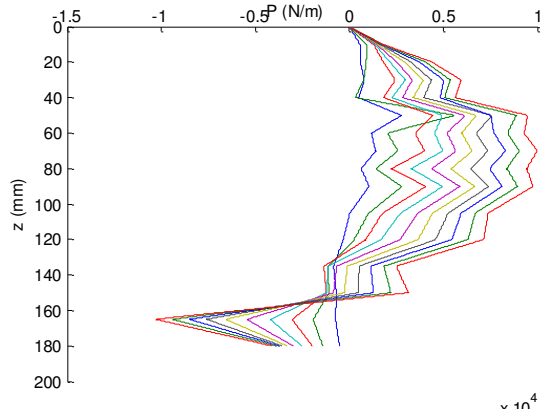

Figure A1-239: Soil reaction vs depth

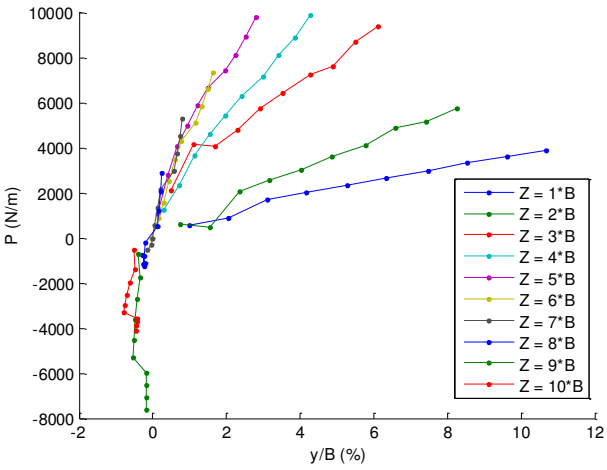

Figure A1-240: monotonic p-y curves

Test : C13P7FL1G (Cyclic loading)

The figures represent the cycles 1, 10, 100, 1000

Loading : line complete and unloading : hatched line

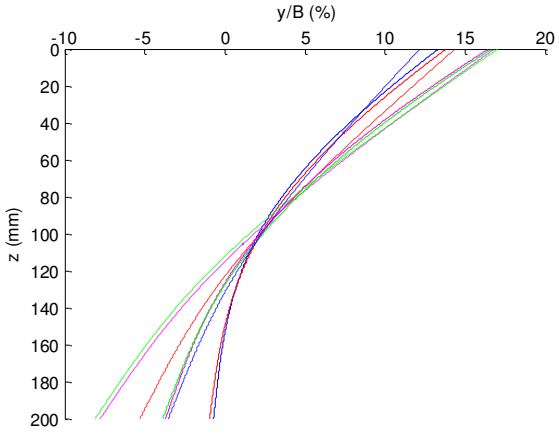

Figure A1-241 : lateral displacement vs depth

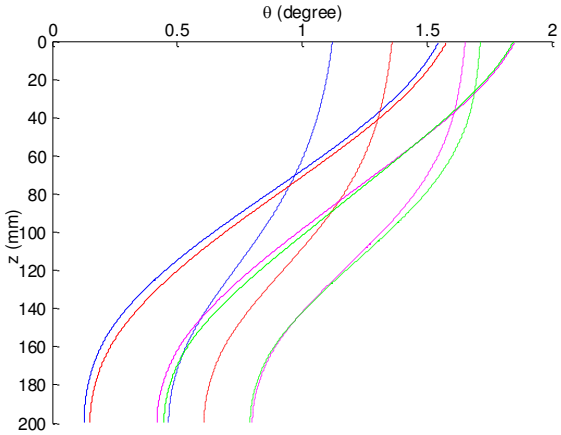

Figure A1-242: rotation vs depth

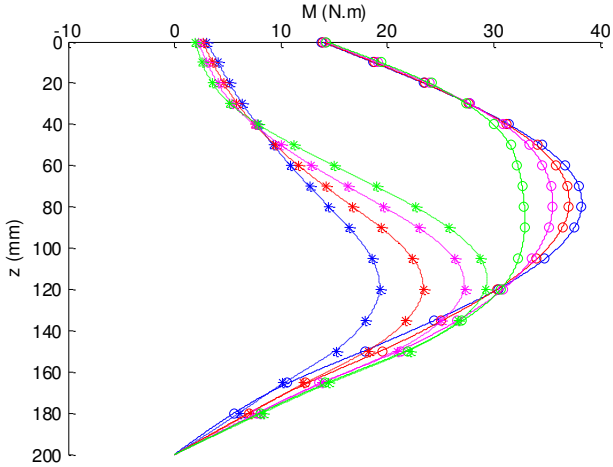

Figure A1-243: moment vs depth

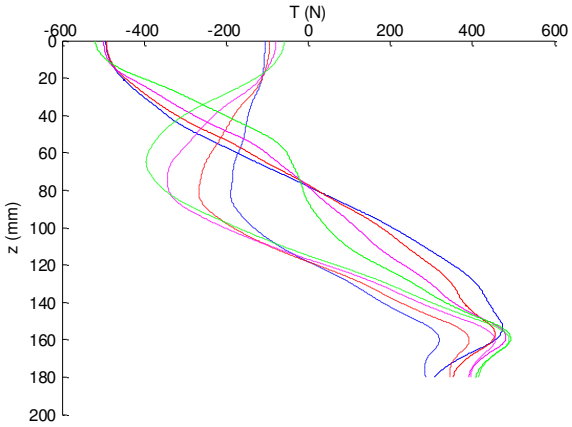

Figure A1-244: shear force vs depth

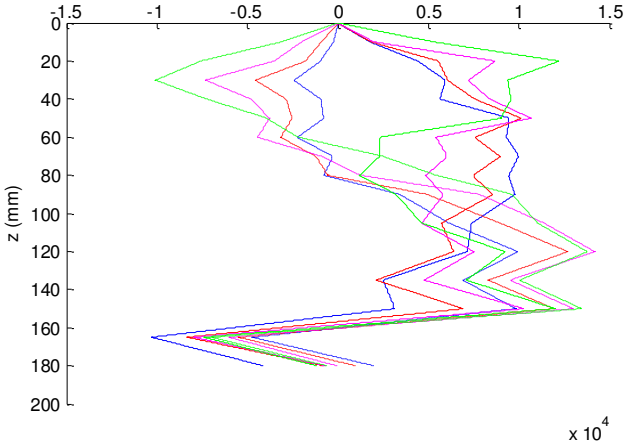

Figure A1-245: Soil reaction vs depth

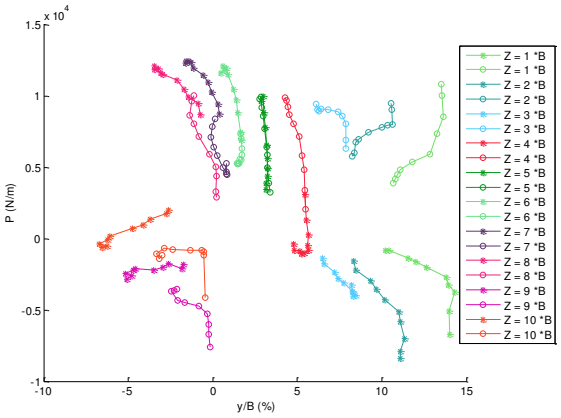

Figure A1-246: cyclic p-y curves

Strongbox C14 D_r = 99% (Dry)

Model pile : instrumented pile

Test : C14P1FL1G (Monotonic loading)

The figures represent the increase of the lateral loading with step of 50 N

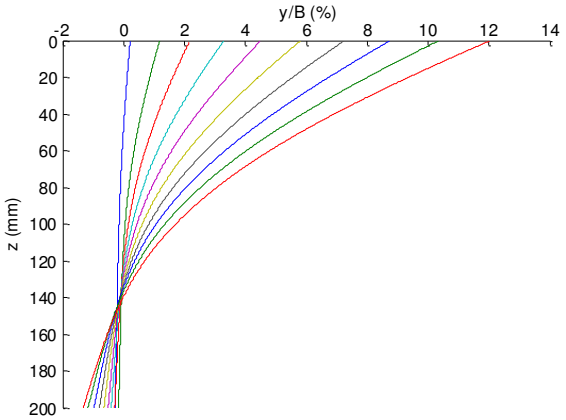

Figure A1-247 : lateral displacement vs depth

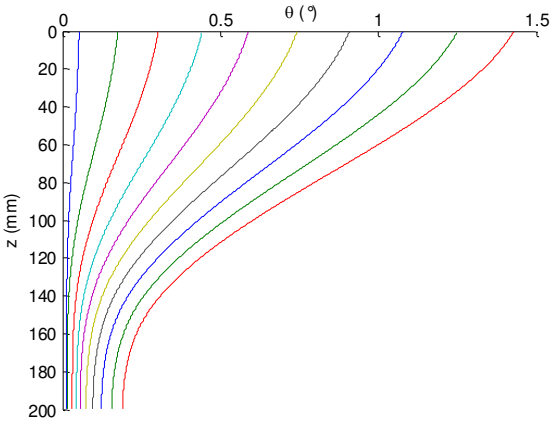

Figure A1-248: rotation vs depth

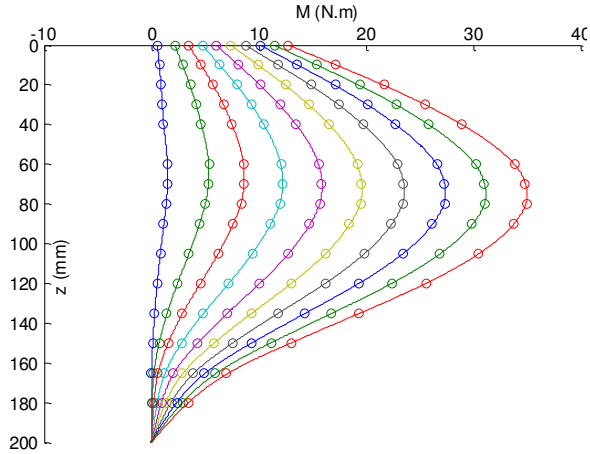

Figure A1-249: moment vs depth

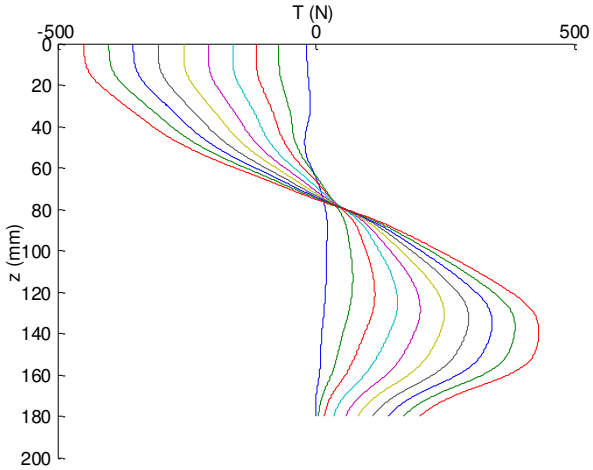

Figure A1-250: shear force vs depth

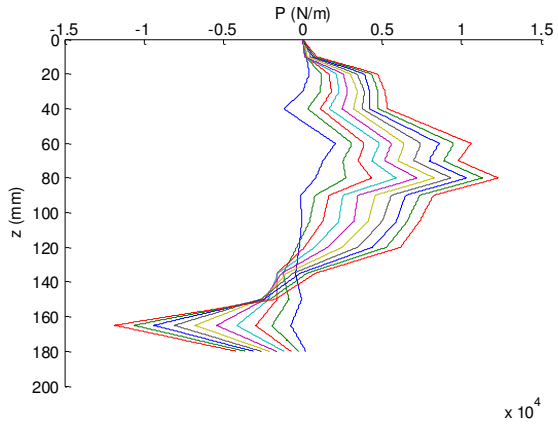

Figure A1-251: Soil reaction vs depth

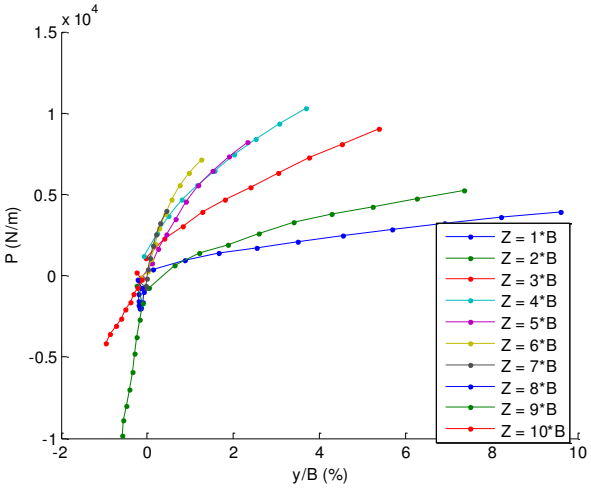

Figure A1-252: monotonic p-y curves

Test : C14P1FL1G (Cyclic loading)

The figures represent the cycles 1, 10, 100

Loading : line complete and unloading : hatched line

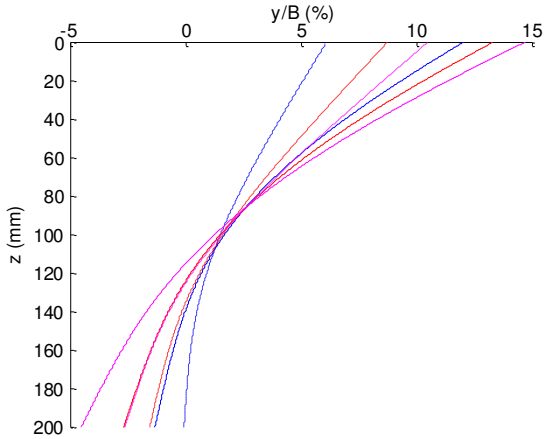

Figure A1-253 : lateral displacement vs depth

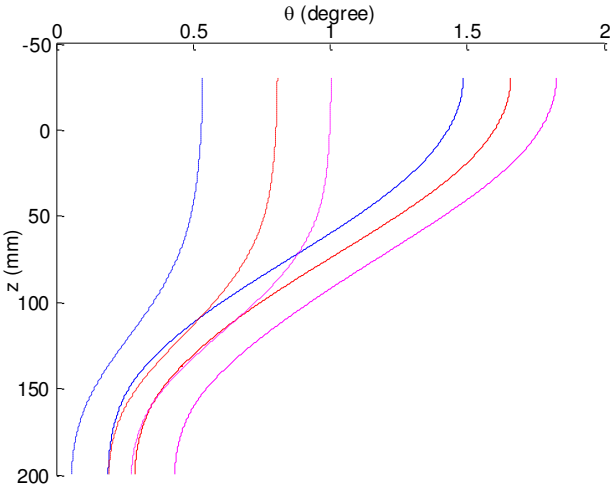

Figure A1-254: rotation vs depth

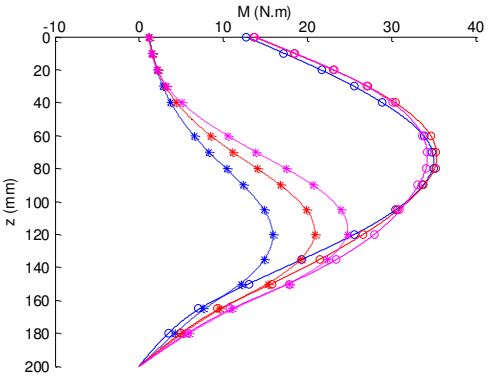

Figure A1-255: moment vs depth

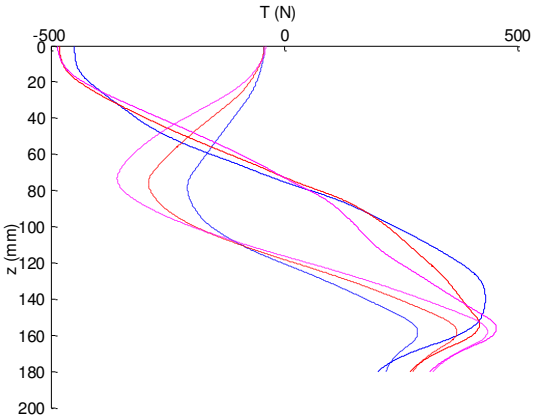

Figure A1-256: shear force vs depth

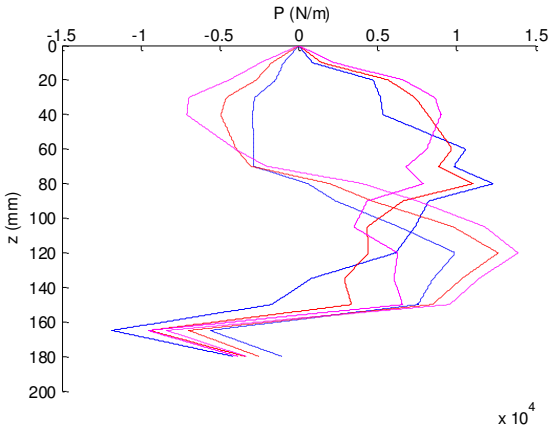

Figure A1-257: Soil reaction vs depth

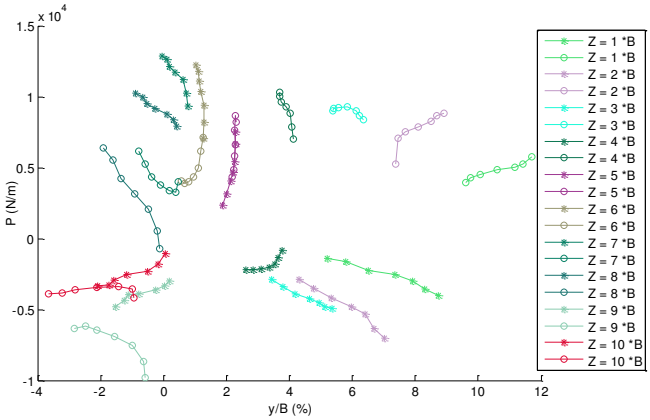

Figure A1-258: cyclic p-y curves

Model pile : instrumented pile

Test : C14P2FL100G (Monotonic loading)

The figures represent the increase of the lateral loading with step of 50 N

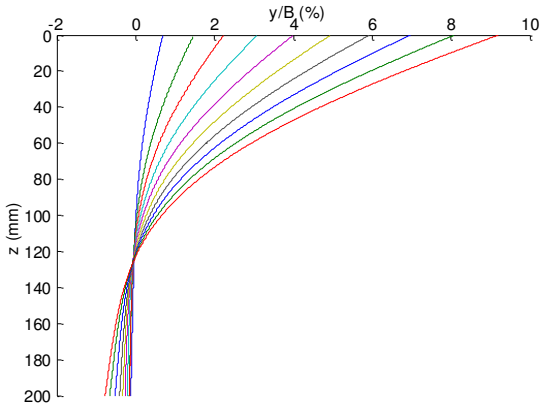

Figure A1-259 : lateral displacement vs depth

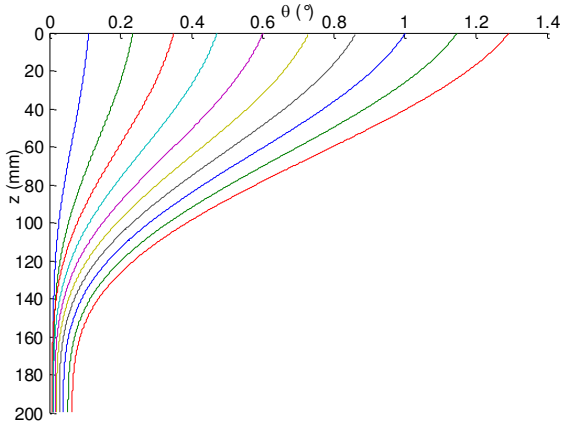

Figure A1-260: rotation vs depth

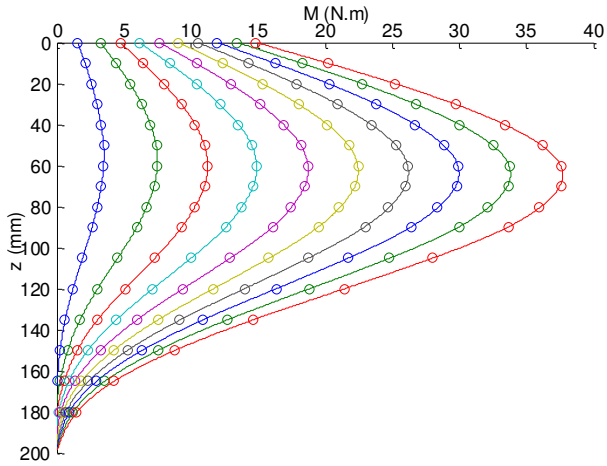

Figure A1-261: moment vs depth

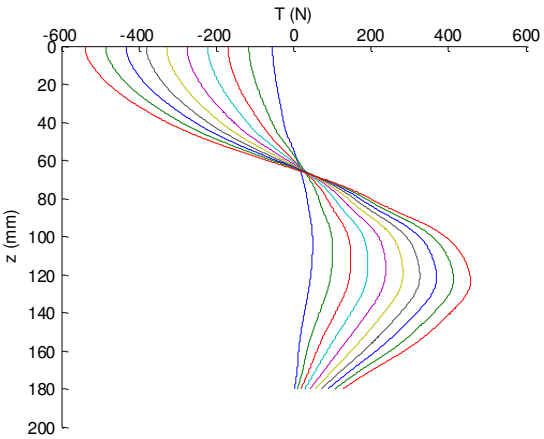

Figure A1-262: shear force vs depth

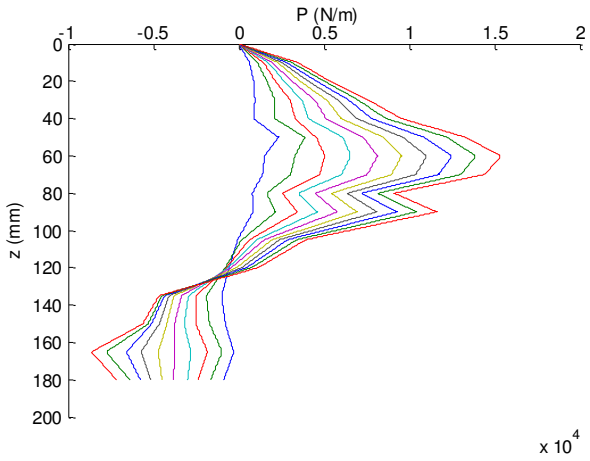

Figure A1-263: Soil reaction vs depth

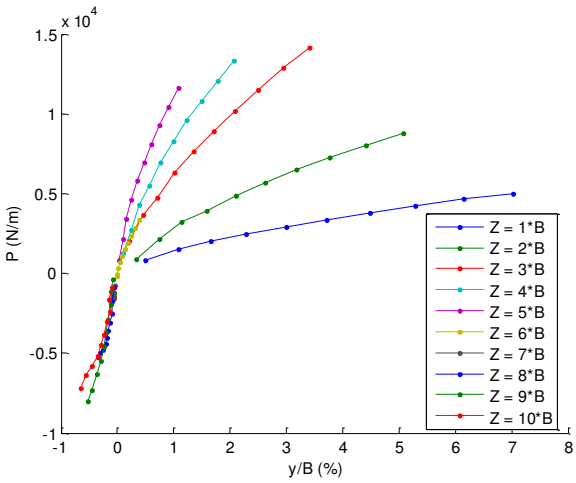

Figure A1-264: monotonic p-y curves

Test : C14P2FL100G (Cyclic loading)

The figures represent the cycles 1, 10, 100

Loading : line complete and unloading : hatched line

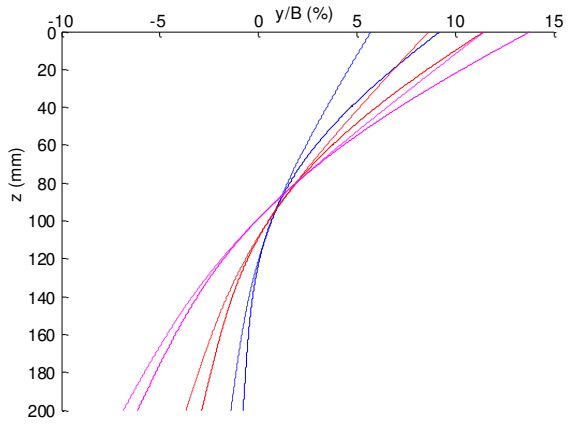

Figure A1-265 : lateral displacement vs depth

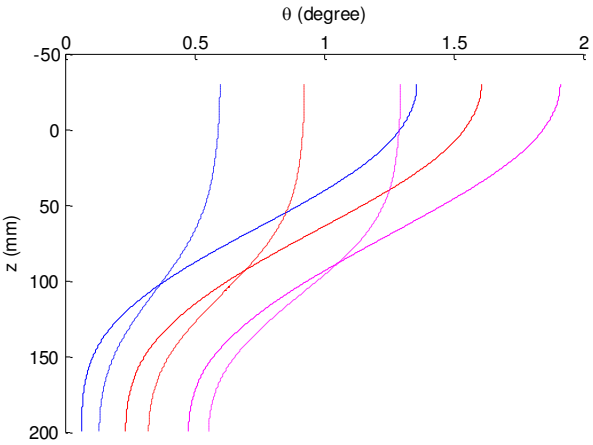

Figure A1-266: rotation vs depth

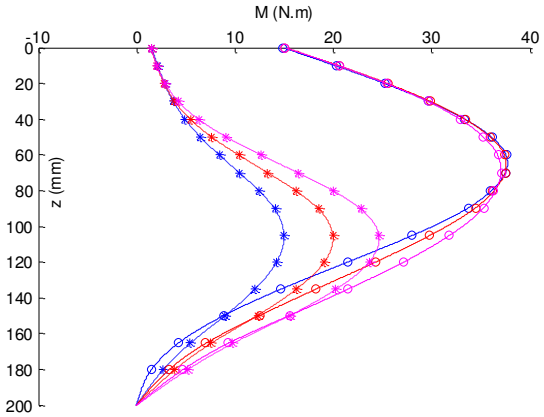

Figure A1-267: moment vs depth

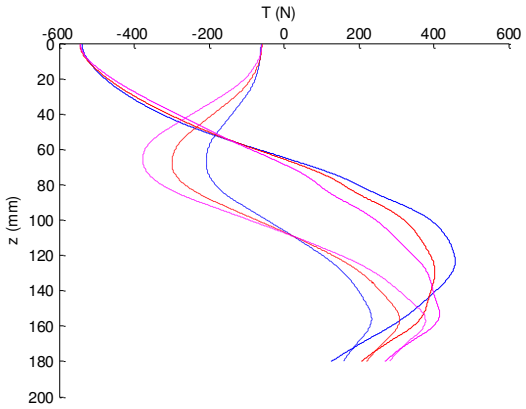

Figure A1-2668: shear force vs depth

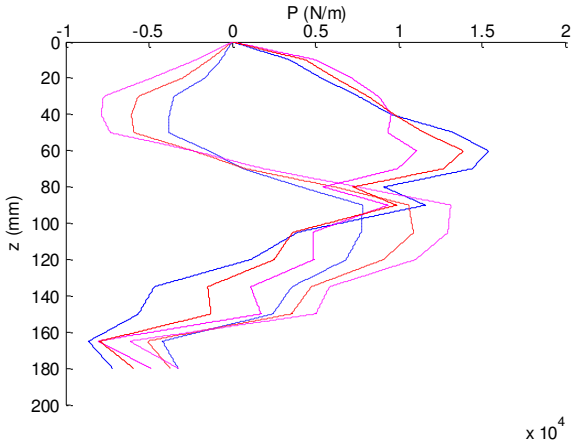

Figure A1-269: Soil reaction vs depth

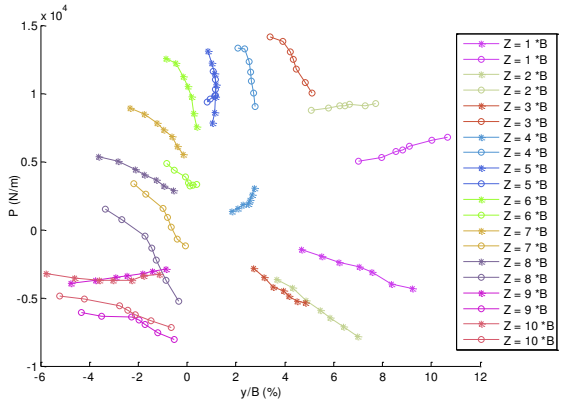

Figure A1-270: cyclic p-y curves

Model pile : instrumented pile

Test : = C14P3FH1G (Monotonic loading)

The figures represent the increase of the lateral loading with step of 50 N

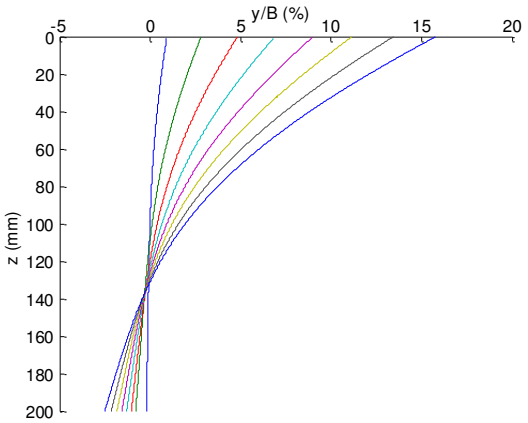

Figure A1-271 : lateral displacement vs depth

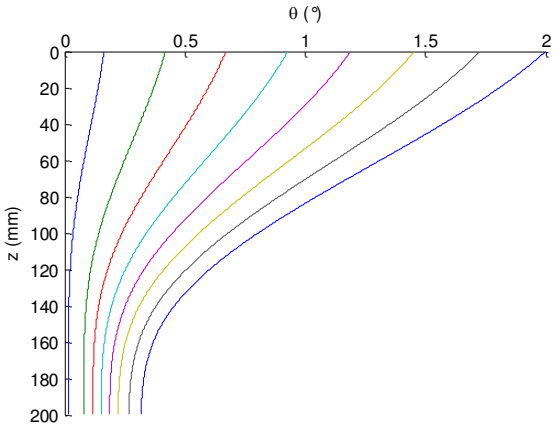

Figure A1-272: rotation vs depth

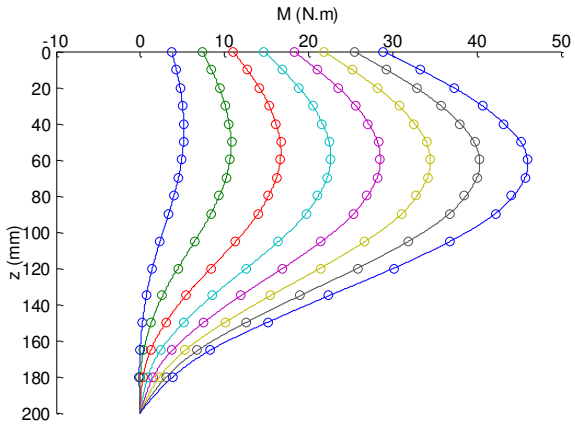

Figure A1-273: moment vs depth

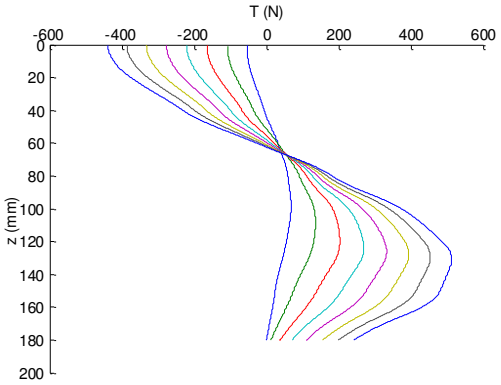

Figure A1-274: shear force vs depth

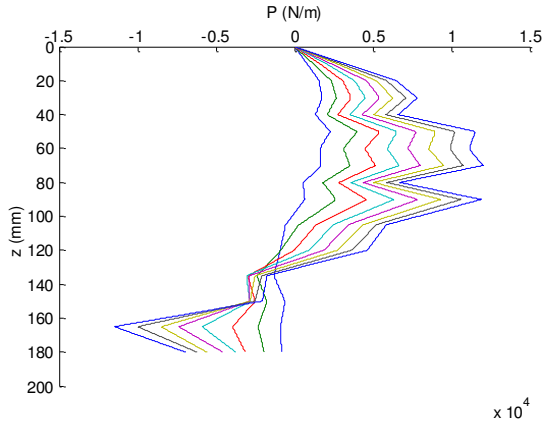

Figure A1-275: Soil reaction vs depth

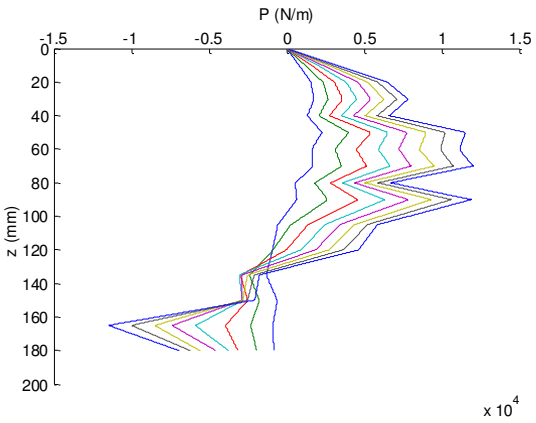

Figure A1-276: monotonic p-y curves

Test : C14P3FH1G (Cyclic loading)

The figures represent the cycles 1, 10, 100,1000

Loading : line complete and unloading : hatched line

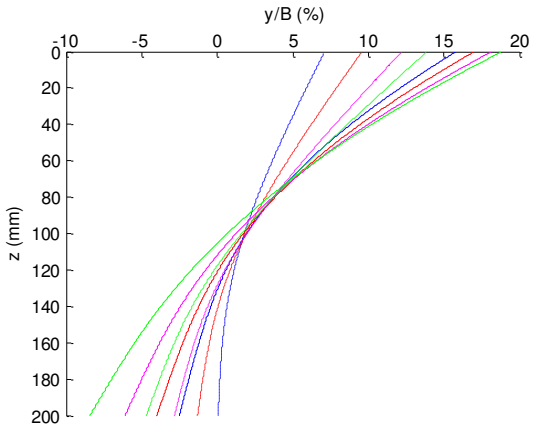

Figure A1-277 : lateral displacement vs depth

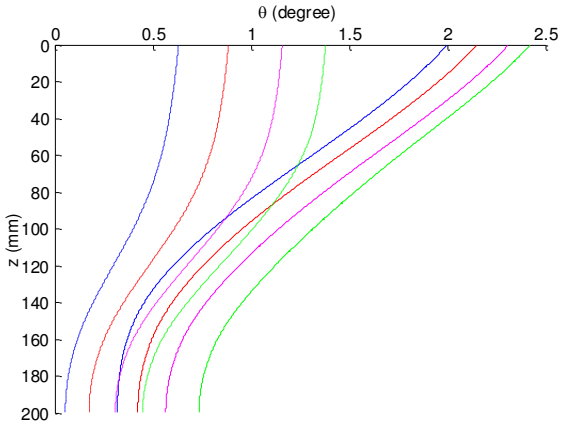

Figure A1-278: rotation vs depth

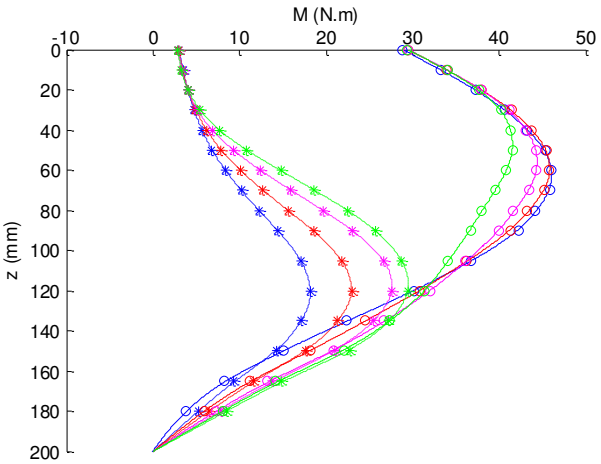

Figure A1-279: moment vs depth

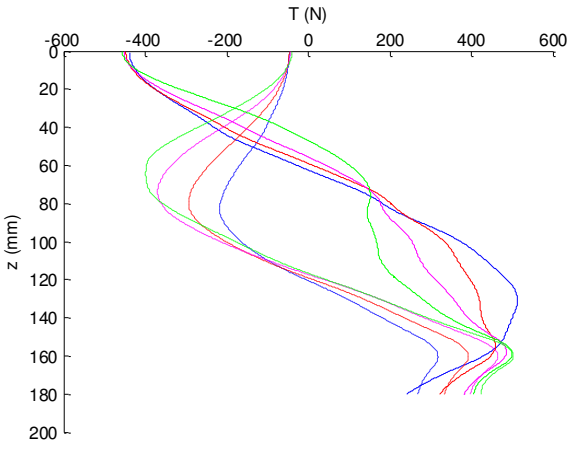

Figure A1-280: shear force vs depth

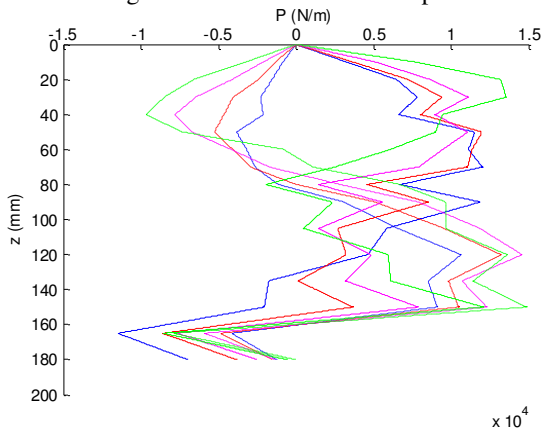

Figure A1-281: Soil reaction vs depth

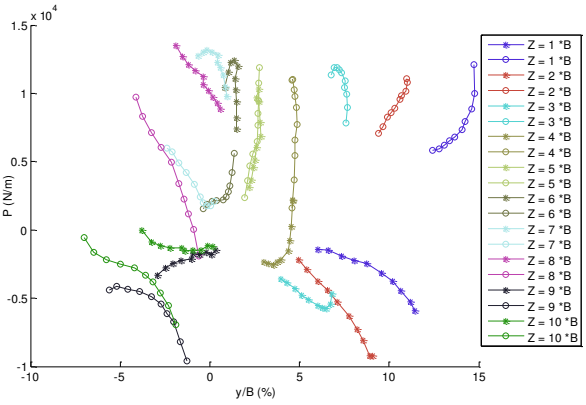

Figure A1-282: cyclic p-y curves

Model pile : instrumented pile

Test : C14P4FH100G (Monotonic loading)

The figures represent the increase of the lateral loading with step of 50 N

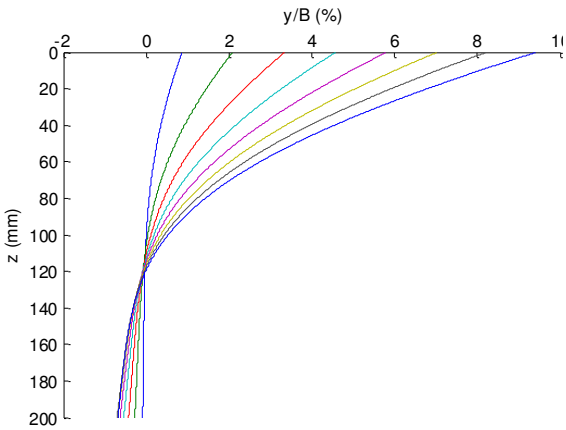

Figure A1-283: lateral displacement vs depth

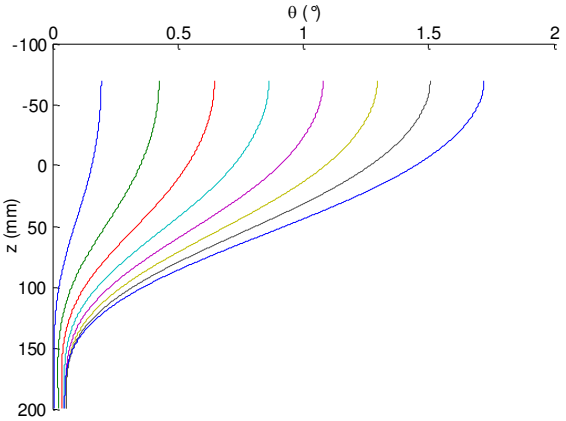

Figure A1-284: rotation vs depth

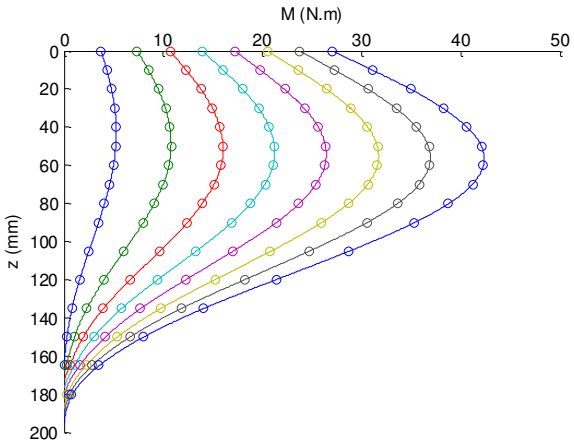

Figure A1-285: moment vs depth

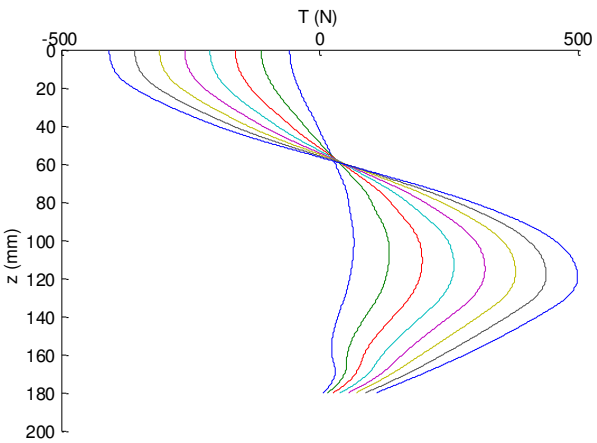

Figure A1-286: shear force vs depth

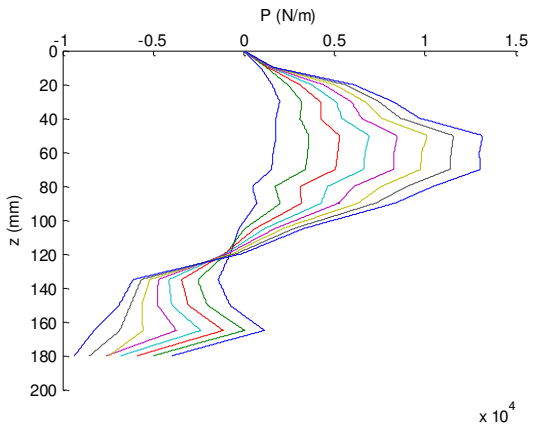

Figure A1-287: Soil reaction vs depth

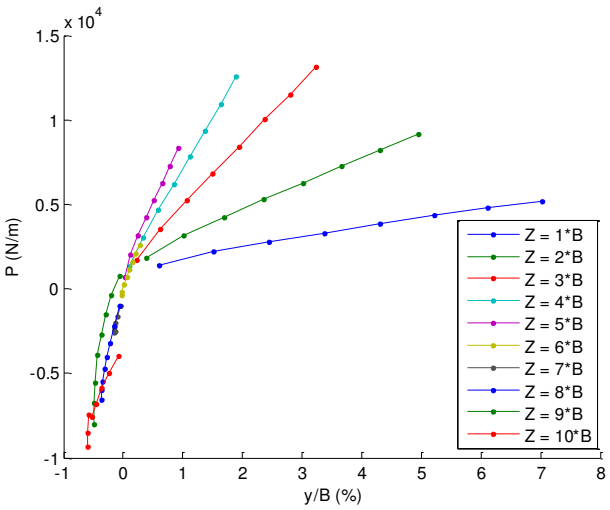

Figure A1-288: monotonic p-y curves

Test : C14P4FH100G (Cyclic loading)

The figures represent the cycles 1, 10, 100,1000

Loading : line complete and unloading : hatched line

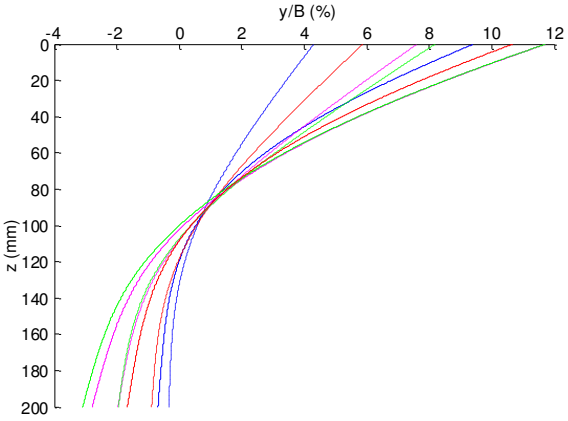

Figure A1-289 :lateral displacement vs depth

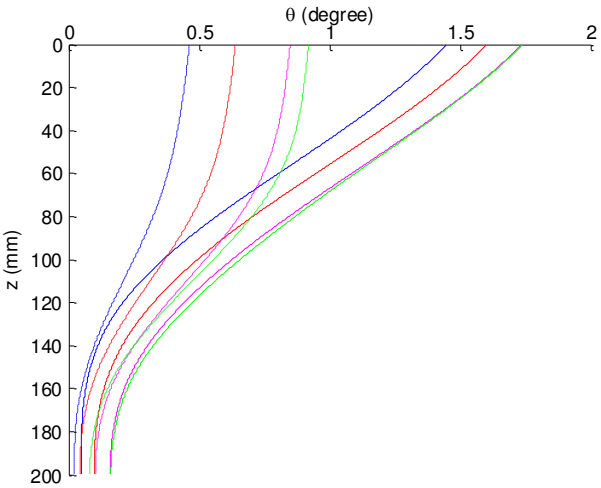

Figure A1-290: rotation vs depth

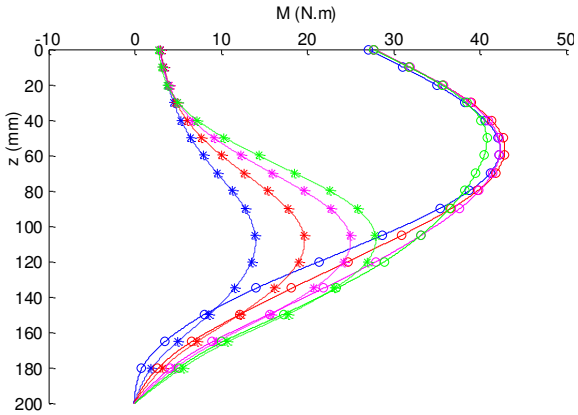

Figure A1- 291: moment vs depth

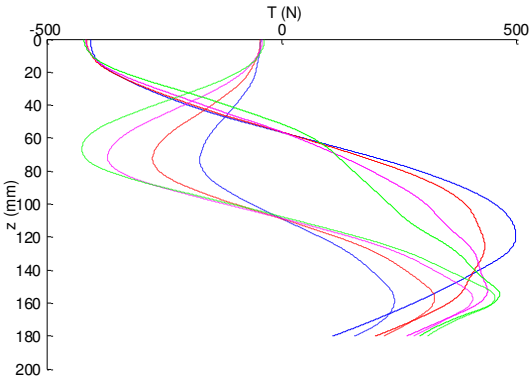

Figure A1-292: shear force vs depth

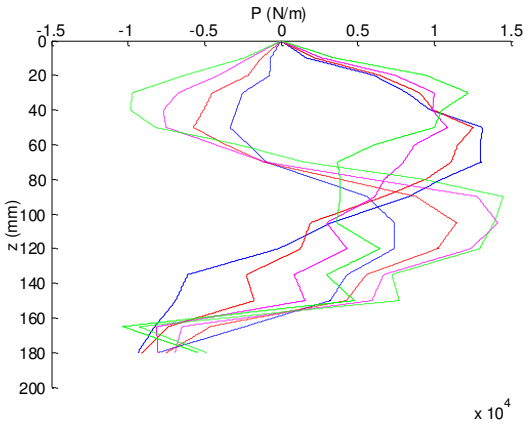

Figure A1-293: Soil reaction vs depth

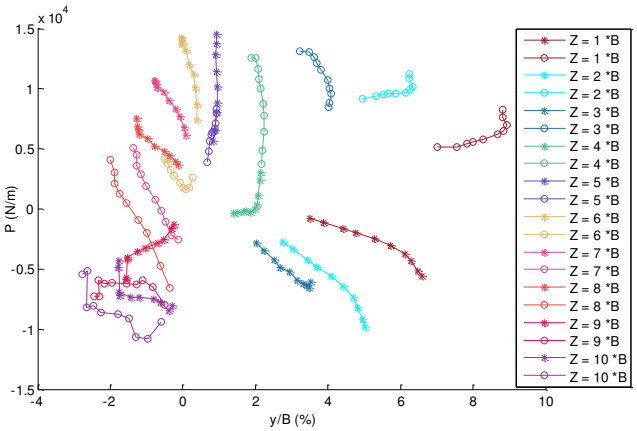

Figure A1-294: cyclic p-y curves

Appendix 2 : Model pile instrumented with strain gauges and pile calibration

One pile fully instrumented has been used for lateral loading tests. The instrumentation is installed inside, in order to be able to jack the pile before loading.

The calibration of the instrumented model pile is necessary to determine the coefficient of proportionality between the electrical response of the strain gauges and: 1) the bending moment in the case of lateral loading; 2) the axial force in the case of the axial loading. There are 17 levels of strain gauges stuck inside the pile, installed in quarter-bridge configuration. The calibration of the pile was done firstly under lateral loading so the pile needed to be encased at one extremity and submitted on the other side to well-known loads. The second step of the calibration process will be to calibrate also the pile under axial loading. To realize this step the pile was charged axially using a press machine.

1. Model pile

The model pile is 18 mm aluminum pile (Table A2-1) instrumented using 17 levels of quarter bridge gauges as presented in the Figure A2-1. The gauges are numerated from 1 to 34, the even numbers are at one side and the odd at the other side. Only 16 levels are inside the sand. This is due to a shift of 10 mm of the location of the gauges done during the instrumentation of the pile compared to the ordered positions. The embedded length of the pile is 200 mm and the total length is 300 mm. It must be noted that before the calibration the total length of the pile was 350 mm. The pile was initially ordered with an additional 50 mm at the tip side. This additional length is necessary to fix the pile at it tip during the calibration process. Once the calibration is realized the additional length was cut.

Table A2-1: pile characteristics

	Internal diameter (mm)	External diameter (mm)	Moment of inertia (m^4)	Bending stiffness ($N.m^{-2}$)
Instrumented pile	15	18	2.67×10^-9	197.43

2. Lateral calibration: flexion beam

2.1 Calibration principales

Based on beam theory, the pile (Figure A2-1) is tested in configuration where the boundary conditions are well-known. Clamped at one extremity, the model pile is subjected to a load

applied at the other extremity by successive steps, for which the electrical responses of the 34 strain gauges are recorded. The use of the quarter-bridge leads to that the needed coefficient of the proportionality isn't directly between the electrical response of each gauge and the moment at this gauge. The coefficient will be between the difference of the response of the two gauges installed at the same level and the bending moment at this level. So in order to extract this coefficient firstly, the electrical response of all the gauges is recorded then the difference is calculated.

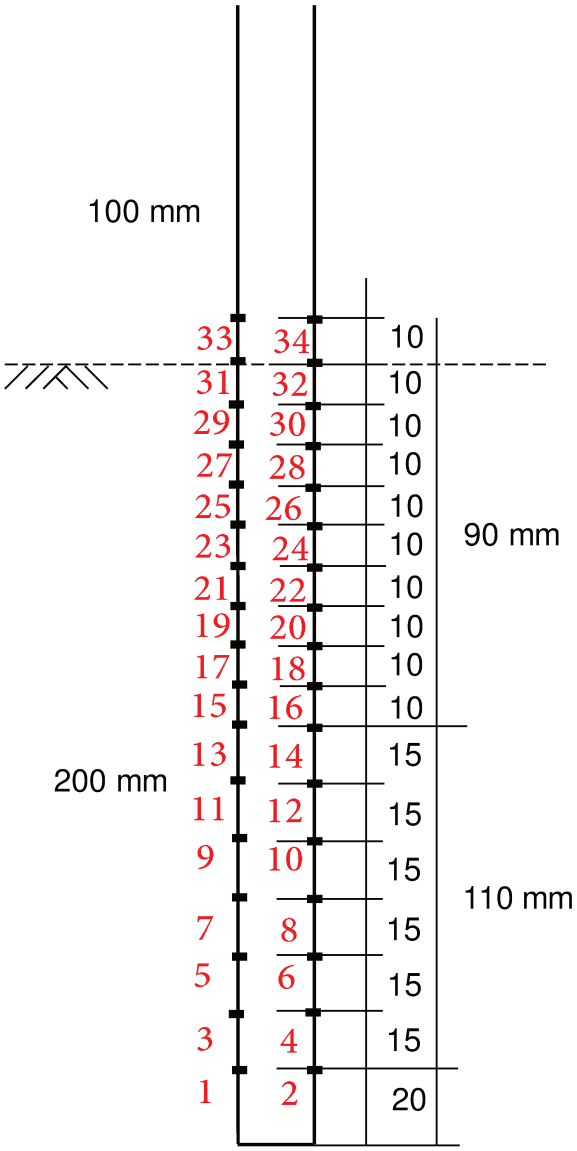

Figure A2-1: Instrumented pile

2.2 Calculation of the gauges coefficients

In order to get the electrical response of the strain gauges (in mV), they must be plugged to the DAS (Data Acquisition System).

As explained previously, the needed coefficient (C_i) will be between the differences of the response of the pair of strain gauges at the same elevation i (n_i) and the moment at this level given as $M(z_i)$.

$$C_i = \frac{M(z_i)}{n_i} \quad (1)$$

The moment at the level z_i can be given as : $M(z_i) = P(a-z_i)$ for a fixed beam in flexion.

So $C_i = \frac{P(a-z_i)}{n_i}$ (2)

And z_i is the distance between the fixed support and the gauge i.

a is the distance between the fixed support and the applied load (Figure A2-2).

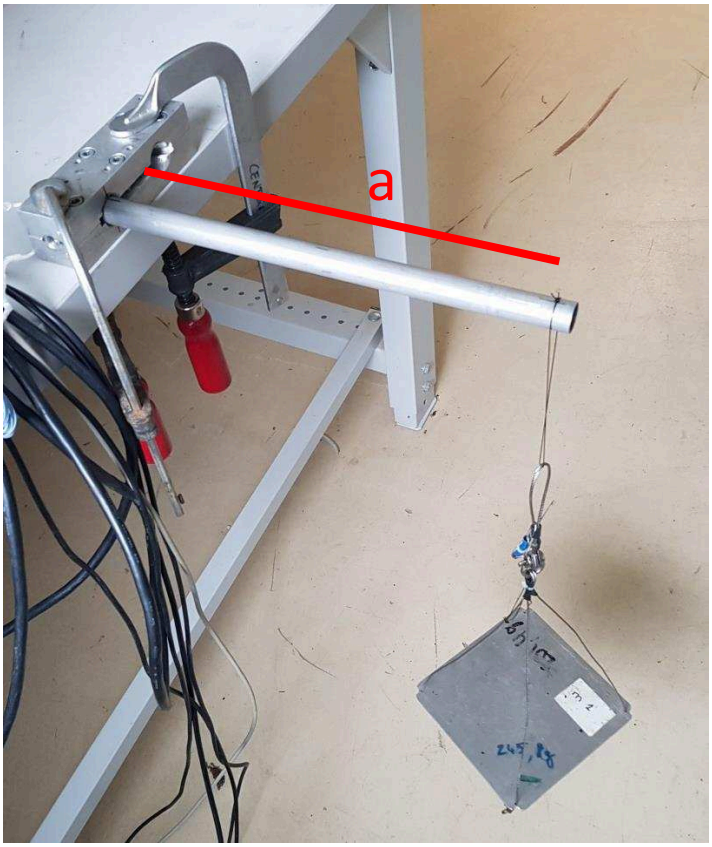

Figure A2-2: Pile calibration

2.3 Calculation of the maximum admissible loading

It is important that the pile doesn't leave the elastic domain, under loading, and especially during calibration phase. It is so necessary to determine the maximum admissible load that can be applied to the pile to not generate irreversible deformation inside the pile.

The elasticity limit of the aluminum AU4G type 2017A used for the fabrication of the pile is given as:

σ_e = 245 MPa.

The maximum stress will be:

$\sigma_x = \frac{M(z)}{I}\frac{B}{2}$ (3) avec M(z) = Pa (4)

The moment of inertia of a tube is: $I = \frac{\pi}{64}(B^4 - b^4)$ (5)

With: B the external diameter of the tube and b his internal diameter.

During the calibration, the loading is applied at a = 310 mm from the fixed support. So the maximum loading that can be applied on the pile is:

$P_{max} = \frac{\left[\frac{\frac{\pi}{64}(B^4-b^4)}{\frac{B}{2}}\right]}{a}$ = 234 N

Taking into consideration the uncertainty that can exist during the calibration of the pile. It is preferable to limit the calibration loading at a maximum of 25% of the plastic limit previously calculated.

In this study, the calibration loading is limited to 5 kg and load is applied in 5 steps of 1 kg.

Table A2-2: Calibration loads

m (kg)	1	2	3	4	5
P (N)	9.81	19.62	29.43	39.24	49.05
% of the elastic limit	4.2	8.4	12.6	16.8	21

2.4 Calibration results

Four different configurations are used in the lateral calibration of the pile by varying the application point of the load between the tip and head of the pile and the position of the even and odd gauges.

Table A2-3: Calibration configurations

	Load position	Gauges position
Config 1	Tip	Even in the upper side
Config 2	Tip	Odd in the upper side
Config 3	Head	Even in the upper side
Config 4	Head	Odd in the upper side

2.5 Gauges coefficients

For each configuration the coefficient between the differences of the response of the gauges in the same level and the moment at this level is calculated and presented in the Table A2-4.

Table A2-4: Calibration coefficients values Ci (Nm/V)

Gauges level	config 1	config 2	config 3	config 4	Average value
1 - 2	29.7545	29.7545	30.74159	30.26965	30.13006
3 - 4	29.01064	28.90885	29.87092	29.52954	29.32999
5 - 6	29.91249	29.69351	30.41127	29.9797	29.99924
7 - 8	29.91713	29.88001	30.53535	30.16428	30.12419
9 - 10	30.21226	29.82451	30.57666	30.0333	30.16168
11 - 12	29.61546	29.53266	30.24983	29.85021	29.81204
13 - 14	30.15392	29.84959	30.42741	29.99165	30.10564
15 - 16	29.84792	29.80114	30.34009	29.94193	29.98277
17 - 18	30.09001	29.97881	30.76118	30.17956	30.25239
19 - 20	30.37098	30.11629	30.6818	30.24708	30.35404
21 - 22	30.52274	30.31993	30.94081	30.421	30.55112
23 - 24	29.99165	29.78762	30.30843	30.00099	30.02217
25 - 26	30.43317	30.28773	30.91565	30.3463	30.49571
27 - 28	29.95878	29.75783	30.33001	29.94193	29.99714
29 - 30	29.81388	29.85112	30.31078	29.92051	29.97407
31 - 32	29.6275	29.5674	29.89485	29.61546	29.6763
33 - 34	30.09001	29.9272	30.34009	30.17956	30.13422

3. Axial calibration

3.1 Calibration principles

The main principle of the axial calibration is that the applied axial load on the pile must be found identical at any level in the pile. Taking this into account the pile is loaded axially with different increasing load steps and the variation of the sum of the electrical response of the two gauges at each level of the pile is considered proportional to the applied load by a coefficient Ci.

3.2 Calculation of the maximum admissible loading

It is important during the calibration of the pile to pay attention of the axial admissible loading to prevent any risk of buckling of the pile. In order to stay in the safe zone and as the buckling load depend on the limit conditions of the pile, the worst scenario is considered to exist for the limit condition (one end fixed and the other end free to move laterally) and the buckling is given as:

$$P_b = \frac{\pi^2 E I}{4L^2} = 3970 \text{ N} \quad (6)$$

The maximum applied load on the pile is limited to 25% of the buckling load. In this study the load is limited to 1000 N.

3.3 Calibration process

The calibration of the pile is realized with the use of a press machine (Figure A2-3) and the different applied steps are adjusted with the use of a dynamometric ring (Figure A2-4). The load is applied with the use of a five steps of 200 N each up to the maximum fixed load of 1000 N.

3.4 Axial coefficients

The coefficients between the axial applied load and the sum of the variation of the electrical response of the two gauges at the same level in the pile are given in Table A2-5.

Table A2-5: Calibration coefficients values Ci (N/V)

1 - 2	6313.131
3 - 4	6242.197
5 - 6	6295.247

7 - 8	6337.136
9 - 10	6343.165
11 - 12	6331.117
13 - 14	6379.585
15 - 16	6459.948
17 - 18	6561.68
19 - 20	6574.622
21 - 22	6620.324
23 - 24	6581.112
25 - 26	6680.027
27 - 28	6646.726
29 - 30	6640.106
31 - 32	6693.44
33 - 34	6823.61

Figure A2-3: Axial calibration

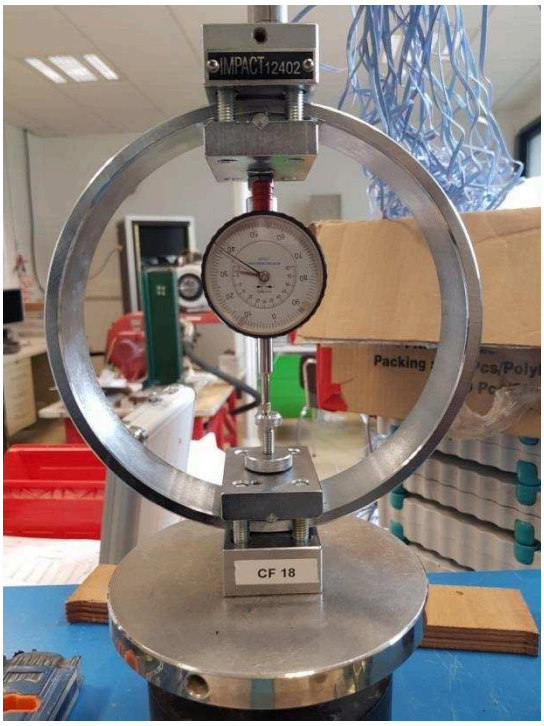

Figure A2-4: Dynamometric ring

Appendix 3 : Centrifuge force inside the sand massif

The centrifuge modelling consists of the use of small scale model of geotechnical work, installed in a high field of gravity to permit the replication of the stress state that exists in the prototype (at full scale). The increase of the acceleration due to centrifuge rotation leads to the reproduction, inside the sand model, of the same stresses that exist in the prototype . A model of height of h can represent a prototype massif of height h_p= N×h_m when subjected to a centrifuge acceleration of N times the earth gravity.

The centrifuge acceleration depends on the rotation speed ω and the radius R_N. Schofield (1980) has indicated that the vertical stress profile inside the sand massif isn't linear but parabolic. The objective of this appendix is to remind the shape of the centrifuge force profile inside the soil model and to discuss the application point where the centrifuge acceleration must be applied.

1. Profile of the centrifuge force inside the sand model

The vertical stress profile inside a prototype geotechnical work can be expressed with the density ρ, the earth gravity g and the depth coordinate z, using the following linear formula:

$$\sigma_v^p = \rho g z \tag{1}$$

Assuming that the centrifuge model (located between the centrifuge radius R_0 and R_1, respectively for the top and the bottom of the soil model) is subjected to a centrifuge acceleration equal to N times the earth gravity, normal to the "horizontal surface" of the model, the vertical stresses inside the model (Figure A3-1) can be calculated as:

$$\sigma_v^m = \rho G(R - R_0) \tag{2}$$

The acceleration G inside the sand mass depends on two parameters: the rotation speed of the centrifuge (ω^2) and the radius of the application of the stresses (R):

$$G = R\omega^2 \tag{3}$$

Taking R_N as the radius of the application of the acceleration, the rotation speed of the centrifuge can be expressed as:

$$\omega^2 = \frac{G}{R_n} \tag{4}$$

Considering that G=Ng at R = R_N the rotation speed is:

$$\omega^2 = \frac{Ng}{R_N} \tag{5}$$

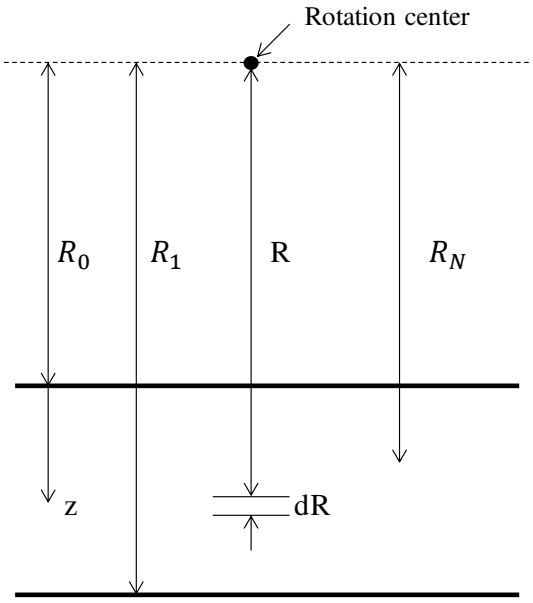

R: Radius location of a surface element dS

R_0: Radius between the rotation axes of the machine and the strongbox surface

R_1: Centrifuge radius

R_N: Radius of the application of the Centrifuge acceleration

z : Relative depth of the strongbox

Considering an elementary volume dV = dR.dS for which the gravity will be constant on the height dR. The vertical stress on this element is:

$$d\sigma_{vm} = \frac{\rho G dV}{dS} = \rho R \omega^2 dR \tag{6}$$

So the vertical stress in a depth corresponding to a radius R can be given by the following equation:

$$\sigma_{vm} = \int_{R_0}^{R} \rho R \omega^2 dR = \frac{\rho \omega^2}{2}(R^2 - R_0^2) = \frac{\rho N g}{2R_N}(R^2 - R_0^2) \tag{7}$$

The optimal depth for the application of the centrifuge acceleration can be defined using variant method. Cooke 1990 has defined it as the point where the difference between the theorical profile and the applied one is minimal. Considering ε is this difference.

$$\varepsilon = \rho N g(R - R_0) - \frac{\rho N g}{2R_N}(R^2 - R_0^2) \tag{8}$$

So

$$\varepsilon = \frac{\rho N g}{2R_N}[2R_N(R - R_0) - R^2 + R_0^2]$$

ε is minimal when the area limited between the two profile is equal to zero (Figure A3-2):

$$\int_{R_0}^{R_1} \varepsilon dR = 0$$

$$\frac{\rho N g}{2R_N} \int_{R_0}^{R_1} (2R_N(R - R_0) - R^2 + R_0^2) dR = 0$$

$$\frac{\rho N g}{2R_N} \left[R_N R^2 - 2R_N R_0 R - \frac{R^3}{3} + R_0^2 R \right]_{R_0}^{R_1} = 0$$

The minimal difference is obtained for: $R_N = \frac{2}{3} R_0 + \frac{1}{3} R_1 = R_0 + \frac{1}{3} (R_1 - R_0)$

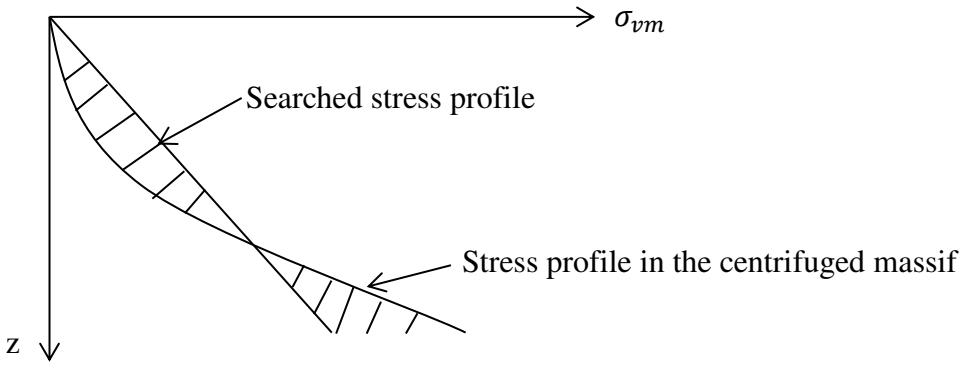

Figure A3-2: Verticals stresses profiles (searched and inside the centrifuged massif)

2. Centrifuge force at the surface of the sand

The surfaces where the centrifuge generates the same acceleration when it is in rotation can be defined as cylinders around the axis of rotation of the centrifuge. These surfaces are also called the iso-g surfaces. The surface of the sand inside the strongboxes is plan which means, if the centrifuge force is applied at the middle of the surface of the sand, that the centrifuge force at the extremities of the strongbox are bigger. It is important to quantify the increase of the g level at the location of the realized tests.

The area where the tests can be realized is limited by a usable surface. This surface is 20 cm far from both sides of the strongbox at the small sides and 10 cm far at the long sides (Rosquoet, 2004). This means that the longitudinal usable length of the strongbox is 80 cm. If the centrifuge force is applied at the centre of this surface, the difference of the g level must be quantified at the farthest point (40 cm from the centre). At this point the variation of the g level is in order of 0.52%, so it can be assumed that almost no effect is considered to exist due to this augmentation on the realized tests.

3. Conclusion

Finally the centrifuge acceleration must be applied **at the third of the height** of the sand mass from the surface to best approach the prototype profile of the vertical stresses.

The augmentation of the acceleration level at the positions of the realised tests is 0.52%. No effect is considered to exist due to this augmentation on the realized tests.

Cooke B. (1991). Selection of operative centrifuge radius to minimize stress error in calculations. Canadian Geotechnique **28**(1). Pp 160-161.

Rosquoet, F. 2004. Pieux sous charge latérale cyclique. Phd Ecole centrale de Nantes, Université de Nantes. Pp 66-69.

Schofield A.N. (1980). Cambridge geotechnical centrifuge operation. Geotechnique **30**(3). Pp 227-268.

Appendix 4 : Characterization of sand mass reconstituted in rectangular strongboxes

The characterization of the used sand mass was done with the use of calibration boxes for the determination of the real density of the reconstituted sand and some CPT tests in order to check their homogeneity.

1. Determination of the unit dry weight of the pluviated sand

The unit dry weight of each prepared sand strongbox has been verified with the use of calibration boxes which were installed inside the strongbox prior to the pluviation (Figure A4-1). When the strongbox was filled with the pluviated sand, the density box was also been filled with the sand which insure that the sand inside this box is similar to the surrounding sand in the strongbox. This process is similar to the one for identifying meteorological pluviometry. After the realization of the centrifuge test, at the time of the emptying of the rectangular strongbox, the density box was extracted then shaved and weighted in order to determine the unit dry weight of the used sand.

Figure A4-1: Calibration box inside the sand rectangular strongbox

2. Pluviation parameters and prepared densities

The air pluviation technique (Figure A4-2) is used widely in geotechnical laboratory in order to prepare sand samples of high level of homogeneity and because of the possibility to prepare sand samples of wide ranges of densities and in high accuracy only by changing some

pluviation parameters. IFSTTAR-Nantes is equipped with a home-made pluviation machine where the desired sand density can be adjusted by varying the high of the hopper (Figure A4-3), the width of it slit, it horizontal speed and the number of the round trip that the hopper realize above the strongbox before readjusting the hopper elevation. In the present study two desired densities where prepared by changing the four parameters mentioned previously. The verification of the density was realized by the use of the calibration boxes and described in the previous section. The density was verified inside one strongbox for each density then the same configuration for the pluviation parameters was used for the rest of the realized strongboxes. The reason is to eliminate any perturbation in the behaviour of the piles due to the existence of the boxes at the bottom of the strongboxes.

For the medium dense sand (1.59 g/cm^3) the following parameters are used:

Hopper high: 60 cm

Slit width: 4 mm

Horizontal frequency: 11 Hz

Number round-trip: 1

For the dense sand (1.70 g/cm^3) the following parameters are used:

Hopper high: 90 cm

Slit width: 3 mm

Horizontal frequency: 50 Hz

Number round-trip: 4

In the case when the sand needs to be saturated the strongbox is then connected to a water tank by the underside up to full saturation which gives effective unit weight of 0.99 g/cm^3 and 1.04 g/cm^3 for the medium dense saturated sand and the dense saturated sand respectively.

Figure A4-2: Air pluviation lab

Figure A4-3: The Hopper machine

3. CPT tests

The geotechnical characteristics of each strongbox and the homogeneity of the sand inside it have been verified with the use of penetration tests. In each strongbox several CPT test have been realized at 100×g in different location. Figure A4-4 and Figure A4-5 show the results of the CPT tests realized in the medium dense and dense dry sand.

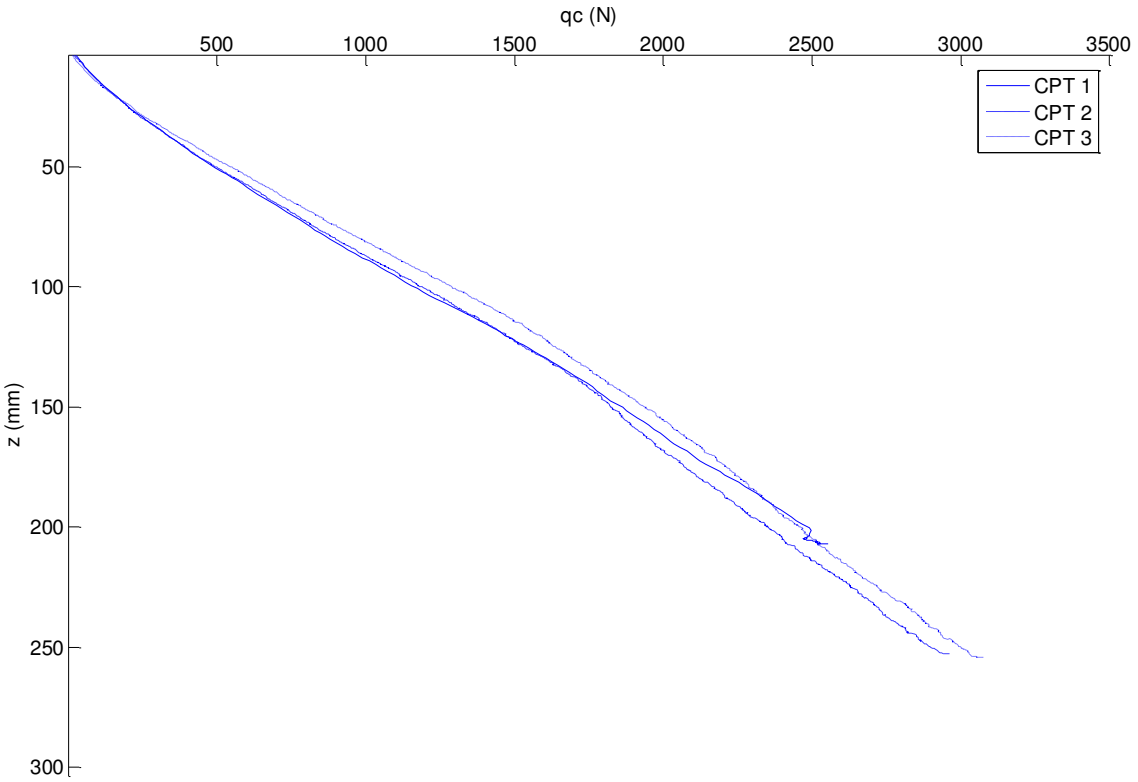

Figure A4-4: CPT in medium dry sand (model values)

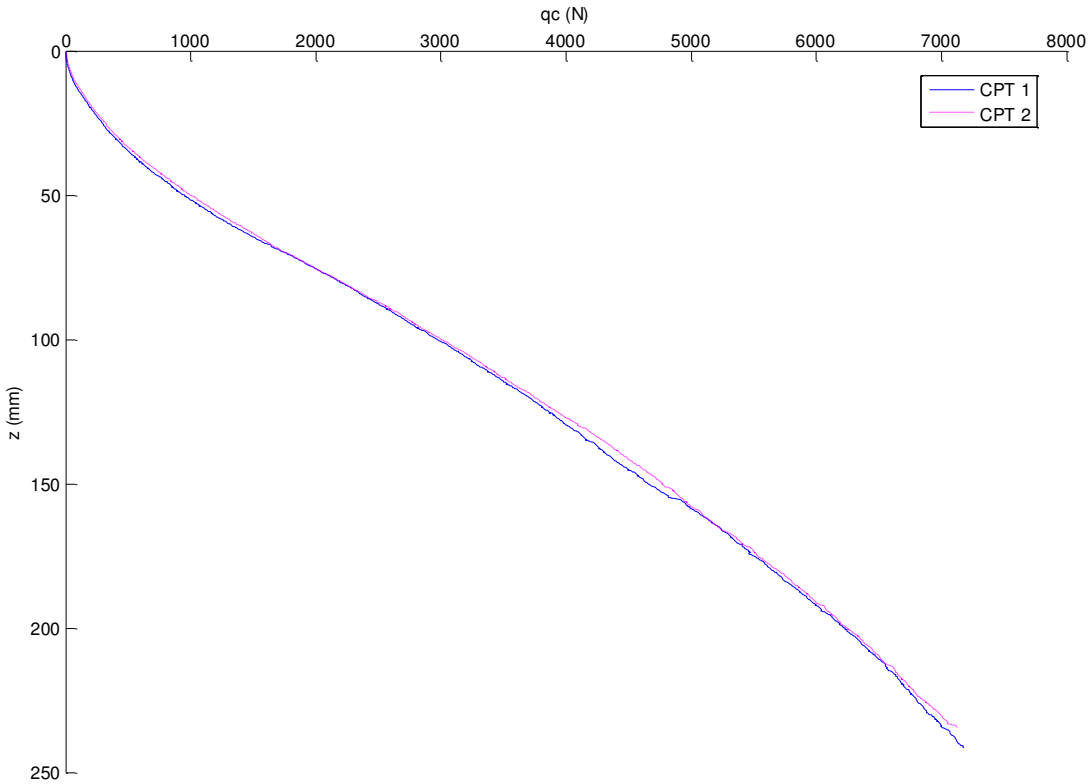

Figure A4-5: CPT in dense dry sand (model values)

At the end, one CPT profile has been chosen to represent the geotechnical characteristic of each condition of the used sand (dense, medium dense, dry or saturated). Figure A4-6 shows the CPT profile in each sand condition. These profiles have been also used in the calculus following the geotechnical standards in order to determine the axial capacity of the tested piles.

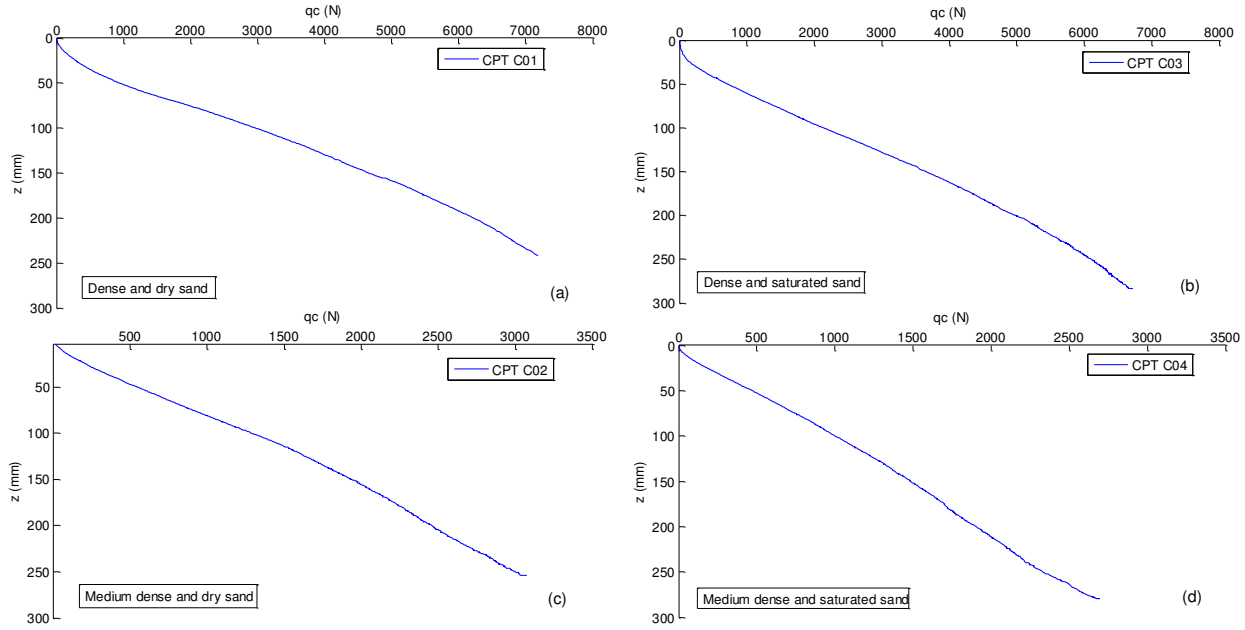

Figure A4-6: CPT in (a) dense dry sand (b) dense saturated sand (c) medium dense dry sand (d) medium dense saturated sand (model values)

Appendix 5 : Determination of the maximum and minimum dry unit weight

The maximum and minimum dry unit weight are used in the procedure of calculation of the relative density of the soil this is why it is important to have precise information of these parameters for the sand used. The procedure applied in this annex for the calculation of the max and min dry unit weight is obtained from the French standards (NF P 94-059).

1. Determination of the relative density:

The relative density can be calculated using the following formula:

$$I_D = \frac{e_{max} - e}{e_{max} - e_{min}} = \frac{\frac{1}{\rho_{dmin}} - \frac{1}{\rho_d}}{\frac{1}{\rho_{dmin}} - \frac{1}{\rho_{dmax}}} \quad (1)$$

with $e_{max} = \frac{\rho_s}{\rho_{dmin}} - 1$ and $e_{min} = \frac{\rho_s}{\rho_{dmax}} - 1$

Where:

e is the void ratio of the material

e_{max} is the maximum void ratio of the material

e_{min} is the minimum void ratio of the material

ρ_s is the dry unit weight of the solid particles

ρ_d is the unit dry weight of the material

ρ_{dmax} is the maximum unit dry weight of the material

ρ_{dmin} is the minimum unit dry weight of the material

1.1 Determination of the minimum unit dry weight

In order to determine the minimum unit dry weight the following steps must be realized:

- Filling the test cylindrical mold (Figure A5-1) with sand using the minimum possible drop height.

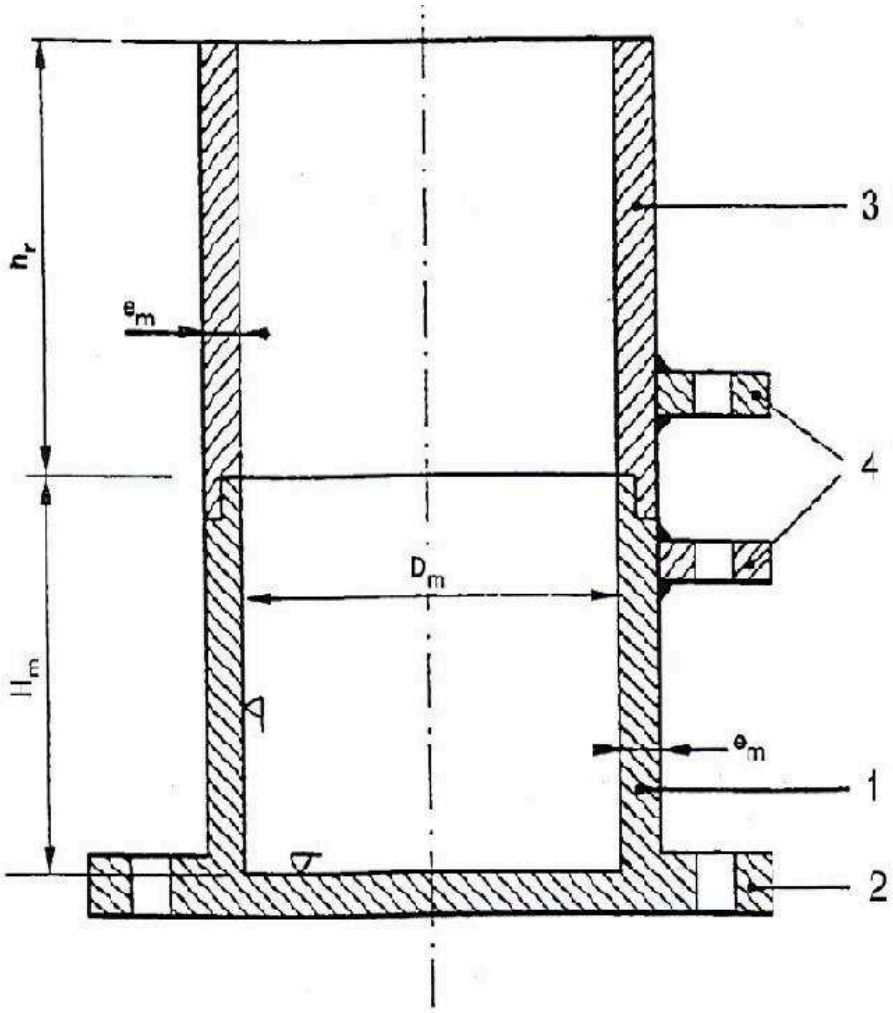

D_m = 10cm H_m = 11.6cm

h_r = 5.1cm e_m = 0.5 cm

Legend

1 Test mold
2 Monting brackets of the mold on the vibration table
3 Rise
4 Assembly of the rise on the mold

Figure A5-1: the test mold with its rise

- At the end of the mold filling, the sand surmounting the mold will take a conical form (Figure A5-2).

Figure A5-2: the test mold with the conical sand at the end of the filling step

- The exceeding sand over the superior plane of the mold must be removed very carefully to eliminate any risk of densification of the underlying soil.
  Several steps of 1cm of height must be done using a ruler with the use of a translation movement parallel to the superior plane of the mold.
- At the end of the shaving step (Figure A5-3), the mass of the mold with the sand is measured.
- The minimum unit dry weight can be obtained using the following formula:

$$\rho_d = \frac{m_d}{V_m} \qquad (2)$$

Where:

m_d is the dry weight of the sand ($m_d = m - m_m$)

V_m is the inside volume of the test mold

m is the mass of the mold and it content

m_m is the mass of the test mold

- In order to minimize any possible uncertainty, the measure of the minimum unit dry weight is repeated three times then the average value obtained from these 3 times is considered as the minimum unit dry weight of the used sand.

Figure A5-3: the test mold after shaving the extra sand

1.2 Determination of the maximum unit dry weight

To determinate the maximum unit dry weight the steps described in the previous section to fill the test mold and shave the extra sand must be repeated then the procedure must follow this sequence:

- Mount the cylindrical rise of the test mold.
- Fix the test mold on the vibration table.
- Put an overload weight of about 5 kg on the mold (Figure A5-4).
- Adjust the vibration table with a frequency of 50 Hz.
- Vibrate the material for 8 min.
- Remove the overload and the rise.
- Calculate the volume of the sand (V_m) then do the measurement of the weight of the test mold with the sand.

- The maximum unit dry weight can be obtained using the following formula:

$$\rho_d = \frac{m_d}{V_m} \qquad (3)$$

Where:

m_d is the dry weight of the sand ($m_d = m - m_m$)

V_m is the inside volume of the test mold

m is the mass of the mold and it content

m_m is the mass of the test mold

- In order to minimize any possible uncertainty, the measure of the maximum unit dry weight is repeated three times then the average value obtained from these 3 times is considered as the maximum unit dry weight of the used sand.

Figure A5-4: the test mold on the vibration table

2. Application to Fontainebleau NE 34:

Mold weight = 3278 g

Mold volume = 942.39 cm^3

Determination of the minimum dry weight:

Test 1: Weight of the mold + sand = 4652 g

Test 2: Weight of the mold + sand = 4656 g

Test 3: Weight of the mold + sand = 4656 g

Average of the Weight of the mold + sand = 4654.6 g

Average weight of the sand = 1376.6 g

$\rho_{dmin} = \frac{m_d}{V_m} = \frac{1376.6}{942.39}$ = 1.46 g/cm^3

It is necessary to note that the obtained value of the ρ_{dmin} although the repetition of the method 3 times seem to be higher than what exist in the literature (Rosquoet 2004, Silva 2014). This variation can be originated from several causes, from the fact that the method used in the determination of the ρ_{dmin} is user dependent (the filling of the mold and the removing of the extra sand) to the fact that the NE34 come from natural deposits and it has properties that can differ from one slot to another.

Determination of the maximum dry weight:

In this test after the remove of the rise, the extra sand above the horizontal plane of the mold was shaved so it is considered that the sand volume is equal to the mold volume.

Test 1: Weight of the mold + sand = 4890 g

Test 2: Weight of the mold + sand = 4891 g

Test 3: Weight of the mold + sand = 4889 g

Average of the Weight of the mold + sand = 4890g

Average weight of the sand = 1612 g

$\rho_{dmax} = \frac{m_d}{V_m} = \frac{1612}{942.39}$ = 1.71 g/cm^3

3. Uncertainty calculus:

Uncertainty on diameter measurement of the mold: 0.00531 mm

Uncertainty on height measurement of the mold: 0.00522 mm

Combined uncertainty on the volume of the mold: 1.19909 mm^3

minimum dry weight:

Uncertainty on the mass of the sand: 1.3361 g

Combined uncertainty on the ρ_{dmin} = 0.00644 g/cm^3

So ρ_{dmin} can be written as : 1.46 ± 0.01288 (k=2) g/cm^3

maximum dry weight:

Uncertainty on the mass of the sand : 0.58372 g

Combined uncertainty on the ρ_{dmax} = 0.00663 g/cm^3

So ρ_{dmax} can be written as : 1.71 ± 0.01326 (k=2) g/cm^3

4. Summary:

	Min	Max
ρ_d (g/cm^3)	1.46	1.71
e	0.549	0.753
n	0.354	0.429

Appendix 6 : Laser particle size distribution

Laser particle size distribution

The Fontainebleau sand grain size distribution is analysed using a laser apparatus. This method dates of the 1970s and permits to measure the size of the particles, or more exactly their radius (assuming a spherical shape), and also to determine their statistic frequency vs their size. The resolution of this method is well above that of the conventional sieve analysis test (the laser size distribution method permit to measure sizes of particles between 0.01 and 3500 µm). It is also quickly realized but, as the assumption of spherical grains is strong, it is more used as an indicator than the "true" particle size distribution. The results are presented versus the volume instead of the mass.

An intact Fontainebleau NE34 sand is compared with a sand sample extracted from the plug created inside the open-ended pile C1O16 during its installation, using the size distribution by laser machine Mastersizer 3000 of IFSTTAR-Nantes (figure A6-1 and Table A6-1). The grading graphs obtained are compared in order to clarify the potential evolution of the sand trapped inside the open piles.

Figure A6-1: Size distribution by laser machine of IFSTTAR

1. The laser size distribution experience

The experimental set up of the sand size distribution by laser is simple and only a small quantity of sand is needed (about a half spatula of sand for each test). The order of the tasks that must be realized during the experiment is already programed inside a computer program that is connected to the size distribution by laser machine. The sand sample is poured inside the water recipient of the machine (figure A6-2) because the water is used as a dispersing material. During the test the only thing that needed to be done is to provide water to the machine when it is needed and to disperse the sand into the water recipient when the machine asks for. The quantity of the sand that must be dispersed can be known using an obscuration index inside the machine program (in order to realize the test an obscuration index between 4% and 8% is needed). In the case of the used sand, this obscuration index corresponds to about a half of spatula of Fontainebleau sand. The test is repeated three times for each sand and the average result of the three tests is finally given.

Figure A6-2: Water recipient

2. Test results

2.1 Intact Fontainebleau NE 34 sand

At the end of the three tests realized on three samples from the intact Fontainebleau NE34 sand the average result of the three tests is given. Figure A6-3 shows that the Fontainebleau sand is a poorly graded sand and that the minimum grain size is 80 µm and the maximum is 400 µm. The majority part of the grains has a size between 160 and 315 µm.

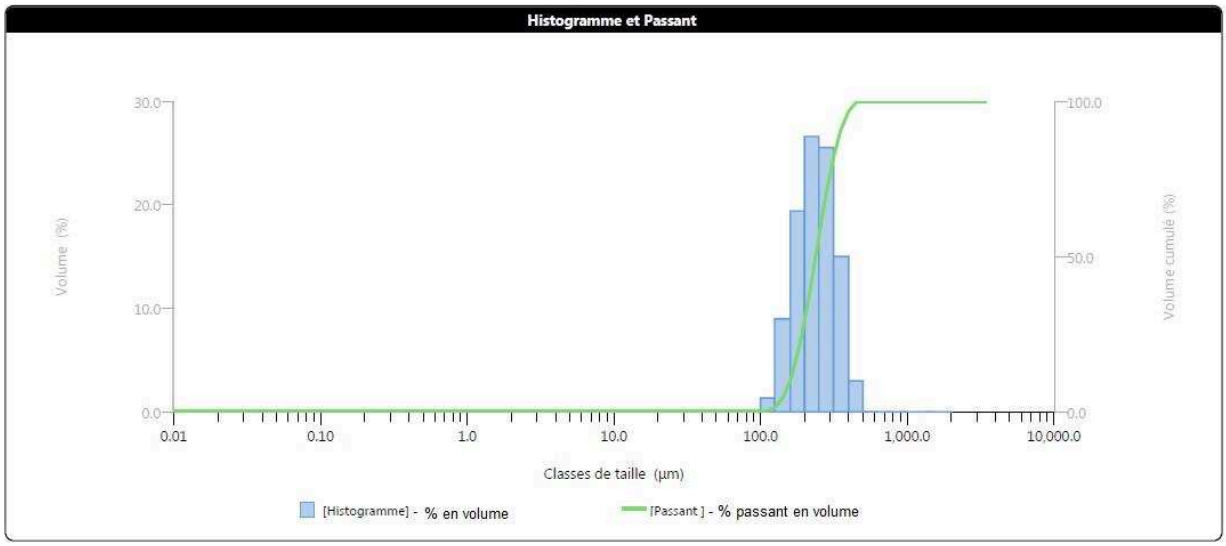

Taille (µm)	% Volume Passant	Taille (µm)	% Volume Passant	Taille (µm)	% Volume Passant	Taille (µm)	% Volume Passant	Taille (µm)	% Volume Passant	Taille (µm)	% Volume Passant
0.0100	0.00	0.160	0.00	1.25	0.00	10.0	0.00	80.0	0.00	560	100.00
0.0250	0.00	0.200	0.00	1.60	0.00	12.5	0.00	100	0.04	630	100.00
0.0320	0.00	0.250	0.00	2.00	0.00	16.0	0.00	125	1.37	800	100.00
0.0400	0.00	0.315	0.00	2.50	0.00	20.0	0.00	160	10.36	1000	100.00
0.0500	0.00	0.400	0.00	3.15	0.00	25.0	0.00	200	29.79	1500	100.00
0.0630	0.00	0.500	0.00	4.00	0.00	31.5	0.00	250	56.43	2000	100.00
0.0800	0.00	0.630	0.00	5.00	0.00	40.0	0.00	315	81.99		
0.100	0.00	0.800	0.00	6.30	0.00	50.0	0.00	400	97.00		
0.125	0.00	1.00	0.00	8.00	0.00	63.0	0.00	500	100.00		

Taille (µm)	% Volume Dans	Taille (µm)	% Volume Dans	Taille (µm)	% Volume Dans	Taille (µm)	% Volume Dans	Taille (µm)	% Volume Dans	Taille (µm)	% Volume Dans
0.0100	0.00	0.160	0.00	1.25	0.00	10.0	0.00	80.0	0.04	560	0.00
0.0250	0.00	0.200	0.00	1.60	0.00	12.5	0.00	100	1.33	630	0.00
0.0320	0.00	0.250	0.00	2.00	0.00	16.0	0.00	125	8.99	800	0.00
0.0400	0.00	0.315	0.00	2.50	0.00	20.0	0.00	160	19.43	1000	0.00
0.0500	0.00	0.400	0.00	3.15	0.00	25.0	0.00	200	26.64	1500	0.00
0.0630	0.00	0.500	0.00	4.00	0.00	31.5	0.00	250	25.56	2000	
0.0800	0.00	0.630	0.00	5.00	0.00	40.0	0.00	315	15.02		
0.100	0.00	0.800	0.00	6.30	0.00	50.0	0.00	400	2.99		
0.125	0.00	1.00	0.00	8.00	0.00	63.0	0.00	500	0.00		

Figure A6-3: Results of the size distribution of Fontainebleau NE34

2.2 Results of the plugged Fontainebleau NE 34 sand inside the open piles

The same study has been repeated on three samples from the trapped sand inside the open pile in order to study if there is any changing in the grading of this sand caused by the plugging. Figure A6-4 shows the average result obtained from the tests on these samples. This figure shows clearly a change in the overall grading of the sand. This sand includes finer grains than

the intact sand. The minimum grain size passes from 80 µm to 0.63 µm and 13.46 % in volume of the sand are smaller from 80 µm. These results prove that crushing occurs inside the pile plug.

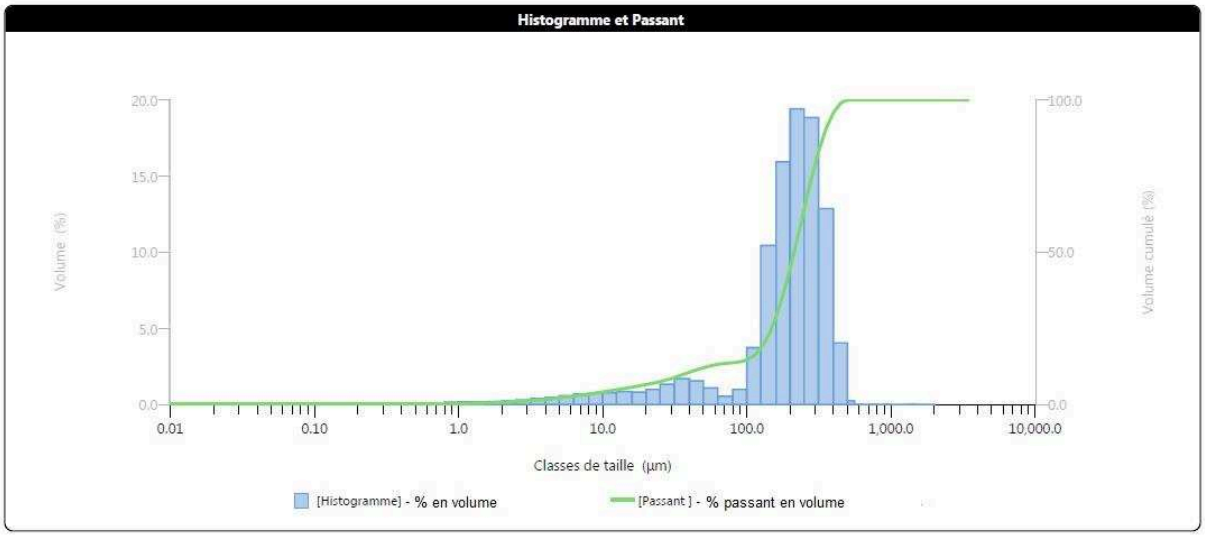

Taille (µm)	% Volume	Passant
0.0100	0.00	
0.0250	0.00	
0.0320	0.00	
0.0400	0.00	
0.0500	0.00	
0.0630	0.00	
0.0800	0.00	
0.100	0.00	
0.125	0.00	

Taille (µm)	% Volume	Passant
0.160	0.00	
0.200	0.00	
0.250	0.00	
0.315	0.00	
0.400	0.00	
0.500	0.00	
0.630	0.00	
0.800	0.03	
1.00	0.18	

Taille (µm)	% Volume	Passant
1.25	0.34	
1.60	0.51	
2.00	0.70	
2.50	0.94	
3.15	1.24	
4.00	1.63	
5.00	2.08	
6.30	2.66	
8.00	3.36	

Taille (µm)	% Volume	Passant
10.0	4.08	
12.5	4.83	
16.0	5.67	
20.0	6.49	
25.0	7.47	
31.5	8.80	
40.0	10.49	
50.0	12.03	
63.0	13.11	

Taille (µm)	% Volume	Passant
80.0	13.64	
100	14.63	
125	18.35	
160	28.78	
200	44.69	
250	64.07	
315	82.89	
400	95.74	
500	99.77	

Taille (µm)	% Volume	Passant
560	100.00	
630	100.00	
800	100.00	
1000	100.00	
1500	100.00	
2000	100.00	

Taille (µm)	% Volume	Dans
0.0100	0.00	
0.0250	0.00	
0.0320	0.00	
0.0400	0.00	
0.0500	0.00	
0.0630	0.00	
0.0800	0.00	
0.100	0.00	
0.125	0.00	

Taille (µm)	% Volume	Dans
0.160	0.00	
0.200	0.00	
0.250	0.00	
0.315	0.00	
0.400	0.00	
0.500	0.00	
0.630	0.03	
0.800	0.15	
1.00	0.16	

Taille (µm)	% Volume	Dans
1.25	0.17	
1.60	0.19	
2.00	0.23	
2.50	0.30	
3.15	0.39	
4.00	0.46	
5.00	0.58	
6.30	0.70	
8.00	0.72	

Taille (µm)	% Volume	Dans
10.0	0.75	
12.5	0.84	
16.0	0.82	
20.0	0.98	
25.0	1.33	
31.5	1.69	
40.0	1.54	
50.0	1.08	
63.0	0.53	

Taille (µm)	% Volume	Dans
80.0	0.98	
100	3.72	
125	10.43	
160	15.91	
200	19.39	
250	18.82	
315	12.85	
400	4.03	
500	0.23	

Taille (µm)	% Volume	Dans
560	0.00	
630	0.00	
800	0.00	
1000	0.00	
1500	0.00	
2000		

Figure A6-4: Results of the size distribution of Fontainebleau NE34 of the plugged piles

The Figure A6-5 shows the difference of the volumes of the different ranges of the grains sizes distributions of the sand between the intact sand and the plugged one. The negative values indicate an increase in the volume of the corresponding grains sizes ranges between the intact and the plugged sand due to the crush of the sand. On the other hand the positive volumes indicate the sizes ranges that decreased in volumes due to the crush of the sands of these ranges. This graph confirms that the coarser fractions have been reduced in volume, and crushed for becoming finer fractions.

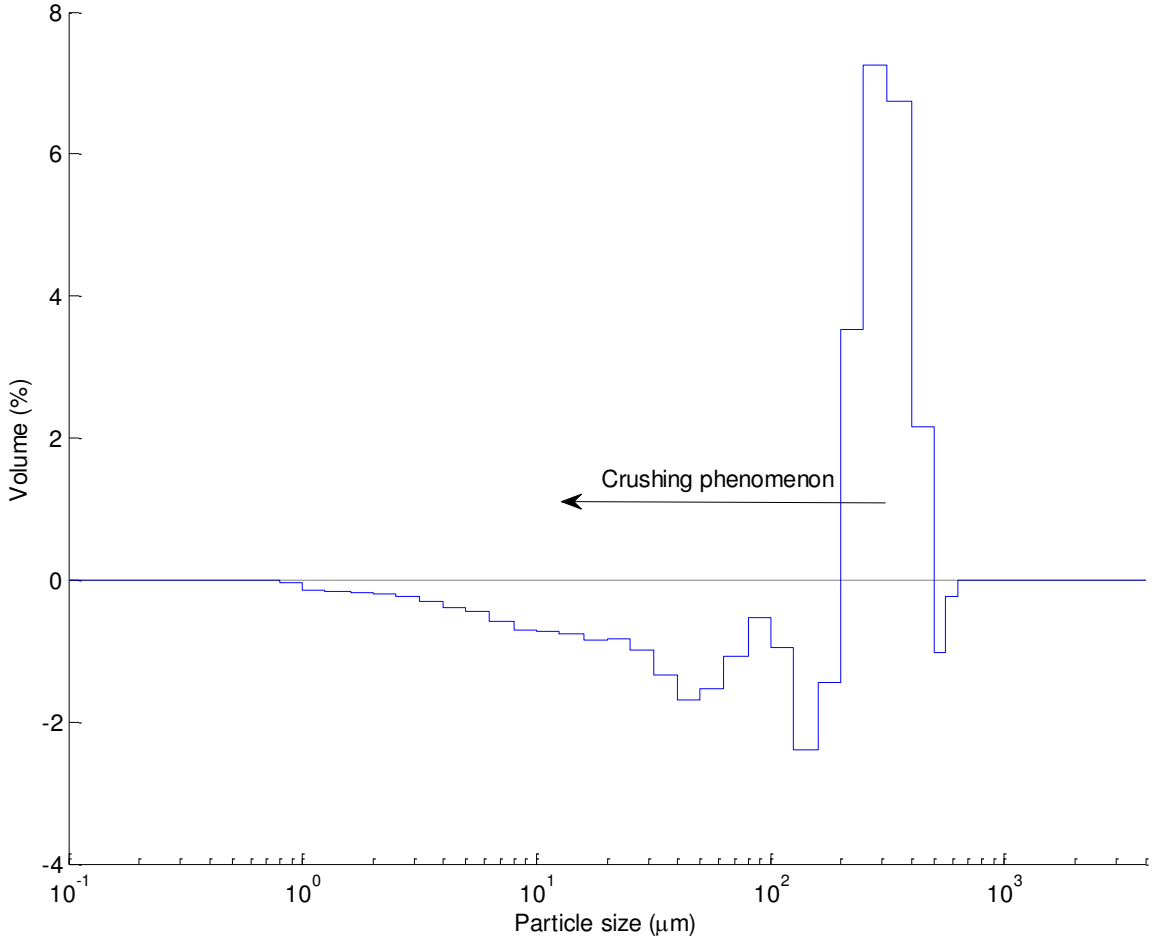

Figure A6-5: Evolution of the volume of the different particles sand sizes due to the plug

Table A6-1: Laser size distribution apparatus specifications

Specification	**Mastersizer 3000**	
	Parameters	**Specifications**
Generals	Principle Acquisition frequency Typical measure time	diffraction with laser light 10 kHz <10 sec
Optics	Red light source Blue light source Lens set up	Maxi. 4 mW He-Ne, 632.8 nm LED 10 mW nominal, 470 nm Inverse Fourier (convergent light beam)
Detector	Arrangement Angular range Alignment	network of logarithmically spaced detectors From 0.015 to 144 degrees Automatic
Sizes	Range of sizes Numbers of size distribution ranges Precision Repeatability Reproducibility	From 0.01 to 3500 µm 100 ranges Better than 1% Variation better than 0.5% Variation better than 1%
Software	21 CFR part 11	Allows an operation mode that respect the ER/ES
System	Dimensions of the optic bench Weight Alimentation Product storage conditions Operational conditions	690 mm × 300 mm × 450 mm (L×l×H) 30 kg 100/240 V, 50/60 Hz -20°C to +50°C, 10% - 80% of relative humidity +10°C to +35°C, 10% - 80% of relative humidity

Appendix 7 : Sensors list

Sensors list

Different sensors were used in the present study and will be grouped in three tables: Table A7-1 is for the force sensors, Table A7-2 and Table A7-3 are for the displacement sensors.

Table A7-1: Force sensors

Sensor	Utilization	Manufacturer	Serial number	Measure minimum (N)	Measure Maximum (N)	Linearity gap*	Hysteresis gap*
XF3057	Instrumented rigid pile (Pile 1)	FGP	S130MG	-17000	+17000	±0.139%	±0.205%
FN3070	Vertical hydraulic jack	FGP	04	-25000	+25000	±0.2 %	
F521-06TC	Horizontal electrical jack	TME	47954	-2500	+2500	±0.15%	±0.15%

*: The gaps are in function of the measure rang of the sensor

Table A7-2: Displacement sensors

Sensor	Utilization	Manufacturer	Serial number	Measure range (mm)	Repeatability gap*	Linearity gap*	Hysteresis gap
MSE/0350S010-1E01	Vertical hydraulic jack	TWK	1246 0428	300	0.001%	0.01%	4 µm
-	Horizontal electrical jack	Exlar	-	150	-	-	-

*: The gaps are in function of the measure rang of the sensor

Table A7-3: Displacement laser sensor

Sensor	Utilization	Manufacturer	Serial number	Measure width range (mm)	Measure width range (mm)	Measure diameter range (mm)
OCX7-11170024	Lateral laser sensor	BAUMER	70000181 7028	75-125	150-250	30-130

Appendix 8 : Publications list

1. Publications in journals

[1] El Haffar I., Blanc M., Thorel L. 2017 Impact of pile installation method on the axial capacity in sand. Géotechnique Letters, 7, 260-265, http://dx.doi.org/10.1680/jgele.17.00036

[2] El Haffar I., Blanc M., Thorel L. 2018 Axial capacity of piles jacked in sand. Parametric study in centrifuge. (submitted to International journal of physical modelling in geotechnics).

[3] El Haffar I., Blanc M., Thorel L. 2018 Impact of pile roughness on the shaft resistance in sand. (submitted to Proceedings of the Institution of Civil Engineers - Geotechnical Engineering).

[4] El Haffar I., Blanc M., Thorel L. 2018 Monotonic lateral loading on single piles in sand: parametric centrifuge modelling in eccentricity, saturation and installation mode. (submitted to Géotechnique).

[5] El Haffar I., Blanc M., Thorel L. 2018 Cyclic lateral loading on single piles in sand: parametric centrifuge modelling in eccentricity, saturation and installation mode. (submitted to Canadian Geotechnical Journal).

2. Publications in nationals and internationals conferences

[1] El Haffar I., Blanc M., Thorel L., 2018. General study on the axial capacity of piles of offshore wind turbines jacked in sand. 9th ICPMG London 17-20th july. (accepted).

[2] El Haffar I., Blanc M., Thorel L., 2018. Effect of the installation methods of piles in cohesionless soil on their axial capacity. 9th ICPMG London 17-20th july. (accepted).

[3] El Haffar I., Blanc M., Thorel L. 2017 L'effet de la méthode d'installation sur la capacité des pieux en traction. AUGC Nantes. 7p.

[4] El Haffar I., Blanc M., Thorel L. 2018 Capacité axiale de pieux foncés dans du sable - essais en centrifugeuse. Dans : Delage P., Chevalier C., Cui Y.J. & Semblat J.F. (Eds.), 2018. Actes des 9èmes Journées Nationales de Géotechnique et de Géologie de l'Ingénieur, 13-15 juin 2018 (online). Marne-la-Vallée : IFSTTAR-ENPC, 2018.

Collection Actes Interactifs de l'Ifsttar, AII3. 978-2-85782-742-9. Online at the address http://www.ifsttar.fr/collections/ActesInteractifs/AII3.

[5] El Haffar I., Blanc M., Thorel L. 2018 Effet de la methode d'installation sur le chargement lateral d'un pieu - essais en centrifugeuse. Dans : Delage P., Chevalier C., Cui Y.J. & Semblat J.F. (Eds.), 2018. Actes des 9èmes Journées Nationales de Géotechnique et de Géologie de l'Ingénieur, 13-15 juin 2018 (online). Marne-la-Vallée : IFSTTAR-ENPC, 2018. Collection Actes Interactifs de l'Ifsttar, AII3. 978-2-85782-742-9. Online at the address http://www.ifsttar.fr/collections/ActesInteractifs/AII3.

UNIVERSITE BRETAGNE SCIENCES LOIRE POUR L'INGENIEUR

CENTRALE NANTES

Titre : Modélisation physique et étude du comportement de fondations profondes d'éoliennes offshore dans du sable

Mots clés : Pieu, capacité axial, chargement latéral, courbes p-y, modèles réduits centrifugés.

Résumé : La capacité axiale et latérale des pieux foncés dans du sable de Fontainebleau NE34 ont été étudié à l'aide d'essais sur modèles réduits centrifugés.

L'effet de la méthode d'installation, de la densité et de la saturation du sable, du diamètre du pieu, de la géométrie de sa pointe (ouvert /fermé) et de sa rugosité sur la capacité axiale a été étudié. Une augmentation significative de la capacité en traction est observée dans les pieux foncés cycliquement, contrairement aux pieux foncés d'une manière monotone à 100 × g. La saturation du sable dense accélère la formation du bouchon lors de l'installation du pieu. L'augmentation de la rugosité du pieu et de la densité du sable accroissent significativement le frottement latéral des pieux testé. Dans tous les cas, les capacités de pieux sont comparées aux codes de dimensionnement des éoliennes offshore.

Une étude paramétrique de l'effet de la méthode d'installation, de l'excentricité de la charge et de la saturation du sable sur la réponse latérale des pieux foncés est ensuite réalisée grâce à l'utilisation d'un pieu instrumentée. Le pieu est chargé d'une manière monotone puis un millier de cycles sont appliqués. Une nouvelle méthode a été développée pour la détermination des constantes d'intégration pour déterminer le profil de déplacement latéral du pieu. La méthode d'installation influence directement le comportement global (moment maximum et déplacement latéral) et local (courbes p-y) des pieux. L'effet de l'excentricité de la charge et de la saturation du sable sur le comportement des pieux est également présenté. Dans chaque cas, une comparaison avec les courbes p-y extraites du code DNVGL est réalisée.

Title : Physical modeling and study of the behavior of deep foundations of offshore wind turbines in sand

Keywords : Pile, axial capacity, lateral loading, p-y curves, centrifuge modeling.

Abstract : The axial and lateral capacity of piles jacked in Fontainebleau sand NE34 are studied using centrifuge modelling at 100×g.

The effect of the installation method, sand density and saturation, pile diameter and pile tip geometry (open or closed-ended) and pile roughness on the axial capacity of piles are firstly studied. A significant increase in the tension capacity is observed in cyclically-jacked piles unlike piles monotonically jacked at 100×g. The saturation of dense sand accelerates plug formation during pile installation. The increase in pile roughness and sand density increases significantly the shaft resistance of the piles tested here. For all the cases, pile capacities are compared with the current design codes for offshore wind turbines.

A parametric study of the effect of the installation method, load eccentricity and sand saturation on the lateral response of jacked piles is then realized using of an instrumented pile. The pile is loaded monotonically, then a thousand cycles are applied. A new methodology has been developed for determining of the constants needed in the integration procedure to identify the lateral displacement profile of the pile. The installation method influences directly the global (maximum moment and lateral displacement) and local behaviour (p-y curves) of the piles. The effect of the load eccentricity and sand saturation on the behaviour of the piles is also presented. In each case a comparison with the p-y curves extracted from the DNVGL code is realized.